

AUTONOMIC INNERVATION AND CONTROL OF CHRONOTROPY IN THE
ZEBRAFISH HEART

by

Matthew R. Stoyek

Submitted in partial fulfilment of the requirements
for the degree of Doctor of Philosophy

at

Dalhousie University
Halifax, Nova Scotia
August 2016

© Copyright by Matthew R. Stoyek, 2016

This thesis is dedicated to my wife Jacqueline,

Who has endured countless late nights and the endless mumbled thoughts of someone whose mind was focused on ongoing experiments, papers, or presentations, but who offered me only compassion and support despite my scientific predilection.

TABLE OF CONTENTS

LIST OF TABLES	ix
LIST OF FIGURES	x
ABSTRACT	xii
LIST OF ABBREVIATIONS USED	xiii
ACKNOWLEDGEMENTS	xv
CHAPTER 1 INTRODUCTION	1
1.1 An overview of the autonomic nervous system and the intracardiac nervous system.....	2
1.1.1 Overview of the autonomic nervous system	2
1.1.2 The intracardiac nervous system.....	4
1.1.3 Difficulties in studying the intracardiac nervous system.....	6
1.2 The zebrafish as an alternative model for studies of integrative cardiac control.....	7
1.2.1 Anatomy of the teleost heart	7
1.2.2 Innervation of the teleost heart.....	8
1.2.3 Pacemaker function of the teleost heart	11
1.3 Relevance and thesis objectives.....	13
1.3.1 Relevance	13
1.3.2 Thesis objectives.....	14
CHAPTER 2 ANATOMY OF THE ZEBRAFISH INTRACARDIAC NERVOUS SYSTEM.....	20
2.1 Introduction.....	21
2.2 Methods.....	24
2.2.1 Animals	24
2.2.2 Heart isolation	24
2.2.3 General and neurotransmitter-specific labelling	24
2.2.4 Tracing extrinsic vagosympathetic inputs.....	26
2.2.5 Imaging and data processing.....	27
2.3 Results	28
2.3.1 Overview of innervation pattern	28

2.3.2	Sinoatrial plexus.....	28
2.3.3	Identification of putative pacemaker cells in the sinoatrial valve.....	32
2.3.4	Atrioventricular junction.....	32
2.3.5	Outflow tract.....	33
2.4	Discussion.....	34
2.4.1	Intracardiac neurons at the venous pole.....	34
2.4.2	Sinoatrial plexus innervation.....	40
2.4.3	Putative pacemaker cells.....	42
2.4.4	Innervation of the atrioventricular junction.....	43
2.4.5	Conclusions.....	45
CHAPTER 3 AUTONOMIC CONTROL OF CHRONOTROPY IN THE ZEBRAFISH.....		55
3.1	Introduction.....	56
3.2	Methods.....	59
3.2.1	Animals.....	59
3.2.2	Heart isolation.....	59
3.2.3	Whole heart electrocardiograms and vagosympathetic nerve trunk stimulations.....	59
3.2.4	Isolated ventricular pacemaker recordings.....	60
3.2.5	Branchiocardiac trunk stimulation.....	60
3.2.6	Pharmacological agents.....	60
3.2.7	Voltage optical mapping.....	60
3.2.8	Pacemaker cell immunohistochemistry.....	61
3.2.9	Imaging and data analysis.....	61
3.3	Results.....	62
3.3.1	Viability of heart function <i>in vitro</i>	62
3.3.2	Electrical stimulation of cardiac rami of vagosympathetic trunks.....	62
3.3.3	Effects of cholinergic and adrenergic agents on R-R interval.....	63
3.3.4	Autonomic effects on atrioventricular region activity.....	63
3.3.5	Effect of branchiocardiac trunk stimulation.....	64
3.3.6	Imaging of the origin and spread of cardiac excitation.....	64

3.3.7 Anatomical identification of putative pacemaker cells in the sinoatrial and atrioventricular regions.....	66
3.4 Discussion	68
3.4.1 Receptor-mediated mechanisms of chronotropic modulation	68
3.4.2 Properties and neural control of pacemaker loci.....	70
3.4.3 Influence of the branchiocardiac trunk on heart rate	72
3.4.4 Anatomical relationship of muscarinic and adrenergic receptors with putative pacemaker cells	73
3.4.5 Conclusions.....	76
 CHAPTER 4 EFFECTS OF VAGAL NERVE STIMULATION ON PACEMAKER ACTIVITY AND INTRACARDIAC NEURONAL ACTIVATION IN THE ZEBRAFISH.....	
4.1 Introduction	88
4.2 Methods.....	90
4.2.1 Animals	90
4.2.2 Heart isolation	90
4.2.3 Vagosympathetic nerve stimulation for assessment of intracardiac neurons by cFOS	91
4.2.4 Vagosympathetic nerve stimulation for assessment of intracardiac neurons by phosphorylated extracellular signal-regulated kinase.....	91
4.2.5 cFOS and phosphorylated extracellular signal-regulated kinase immunohistochemistry	92
4.2.6 Controls.....	92
4.2.7 Voltage optical mapping	93
4.2.8 Vagosympathetic nerve stimulation for assessment of pacemaker shift	93
4.2.9 Pharmacological blockade	94
4.2.10 Data presentation.....	94
4.3 Results	94
4.3.1 Intracardiac neuron activation revealed by cFOS-like immunoreactivity	94

4.3.2	Intracardiac neuron activation as revealed by phosphorylated extracellular signal-regulated kinase-like immunoreactivity	95
4.3.3	Pacemaker activity <i>in vitro</i>	96
4.3.4	Effects of graded vagosympathetic nerve stimulation on pacemaker activity within the sinoatrial region.....	96
4.4	Discussion	97
4.4.1	Intracardiac neuron activation revealed by cFOS- and phosphorylated extracellular signal-regulated kinase-like immunoreactivity	98
4.4.2	Pacemaker site changes in response to vagosympathetic nerve stimulation.....	100
4.4.3	Conclusions.....	103
CHAPTER 5 CARDIAC DISTRIBUTION AND CHRONOTROPIC EFFECTS OF SEROTONIN IN THE ZEBRAFISH		
115		
5.1	Introduction	116
5.2	Methods.....	117
5.2.1	Animals	117
5.2.2	Heart isolation	118
5.2.3	Immunohistochemical detection of serotonin and tryptophan hydroxylase	118
5.2.4	Whole-heart electrocardiogram recordings.....	119
5.2.5	Pharmacological agents.....	119
5.2.6	Imaging, data analysis and presentation	119
5.3	Results	120
5.3.1	Cardiac distribution of serotonin detected by immunohistochemistry	120
5.3.2	Basal heart rate.....	122
5.3.3	Effects of serotonin on R-R interval	123
5.4	Discussion	123
5.4.1	Distribution of serotonin within the zebrafish heart	123
5.4.2	Serotonin effects on heart rate	127

5.4.3 Conclusions	130
CHAPTER 6 THE ISOLATED ZEBRAFISH HEART AS A MODEL TO STUDY THE CHRONOTROPIC EFFECTS OF VAPOUR	
ANAESTHETICS	138
6.1 Introduction	139
6.2 Methods	141
6.2.1 Animals	141
6.2.2 Heart isolation	142
6.2.3 Measurement of heart rate and vagosympathetic nerve electrical stimulation	142
6.2.4 Potential effects of tricaine as overdosing agent.....	142
6.2.5 Anaesthetic agents.....	143
6.2.6 Anaesthetic test procedures.....	143
6.2.7 Pharmacologic agents	144
6.2.8 Data analyses.....	145
6.3 Results	145
6.3.1 Heart function <i>in vitro</i>	145
6.3.2 Time course of anaesthetic-induced changes in heart rate and atrioventricular delay.....	145
6.3.3 Concentration-dependent changes in heart rate and atrioventricular delay	146
6.3.4 Effects of autonomic blockade and vagosympathetic nerve stimulation.....	146
6.4 Discussion	147
6.4.1 Effects of anaesthetics on heart rate and atrioventricular delay.....	149
6.4.2 Concentration-dependent effects.....	151
6.4.3 Effects of autonomic blockade and vagosympathetic nerve stimulation.....	153
6.4.4 Conclusions.....	155
CHAPTER 7 CONCLUSIONS	170

CITATIONS	176
APPENDIX A Expanded methods	196
APPENDIX B Table of immunohistochemical agents.....	224
APPENDIX C Results of studies in goldfish (<i>Carassius auratus</i>).....	228
APPENDIX D Copyright permissions	243

LIST OF TABLES

Table 1 Summary of effects of desflurane, isoflurane, sevoflurane on heart rate or atrioventricular delay as compared to pre-treatment values.	158
Table 2 Summary of effects of vagosympathetic nerve stimulation on heart rate during exposure to desflurane, isoflurane, or sevoflurane.	159

LIST OF FIGURES

Figure 1.1	Overview of the zebrafish heart.....	18
Figure 2.1	Organization of the intracardiac nervous system with general neuronal antibodies.....	47
Figure 2.2	Localization of neurotransmitter-specific elements and presumptive pacemaker tissue in the sinoatrial valve region.....	49
Figure 2.3	Intracardiac tracing of extrinsic vagosympathetic inputs to the sinoatrial plexus.....	51
Figure 2.4	Innervation of the atrioventricular region and the outflow tract	53
Figure 3.1	Chronotropic responses to vagosympathetic nerve stimulation and autonomic agents	77
Figure 3.2	Atrioventricular dissociation, modulation of atrioventricular region activity, and stimulation of branchiocardiac nerve trunk	79
Figure 3.3	Optical mapping of origin and spread of excitation in atrium and ventricle	81
Figure 3.4	Regional distribution of putative pacemaker cells and muscarinic receptors detected by immunohistochemistry	83
Figure 3.5	Regional distribution of beta-adrenergic receptors associated with putative pacemaker cells and myocardium.....	85
Figure 4.1	Organization of intracardiac neurons demonstrating cFOS- and phosphorylated extracellular signal-regulated kinase-like immunoreactivity following left vagosympathetic nerve stimulation	105
Figure 4.2	Organization of intracardiac neurons demonstrating cFOS- and phosphorylated extracellular signal-regulated kinase-like immunoreactivity following right vagosympathetic nerve stimulation	107
Figure 4.3	Proportion of intracardiac neurons activated by vagosympathetic nerve stimulation	109
Figure 4.4	Maps of the initial pacemaker site breakthrough in the sinoatrial region with varying levels of the left cardiac vagosympathetic nerve	111
Figure 4.5	Maps of the initial pacemaker site breakthrough in the sinoatrial region with varying levels of the right cardiac vagosympathetic nerve	113
Figure 5.1.	Serotonin immunoreactivity in the atrial wall	132
Figure 5.2	Organization of serotonin immunoreactivity in the sinoatrial region....	134
Figure 5.3	Chronotropic responses to serotonin and serotonergic agents.....	136

Figure 6.1	Schematic of the perfusion and electrocardiogram recording system for the zebrafish heart.....	159
Figure 6.2	Time-dependent chronotropic responses of the isolated zebrafish heart to anaesthetics.....	161
Figure 6.3	Concentration-dependent chronotropic responses of the isolated zebrafish heart to anaesthetics relative to a 1.0 human minimum alveolar concentration (MAC).....	163
Figure 6.4	Effects of anesthetic exposure during autonomic blockade on heart rate	165
Figure 6.5	Effects of vagosympathetic nerve stimulation on HR during anesthetic exposure.....	167
Figure C1	Overview of cardiac innervation and putative pacemaker tissues in goldfish	229
Figure C2	Innervation of the atrial wall in goldfish	231
Figure C3	Innervation of the atrial funnel, ventricle, and ventriculobulbar junction in goldfish.....	233
Figure C4	Innervation of the ventricular wall, ventriculobulbar junction, and outflow tract in goldfish	235

ABSTRACT

In the vertebrate heart the intracardiac nervous system is a common pathway for autonomic control of cardiac output, comprising a population of intracardiac neurons in ganglia embedded within nerve plexi. These neural elements modulate the activity of effectors within the heart to adjust cardiac output, maintaining optimal perfusion of the body tissues under a wide range of metabolic activities. Investigation of the specific functional roles of subpopulations of intracardiac neurons within the circuitry mediating cardiac control in vertebrates has been hampered by a lack of knowledge about the detailed anatomical organization of the intracardiac nervous system. This work has revealed within the zebrafish intracardiac nervous system a complex neuroanatomy in which extrinsic innervation reached all regions of the heart; populations of intracardiac neurons were present at the sinoatrial and atrioventricular junctions, and adrenergic, cholinergic, nitroergic and peptidergic neurotransmitter phenotypes were expressed. Stimulation of individual extrinsic cardiac nerves and application of cholinergic and adrenergic agents showed that the zebrafish heart contains all the classic vertebrate hallmarks of cardiac control, establishing this preparation as a viable model for studies of integrative autonomic control of cardiac function. Disruption of electrical activity within the sinoatrial region during periods of simulated extrinsic input to the heart illustrated the complex neural mechanisms involved in rate control. In addition, it was found, using detection of activity-dependent markers, that distinct populations of intracardiac neurons were activated during vagal stimulation. This represents the first use of these markers in the heart, establishing a new method to investigate cardiac function. Further, the use of the isolated zebrafish heart for studies of clinically relevant issues was validated. These studies focused on pathways that may be responsible for cardiac dysfunction known to occur in those on serotonergic anti-depressants as well as in patients during clinical anesthesia. The results of this work offer a new model for studies of the direct and neurally mediated pathways involved in heart rate regulation. Overall, the results from these studies contribute significant advances to the establishment of the zebrafish as a new model for studies of integrative autonomic cardiac control.

LIST OF ABBREVIATIONS USED

%	percent	HCN3	hypolarization-activated, cyclic nucleotide-gated channel 3
°C	degrees Celsius		
5-HT	serotonin		
5-HTT	serotonin transporter	HCN4	hypolarization-activated, cyclic nucleotide-gated channel 4
A	atrium		
AB	autonomic blockade		
ACh	acetylcholine	HEX	hexamethonium
AcT	acetylated tubulin	HR	heart rate
aE	atrial electrode	Hu	human neuronal protein C/D
ANOVA	analysis of variance		
ANS	autonomic nervous system	Hz	hertz
AP	action potential	ICN	intracardiac neuron
ATR	atropine	ICNS	intracardiac nervous system
AV	atrioventricular		
AVd	atrioventricular delay	IEG	immediate early gene
AVP	atrioventricular plexus	IR	immunoreactive
AVR	atrioventricular region	ISF	isoflurane
AVtr	atrioventricular nerve trunk	Isl1	Islet 1
		ISO	isoproterenol
AVV	atrioventricular valves	K ⁺	potassium (ion)
BA	bulbus arteriosus	KCl	potassium chloride
BCT	branchiocardiac trunk	KET	ketanserin
BSA	bovine serum albumin	L	litre
Ca ²⁺	calcium (ion)	LIR	like immunoreactivity
CaCl ₂	calcium chloride	lvG	left ventral ganglia
ChAT	choline acetyltransferase	LX	left vagosympathetic trunk
Cl ⁻	chloride (ion)	LXG	left vagosympathetic trunk ganglia
CNS	central nervous system		
DC	ducts of Cuvier	M ₂ R	muscarinic receptor subtype 2
dG	dorsal ganglia		
DSF	desflurane	MAC	minimum alveolar concentration
ECG	electrocardiogram		
ERK	extracellular signal-regulated protein	mg	milligram
		MgSO ₄	magnesium sulfate
FLX	fluoxetine	min	minute
G	ganglia	mL	millilitre
h	hour	mm	millimetre
HCN	hypolarization-activated, cyclic nucleotide-gated channel	mM	millimolar
		ms	millisecond
HCN1	hypolarization-activated, cyclic nucleotide-gated channel 1	MS-222	tricaine methanesulfonate
		MUS	muscarine
		NA	numerical aperture
		Na ⁺	sodium (ion)
		NaCl	sodium chloride

NaH ₂ PO ₄	monosodium phosphate	SBP	serotonin binding protein
NaHCO ₃	sodium hydrogen carbonate (bicarbonate)	SEM	standard error of the mean
NANC	non-adrenergic, non-cholinergic	SIF	small intensely fluorescent
NE	norepinephrine	SNS	sympathetic nervous system
NGS	normal goat serum	SPIP	spiperone
NIC	nicotine	SSRI	selective serotonin reuptake inhibitor
nm	nanometre	SV	sinus venosus
nNOS	neuronal nitric oxide synthase	SV2	synaptic vesicle protein 2
NO	nitric oxide	SVF	sevoflurane
O	ostium	TCA	tricyclic antidepressant
P	probability	TH	tyrosine hydroxylase
PBS	phosphate buffered saline	TIM	timolol
PBS-T	phosphate buffered saline with Triton X100	TPH	tryptophan hydroxylase
pERK	phosphorylated extracellular signal regulated protein	TRITC	tetramethylrhodamine isothiocyanate
PFA	paraformaldehyde	V	ventricle
pH	power of hydrogen	VA	ventral aorta
Phal	phalloidin	VACHT	vesicular acetylcholine transporter
pLXG	proximal left vagosympathetic trunk ganglia	vE	ventricular electrode
PNS	parasympathetic nervous system	vG	ventral ganglia
pRXG	proximal right vagosympathetic trunk ganglia	VIP	vasoactive intestinal polypeptide
rvG	right ventral ganglia	vSAP	ventral sinoatrial plexus
RX	right vagosympathetic trunk	VSN	vagosympathetic nerve trunk
RXG	right vagosympathetic trunk ganglia	β ₁ AR	beta adrenergic receptor subtype 1
s	second	β ₂ AR	beta adrenergic receptor subtype 2
SAP	sinoatrial plexus	βAR	beta adrenergic receptor
SAP	sinoatrial plexus	μA	microampere
SAR	sinoatrial region	μg	microgram
SAV	sinoatrial valves	μL	microlitre
		μm	micrometre
		μs	microsecond
		μM	micromolar

ACKNOWLEDGEMENTS

I have been fortunate to have support and guidance from many individuals to whom I owe an incredible amount of gratitude. I would like to first thank my supervisors, Dr. F.M. Smith and Dr. R.P. Croll, for taking a chance on a student who came to them many years ago looking for a way to get into research, but who really did not understand how it worked. They have made themselves available, and offered creative input and helpful critiques throughout the planning and execution of my thesis work, and who have greatly helped me in bettering myself as a researcher. I would like to offer special thanks Dr. T.A. Quinn, who selflessly dedicated countless hours to building, refining and troubleshooting the apparatus and software for the optical mapping studies, and without whose expertise these projects would not have been possible. I would also like to thank Dr. R.A. Rose and Dr. K. Semba, who as my supervising committee offered insightful feedback and constructive criticisms, helping to guide my thesis project. I would like to acknowledge K. Smith and J. Kennedy who helped me with testing, developing and refining immunohistochemistry protocols. I would also like to acknowledge the National Science and Engineering Research Council of Canada, who provided me with funding during my thesis research. Finally, over the years my family and friends have offered immense support for my endeavours, scientifically and otherwise. It has been this support that has allowed me to complete this stage of my academic life.

CHAPTER 1

INTRODUCTION

1.1 An overview of the autonomic nervous system and intracardiac nervous system.

The maintenance of cardiovascular homeostasis is a key component in vertebrate survival. In particular, as factors such as oxygen availability or temperature vary in the external environment, or when internally driven processes such as exercise or feeding are engaged, the supply of oxygen and nutrients to support the changing metabolic demands of working tissues must adapt quickly. Cardiac output must therefore be modulated rapidly to match the short-term tissue perfusion demands. The output from the heart is a function of heart rate and stroke volume: rate is set by the timing of pacemaker cell discharge, while stroke volume is set by the degree of filling of cardiac chambers and by the contractility of myocytes throughout the myocardium. In all gnathostome vertebrates, the autonomic nervous system (ANS) innervates the heart to provide fast, reflex-driven modulation of the activity of both of these effector types (Nilsson, 1983; 2011; Donald, 1998; Jänig, 2006) to maintain homeostasis. The intracardiac nervous system (ICNS) acts as a common pathway for autonomic control of the vertebrate heart, comprising a population of intracardiac neurons (ICNs) in ganglia embedded within nerve plexi. Together these neural elements modulate the activity of effectors within the heart to adjust cardiac output, thus maintaining optimal perfusion of the gas exchange organ and body tissues under a wide range of metabolic activities.

1.1.1 Overview of the ANS.

Langley (1921) and Cannon (1915) were the first to describe the structural, functional and pharmacological properties of visceral control by the autonomic nervous system. Traditionally the ANS is described as a motor (efferent) system that provides

control over visceral functions critical to maintaining homeostasis (Loewy, 1990), especially cardiovascular homeostasis. The ANS is composed of two principal efferent divisions, the parasympathetic (PNS) and sympathetic (SNS) nervous systems. Classically, in terms of control of organ function, these divisions have been viewed as having a reciprocal antagonistic relationship; the PNS being involved in inhibitory function and the SNS in excitatory (Cannon, 1915; Langley, 1921). The motor component of the SNS and PNS is formed of serially connected neurons (Loewy, 1990); the preganglionic neurons whose cell bodies lie within the central nervous system (CNS) and project axons synapsing on post-ganglionic neurons which in turn project axons that innervate target tissues.

In the PNS short efferent axons are projected from post-ganglionic neurons that lie near or within the tissues that they target. In contrast, sympathetic cell bodies are found in para- and prevertebral ganglia and project post-ganglionic efferent axons to their target tissues over a further distance. In addition to this anatomic distinction, there also exists a distinction based upon the neurotransmitters used within each limb. Pre-ganglionic parasympathetic and sympathetic neurons act through release of the neurotransmitter acetylcholine (ACh), and are termed cholinergic. In the PNS ACh acts at excitatory nicotinic receptors on post-ganglionic neurons, while post-ganglionic release of ACh acts on inhibitory muscarinic receptors in the target tissues. At post-ganglionic sites, while parasympathetic release is cholinergic, sympathetic action is via adrenergic pathways by release of norepinephrine (NE). It should also be noted at this point that while parasympathetic release occurs in close proximity to target neurons, sympathetic targets can also be under the influence of circulating catecholamines (Cannon, 1915) producing widespread autonomic neuroendocrine responses (Loewy, 1990). The ANS, however, is

not strictly an efferent system (Loewy, 1990). Almost all visceral autonomic nerves have sensory fibres intermixed with motor fibres, functioning in a feedback system to integrate and relay information to the CNS, which modulates autonomic motor outflow, contributing to control of the end organ (Loewy, 1990).

1.1.2 The intracardiac nervous system.

In the vertebrate heart, the activity of cardiac effector cells (e.g.: myocytes) is modulated by autonomic reflexes (Laurent *et al.*, 1983; Nilsson, 1983) as mentioned above, as well as acting through the ICNS. In the SNS, cardioaugmentatory impulses originate from preganglionic neurons in spinal cord nuclei. Postganglionic neurons project axons to the heart via the cardiac nerves, where they enter the ICNS and project to cardiac effector cells. In the PNS, cardioinhibitory impulses originate from brainstem vagal motor nuclei, projecting in the vagosympathetic trunks to synapse on postganglionic neurons in the ICNS. Postganglionic neurons then innervate the myocardium (Burnstock, 1969; Nilsson, 1983; 2011; Gibbins, 1994; Donald, 1998; Funakoshi and Nakano, 2007). Traditionally, it is viewed that this system maintains a balance of excitatory and inhibitory signals to the main cardiac effectors, the pacemaker cells and cardiac myocytes, providing fast-acting integrative neural control of cardiac output. The detailed organization, as well as identities and distribution of subpopulations of ICN that control specific cardiac function, however, has been hampered by a lack of knowledge about the detailed anatomical organization of the ICNS.

In the classical model of autonomic innervation of the heart, ICNs represent the a common pathway for information relayed from PNS preganglionic neurons to the

myocardium. Work in the last two decades in mammalian hearts has, however, shown that this view is overly simplistic given the neurochemical complexity (Steele *et al.*, 1994; Leger *et al.*, 1999; Hoover *et al.*, 2009), distributed nature (Armour *et al.*, 1997; Yuan *et al.*, 1994; Pauza *et al.*, 2000; Leger *et al.*, 1999) and capability for local information processing within the ICNS. A major issue requiring clarification in the control of cardiac functions by the ICNS is the distribution and connectivity of the ICN within this system. In the mammalian heart, ICN somata are widely distributed in ganglia throughout both atria (Steele and Choate, 1994; Steele *et al.*, 1994; Armour *et al.*, 1997; Leger *et al.*, 1999; Pauza *et al.*, 2000), but with few exceptions (i.e. Pardini *et al.*, 1987, canine; Steele and Choate, 1994, guinea pig) the projection patterns of subpopulations of ICNs to specific targets have not been established.

A more complex and integrative view of autonomic control over cardiac output has recently emerged after descriptions of sympathetic and parasympathetic interactions within the ganglia of the heart that are more complex than described by the classical model. Leger (1999) described the presence of small catecholaminergic cells within the ICNS of the guinea pig, proposed as putative small intensely fluorescent (SIF) cells, that could potentially modulate cardiac neural activity and have been shown to have cholinergic innervation. A recent study described neuronal somata that exhibit colocalised immunoreactivity for choline acetyltransferase (ChAT, a rate limiting enzyme in the synthesis of acetylcholine) and tyrosine hydroxylase (TH, a rate limiting enzyme in the synthesis of NE) within ganglia of the mouse heart (Rysevaite *et al.*, 2011) suggesting that parasympathetic and sympathetic transmitters could occur within the same ICN. Such findings have begun to complicate the classic viewpoint of autonomic control of the heart.

Functional (Smith, 1999) and anatomic data (Gagliardi *et al.*, 1988) have shown that ICNs within a particular region of the heart can receive inputs from parasympathetic preganglionic, sympathetic postganglionic, other ICNs as well as from afferent axons from other areas of the heart. Acute (Armour *et al.*, 1998) and chronic decentralization (Smith, 2001a), isolation of a heart from the CNS, have shown that ICNs in the mammalian heart remain viable and responsive to changes in the cardiac milieu. Additionally, it has been shown using simultaneous recordings in the mammalian heart that both parasympathetic (vagal) and sympathetic (cardiopulmonary) nerves could be co-activated (Kollai and Koizumi, 1979; Koizumi *et al.*, 1982). In experiments in which ICN activity was recorded in the beating mammalian heart during stimulation of the cardiac vagal nerves, less than 20% of ICNs received direct inputs from the extrinsic nerves (see Armour, 2008). It was hypothesized from these findings that these ICNs could potentially be acting as interconnecting neurons. Perhaps most interesting among these studies is Smith's (1999) finding that adrenergic input could augment the effects of cholinergic activation of ICNs. In this experiment adrenergic/cholinergic interactions augmented action potential (AP) firing of ICNs that did not occur in the presence of only one input.

1.1.3 Difficulties in studying the ICNS.

The neural control of the heart has been extensively studied in many mammalian models (mice, rats, dogs and guinea pigs) by means of extracardiac nerve stimulations. The ICNS and its associated innervation comprise more than 10^6 ICNs in the human heart (Pauza *et al.*, 2002) and more than 10^5 ICNs in the heart of a dog (Pauza *et al.*, 2002; Armour and Ardell, 2004). Even small hearts such as that of the guinea pig contain at least

1500-2000 ICNs (Leger *et al.*, 1999). Previous reports have shown that activity in the ICNS is modified by interventions affecting cardiac function (Armour *et al.*, 1993; Huang *et al.*, 1993; Murphy *et al.*, 2000; Smith *et al.*, 2001a, b; Arora *et al.*, 2003). Despite these advances, our current understanding of the mechanisms of intracardiac integration of autonomic inputs and the details of the anatomical and functional connections between the ICNS and cardiac effectors are incomplete. In mammalian hearts a major difficulty in studying the role of function-specific components of the ICNS, is that this system is deeply embedded in, and distributed throughout, the walls of both atria and ventricles. These components are therefore largely inaccessible for integrative studies. One solution to this problem is the use of reduced experimental preparations representing a subset of the ICNS, such as isolated tissues containing ICN in ganglionated plexi, to study properties of control circuits *in vitro* (Smith, 1999; Ardell *et al.*, 2014). This approach, however, eliminates the majority of intracardiac neuronal connections; so only limited conclusions may be drawn about the roles of localized circuitry in controlling overall cardiac function. To overcome such limitations, I thus propose to use the smaller, a simplified vertebrate heart, that of the zebrafish, a widely used model for fundamental questions in genetics, molecular biology and organ function, to investigate autonomic cardiac control in an intact organ.

1.2 The zebrafish as an alternative model for studies of integrative cardiac control

1.2.1 Anatomy of the teleost heart.

Over the course of evolution, teleosts have become the most numerous vertebrate group, making up more than half of extant vertebrate species. Members of this group have radiated and diversified to occupy all available aquatic habitats, with variations in the

morphology of their circulatory systems reflecting this diversity (Johansen and Burggren, 1980; Satchell, 1991; Farrell and Jones, 1992). The basic function of the heart, to generate flow sufficient to maintain circulatory homeostasis, is conserved from fish to humans (Farrell and Jones, 1992). In teleosts the heart sits caudal to the gills contained within a pericardial sac (Figure 1.1). Deoxygenated blood flows unidirectionally from the dorsal aorta through the body tissues, collecting in sinus venosus. A bicuspid valve (two valve leaflets) is found at the sino-atrial junction. Sequential contractions eject blood first from the atrium to the ventricle, and then from the ventricle to the bulbus arteriosus. A valve comprised of four leaflets is found at atrio-ventricular junctions, preventing the retrograde flow of blood to the atrium during ventricular contraction. The bulbus arteriosus, composed of vascular smooth muscle and elastin, acts in a similar manner as the mammalian aortic arch and dampens pressure pulsations before blood leaves through the ventral aorta. Blood is passed through the dorsal aorta and to the gills, supplying oxygenated blood to all body tissues (Santer, 1985).

1.2.2 Innervation of the teleost heart.

In the majority of teleosts investigated to date, the heart receives dual extrinsic innervation from the parasympathetic (PNS; cardioinhibitory) and sympathetic (SNS; cardioaugmentatory) limbs of the ANS (Holmgren, 1977; Laurent *et al.*, 1983; Santer, 1985; Gibbins, 1994; Morris and Nilsson, 1994; Donald, 1998). Hearts in all except the most primitive teleosts are dually innervated by axons from cholinergic parasympathetic and adrenergic sympathetic postganglionic neurons (Nilsson, 2010). Parasympathetic preganglionic neurons, located in brainstem vagal nuclei, project bilaterally via the vagus

nerves to synapse on postganglionic cholinergic ICNs projecting to cardiac effectors. Sympathetic preganglionic neurons in the intermediolateral zone of the spinal cord project to postganglionic neurons in ganglia associated with the vagal roots. Postganglionic sympathetic neurons then project either to cardiac effectors or, in some cases, on ICN within intracardiac ganglia (Burnstock, 1969; Nilsson, 1983; Laurent *et al.*, 1983; Santer, 1985; Gibbins, 1994; Donald, 1998; Funakoshi and Nakano, 2007; Nilsson, 2010). The most common arrangement of this dual innervation in teleosts is that axons from both limbs of the autonomic nervous system enter the heart together from the vagal cardiac rami. In accordance with this, it has been shown in the goldfish (Newton *et al.*, 2014; Appendix B) that vagal rami appear to carry both cholinergic and adrenergic extrinsic cardiac innervation; confirming that in this species the vagi are in fact vagosympathetic trunks (Gibbins, 1994; Holmgren and Jensen, 1994; Nilsson, 2010). Thus, in evolutionary terms, the elements of the ANS which collectively mediate neural regulation of the teleost heart represent the earliest version of this system that contains all of the elements of cardiac control that are elaborated in more recently evolved vertebrates (Gibbins, 1994; Donald, 1998).

Innervation patterns of the teleost heart have been found to differ regionally within a single species and among the hearts of different species. In general, it has been shown that at the sino-atrial junction the vagal nerves innervate a group of postganglionic cell bodies (*Salmo trutta* and *Salmo iredis*, Yamauchi and Burnstock, 1968; Saetersdal, 1974; *Carassius auratus* Newton *et al.*, 2014; see also Appendix B), which forms a dense sino-atrial plexus. Atrial axonal densities are much lower than in the sino-atrial plexus (Donald and Campbell, 1982; Newton *et al.*, 2014), and even further reduced in the ventricle

(Newton *et al.*, 2014). Cholinergic fibres have been described in the atrium and ventricle of teleost species (Holmgren, 1981). Innervation of the ventricle is predominantly adrenergic (Holmgren, 1977; Zaccone, 2009; Newton *et al.* 2014) though this innervation is limited largely to the compact myocardium and plexi surrounding coronary blood vessels.

In addition to the "classical" autonomic adrenergic and cholinergic neurotransmitters, a variety of nitrenergic, peptidergic and other neurotransmitters and neuromodulators are associated with the teleost ICNS. Collectively termed "non-adrenergic, non-cholinergic" (NANC) neurotransmitters, these include neuropeptides (Gibbins, 1989; Nilsson and Holmgren, 1992; Davies *et al.*, 1994; Holmgren, 1995; Zaccone *et al.*, 2009a; 2009b; 2010) and nitric oxide (NO, Olson and Donald, 2009), a neuromodulator generated by activity of the enzyme neuronal nitric oxide synthetase (nNOS). Such neurochemical diversity suggests that the ICNS in fish is capable of complex, receptor-mediated, integrative signal processing in the control of cardiac function.

Functional measures of cardiac modulation have long been established in the teleost. Using a combination of electrical and pharmacological stimulations, Vornanen (1989) established ventricular contractility in the goldfish as being under the control of β -adrenergic receptors by use of force measurements *in vitro*. Axelsson *et al.* (1987) investigated the effects of cholinergic and adrenergic influences on the heart in seven species of teleosts (pollack, *Pollachius pollachius*; cuckoo wrasse, *Labrus mixtus*; ballan wrasse, *Labrus berggylta*; five-bearded rockling, *Ciliata mustela*; tadpole fish, *Raniceps raninus*; eel-pout, *Zoarces viviparus* and short-spined sea scorpion, *Myoxocephalus*

scorpius), the results suggesting a mainly neural adrenergic tonus on the teleost heart.

Their findings are compatible with the view that both a cholinergic inhibitory tonus and an adrenergic excitatory tonus are general features in the control of the teleost heart *in vivo* (Axelsson *et al.*, 1987). Electrical stimulations have been performed at the vagal nerve trunks (Saito, 1973) and by field stimulation methods to electrically pace teleost atria and ventricles (Gannon, 1970). In the latter study atria were shown to possess both cholinergic-inhibitory and adrenergic-augmentor motor innervation while the ventricles possessed only adrenergic-augmentor innervation. Similar antagonistic responses have been shown pharmacologically in the zebrafish as early as four days post fertilization (Schwerte *et al.*, 2006). To date, however, there has been no detailed description of the connectivity of the ICNS and its neural control of cardiac effector cells, such as the pacemaker system, in any teleost species.

1.2.3 Pacemaker function of the teleost heart.

The ANS and ICNS determine the rate and rhythm of the heart, regulate the force production of cardiac myocytes during contraction, and the rate of relaxation following contraction (Haverinen and Vornanen, 2007). Each heartbeat is initiated by an AP that begins in a set of pacemaker cells and subsequently spreads to the atrial and ventricular myocytes, eliciting sequential contraction (Haverinen and Vornanen, 2007). The electrical properties of the teleost heart obey the same biophysical principles as mammals (Sedmera *et al.* 2003; Kopp *et al.* 2005; Arnaout *et al.* 2007; Milan *et al.* 2006; Haverinen and Vornanen, 2007). Activity of the cardiac pacemaker is due to the presence of a spontaneous depolarization, or pacemaker potential, and is an outcome of a complicated

interaction between several ion channels and ion transporters that are driven by a net inward current through the sarcolemma of the pacemaker cells (Haverinen and Vornanen, 2007). Normal electrical excitability of cardiac pacemaker cells results from a balance between depolarizing (inward) and repolarizing (outward) currents. Depolarization is mediated by channels or transporters that enable positively charged Na^+ or Ca^{2+} ions to enter the cell (or negatively charged Cl^- ions to exit) and repolarization results when the K^+ efflux exceeds the sum of the Na^+ and Ca^{2+} influx (Hodgkin & Huxley 1952; Haverinen and Vornanen, 2007).

Even though they possess a comparatively simple two-chambered heart, the zebrafish electrocardiogram (ECG) retains many of the fundamental elements of a mammalian ECG (Figure 1.1). Within the zebrafish ECG the P wave (atrial depolarization), QRS complex (ventricular depolarization) and T wave (ventricular repolarization) are retained (Sedmera *et al.*, 2003; Milan *et al.*, 2006; Huang *et al.*, 2010). From ECGs recorded from zebrafish, calculations of waveform intervals such as Q-T and R-R intervals (see Milan *et al.*, 2006; Arnaout *et al.*, 2007; Chaudhari *et al.*, 2013) have given information on cardiac performance of chronotropic effects (heart rate, Huang, 2010) and dromotropic effects (conduction, Yu *et al.*, 2010).

In teleosts there is extensive physiological evidence that the sinoatrial region is the site of the cardiac pacemaker. In the trout three different types of pacemaker cells have been identified morphologically (spindle, spider and elongated spindle cells, Haverinen and Vornanen, 2007). Saito (1973), Saito and Tenma (1976), Vornanen *et al.* (2010) and Haverinen and Vornanen (2007) have reported pacemaker-type electrical activity recorded from cells located within the base of the sinoatrial valve leaflets. Haverinen and Vornanen

(2007) described tissue here in *Oncorhynchus mykiss* as being responsible for electrical impulses triggering cardiac conduction, though this has been experimentally investigated in a limited number of species (Saito, 1969; Mackenzie, 1913; Yamauchi *et al.* 1973). A hyperpolarization-activated channel, HCN4, has been shown to be crucial in the generation of pacemaker potentials in the mammalian heart (Steiber *et al.*, 2003). Recently HCN4 has been shown to be present in the cardiac tissues of teleosts (Cho *et al.*, 2003; Tessadori *et al.*, 2012). Teleost cardiac pacemaker cells have been identified electrophysiologically in tissue associated with the sinoatrial valves (SAV; Saito, 1973; Saito and Tenma, 1976; Vornanen *et al.*, 2010). In the mammalian heart, pacemaker cells express HCN4 and antibodies directed against this ion channel are now accepted as a marker for the mammalian pacemaker region (Chandler *et al.*, 2009; DiFrancesco, 2010). Tessadori *et al.* (2012) established, using combined *in situ* hybridization and patch clamp methods, that cells in the zebrafish heart which exhibit pacemaker electrical properties also express mRNA for HCN4. Moreover, recent studies in the zebrafish have shown, using optical recordings imaging voltage-sensitive dyes, that the first electrical activity in the cardiac cycle occurs in the SAV region where cell containing HCN4 are concentrated (Sedmera *et al.*, 2003; Tsutsui *et al.*, 2010), offering an tractable effector cell type to investigate in my thesis.

1.3 Relevance and thesis objectives

1.3.1 Relevance.

Recent reports in the field of neurocardiology have shown that dysfunctions of the autonomic nervous system can contribute to the initial development and progression of

many cardiovascular diseases (see review chapters in Armour and Ardell, 2004). Conversely, as these diseases progress, the ANS can support and coordinate the components of the myocardium that remain functional, thus helping maintain tissue perfusion by boosting cardiac output (Armour, 2008). A comprehensive understanding of how the nervous system controls the heart and what can go wrong with this control system is therefore a key factor in developing successful new cardiotherapies. Suppression of activation of the ICNS has been found to reduce the induction of cardiac arrhythmias (Foreman *et al.*, 2004; Cardinal *et al.*, 2006). As was put forth by Armour (2007), we must gain a more comprehensive understanding of the role of the ICNS in the coordination of regional indices of cardiac function in order to target any component within the cardiac neuroaxis that may malfunction in disease states. Given similar innervation patterns to the mammalian heart it is hoped that understanding the relatively simple teleost heart will aid in the understanding of the more complex mammalian heart. The main premise of this thesis is that studies of the zebrafish heart will clarify the overall organization and operation of the ICNS, for the first time in any vertebrate, providing information to guide further studies of the role of the ICNS in regulating global cardiac function.

1.3.2 Thesis objectives.

Though much is known of the ICNS in mammals, there currently exists no global, integrative understanding of how specific effectors within the heart are controlled. Our current understanding of the mechanisms of intracardiac integration of autonomic inputs and the details of the anatomical and functional connections between the ICNS and cardiac effectors is incomplete. The use of reduced experimental preparations representing a

subset of the ICNS, such as isolated tissues containing neurons in ganglionated plexi, to study properties of control circuits *in vitro* (Smith, 1999; Ardell *et al.*, 2014) eliminates intracardiac neuronal connections, so only limited conclusions may be drawn about the roles of localized circuitry in controlling overall cardiac function. Though the small size of the zebrafish heart presents its own technical challenges, its size also permits visualization and accessibility of the entire ICNS in the whole organ.

From these studies I will shed light on several key issues of global cardiac function, which have not previously been possible to examine in mammalian models. In Chapter 2 the neuroanatomy of the zebrafish ICNS, distribution of ICNs and their neurotransmitter phenotypes are described. Taken together, my anatomical observations in the zebrafish heart suggest the potential for regionally precise and function-specific autonomic control of the effectors that determine cardiac output. In particular, the fine details of innervation that I observed in the region in the sinoatrial region (SAR) containing putative pacemaker cells reveal the neuroanatomical substrate by which the discharge activity of these cells may be rapidly modulated. The results of this study will lay the essential neuroanatomical groundwork for further investigations to identify the locations, functional characteristics and of subpopulations of ICNs involved in regulating cardiac output in the hearts of teleosts.

In Chapter 3 I describe establishing the isolated, innervated zebrafish heart as a novel alternative model to investigate the integrative neural control of cardiac pacemaker function through a combined electrophysiological, pharmacological, and anatomical approach. Using ECG recordings, combined with extrinsic nerve stimulation or pharmacological activation, I demonstrate that discrete neural pathways modulate heart

rate through adrenergic and cholinergic mechanisms. Optical mapping of electrical activity confirmed the location of the primary pacemaker within the SAR and a secondary pacemaker in the atrioventricular region (AVR), as well as the capacity for autonomic modulation of both SAR and AVR pacemaker function. Finally, the relationships of cholinergic and adrenergic receptors to putative pacemaker cells are described.

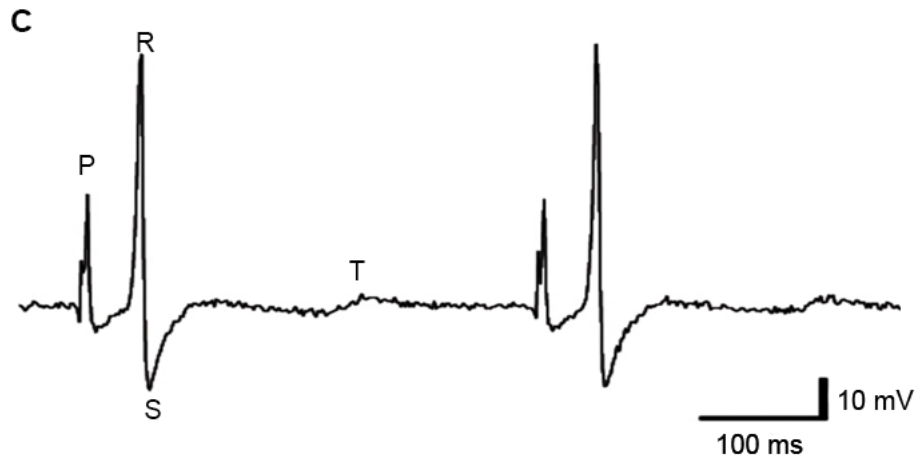
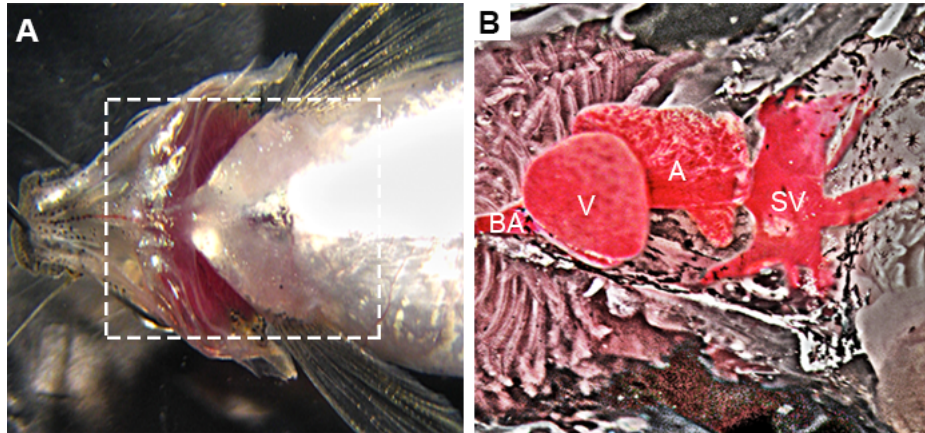
To date, the potential functional differences between the left and right cardiac rami have not been resolved. In canine, left and right vagal inputs evoke differential effects on both the sinoatrial and atrioventricular nodes. In Chapter 3 I show that the R-R interval response to combined vagosympathetic nerve trunk (VSN) stimulation is summative, supporting the idea that stimulation of individual VSN activated different groups of post-ganglionic ‘rate-control’ neurons with minimal interactions within the ICNS. In Chapter 4, distinct populations of ICNs activated during VSN stimulation are investigated using known immunohistochemical markers. In addition, the effects of such activation reveal that the site of sinoatrial pacemaker initiation becomes highly disorganized during vagal activation. Taken together, these results suggest that there are distinct ICN populations at the vagal junctions, which project to ipsilateral effector cells, and ICNs within the medial sinoatrial region which do not receive direct extrinsic input and may represent local processing neurons.

In Chapters 5 and 6, I use the methodologies developed in earlier chapters to validate the use of the isolated zebrafish heart for studies oriented to more clinical issues. In Chapter 5 using immunohistochemical, electrophysiological and pharmacological methods I describe the distribution of serotonin (5-HT) in the heart, its chronotropic effects, and the proportion of these effects acting through the ICNS compared to action

through pacemaker cells. In Chapter 6 I investigate the chronotropic responses to volatile anesthetics and the proportion of these responses resulting from direct effects on the pacemaker versus those acting indirectly through the ANS to alter rate were determined. Thus, these studies will begin to clarify the direct and neurally mediated pathways involved in heart rate regulation that may potentially be responsible for heart dysfunction known to occur in those on serotonergic anti-depressants as well as in patients during clinical anesthesia.

Overall, the results of the studies presented within my thesis contribute significant advances in the establishment of the zebrafish as a new model for studies of integrative autonomic cardiac control.

Figure 1.1: Overview of the zebrafish heart. **A:** Ventral view of an adult zebrafish, showing area of the heart. Dashed box indicates the area highlighted in B. **B:** Ventral view of the adult zebrafish from A, after a ventral midline incision has been made through the body wall and pericardial sac, exposing the heart. A, atrium; BA, bulbus arteriosus; SV, sinus venosus; V, ventricle. **C:** Example of a differential electrocardiogram recording from an adult zebrafish showing P-, R-, S-, and T-waveforms.



CHAPTER 2

ANATOMY OF THE ZEBRAFISH INTRACARDIAC NERVOUS SYSTEM

2.1 Introduction

The general organization of the portion of the autonomic nervous system (ANS) concerned with cardiac control has been studied for almost a century (Langley, 1921; Nilsson, 1983; 2011). Dual innervation of the heart by sympathetic and parasympathetic autonomic limbs of the ANS is conserved from teleost fish to humans (Nilsson, 1983; Nilsson and Holmgren, 1994). In all of these groups neural inputs in extrinsic cardiac nerves converge on the intracardiac nervous system (ICNS), that part of the ANS lying within the heart. This network represents a common pathway for neural control of cardiac output. This system maintains a balance of excitatory and inhibitory signals to the main cardiac effectors, the pacemaker cells and cardiac myocytes, providing fast-acting integrative neural control of cardiac output. The detailed organization of the projection pathways of extrinsic and intrinsic axons within the ICNS, and the identities and distribution of subpopulations of intrinsic cardiac neurons that control specific cardiac functions remain unknown. Knowledge of the neuroanatomy of this system is particularly lacking in fishes, so the early evolution of vertebrate cardiac control is unclear.

In order to begin addressing this issue the neuroanatomy of the ICNS in the goldfish (Newton *et al.*, 2014; Appendix B) was investigated. This study provided, for the first time in any teleost species, details of the general innervation pattern, the neurotransmitter phenotypes and the distribution of axons and neuronal somata within the heart. It was concluded that the ICNS in this species innervates all cardiac regions to provide the neuroanatomical substrate for cholinergic and adrenergic control of effectors determining cardiac output.

A key factor in determining cardiac output is the discharge rate of pacemaker cells. In teleosts these cells have been proposed to be located in the region of the sinoatrial valve (Saito, 1973; Saito and Tenma, 1976; Vornanen *et al.*, 2010). The presence of hyperpolarization-activated, cyclic nucleotide-gated ion channels (HCN), in particular HCN4, is characteristic of mammalian pacemaker cells, but until recently there have been no reliable markers for teleost pacemaker cells. Tessadori *et al.* (2012) provided evidence that cells in this region in the zebrafish heart expressed the message for HCN4 (*in situ* hybridization) and exhibited pacemaker-like electrophysiological properties. These authors also described the expression of the transcription factor Islet-1 (Isl1) in putative pacemaker cells. Newton *et al.* (2014) used immunohistochemical methods in the goldfish heart to show that HCN4 channel protein is present in small cells in the densely innervated sinoatrial valve leaflets.

In the present study previously established methods were applied to study the ICNS in zebrafish, a cyprinid species that has been widely exploited as a representative vertebrate model for investigating the time course, genetics and molecular biology of embryonic development (Woo *et al.*, 1995; Kimmel *et al.*, 1995; Goldstein *et al.*, 1998; Stainier, 2001; Yelon, 2012; Singleman and Holtzman, 2012; Liu and Stainier, 2012; Gould *et al.*, 2013), mutagenesis (entire issue, *Development* 123 [1996]; Stainier *et al.*, 1996; Chen *et al.*, 1996; Warren and Fishman, 1998; Sehnert and Stainier, 2002; Berdugo *et al.*, 2003) and organ function (Briggs, 2002). The zebrafish genome has recently been sequenced and it appears that there may be at least one or more zebrafish orthologues for approximately 70% of human genes (Howe *et al.*, 2013). The high degree of conservation

of the zebrafish genome has allowed for the study of the potential roles of specific genes in many human diseases (Ackermann and Paw, 2003; Dodd *et al.*, 2004).

The zebrafish offers many advantages for cardiac studies. Recent reviews have described rapid progress in establishing the zebrafish heart as a model for regeneration (Ausoni and Sartore, 2009), physiology (Briggs, 2002; Hecker *et al.*, 2008; Nemtsas *et al.*, 2010; Hoage *et al.*, 2012; Sabeh *et al.*, 2012) and the genetic basis of cardiovascular diseases (Ackermann and Paw, 2003; Dahme *et al.*, 2009; Bakkers, 2011; Kloos *et al.*, 2012). These studies have produced significant advances in understanding mechanisms underlying cardiac function, but none has considered the role of integrated neural control of the zebrafish heart.

In all teleosts studied to date cardiac output is modulated by autonomic reflexes engaged by changes in a variety of internal variables such as arterial blood pressure (the baroreflex; Smith *et al.*, 1985) and by alterations in environmental factors such as oxygen and CO₂ (i.e., hypoxic bradycardia; Smith and Jones, 1978; Jonz *et al.*, 2014). Though such reflexes are present in both adult and larval zebrafish (Barrionuevo and Burggren, 1999; Jacob *et al.*, 2002; Steele *et al.*, 2009; Schwerte *et al.*, 2006), the pathways within the ICNS that are targeted by the efferent arms of these reflexes have not been established. In the present study immunohistochemical and neurotracing techniques were used to map the general innervation pattern of the zebrafish heart, the distribution and neurotransmitter phenotypes of neural elements within the ICNS and the projections of extrinsic axons into this system. HCN4 and Isl1 immunohistochemistry were used to identify and locate putative pacemaker cells, as well as a synaptic vesicle marker to label the terminals of axons innervating these cells.

2.2 Materials and Methods

An expanded Methods section is provided in Appendix A.

2.2.1 Animals.

A total of 60 adult AB wild type zebrafish (12-18 months post fertilization; mixed sex; mean standard body length 44 ± 7 mm (\pm SEM) were used in this study. Institutional approval for animal use in this study was obtained from the Dalhousie University Committee on Laboratory Animals.

2.2.2. Heart Isolation.

Fish were anesthetized in a buffered solution of tricaine (MS-222) in tank water until respiratory opercular movements had ceased and the animals lacked responses to pinching with forceps. A ventral midline incision exposed the bulbus arteriosus, ventricle, atrium, sinus venosus and attached proximal segments of the ducts of Cuvier (containing the vagus nerves) which were then removed for immunohistochemical processing. Tissues were fixed overnight in 4% paraformaldehyde (PFA) or 9:1 (v/v) solution of methanol and formalin prior to processing for immunohistochemistry in whole-mount format.

2.2.3 General and neurotransmitter-specific labeling.

The general procedures used for immunohistochemistry in this study were similar to those described in previous publications on cyprinid neuroanatomy (Finney *et al.*, 2006; Robertson *et al.*, 2008; Dumbarton *et al.*, 2010; Newton *et al.*, 2014).

The primary antibodies used in this study have been used previously in zebrafish and in the goldfish heart, a cyprinid species closely related to the zebrafish (see Appendix B). In the present study, to determine the general innervation of the heart antibodies against acetylated tubulin (AcT, axons) combined with human neuronal protein C/D (Hu, neuronal somata) have been used. An antibody against synaptic vesicle protein 2 (SV2) was used to detect axon terminals. Cholinergic axons and somata were detected by immunoreactivity for choline acetyltransferase (ChAT), an enzyme involved in acetylcholine (ACh) synthesis. In a subset of specimens an antibody against vesicular acetylcholine transporter (VAChT) was used together with ChAT to double-label putative cholinergic elements. The VAChT antibody used was the same as used by Shakarchi *et al.* (2013), who reported that pre-adsorption with a synthetic peptide that corresponded to the C-terminus sequence eliminated immunoreactivity in the zebrafish gill. The expression of tyrosine hydroxylase (TH), the rate-limiting enzyme in the synthesis of noradrenaline (NE), indicated adrenergic elements. Neurons capable of generating nitric oxide were detected by the presence of neuronal nitric oxide synthase (nNOS). An antibody directed against vasoactive intestinal polypeptide (VIP) demonstrated the distribution of this peptide in neural elements in the heart.

To label putative pacemaker cells, an antibody against HCN4 was used. Expression of the transcription factor Islet-1 (Isl1) has been shown to partly overlap that of HCN4 in the zebrafish heart (Tessadori *et al.*, 2012), so an analysis of the distribution of immunoreactivity for this factor in has been included in this study. The anti-Isl1 antibody used here (Isl1) was the same as that used by Tessadori *et al.* (2012) and others in zebrafish (Ericson *et al.*, 1992; Kuscha *et al.*, 2012).

For all antibodies used in this study, negative control tissues were processed as outlined above, except that either the primary or secondary antibody was omitted. In all trials this eliminated detection of histofluorescence. As a control for the anti-HCN4 antibody, the HCN4 antibody was pre-treated with fusion protein (1 μg primary antibody: 3 μg fusion protein). Tissue was then incubated in the presence of the pre-adsorbed antibody following the procedures outlined above. In 6 trials no immunoreactivity was observed.

In order to determine how immunohistochemically labelled neuronal elements were related to the regional structure of the myocardium, some specimens were double-labelled with the F-actin marker phalloidin (Phal; Small *et al.*, 1999; Newton *et al.*, 2014), conjugated with tetramethyl rhodamine isothiocyanate to show cardiac myocytes.

2.2.4 Tracing extrinsic vagosympathetic inputs.

To visualize the intracardiac projections and termination patterns of axons in the cardiac rami of the vagosympathetic trunks a combination of the actively transported neurotracer neurobiotin and a fluorescent styryl dye, FM1-43X was utilized. This dye, which appears to label the membranes of recycled synaptic vesicles, becomes concentrated in active synaptic terminals over time (Betz *et al.*, 1992) so will accumulate in the intracardiac terminals of extracardiac axons when those axons are stimulated. In this procedure hearts were isolated as described above and pinned to the rubber bottom of a chamber perfused with zebrafish saline. A length of approximately 1 mm of the left or right vagosympathetic trunk was freed from the wall of the duct of Cuvier and the cut end of the nerve was drawn by suction into a tip of a closely fitting glass pipette filled with

saline. This was then replaced with a solution containing neurobiotin and FM1-43X (1 mM each) in distilled water. This preparation was maintained at room temperature for 6-8 hours and maintained spontaneous cardiac contractions throughout this period. The nerve was then removed from the pipette and hearts were perfused for a further 2-3 hours. During the last hour of this period the dye-loaded nerve was stimulated with a bipolar wire electrode driven by a constant-current stimulator to load axonal terminals with FM1-43X. Trains of rectangular pulses were delivered every 5 minutes for a total of 12 stimulation periods. Following this procedure hearts were fixed as described above for immunohistochemistry. The presence of neurobiotin in neural elements was detected with avidin conjugated to AlexaFluor 488. Two controls were used for this procedure: nerves were loaded with neurobiotin and FM1-43X but not stimulated, or neurobiotin without FM1-43X was applied and nerves were stimulated. In both cases no terminals were observed.

2.2.5 Imaging and data presentation.

Tissues were viewed using a Zeiss LSM510 confocal microscope using Zeiss Zen2009 software. These images were processed into plates with Photoshop CS6. During composition of the figure plates some images originally in color were converted to greyscale values; the brightness of these images was adjusted so that panel-to-panel contrast in the plate was consistent. Numerical values were expressed as mean \pm 1 SEM. One-way ANOVA was used to detect significant differences among means.

2.3 Results

2.3.1 Overview of innervation pattern.

A wholemount preparation of the entire zebrafish heart, in which the ICNS was demonstrated with the pan-neuronal markers AcT and Hu, showed that all cardiac chambers were innervated (Figure 2.1A). The organization of the ICNS is summarized in the schematic diagram in Figure 1B. A major nerve plexus, termed the sinoatrial plexus (SAP), was located at the venous pole of the heart, circumscribing the sinoatrial valve (SAV). The majority of neuronal somata within the heart were associated with the SAP. This plexus received inputs from the cardiac vagosympathetic rami entering the heart close to the valvular commissures (Figure 2.1A). Most axons from these rami appeared to terminate within the plexus while a few projected to the atrial wall or toward the atrioventricular junction in one or two major nerve trunks. The atrioventricular plexus (AVP) surrounded the valve at this junction and contained a small population of somata. The ventricular myocardium and walls of the bulbus arteriosus were innervated by axons arising from the venous pole, as well as from nerves entering the heart along the ventral aorta. In the sections below details of regional cardiac innervation are presented and the distributions of neuronal elements with neurotransmitter-specific phenotypes are mapped.

2.3.2 Sinoatrial plexus.

The region surrounding the bicuspid sinoatrial valve represented the most intensely innervated area of the heart in this species (Figure 2.1A, B, C). AcT-Hu labelling suggested that axons entered the SAP from both vagosympathetic trunks (Figure 1D, E), which joined the heart close to the commissures of the sinoatrial valve.

After entering the SAP, the majority of extrinsic axons coursed around the ostium within the basal structure of the valve leaflets as shown in the example in Figure 1C (the myocyte marker Phal shows the organization of myocytes in the leaflets). The density of the neuropil varied by region within the SAP, with axons being most plentiful in the dorsal region between the junctions of the extrinsic nerves with the plexus (dSAP, Figure 2.1C, F) compared with the ventral SAP (vSAP, Figure 2.1C, G). Transmitter-specific labelling of intracardiac neuronal elements and putative pacemaker cells is shown in the examples in Figure 2. The majority of axons and many terminals within the SAP appeared to be ChAT-positive (Figure 2.2A, B). There were also TH-positive axons in the extrinsic nerves, and both axons and terminals expressing TH were present throughout the SAP (Figure 2.2C, D). In addition to ChAT- and TH-positive terminals in the SAP, there were putative axonal varicosities labelled with anti-VIP that were distributed in a punctate pattern, in all regions of the SAP (Figure 2.2F). The distribution of transmitter specific markers are summarized in Figure 2.2J.

In addition to the distributions of axons within the SAP, immunolabelling showed that somata of intracardiac neurons were distributed throughout this plexus (Figure 2.1C-G; Figure 2.2). To quantify the distribution of ganglionic neuronal somata labelled with AcT-Hu within the SAP, this area was divided into four sub-regions: the zones around the junctions of the right and left vagosympathetic nerves with the plexus and the dorsal and ventral zones between these junctions. Within these sub-regions, neuronal somata were clustered into groups designated right and left vagal ganglia (RXG, LXG), dorsal ganglia (dG) and ventral ganglia (vG). The division of the ventral ganglia into two parts, right (rvG) and left (lvG), resulted because of the mid-ventral split to lay out the map; these two

parts would be contiguous in the intact heart. The total number of neurons in all regions of the SAP detected by AcT-Hu was 197 ± 23 ($n=6$). The vG (lvG and rvG combined) had significantly less somata (23 ± 5 ; $n=6$; 12% of total number) than the dG (52 ± 7 ; 26%), LXG (54 ± 8 ; 27%) and RXG (67 ± 10 ; 34%).

Within the SAP subsets of neuronal somata labelled with AcT-Hu were positive for anti-ChAT (Figure 2.2A, B), anti-TH (Figure 2.2D) and anti-nNOS (Figure 2.2E). ChAT-positive cells represented the most common phenotype in the SAP (181 ± 12 , $n=6$; Figure 2.2A, B), representing 92% of the mean total number of somata labelled with AcT-Hu. In a subset of three specimens ChAT and VAcHT antibodies were used together; in all three specimens there was complete overlap between these labels (data not shown). Cells expressing nNOS (14 ± 3 , $n=6$; Figure 2.2E) represented 7 % of the total number. In five of six specimens, a mean of 5 ± 3 TH-positive somata was detected (Figure 2.2D). The distribution of subsets of neurons expressing these phenotypes is shown in schematic form (Figure 2.2J).

While immunolabelling showed the overall innervation, it did not permit the discrimination of axons originating extrinsically from those originating within the SAP. The projection patterns of inputs from the vagosympathetic trunks into the heart were further analyzed by application of a combination of neurobiotin (to label axons and somata) and FM1-43X (to intensify terminal labelling) to the distal cut ends of these nerves. Examples of the outcomes of such tracing experiments are shown in Figure 3, double-labelled with AcT-Hu to differentiate extrinsic from intrinsic axons. The detailed distribution patterns of extrinsic inputs from the cardiac vagi within the SAP were different. Axons entering from the left vagosympathetic trunk terminated in a continuous

pattern spreading from the ipsilateral junctional region across most of the dorsal plexus, extending to the contralateral junctional region (Figure 2.3A). The pattern of projections into the ventral SAP was sparser than that in the dorsal region, also extending to the contralateral junctional area. Conversely, axons from the right vagosympathetic trunk appeared to terminate in more limited regions of the SAP than those from the left trunk. There appeared to be two distinct terminal fields in the ipsilateral SAP proximal to the junctional region and a third field in the dorsal SAP that was proximal to the left junctional region (Figure 2.3B). Axons from the right trunk also projected to the proximal half of the ventral SAP, but this projection was sparser than that to the same region from the left vagosympathetic trunk. Within all regions of the SAP, terminals of extrinsic axons, which label only with neurotracer, and thus show only in green, appeared to surround neuronal somata, as in the example shown in Figure 3C.

A small cluster of neurobiotin-positive somata was observed in the dorsal SAP proximal to the junction of the right vagosympathetic trunk (region outlined by box, Figure 3B). These somata (arrows, Figure 2.3D) were ovoid-shaped, with their long axes measuring approximately 10 μm . Such somata could be clearly distinguished by shape, size and label content from AcT-Hu-labelled somata in the adjacent neuropil. A process, presumably the axon, appeared to emerge from one end of each neurobiotin-labelled soma (Figure 2.3D) and could be followed to the adjacent junctional region and into the nerve trunk (not shown). It is possible, since these somata were labelled via transport of the tracer in axons coursing in the vagosympathetic trunk, that they represented intracardiac sensory neurons with their axons projecting centripetally.

2.3.3. Identification of putative pacemakers in sinoatrial valve.

The general location of the cardiac pacemaker in the sinoatrial region of the heart is conserved across the vertebrates. In the zebrafish heart a combination of HCN4 and Isl1 immunohistochemistry was used to determine the occurrence and distribution of putative pacemaker cells in this region. In the sinoatrial valve, small ovoid- or spindle-shaped cells labelled with anti-HCN4 were observed in a band in the medial intra-vagal regions and toward the free margin of both valve leaflets (Figure 2.2G-I). Figure 2G shows a detailed view of HCN4-positive cells in which the labelling was punctate, appearing to be associated with both the membrane and the cytoplasm. These cells were co-labelled with anti-Isl1, which appeared to be evenly distributed throughout the cytoplasm (Figure 2.2G). Multiple axon terminals expressing the synaptic vesicle marker SV2 were closely apposed to individual HCN4-positive cells in the valve leaflets (Figure 2.2H). Double-labelling trials with Phal (Figure 2.2I) showed that HCN4-positive cells were embedded among cardiac myocytes in the leaflet structure. The position of putative pacemaker cells relative to the SAP is shown schematically in Figure 2J.

2.3.4 Atrioventricular junction.

Figure 2.4A shows an overview of the innervation pattern of the atrium, atrioventricular region and a portion of the ventricle proximal to the atrium, labelled with a combination of AcT-Hu and neurotracer. Two large nerve trunks coursed in the atrial wall from the SAP toward the atrioventricular junction; from these trunks a mesh of fine axons innervated the atrial wall. Some of the axons in the nerve trunks appear to have originated extrinsic to the heart, as indicated by double-labelling with neurotracer (Figure 2.4A). A

plexus was present around the atrioventricular valve (AVP; boxed region, Figure 2.4B) that received contributions from the atrial nerve trunks. Neuronal somata were clustered into small ganglia (arrow, Figure 2.4B) associated with this plexus and a majority, if not all, of the ganglionic somata appeared to be cholinergic (Figure 2.4C). There was also a relatively dense network of TH-positive axons in the AVP region (Figure 2.4D), with some of these axons innervating the leaflets of the atrioventricular valve (not shown). Multiple axon terminals expressing the synaptic vesicle marker SV2 were closely apposed to individual HCN4-positive cells (Figure 2.4E) in the bases of the valve leaflets (asterisk*, Figure 4B) and in atrial tissue proximal to this valve. Such cells appeared similar in size and morphology to HCN4-positive cells in the sinoatrial region (cf Figure 2.2G-I). A network of fine AcT-Hu positive axons innervated the ventricle wall; larger nerve trunks were associated with coronary blood vessels (Figure 2.4F).

2.3.5 Outflow tract.

AcT-Hu labelling in the bulbus arteriosus indicated that tissue here may have been innervated by axons from two sources (Figure 2.4G-H). Innervation arising from the venous pole of the heart consisted of a meshwork of fine axons in the wall of the bulbus (BA, Figure 2.4G); these axons arose from extensions of ventricular nerve trunks that could be traced to the AVP. At least some of these axons were immunoreactive for TH (Figure 2.4I). In addition to innervation coursing into the bulbus from the ventricle, a major nerve trunk entered the bulbus arteriosus from the wall of the ventral aorta (arrow, Figure 2.4G, H). This trunk coursed in a cephalo-caudal direction in the bulbus wall and crossed the bulbo-ventricular junction to innervate parts of the ventricular wall proximal to

this junction. This nerve trunk, designated as the branchio-cardiac nerve trunk (BCT), as it appeared to emerge from the ventrocaudal aspect of the fourth gill arch (not shown) and travel into the heart. Some of the axons within this trunk were also TH-positive (Figure 2.4H).

2.4 Discussion

In this study, the neuroanatomy of the zebrafish intracardiac nervous system, the patterns of extrinsic innervation of this system at the venous and arterial poles of the heart, the distribution of intracardiac neurons and the neurotransmitter phenotypes of some neuronal subpopulations has been characterized. In addition details of putative pacemaker cells and their innervation at the sinoatrial and atrioventricular junctions have been described. In the sections below, the organization of the components of the ICNS and the insights such organization may provide for understanding autonomic modulation of the effectors that determine cardiac output are discussed.

2.4.1 Intracardiac neurons at venous pole.

In this study a combination of antibodies against AcT and Hu was used to identify intracardiac neuronal somata and axons. Previous neuroanatomical studies have established the utility of this combination of labels to detect neuronal somata in the zebrafish intestine (Bisgrove *et al.*, 1997; Olsson, 2009) and in the goldfish heart (Newton *et al.*, 2014). Though this technique appeared to label most of the neurons in the organs studied in these species, there remains some uncertainty that all neuronal somata were labelled (see Olsson, 2009 for discussion). It therefore must be recognized that, since AcT-

Hu immunohistochemistry may not have labelled all neuronal somata, regional and total counts of neurons in the zebrafish heart must be interpreted conservatively.

A principal finding in this study was that most of the intracardiac neurons (ICN) were situated within the SAP, in the vicinity of the sinoatrial valve; there was also a smaller population of neurons associated with the AVP. This conforms to the overall pattern seen in other teleost hearts (Laurent *et al.*, 1983; Zaccone *et al.*, 2009, 2010; 2012; Newton *et al.* 2014). Newton *et al.* (2014) provided the only previous report with a quantitative analysis of ICNs in a teleost heart, indicating that the mean total number of ICNs was 723 ± 78 (SE) in the goldfish heart. In the present study it was found that just over one-quarter of that number (mean total 197 ± 23) are present in the zebrafish heart. The meaning of the absolute number of ICNs per heart is not clear. Furthermore, the relationship of the total number of ICNs present in any vertebrate heart to the capability for control of the myocardium also remains unresolved. One possibility is that the number of ICNs required to control cardiac function may be related to body or cardiac mass. In mammals, the vertebrate group in which cardiac innervation has been studied in the most detail, the number of ICNs per heart tends to increase as body size increases (i.e. guinea pig, ~1500 somata [Leger *et al.*, 1999]; canine, 10,000-20,000 [Yuan *et al.*, 1994]; human, ~100,000 [Pauza *et al.*, 2000]) but no clear correlation between neuron number and cardiac mass has so far been established in any vertebrate.

In the goldfish heart there is a regional difference in density of ICN within the SAP, with the dorsal region containing significantly more neurons than the regions around the vagosympathetic trunk-SAP junctions or the ventral region (Newton *et al.*, 2014). In the present study the ventral region of the zebrafish SAP had significantly fewer ICN than

the other regions. While this aspect of the ICNS has only been investigated in two species, a pattern is emerging to suggest that ICNs may be concentrated in the dorsal and junctional regions in the SAP. Whether the findings in these species represent a general teleost trend is not yet clear. If this pattern is consistent across a broad range of teleosts, it may indicate a correlation between the somatic location of ICNs that have function-specific roles and the site of effectors, such as pacemaker cells, that are targeted by those neurons.

The specific neurotransmitter expressed in a particular subpopulation of peripheral autonomic neurons ("function-specific chemical coding"; Jänig, 1996) has been considered as a useful anatomical indicator of neurons in particular pathways involved in visceral control. In this study immunohistochemical detection of markers for neurons expressing cholinergic, adrenergic and nitrergic phenotypes in the SAP, and the distribution of cells expressing these phenotypes has been described. This was undertaken as a necessary first step in understanding the functional roles of these neurons.

Cholinergic neurons in the heart represent postganglionic efferent neurons in the parasympathetic limb of the autonomic outflow pathway for control of cardiac output, in the traditional view of the ANS. This view has been extended from its original application in mammals to apply across most vertebrates (Nilsson, 1983; 2011; Donald, 1998). According to this model, such neurons release ACh to alter cardiac efferent activity through actions on muscarinic postjunctional receptors. There are to date relatively few studies demonstrating putative cholinergic neurons in the hearts of teleost species (e.g., bichar, catfish, mullet: Zacccone *et al.*, 2009; 2010; 2012). These authors reported relatively low numbers and a high degree of variability among species for the occurrence of this neuronal phenotype. Such variability may have been related to the method used for

detecting these neurons: immunohistochemistry for acetylcholinesterase gave the lowest estimates (Zaccone *et al.*, 2009, 2010) while a higher number of cholinergic neurons was reported with the use of ChAT immuneoreactivity (Zaccone *et al.*, 2012). Furthermore, none of these studies attempted to evaluate the total number of intracardiac neurons to obtain a more accurate estimation of the relative proportion of cholinergic cells to the total cell population.

To address this ChAT and AcT-Hu double-labelling was performed in the same specimens. It was found that the vast majority of neurons in the SAP expressed ChAT (92% of total) and were cholinergic. This was confirmed by ChAT and VAcT double-labelling in which there was complete overlap of these labels. In contrast, in the goldfish slightly less than half of SAP neurons were cholinergic (Newton *et al.*, 2014). Assuming that these estimates of cell numbers accurately reflected the actual numbers in the hearts of these species (but see caveat above), the difference in relative proportion of cholinergic neurons to the total number may be species-specific. Additional studies with alternative cholinergic markers, such as the vesicular acetylcholine transporter used by Shakarchi *et al.* (2014) and in the present study in zebrafish, should now be done in a wider range of teleosts to help resolve this issue.

At least some of the cholinergic intracardiac neurons in the fish heart will be postganglionic efferent cells projecting to cardiac effectors, according to the traditional ANS model. The finding that in the goldfish, slightly less than half of the intracardiac neurons in the SAP expressed ChAT (Newton *et al.*, 2014), while nearly all neurons in the zebrafish SAP were cholinergic suggests that there may be a higher proportion of neurons in the zebrafish heart involved in direct efferent control. Expression of a cholinergic

phenotype does not mean that neurons are limited to a primary efferent role. For instance, in the wall of the small intestine, different subpopulations of cholinergic neurons act as sensory receptor cells, interneurons or control effector cells (Furness *et al.*, 2004). It is thus likely that, in the teleost heart, cholinergic neurons may play multiple roles and warrants further investigation.

The presence of TH in neurons implies that these cells could be capable of synthesizing norepinephrine and epinephrine, neurotransmitters released by sympathetic autonomic postganglionic neurons for adrenergic control of the viscera. Previous findings in zebrafish reinforce previous reports of such cells in the hearts of several teleosts (Zaccone, 2009; 2010; 2011; 2012; Newton *et al.*, 2014) including zebrafish (present study), and suggest that the presence of TH-positive somata may be a general feature of the teleost heart. This arrangement does not, however, conform to the general model of organization of the peripheral ANS, in which postganglionic somata in the sympathetic autonomic pathway are located at a distance from the organs they innervate (Nilsson, 1983; Nilsson and Holmgren, 1994). As has been speculated previously (Newton *et al.*, 2014), such neurons may be adrenergic postganglionic cells that have been displaced from sympathetic autonomic ganglia into the heart, but their role in sympathetic autonomic control of the heart remains unresolved.

Axons and putative varicosities containing TH were present within the SAP in the present study. Some TH-positive axons originated extracardially, coursing from the vagosympathetic trunks into the SAP. There were also TH-positive somata within the SAP (see above), so some of the axons and varicosities expressing TH could have come from intrinsic cardiac neurons. Collectively these elements may represent the final pathway for

adrenergic sympathetic postganglionic inputs to the heart, but whether they release adrenergic neurotransmitters is not known. The projection pathways or connectivity patterns of these TH-positive elements within the heart were unable to be determined. In the goldfish heart there were similar TH-positive elements (Newton *et al.*, 2014) and axons expressing TH are common to the hearts of several other teleosts (Zaccone *et al.*, 2009; 2010, 2011).

Nitric oxide synthase has been reported in intracardiac neurons in a variety of teleosts (Davies *et al.*, 1994; Bruning *et al.*, 1996; Zaccone *et al.*, 2009; 2010; 2011; 2012; Newton *et al.*, 2014). In the zebrafish heart it was observed that about 7% of SAP neurons express nNOS. The potential role for these neurons in the heart is not clear, but it has been suggested that nitric oxide released from intracardiac sources is involved in modulating cardiac effector cells (reviewed in Tota *et al.*, 2005).

A number of peptide neurotransmitters and neuromodulators are expressed by peripheral autonomic neurons in teleosts (Davies *et al.*, 1994; Zaccone *et al.*, 2009; 2010; reviewed by Nilsson, 2011 and others). Vasoactive intestinal polypeptide is commonly expressed in axons within the hearts of teleosts, including in the goldfish (Newton *et al.*, 2014). VIP was detected in axons and putative varicosities in the zebrafish SAP, so the presence of VIP in this species conforms to its presence in other teleosts.

2.4.2 SAP innervation.

In many teleosts the vagosympathetic trunks, combining axons of both the parasympathetic and sympathetic autonomic limbs, form the major pathway at the venous pole of the heart for extracardiac inputs into the ICNS (Nilsson and Holmgren, 1994;

Nilsson, 2011). The current results in the zebrafish support this trend; no evidence of separate sympathetic nerves to the heart during dissections to remove the heart, or in cardiac wholemounts was observed.

The SAP in the zebrafish heart, as visualized with AcT-Hu immunohistochemistry, consisted of a rich neuropil in association with neuronal somata; this was also a major feature of the goldfish heart (Newton *et al.*, 2014). However, in neither preparation could intrinsic cardiac neural elements be distinguished from those of extrinsic origin. In order to evaluate the pattern of innervation of the ICNS by extrinsic axons and the organization of the terminal fields of these axons in the zebrafish heart, a combination of neurobiotin, an actively transported neurotracer, and FM1-43X, was applied to the proximal stumps of the cardiac vagi. This is the first description of extrinsic cardiac inputs to a teleost heart using neurotracing techniques, and the first use of the combination of a neurotracer and FM1-43X in fish. Here the capability of FM1-43X to accumulate in axon terminals over time when the axons are electrically stimulated (Betz *et al.*, 1992) was utilized to intensify the fluorescent signal in these terminals so that they could be identified as extrinsic.

The entire SAP was innervated by extrinsic axons in the vagosympathetic trunks, and there was a general trend for terminals from axons in each trunk to be concentrated in the SAP near the region where that trunk joined the SAP. This pattern was correlated with the observation that major collections of ganglia were also grouped in these regions. In fact intense terminal baskets around individual ICNs were observed in these junctional regions, so a subset of the extrinsic axons appeared to form synapses on these cells. As well, some axons from each trunk projected around the plexus from their respective trunk-SAP junction toward the other junction, with more of these projections terminating in the

dorsal region than in the ventral region. This distribution of terminals also correlated with the distribution of ICNs in these regions; there were more neurons in the dorsal than in the ventral region. It could therefore be inferred from this qualitative analysis that some extrinsic axons terminated close to SAP ICNs, and that there were more such terminals where there were more neurons in the SAP. These inputs may represent pre-to-postganglionic connections in the parasympathetic autonomic outflow pathway.

There were also bilateral differences in projection patterns of vagosympathetic axons into the SAP, with axons from the left trunk extending in a continuous pattern that extended about three-quarters of the way around the SAV, while those from the right trunk appeared to target discrete regions within the SAP. The nearest effector cells to the SAP are pacemaker cells (see section 2.4.3), so it is possible that the bilateral difference in axonal projection pattern may reflect differential control of heart rate. Although Saito and Tenma (1976) found no laterality in the cardiac rate response to vagosympathetic trunk stimulation in the carp, the anatomical observations in the current study suggest that there could be the potential for differential effectiveness of activity in these nerves to alter cardiac function in zebrafish.

A particularly intriguing finding from the tracer studies was the detection of what appeared to be neuronal somata in the SAP labelled with neurobiotin (example Figure. 3D). These somata were presumably labelled by transport of the tracer along their axons in the extrinsic nerve where the tracer was applied. Given that transport of the neurotracers would be along the axons to somata, this suggests that these cells represent the first examples in fishes of afferent neurons with their cell bodies located within the heart and projecting axons centripetally. Anatomical evidence for such an arrangement has been

shown in the rat heart (Cheng *et al.*, 1997) and electrophysiological recordings have been made from presumptive intracardiac afferent neurons in the canine heart (Ardell *et al.*, 1991). If these labelled neurons in the zebrafish heart are in fact afferent neurons, they may provide cardiosensory inputs to local, intracardiac control circuits and to central autonomic circuits. The somata of these neurons, and in fact, some axons, labelled for neurotracer, but did not show immunoreactivity for AcT-Hu. The efficacy of AcT-Hu to label all somata has been previously discussed (see above; Olsson, 2009). Thus, these results are taken as the first support for these ideas.

2.4.3 Putative pacemaker cells.

In the mammalian heart HCN4 channels are responsible for a major portion of the diastolic depolarizing current in pacemaker cells, and expression of this protein has been recognized as a marker for such cells (Christoffels *et al.*, 2010). In the heart of the hagfish, orthologues of all members of the HCN channel family (HCN1-4) were expressed but the dominant form present was HCN3 (Wilson *et al.*, 2013). In the goldfish heart HCN4 immunohistochemistry labels cells in the sinoatrial valve leaflets (Newton *et al.*, 2014). In the zebrafish heart Tessadori *et al.* (2012) reported that cells in the vicinity of the sinoatrial valves expressed message for the HCN4 ion channel protein and were also immunoreactive for the transcription factor Isl1; such cells also displayed the electrophysiological characteristics of pacemakers. HCN4 immunoreactivity was detected in cells in the leaflets of the sinoatrial valve, which were double-labelled with Isl1. Taken together, results from the previous studies in zebrafish and goldfish along with the findings of the present study, suggest that this combination of antibodies may constitute a valid

anatomical marker for pacemaker cells. It remains to be confirmed whether the HCN4-Is11-positive cells detected in this study have pacemaker-like discharge properties.

In the goldfish heart it was observed that AcT-Hu-positive axons approached HCN4-expressing cells in the sinoatrial valve leaflets (Newton *et al.*, 2014), suggesting that these cells were innervated from the SAP. In the present study, using the synaptic vesicle marker SV2, a rich terminal field surrounded HCN4-positive cells has been shown, supporting the concept that autonomic transmitters released from these terminals would modulate the discharge activity of these cells.

2.4.4 Innervation of the atrioventricular junction and outflow tract

In the goldfish heart the atrioventricular plexus is innervated by axons in one or more nerve trunks running in the atrial wall from the SAP to the AVP (Newton *et al.*, 2014). Because of the smaller size of the zebrafish heart it is possible to visualize these trunks in their entirety. Intrinsic innervation to the AVP coursed through the atrium in two main trunks arising from either side of the SAP and coursing to the ipsilateral sides of the AVP. An asymmetry of intrinsic and extrinsic axons existed in these pathways; only the pathway arising from the left vagal junction contained intrinsic and extrinsic axons, as demonstrated by the presence of neurotracer in these nerves. In fact, some of the extrinsic axons traversed the AVP and projected into the ventricular wall toward the bulbus arteriosus. It is tempting to speculate that these axons may represent sympathetic autonomic postganglionic axons originating from cell bodies in the paravertebral ganglion chain. Double-labelling experiments with neurobiotin and TH needs to be performed to clarify this issue.

The ventricle in the fish heart beats spontaneously when separated from the atrium, with a much slower rate than that set by the sinoatrial pacemaker (Farrell and Jones, 1992) and it has been postulated that there is a secondary pacemaker in the ventricle proximal to the atrioventricular valves or within the valve region. To date there have been no reliable anatomical markers for such a pacemaker in fish. The observation of small HCN4-positive cells within the atrioventricular valve leaflets imply that these cells may constitute a "ventricular" pacemaker. The AVP surrounded the valves, with a small number of ganglia containing neuronal somata that were cholinergic; these neurons had morphology similar to that of such cells in the SAP. In the AVP there were also TH-positive axons. The overall innervation pattern at the AVP was thus similar to that observed in the goldfish heart (Newton *et al.*, 2014). It is therefore possible that potential pacemaker cells in this region could be under autonomic control by nearby cholinergic neurons and adrenergic axons, and thus represent a general trend in teleosts.

There was evidence of innervation from two sources in the bulbus arteriosus. Axons originating either from the AVP or from the venous pole of the heart projected in the ventricular wall to the ventriculo-bulbar junction and into the bulbus wall, as demonstrated by AcT-Hu labelling; some of these axons were TH-positive and may have been adrenergic. Autonomic modulation of the ventricular myocardium and bulbar smooth muscle via these projections would thus have originated from axons in the vagosympathetic trunks and the venous pole of the heart. The second source of bulbus innervation was from a nerve trunk coursing along the ventral aorta, into the wall of the bulbus, and crossing the bulbo-ventricular junction to the proximal ventricular wall. Given its pathway, this has been termed the branchio-cardiac tract. The ultimate origin of this

nerve tract could not be observed, but in some specimens it ran in the wall of the ventral aorta from the last gill arch. There were some TH-positive axons in this nerve, and at least some of the fine meshwork of TH-positive innervation of the bulbus wall arose from this nerve. These findings complement the earlier report in the goldfish heart of innervation in the bulbus wall that appeared to originate cephalad to the heart (Newton *et al.*, 2014). There has been long-standing speculation that some innervation of the teleost heart enters via the arterial pole (Gannon and Burnstock, 1969; Holmgren, 1977; Donald, 1998); current results suggest that the branchio-cardiac tract may constitute such innervation. While some of the axons in this nerve may be adrenergic, the effects of activating this nerve on the bulbus and ventricle remain to be determined. It is tempting, however, to speculate that the branchio-cardiac tract may represent a pathway for reflex control of the heart originating in the gills, potentially from respiratory chemoreceptors (Jonz *et al.*, 2014).

2.4.5 Conclusions.

Taken together, these observations in the zebrafish heart suggest the potential for regionally precise and function-specific autonomic control of the effectors within the heart that affect cardiac output. In particular, the fine details of innervation that observed in the region near the SAP containing putative pacemaker cells, reveal the neuroanatomical substrate by which the discharge activity of these cells may be rapidly modulated. Neurons in the SAP proximal to the pacemaker region may thus constitute the a common pathway for autonomic control of heart rate. Moreover, the somata in the AVP may modulate the discharge rate of putative pacemakers associated with the atrioventricular valve. The

results of this study have thus laid the essential neuroanatomical groundwork for further investigations to identify the locations, functional characteristics and connectivity of subpopulations of intracardiac neurons involved in regulating cardiac output in the hearts of teleosts.

Figure 2.1. Organization of intracardiac nervous system demonstrated with acetylated tubulin (AcT) and human neuronal protein (Hu) immunohistochemistry. **A, B:** Whole-mount of heart (A) and schematic (B) show an overview of the chambers of the heart and the major elements of cardiac innervation. Schematic represents the heart as it would appear after removal from the body for making wholemount cardiac preparations. Blood passes serially from the paired ducts of Cuvier (DC) into the sinus venosus (SV), through the sinoatrial valves and into the atrium (A), then into the ventricle (V), the bulbus arteriosus (BA) and ventral aorta (VA) to the gills. The box in the lower part of panels A and B outlines the region containing the sinoatrial valve where the sinoatrial plexus (SAP) was located. The uppermost box indicates the region of the atrioventricular plexus (AVP) at the junction of A and V. RX, LX: right and left vagosympathetic trunks. **C-G:** Details of innervation in the region of the sinoatrial valves (O: valve ostium). **C:** Cardiac myocytes were labelled with phalloidin (Phal); arrows indicate neuronal somata. dSAP, vSAP: dorsal and ventral regions, respectively, of SAP. **D, E:** Details of SAP where LX and RX, respectively (arrows), enter the plexus. Somata were clustered into ganglia in each region. **F, G:** Dorsal and ventral SAP, between the areas shown in panels D, E. Arrows indicate somata. Scale bars: 1 mm in A; 250 μm in B; 100 μm in C, D; 75 μm in E, F.

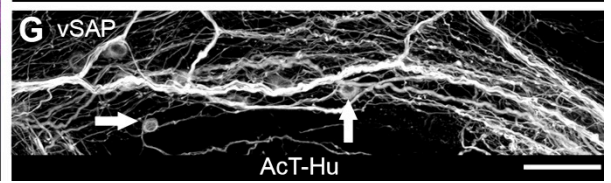
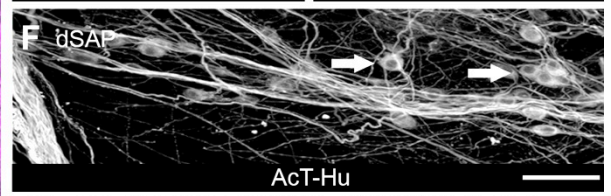
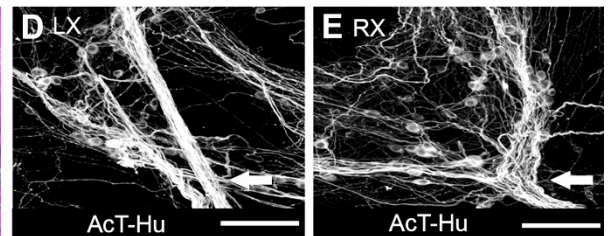
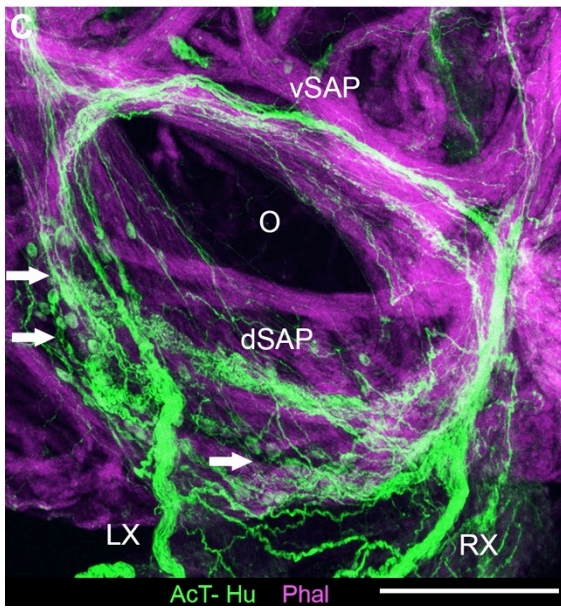
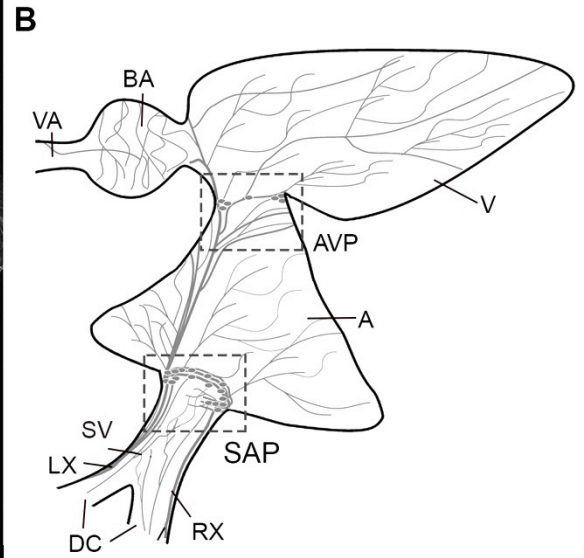
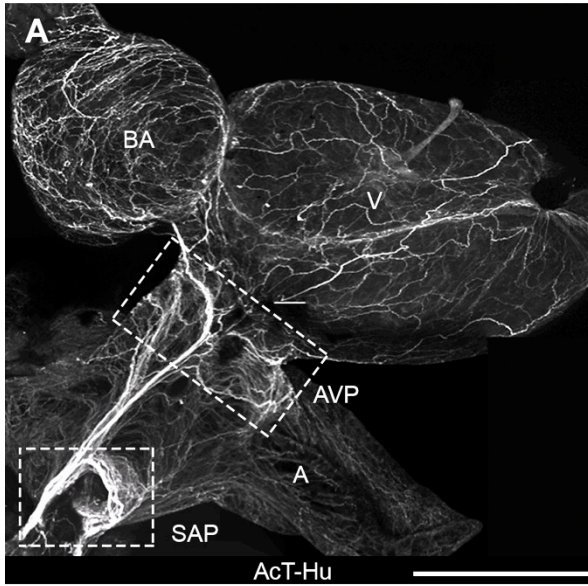


Figure 2.2. Localization of neurotransmitter-specific elements and presumptive pacemaker tissue in sinoatrial valve region. **A, B:** Choline acetyltransferase (ChAT) labelled axons and somata at junctions of left (A) and right (B) vagosympathetic nerves with SAP. **C, D:** Tyrosine hydroxylase (TH)-positive axons in same regions as shown in panels A, B. Arrows in D indicate TH-positive somata. **E:** Anti-neuronal nitric oxide synthase (nNOS) labelled axons and somata in the dorsal SAP; somata were located in a ganglion here (dG). **F:** Vasoactive intestinal polypeptide (VIP)-positive axons and terminals were located in dorsal SAP. **G:** Putative pacemaker cells in base of dorsal sinoatrial valve were double-labelled with antibodies against hyperpolarization activated, cyclic-nucleotide gated ion channels (HCN4) and Islet-1 (Isl1). **H:** Anti-synaptic vesicle 2 (SV2) labelled axon terminals (arrows) proximal to HCN4-positive cells. **I:** HCN4-positive cells embedded in myocytes (Phal) in ventral valve leaflet. **J:** Schematic of SAP region oriented to show locations of elements expressing specific phenotypes (color-coding key on right side). To obtain this tissue orientation a transverse cut was made through the ventral sinoatrial valve leaflet between junctions of the left and right vagosympathetic trunks with the SAP (diagram, lower left); tissue was then flattened and spread. Atrium is shown at upper edge of panel. Neurons were clustered into ganglia (G) by region; from left to right these are left ventral (lvG), left vagal (LXG); dorsal (dG), right vagal (RXG); right ventral (rvG). In all preparations there were varying numbers of neurons in small ganglia associated with the vagosympathetic trunks near the SAP (proximal left and right vagal [pLXG, pRXG]). Putative pacemaker cells were double color-coded to indicate combined HCN4-Isl1 labelling. Scale bars: 100 μm in A-D; 50 μm in E, F; 5 μm in G; 2 μm in H; 10 μm in I.

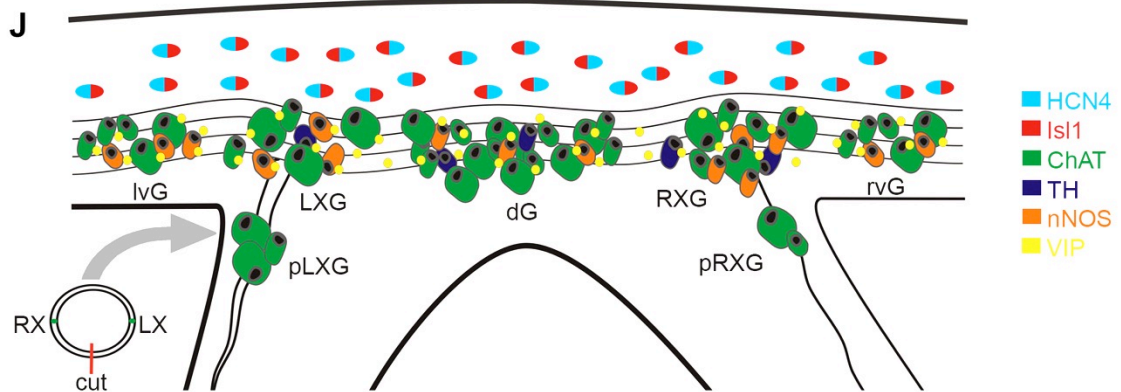
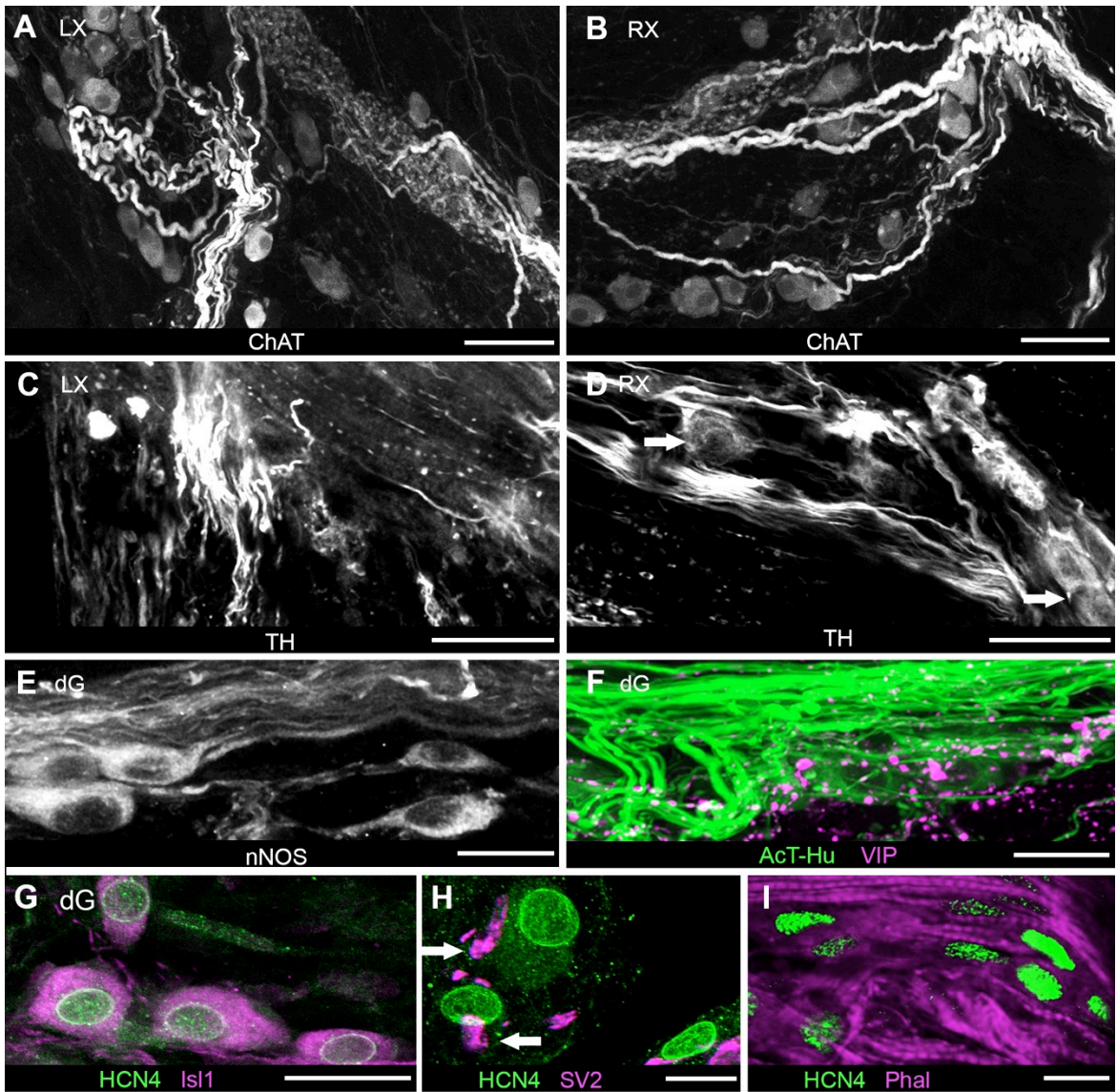


Figure 2.3. Examples of intracardiac tracing of extrinsic vagosympathetic inputs to SAP by neurobiotin and FM1-43X application to proximal stumps of nerve trunks (neurobiotin visualized with avidin secondary). **A, B:** Axons and terminals within SAP shown after tracer application to left (A, LX) and right (B, RX) extrinsic nerves; both tissue samples were double-labelled with AcT-Hu. **C:** Details of terminals associated with extrinsic axons in neuropil near junction of right vagosympathetic trunk with SAP (box in panel B). Some labelled terminals appeared to be apposed to AcT-Hu-positive neuronal somata (arrows). **D:** Arrows indicate putative somata (arrows) and associated axons labelled with neurobiotin, among larger AcT-Hu-positive somata and neuropil. Scale bars: 100 μm in A, B; 50 μm in C; 20 μm in D.

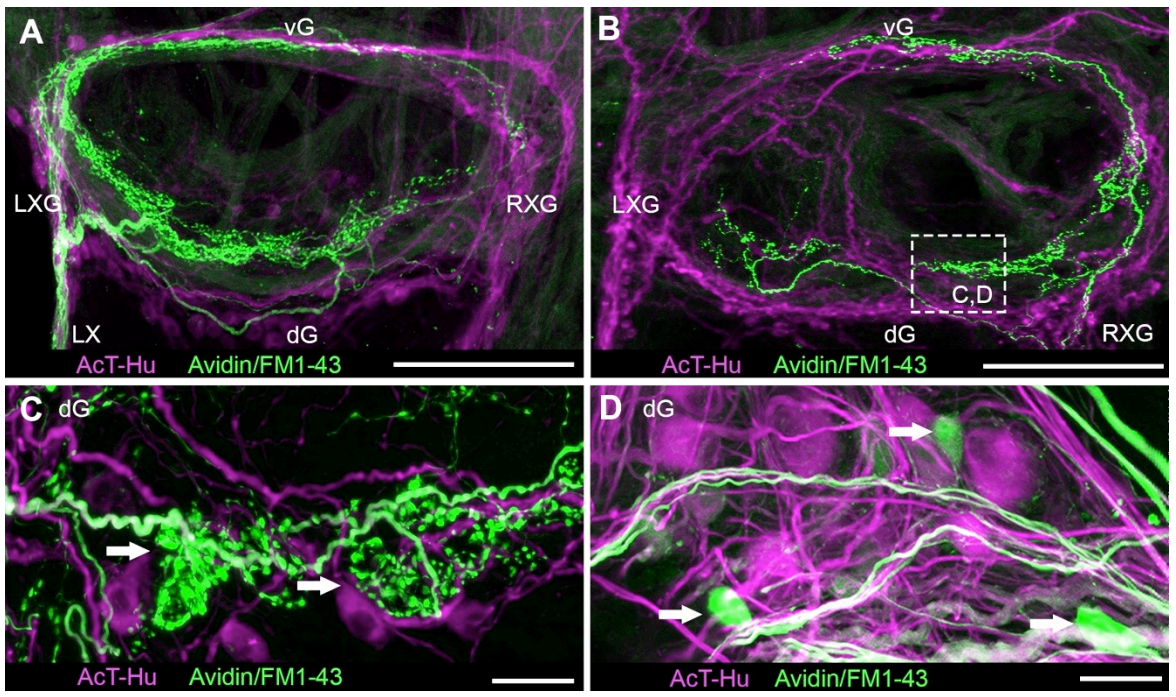
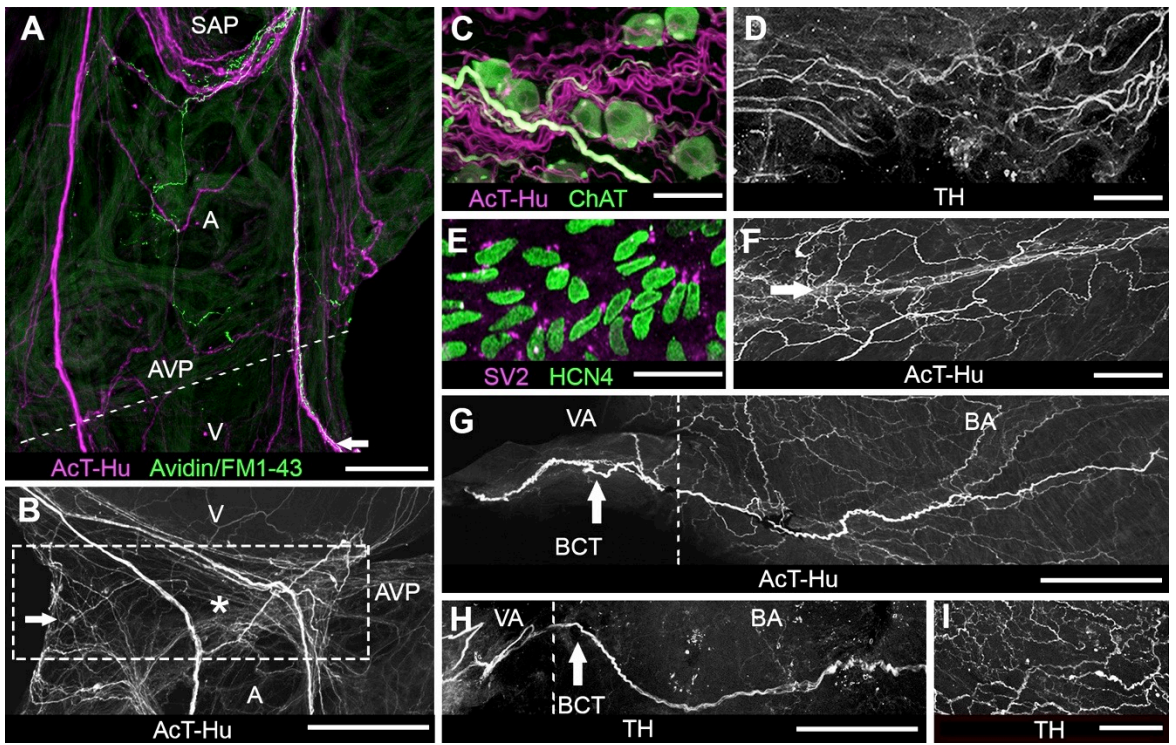


Figure 2.4. Innervation of atrioventricular region and outflow tract. **A:** Atrium and ventricle double-labelled with AcT-Hu and neurotracer (Avidin/FM1-43X, applied to right vagosympathic trunk) shows nerve trunks arising from SAP (upper part of panel) and projecting toward atrioventricular junction (marked by dashed line; AVP: site of atrioventricular plexus). Some axons continued from AVP into ventricle (V) at lower edge of panel. Presence of neurotracer indicates that a portion of axons originated extrinsic to the heart. **B:** Enlargement of region containing AVP (box) from another specimen labelled with AcT-Hu shows contribution of atrial nerve trunks to plexus; a small ganglion is indicated by the arrow; asterisk marks atrioventricular valve. **C:** Detail of AVP shows cholinergic somata associated with cholinergic and non-cholinergic axons in neuropil. **D:** TH-labelled axons in AVP neuropil. **E:** HCN4-positive cells located in region of atrioventricular valves (* panel B). **F:** AcT-Hu-positive axons within atrioventricular valve leaflets (near *). **G:** AcT-Hu-labelled innervation in walls of outflow tract (BA, bulbus arteriosus; VA, ventral aorta). Dashed line marks border between VA and BA. A prominent nerve trunk (branchio-cardiac trunk, BCT, arrowhead) coursed cephalo-caudally in the wall of the BA toward the ventricle (right edge of panel). **H:** TH labelled a subset of axons in the BCT (arrow). **I:** BA wall was innervated with a network of fine TH-positive axons. Scale bars represent 500 μm in A; 100 μm in B; 50 μm in C, D, E, G, I; 75 μm in F, H.



CHAPTER 3

AUTONOMIC CONTROL OF CHRONOTROPY IN THE ZEBRAFISH

3.1 Introduction

An essential aspect of cardiac function is the ability to adjust cardiac output to meet the continually varying metabolic demands of the body. To match these demands, the autonomic nervous system (ANS) alters pacemaker rate and myocardial contractility *via* reflexes acting through the intracardiac nervous system (ICNS). The sympathetic and parasympathetic limbs of the ANS dually innervate the vertebrate heart (Farrell & Jones, 1992; Nilsson, 2011). Reflex output from autonomic centres in the central nervous system are carried by cardiac rami of the vagosympathetic nerve trunks (VSN) to the ICNS, which represents the a common pathway for neuronal control of cardiac function.

Our current understanding of the mechanisms of intracardiac integration of autonomic inputs and the details of the anatomical and functional connections between the ICNS and cardiac effectors is incomplete. In particular, the relationship between the pattern of innervation of pacemaker cells by the ICNS and the responses of these cells to activation of this system are not clear. In mammalian hearts a major difficulty in studying the role of function-specific components of the ICNS, such as those involved in controlling rate, is that this system is deeply embedded in, and distributed throughout, the walls of both atria and ventricles. These components are therefore largely inaccessible for integrative studies. One solution to this problem is the use of reduced experimental preparations representing a subset of the ICNS, such as isolated tissues containing neurons in ganglionated plexi, to study properties of control circuits *in vitro* (Smith, 1999; Ardell *et al.*, 2014). This approach, however, eliminates intracardiac neuronal connections, so only limited conclusions may be drawn about the roles of localized circuitry in controlling overall cardiac function.

The isolated whole zebrafish heart has numerous advantages over traditional mammalian models for investigating the organization and function of the ICNS, which have been employed in the present study. The initiation of excitation by a discrete group of sinoatrial pacemaker cells, and the propagation of this signal through the atrial and ventricular myocardium, are strikingly similar between the two-chambered hearts of zebrafish to the four-chambered hearts of adult mammals (Barusscotti and Robinson, 2007; Christoffels *et al.*, 2010). Recent reports (Briggs, 2002; Chi *et al.*, 2008; Dvornikov *et al.*, 2014; Nemtsas *et al.*, 2010; Rider *et al.*, 2012; Tessadori *et al.*, 2012) have established the zebrafish heart as a powerful tool for studying cardiac electrophysiology, with the potential to provide broad insights into cardiovascular function. In a previous study (Stoyek *et al.*, 2015; Chapter 2), the basic structure of the ICNS in zebrafish was described, which is consistent with that of humans and other mammalian models (Irisawa, 1978; Mangoni and Nargeot, 2008; Pauza *et al.*, 2013; Pauza *et al.*, 2014; Li *et al.*, 2015). The isolated zebrafish heart thus has technical advantages that may be exploited to better understand the role of the ICNS in modulating chronotropy (Stoyek *et al.*, 2015).

Axons entering the zebrafish heart from the cardiac rami of the VSNs form terminals close to putative pacemaker cell that express hyperpolarization-activated, cyclic nucleotide-gated channel 4 (HCN4) in the sinoatrial region (SAR). In zebrafish and mammalian species HCN4 channels are known to contribute a major portion of the diastolic depolarizing current in cardiac pacemaker cells (Irisawa, 1978; Mangoni and Nargeot, 2008; Pauza *et al.*, 2013; Pauza *et al.*, 2014; Li *et al.*, 2015).

Immunohistochemical evidence also shows that juxta-pacemaker terminals contain the neurotransmitters acetylcholine (ACh; parasympathetic, cardio-inhibitory) and

norepinephrine (NE; sympathetic, cardio-excitatory), providing the neuroeffector substrate for autonomic control of pacemaker rate (Stoyek *et al.*, 2015). At the atrioventricular region (AVR) a second population of HCN4-expressing cells has been identified (Stoyek *et al.*, 2015). This anatomical finding is consistent with optogenetic evidence (Arrenberg *et al.*, 2010) that the zebrafish heart may contain a secondary pacemaker in this region, a situation similar to that in the mammalian heart (Goldberg *et al.*, 1973; Saito and Tenma, 1976; Shibata *et al.*, 2009; Arrenberg *et al.*, 2010). An important advantage of the zebrafish heart is that the majority of the neurons within the ICNS are located in the basal regions of the sinoatrial valves, are visible using standard microscopy and are accessible for electrophysiological analyses (Stoyek *et al.*, 2015).

In the present study, the isolated, innervated zebrafish heart was established as a novel model for studies of autonomic control of heart rate (HR). A combined electrophysiological, pharmacological, and anatomical approach was used to investigate the integrative neural control of cardiac pacemaker function. Electrocardiogram (ECG) recordings, combined with extrinsic nerve stimulation or pharmacological activation, demonstrated that discrete neural pathways modulate HR through adrenergic and cholinergic mechanisms. Optical mapping of electrical activity confirmed the location of a secondary pacemaker in the AVR, as well as modulation of both SAR and AVR pacemaker function by neural stimulation. Finally, immunohistochemical methods characterized the relationship of muscarinic cholinergic (M₂R) and beta-2 adrenergic (β_2 AR) receptors to putative pacemaker cells. The results of this study establish the isolated zebrafish heart as a tractable preparation to investigate autonomic control of pacemaker function for improved understanding of integrative cardiovascular physiology.

3.2 Methods

An expanded Methods section is provided in the Appendix A.

3.2.1 *Animals.*

A total of 96 AB strain zebrafish (12-18 months post-fertilization; mixed sex; 35 ± 8 mm standard body length, 693 ± 154 mg mean wet weight) were used. Institutional approval for animal use in this study was obtained from the Dalhousie University Committee on Laboratory Animals.

3.2.2 *Heart isolation.*

Zebrafish were anaesthetised in buffered tricaine (MS-222; 1.5 mM, pH 7.2) and the heart was exposed through a ventral midline incision. Tissues encompassing the ventral aorta (containing the branchiocardiac nerve trunk, BCT), ventricle, atrium, sinus venosus and ducts of Cuvier (containing the cardiac VSN) were removed for *in vitro* recordings or immunohistochemistry. After each experiment hearts were photographed, blotted, and weighed.

3.2.3 *Whole-heart ECG recordings and VSN stimulation.*

Hearts were bath perfused with zebrafish saline and allowed to equilibrate for 30 min. Bipolar wire electrodes were used to deliver trains of rectangular pulses (0.5 ms pulses, 300 μ A, 1-20 Hz) to cardiac VSN. ECG signals were recorded from the atrium and ventricle with bipolar suction electrodes. Cardiac responses were analyzed by measuring the time between R-waves of the ECG (R-R interval). Atrioventricular delay was

measured by the latency between atrial and ventricular R-waves within individual cardiac cycles.

3.2.4 Isolated ventricular pacemaker recordings.

ECG signals were recorded first from intact hearts, followed by isolation of the ventricle, with a small margin of atrial tissue attached. Subsequent ECG recordings were then made from the dissociated atrial and ventricular tissues. Pharmacologic agents were used to evaluate autonomic effects.

3.2.5 BCT stimulation.

The BCT was stimulated in the wall of the ventral aorta between the afferent arteries of the fourth gill arches and the bulbus arteriosus. Stimulation parameters were similar to those for VSN stimulation.

3.2.6 Pharmacological agents.

The agonists nicotine (NIC), muscarine (MUSC), and isoproterenol (ISO) were delivered to the tissues in 200 μ L boluses (all 1 mM) *via* a screw-drive microinjector. Antagonists hexamethonium (HEX; 10 μ M) and atropine (ATR; 10 μ M), and timolol (TIM; 100 μ M) were continuously perfused starting 15 min prior to recording.

3.2.7 Voltage optical mapping.

Electrical activity was recorded in isolated whole hearts or dissociated AVR-ventricular tissue. Tissues were exposed to voltage-sensitive di-4-ANBDQPQ (10 μ M) in

the perfusate for 10 min. The dye was washed out with saline containing blebbistatin (10 μ M) to suppress contractile activity. Blebbistatin was present in perfusate throughout the remainder of the experiments. Stimulation of cardiac VSN (see above) was performed in a subset of these hearts. Data were analysed with custom routines in Matlab.

3.2.8 Pacemaker cell immunohistochemistry.

Hearts were fixed in a periodate-lysine-paraformaldehyde fixative. Antibodies against HCN4 and Islet-1 (Isl1) were used to detect putative pacemaker cells and antibodies against muscarinic receptors subtype 2 (M_2R) and beta-2 adrenoceptors (β_2AR) were used to investigate associated receptors (see Appendix B). An antibody against tyrosine hydroxylase (TH) was used in a subset of tissues to investigate the relationship of β_2AR s to adrenergic innervation. The distribution of M_2R s and β_2AR s was quantified using ImageJ. In all preparations phalloidin (Phal, F-actin marker) was used to label the working myocardium.

3.2.9 Imaging and data analysis.

Tissues were viewed using a Zeiss LSM510 confocal microscope with Zeiss Zen2009 software. Images were processed into plates with Photoshop CS6. During composition of the figure plates the brightness of some images was adjusted so that panel-to-panel contrast in the plate was consistent. All data are presented as means \pm SEM. Data were analyzed using paired Student's t-test or one-way analysis of variance (ANOVA) with Tukey's *post hoc* analysis. P values \leq 0.05 were considered significant.

3.3 Results

3.3.1 Viability of heart function *in vitro*.

In preliminary trials, mean initial HR in the bath was 99 ± 2 beats·min⁻¹ (range 76-129; $n=8$), and varied by <10% in all specimens over a 6 hr period. VSN stimulations performed periodically throughout these trials gave chronotropic responses similar to those measured immediately after isolation, indicating retained functionality. Neither heart area (9.6 ± 0.4 mm²; range 7-12) nor mass (6.25 ± 0.5 mg; range 5-8) was significantly correlated with rate (r -values < 0.05).

3.3.2 Electrical stimulation of cardiac rami of vagosympathetic trunks.

In all preparations, VSN stimulation at a frequency ≥ 15 Hz significantly prolonged the R-R interval (bradycardia), starting with the beat immediately after the initiation of the stimulus and lasting for the duration of the stimulus train (Figure 3.1). At 15 Hz, stimulation of either the right or left cardiac VSN evoked an R-R interval increase of 1.7 ± 0.2 or 1.9 ± 0.3 times the pre-stimulus value, respectively. At a stimulation frequency of 20 Hz, the evoked bradycardia was highly variable, most strikingly resulting in the cessation of beating for the duration of the stimulus period in some hearts (in these cases, the R-R interval was taken as the period of stimulation). Given that 15 Hz stimulation caused a significant change in R-R interval without cardiac standstill in any specimen, this frequency was used to quantify effects of cardiac VSN activation in subsequent experiments except for voltage optical mapping experiments. It was found that in all experiments AV delay was unaltered by VSN at this level. In 15 of the 24 hearts tested,

simultaneous VSN stimulation resulted in a decrease in R-R interval (tachycardia) following cessation of stimulation. This effect had a variable post-stimulus latency to onset (mean 5.1 ± 0.8 s) and duration (mean 11.0 ± 1.8 s), after which the R-R interval returned to the pre-stimulus control value (Figure 3.1B).

3.3.3 Effects of cholinergic and adrenergic agents on R-R interval.

Application of nicotine ($n=6$) significantly prolonged R-R interval to 1.5 ± 0.1 times the control value (NIC, Figure 3.1D), a response qualitatively similar to that evoked by single VSN stimulation at 15 Hz. Both the nicotinic effect and that of VSN stimulation were eliminated by addition of hexamethonium (HEX, Figure 3.1D, shaded). Application of muscarine ($n=6$) also caused a significant increase in R-R interval to 1.4 ± 0.1 times control (MUS, Figure 3.1E). Neither NIC nor MUSC alone evoked a biphasic response (data not shown), as was observed as with VSN. Perfusion of atropine blocked effects of both muscarine and VSN stimulation (ATR, Figure 3.1E, shaded).

Application of isoproterenol ($n=6$) caused a significant decrease in R-R interval to 0.8 ± 0.1 times the pre-application value (ISO, Figure 3.1F). This response was blocked by timolol, which had no effect on the initial increase in R-R interval with VSN stimulation, but did block the post-stimulation decrease in R-R interval (TIM, Figure 3.1F, shaded). It was found that in all experiments atrioventricular (AV) delay was unaltered by autonomic agents.

3.3.4 Autonomic effects on AVR activity.

Atrioventricular delay (Figure 3.2A; mean delay 52 ± 1.8 ms) was highly correlated with pre-stimulus HR ($r = 0.98$), but was unchanged from pre-trials values during VSN stimulations or the application of cholinergic or adrenergic agonists (data not shown).

In the whole heart, depolarization of the ventricle was driven by depolarization of the atrium (Figure 3.2A). Following isolation of the ventricle from the atrium the atrial rate continued unchanged but the mean rate of ventricular contraction fell to 0.3 ± 0.1 times the ongoing atrial rate (1 ventricular beat to ~3-4 atrial beats; Figure 3.2B). Application of NIC to the isolated ventricle significantly increased R-R interval compared with the pre-nicotine interval (Figure 2C), an effect that was blocked by HEX (Figure 3.2C, shaded). Isoproterenol exposure evoked a significant decrease in the ventricular R-R interval, an effect that was blocked by TIM (Figure 3.2C).

3.3.5 Effect of BCT stimulation.

Electrical stimulation of the BCT in the whole heart resulted in a significant decrease in R-R interval to 0.7 ± 0.1 times control (Figure 3.2D). Perfusion of TIM during BCT stimulation eliminated this response, while perfusion of HEX had no effect (Figure 3.2D, shaded). Stimulation of the BCT had no effect on the R-R interval in the isolated ventricle.

3.3.6 Imaging of the origin and spread of cardiac excitation.

In all hearts sampled ($n=6$), the initial site of depolarisation of each heart beat was within the SAR (Figure 3.3B, asterisk). The wave of activation propagated through the

atrial wall in a broad sweep toward the AVR. Mean time to full depolarization of the atrium was 59 ± 5 ms ($n=6$) while mean atrioventricular delay was 55 ± 2 ms. The atrium began to repolarize after this delay (mean atrial action potential duration was 138 ± 10 ms), while the ventricle was still depolarizing. Complete depolarization of the ventricle took 80 ± 8 ms from the invasion of excitation. Mean ventricular action potential duration was 188 ± 7 ms. Mean total duration from initial depolarization of the atrium to full repolarization of the ventricle was 355 ± 4 ms, followed by a delay of 256 ± 8 ms before the next cycle.

Simultaneous VSN stimulation of both cardiac rami at 20 Hz ($n=5$) induced a change in the primary initiation site of electrical activity from the SAR to the AVR (Figure 3.3G-J). In this case, the earliest depolarisation occurred in the AVR, along with multiple foci outside of the SAR, which passed in a retrograde direction through the atrium to the SAR depolarising the atrium. Following depolarisation of the atrium, delay of the depolarising wave front at the AVR (74 ± 5 ms) was significantly increased compared to pre-treatment values, before exciting the ventricle. In these hearts time from initial atrial depolarization to completion of ventricular repolarization (396 ± 3 ms) was also significantly increased compared with pre-treatment values.

Following surgical isolation of the AVR and ventricle from the SAR and atrium, the site of origin of electrical activity was in the AVR (Figure 3.3K-M). Propagation of the AVR-initiated depolarizing wave through the ventricle took significantly longer (97 ± 5 ms) than the ventricular propagation time of a SAR-initiated depolarizing wave in the whole heart.

3.3.7 Anatomical identification of putative pacemaker cells in the SAR and AVR.

HCN4- and Isl1-immunoreactivity (IR) was used to distinguish putative pacemaker cells from the surrounding cardiomyocytes ($n=12$). In the SAR (Figure 4A), cells expressing HCN4-IR formed multiple clusters that congregated toward the basal portions of the sinoatrial valves (Figure 3.4B), corresponding with the region of initial cardiac cycle excitation (Figure 3.3). Within a cluster, the HCN4-positive cells appeared to be contiguous, displacing most of the local myocytes to the cluster margin (Figure 3.4C).

The population of Isl1-positive cells in the SAR completely overlapped the population of HCN4-immunoreactive cells (Figure 3.4C). Cells expressing both markers had spindle-shaped or oval cell bodies, with relatively large oval nuclei. Isl1-IR was more prominent in the cytoplasm, while HCN4-IR appeared to be localized to either the cytoplasm or the cell membrane. Phalloidin labeling was restricted to cardiac myocytes, which predominantly lacked the HCN4 label.

As the antibodies against HCN4, M₂R, and β_2 AR were generated in the same host species, it was not possible to investigate co-expression of these markers. Instead we used the Isl1 antibody to identify putative pacemaker cells to determine the co-localization patterns of these receptors. In the SAR, all Isl1-immunoreactive cells displayed punctate M₂R-IR, which was more heavily concentrated on parts of the cell distal to the nucleus (Figure 3.4D). M₂R-positive punctata were also present on myocytes adjacent to Isl1-immunoreactive cells (Figure 3.4D), but were sparser than the M₂R-IR associated with putative pacemaker cells.

In the AVR, a compact group of HCN4-positive cells was located medially in tissue of the atrioventricular valves (Figure 3.4E). In contrast to HCN4-positive cells in the

SAR, cells in the AVR were smaller, polygonal in shape, and did not co-express Isl1-IR. Thus, we could not use the combination of Isl1- and M₂R-IR to determine whether these receptors were associated with putative pacemaker cells in the AVR (as performed for the SAR). We found that combining phalloidin labeling of local myocytes with M₂R-IR demonstrated that these receptors were present on cell-like structures that were phalloidin-negative (Figure 3.4F), and in the same location as cells labelled with HCN4 in other specimens (Figure 3.4E).

M₂R-IR was also associated with the myocardium of both the atrium and ventricle (Figure 3.4G-I). In a survey of the relative density of receptors in these regions, the atrial myocardium had a significantly higher density (5 ± 1 M₂R-immunoreactive clusters per 100 μm^2) than did the ventricular myocardium (2 ± 1 clusters per 100 μm^2 ; $P < 0.01$).

In the SAR, all Isl1-positive cells displayed punctate β_2 AR-IR, distributed evenly over the cell (Figure 3.5C). β_2 AR -positive punctata were also associated with myocytes proximal to Isl1-IR cells (Figure 3.5D-F), but myocyte-associated β_2 AR-IR was sparser than those associated with putative pacemaker cells.

In the AVR, β_2 AR were present on cell-like structures that were phalloidin-negative (Figure 3.5F), and in the same location as cells labelled with HCN4 in other specimens (Figure 3.5E). β_2 AR -IR was also associated with the myocardium of both the atrium and ventricle (Figure 3.5G-I). In a survey of the relative density of receptors in these regions, the ventricular myocardium had a significantly higher density of β_2 AR -IR (8 ± 2 β_2 AR -IR clusters per 100 μm^2), than did the atrial myocardium (2 ± 1 clusters per 100 μm^2 ; $P < 0.01$).

3.4 Discussion

In this study the viability of the isolated zebrafish heart as a novel model for studies of autonomic control of chronotropy has been established. While reduced, *in vitro* preparations of mammalian hearts including a functional pacemaker have previously been used for similar studies, autonomic elements in these preparations generally have compromised connectivity, thus limiting the capability for full identification of neural mechanisms involved in such functions as pacemaker control. Though the small size of the zebrafish heart presents its own technical challenges, its size also permits visualization and accessibility of the entire ICNS in the whole organ, which has not previously been possible in mammalian models.

3.4.1 Receptor-mediated mechanisms of chronotropic modulation.

In the isolated zebrafish heart, the general function of autonomic control appears to be similar to that observed in the mammalian heart. Cholinergic agents NIC and MUS had parasympathomimetic effects, evoking an increase in R-R interval (the same general chronotropic effect as VSN stimulation). NIC, presumably mimicking the effect of ACh released from vagal terminals, which have previously been shown to contain choline acetyltransferase (the synthetic enzyme of this transmitter; Stoyek *et al.*, 2015), likely activated intracardiac neurons that projected to pacemaker cells. Exposure to the nicotinic receptor antagonist HEX eliminated the responses to both VSN stimulation and NIC, confirming the role of nicotinic cholinergic neurotransmission within the ICNS in VSN-induced bradycardia. MUS acts at cholinergic receptors on pacemaker cells, prolonging the duration of diastolic depolarization and slowing discharge rate (Dhein *et al.*, 2001).

Exposure to the muscarinic antagonist ATR eliminated the bradycardia in response to VSN and MUS, providing functional confirmation that muscarinic receptors play a role in neurogenic bradycardia in the zebrafish heart. The β -adrenergic agent ISO, on the other hand, had an overall sympathomimetic effect, decreasing the R-R interval, while the β -adrenergic antagonist TIM blocked both the post-stimulus tachycardia and the response to ISO, suggesting a robust role for adrenergic control of pacemaker discharge rate.

In the present study, the R-R interval response to simultaneous stimulation of both VSNs was summative, supporting the idea that each nerve activated different groups of post-ganglionic ‘rate-control’ neurons with minimal interactions within the ICNS. This provides functional support both for previous anatomical evidence in zebrafish (Stoyek *et al.*, 2015), and for the anatomical and functional evidence in the mammalian heart that axons of the extrinsic nerves likely target different subpopulations of cardio-inhibitory intracardiac neurons with parallel chronotropic functions (Ardell and Randall, 1986; Lang *et al.*, 1990; Blinder *et al.*, 1998; Akiyama and Yamazaki, 2001; Cheng *et al.*, 2004; Blinder *et al.*, 2007).

In approximately two-thirds of the hearts tested in this study, VSN stimulation at an intensity that evoked significant bradycardia also elicited a variable post-stimulus tachycardia. A biphasic response to vagal stimulation has also been reported in the mammalian heart (Shvilkin *et al.*, 1994). The presence of sympathetic post-ganglionic axons in cardiac vagal rami is conserved from zebrafish to mammals (Nilsson, 2011), and co-activation of these axons, along with vagal preganglionic parasympathetic axons, during VSN stimulation is the most likely explanation for the biphasic response. In the mammalian heart there is partial or complete persistence of the tachycardic portion of the

response to vagal stimulation in the presence of β -adrenergic antagonists, which has been proposed to result from co-release of cardio-acceleratory peptides (Shvilkin *et al.*, 1994; Hancock and Hoover, 2008). As this response was entirely eliminated by β -blockade in this study, peptide release seems an unlikely cause for the post-stimulus tachycardia observed in the zebrafish heart.

3.4.2 Properties and neural control of pacemaker loci.

In the present study, the origin of myocyte electrical activity was located within the SAR, in agreement with previous functional (Saito and Tenma, 1976; Sedmera *et al.*, 2003; Haverinen and Vornanen, 2007; Tsutsui *et al.*, 2010; Tessadori *et al.*, 2012; Lin *et al.*, 2014; Piperhoff *et al.*, 2014) and anatomical (Tessadori *et al.*, 2012; Stoyek *et al.*, 2015) data. The mean time for propagation of atrial excitation, as well as the atrioventricular delay, corresponded with the delay calculated from ECG-derived data, and with values previously reported in other optical imaging studies of the zebrafish heart (Lin *et al.*, 2014; Lin *et al.*, 2015). The location of initiation and spread of excitation observed thus conform with the recognized pattern of normal heart activation in this species, and establish a functional baseline for mapping the effects of VSN stimulation.

In the mammalian heart, it has been suggested that vagal input not only causes bradycardia, but also influences the operational pacemaker site. Previous work has shown that vagal drive can result in a shift of the pacemaker site within the sinoatrial node and the atrial wall, and that under certain conditions the atrioventricular junction can become the dominant pacemaker site (Bouman *et al.*, 1968; Boineau *et al.*, 1988; Shibata *et al.*, 2001; Hucker *et al.*, 2007). In the zebrafish heart, strong simultaneous VSN stimulation (20 Hz)

both induced bradycardia and altered the pattern of initiation and propagation of electrical activity, in a similar manner to that observed in the mammalian heart. In these experiments, the site of first depolarization occurred at the AVR, followed by multiple foci outside of the SAR, which depolarised the rest of the atrium. Following atrial depolarisation, atrioventricular delay was significantly increased compared with pre-stimulus values, before the ventricle was excited. In mammalian hearts, where epicardial light penetration is a limiting factor for complete transmural imaging, the phenomenon of re-entry or transmural breakthrough could offer an explanation for such a shift. As signals were collected from the entire thickness of the tissue in these experiments, however, re-entry or transmural breakthrough would have been visualised in these recordings, so this was not likely a factor in the present study. Thus, in both zebrafish and mammalian hearts, when vagal tone is elevated and bradycardia occurs, there may be an accompanying shift of the primary pacemaker locus from the SAR to a set of pacemaker cells with a lower intrinsic rate near the sinoatrial node or at the atrioventricular junction. This is the first report of a neurally mediated shift in pacemaker locus in the zebrafish heart, and indicates that this powerful system for cardiac control is conserved from fish to mammals.

In the mammalian heart, atrioventricular delay is highly sensitive to autonomic modulation. Yet in the current study it was found that AV delay was unaltered by VSN at 15 Hz or autonomic agents. While the lack of autonomic modulation of conduction may be a zebrafish-specific phenomenon, previous work has shown a high variability in the AV delay in the zebrafish (Lin *et al.*, 2014). It could therefore be possible that the such variability masks any subtle changes in AV delay occurring during autonomic modulation, warranting future investigation.

In mammals, the existence of a primary pacemaker near the sinoatrial junction and one or more subsidiary pacemakers within the atrial wall is well established (Irisawa, 1978; Mangoni and Nargeot, 2008). In this study it was found that the pacemaker at the AVR was also capable of functioning independently after isolation from the atrium, to drive spontaneous ventricular excitation at a rate approximately one-third that of the atrial pacemaker. Optical mapping in the isolated ventricle showed that the initial depolarization occurred in the AVR close to the site of HCN4-labelled cells, and that the activation waveform spread into the ventricular myocardium, establishing the presence of a second major pacemaker locus in the AVR of the zebrafish heart.

The discharge rate of the mammalian atrioventricular pacemaker is modulated by the ANS in a manner similar to autonomic control of the sinoatrial pacemaker (Goldberg *et al.*, 1973; Shibata *et al.*, 2001). In previous work, it was found that the zebrafish AVR is innervated by extrinsic axons from the VSN, as well as a population of intracardiac neurons proximal to the atrioventricular valves (Stoyek *et al.*, 2015; Chapter 2). In the isolated zebrafish ventricle, the general function of the atrioventricular pacemaker and its autonomic control appeared to be similar to that of the atrioventricular node in mammalian hearts. NIC had a parasympathomimetic effect, evoking an increase in R-R interval, while ISO had a sympathomimetic effect, decreasing the interval.

3.4.3 Influence of the BCT on heart rate.

In mammals, cardiac output and lung ventilation can be highly correlated to maximize oxygen uptake (Taylor *et al.*, 1999; Schneider *et al.*, 2012). In many fish there is also a close coordination between cardiac output and gill ventilation frequency partly

driven by oxygen chemoreceptors located in the gills (Smith and Jones, 1978; Jonz *et al.*, 2004) that send afferent inputs to branchio-cardiac reflexes through the central nervous system. In the zebrafish heart the BCT courses along the wall of the ventral aorta and bulbus arteriosus to enter the wall of the ventricle (Stoyek *et al.*, 2015). Though its ultimate origin and destinations have not been traced (Stoyek *et al.*, 2015), it is possible that the BCT may represent a cardiorespiratory pathway that modulates or augments the operation of centrally mediated branchio-cardiac reflexes. When the BCT was electrically stimulated in the whole heart, the net result was an increase in HR. That this response was eliminated in the presence of TIM, but was unaffected by HEX, indicates that these responses likely represented a direct effect of release of adrenergic neurotransmitters from axon terminals at the pacemaker cells. These results bear out previous speculation (Stoyek *et al.*, 2015) that this nerve may represent an alternative input pathway for sympathetic chronotropic control in the zebrafish.

3.4.4 Anatomical relationship of muscarinic and adrenergic receptors with putative pacemaker cells.

The role of M₂R_s in inhibiting cardiac pacemaker discharge is ubiquitous in vertebrates (Lin *et al.*, 2014). In the atria of various mammalian species, including humans, it has been reported that M₂R_s represent the predominant subtype (Peralta *et al.*, 1987; Hulme *et al.*, 1990; Caulfield, 1993). In these species the density of parasympathetic innervation is greatest in the sinoatrial and atrioventricular regions, with receptors mediating negative chronotropic effects by altering pacemaker cell depolarization, potentially through direct inhibition of HCN4 channels (Dhein *et al.*, 2001).

In the present study, considering that the discharge rates of both the SAR and AVR pacemakers were presumably reduced by ACh released from nerve terminals during VSN stimulation and by MUS application, and that these responses were blocked by ATR, it was sought to determine the relationship of M₂R with putative pacemaker cells in the zebrafish heart. In the SAR, there was a high degree of M₂R expression associated with the membrane of Isl1-immunoreactive cells. In the AVR, the M₂R antibody labeled cells in the same region, and with the same apparent morphology as those expressing HCN4. In the atrial myocardium, M₂R label was also associated with myocytes, although label intensity was less than that on the putative pacemaker cells.

β₂ARs are G-protein-coupled receptors that have been shown to mediate positive inotropy and chronotropy in the mammalian heart (McDevitt, 1989; Brodde and Michel, 1999; Ampatzis and Dermon, 2010). In the cat and guinea pig, it was shown that although β₁ARs were the dominant receptor subtype, β₂ARs comprised approximately 25% of the β adrenergic receptors in the atria (McDevitt, 1989; Brodde, 1989). Given higher densities near the SAR in that study, it was postulated that β₂ARs might exert a stronger influence on chronotropy than inotropy (Hedberg *et al.*, 1980; Brodde, 1989; McDevitt, 1989). Previous work in zebrafish has shown that β-adrenoceptors are expressed in the zebrafish heart and exert positive chronotropic effects, although their distribution was not described (Steele *et al.*, 2011).

In the present study, NE released from nerve terminals and application of ISO acted to increase the discharge rates of both the SAR and AVR pacemaker. As TIM blocked both of these responses, the relationship of β₂ARs with putative pacemaker cells in the zebrafish heart was also investigated. Within the SAR, Isl1-immunoreactive cells

had β_2 AR-IR in apparent association with the cell membrane. In the AVR, there was a population of cells in a cluster associated with the bases of the atrioventricular valves that expressed β_2 AR-IR in the same location as HCN4- and M_2 R-positive, phalloidin-negative cells. In the atrial myocardium, β_2 AR-IR was associated with myocytes, although immunoreactivity was sparser than on the putative pacemaker cells. It should be noted that although the adrenergic agents used in this study act across the spectrum of β AR subtypes, and that β_2 ARs represent only a portion of adrenergic receptors, there are no well characterized antibodies for other β AR subtypes for use in zebrafish. Therefore further investigations of the roles of other β AR subtypes in this system should be investigated pharmacologically; confirmation of the anatomical distribution of these receptors must await the availability of suitable antibodies.

In mammalian literature there is considerable debate concerning the roles of the “membrane clock” (driven by the funny current, which is mediated by HCN channels) and the “calcium clock” (driven by spontaneous calcium release from the sarcoplasmic reticulum activating the sodium-calcium exchanger) in the generation and regulation of HR (Lakatta and DiFrancesco, 2009; Lakatta *et al.*, 2009). Previous studies have shown the involvement of both calcium clock (Llach *et al.*, 2011) and membrane clock mechanisms (Warren *et al.*, 2001; Lin *et al.*, 2015) in determining HR in the zebrafish. In the *slo mo* zebrafish mutant, which has a defect in the HCN4 channel, a significant decrease in HR was observed (Warren *et al.*, 2001), which is similar to that observed with HCN4 channel antagonists (Lin *et al.*, 2015). Although the expression of HCN4 channels in the cell membrane and the transcription factor *Isl1* in the cytoplasm have been previously used as anatomical markers for pacemaker cells (Tessadori *et al.*, 2012;

Weinberger *et al.*, 2012; Li *et al.*, 2015), complete identification of this cell population in the zebrafish heart awaits direct electrophysiological evidence. Given that the population of HCN4-positive cells labeled in the zebrafish heart appeared in the appropriate locations, and also displayed intense β_2 AR and M_2 R immunoreactivity that correlated with the chronotropic responses to autonomic activation, it is highly probable that these cells are, in fact, pacemakers.

3.4.5 Conclusions.

The traditional view of a reciprocal and antagonistic system of parasympathetic (inhibitory) and sympathetic (excitatory) innervation, with limited interactions at the level of the heart, is giving way to the recognition of the ICNS as a major site of integration of neural control of cardiac effectors (Armour, 2008; Rajendran *et al.*, 2015). The current study characterizes the properties of neural control of the sinoatrial and atrioventricular pacemakers, as well as the chronotropic responses to stimulation of the cardiac vagal rami and to exogenous pharmacological agents in the isolated, innervated zebrafish heart. Further, putative pacemaker cells in both the SAR and AVR have been shown to express M_2 R, and β_2 AR. In studying pacemaker function in the zebrafish heart, this represents a first step toward understanding the integrative autonomic control of heart rate. It is now possible to utilize this model to identify specific relationships between subpopulations of intracardiac neurons and their targeted effectors to discover basic mechanisms of neural integration involved in modulating cardiac chronotropy.

Figure 3.1. Chronotropic responses to vagosympathetic nerve stimulation and autonomic agents. **A:** *In vitro* view of the heart showing positions of bipolar electrodes recording atrial (aE) and ventricular (vE) surface electrocardiograms (ECG). Scale bar represents 1 mm. **B:** Typical ECG record from atrium (top) and ventricle (bottom) in the same heart before, during and after simultaneous stimulation of cardiac VSN rami (bar below trace). Elongation of R-R interval (bradycardia) during the stimulus period was followed by post-stimulus reduction of R-R interval (tachycardia) relative to pre-stimulus interval. **C:** Proportional change in R-R interval in response to stimulation of the left (LX) or right (RX) VSN, or simultaneous stimulation of both nerves (SIM). * $P < 0.05$ vs. control by one-way ANOVA with Tukey's *post hoc* test; $n=8$ for each. Dashed lines represent pre-intervention R-R interval. **D-F:** Effects of cholinergic and adrenergic agents on R-R interval. **D:** R-R interval increased in response to LX and RX VSN stimulation and local application of nicotine (NIC). Effects of VSN stimulation and NIC application were eliminated during exposure to hexamethonium (HEX, grey shading). **E:** Response to VSN stimulation and local application of muscarine (MUS) were eliminated by atropine (ATR, grey shading). **F:** Isoproterenol (ISO) decreased R-R interval. Exposure to timolol (TIM, grey shading) blocked ISO response without affecting VSN-induced responses. * $P < 0.05$ vs. control by one-way ANOVA with Tukey's *post hoc* test; $n=8$ for each of LX/RX/SIM and $n=6$ for each of NIC/MUS/ISO.

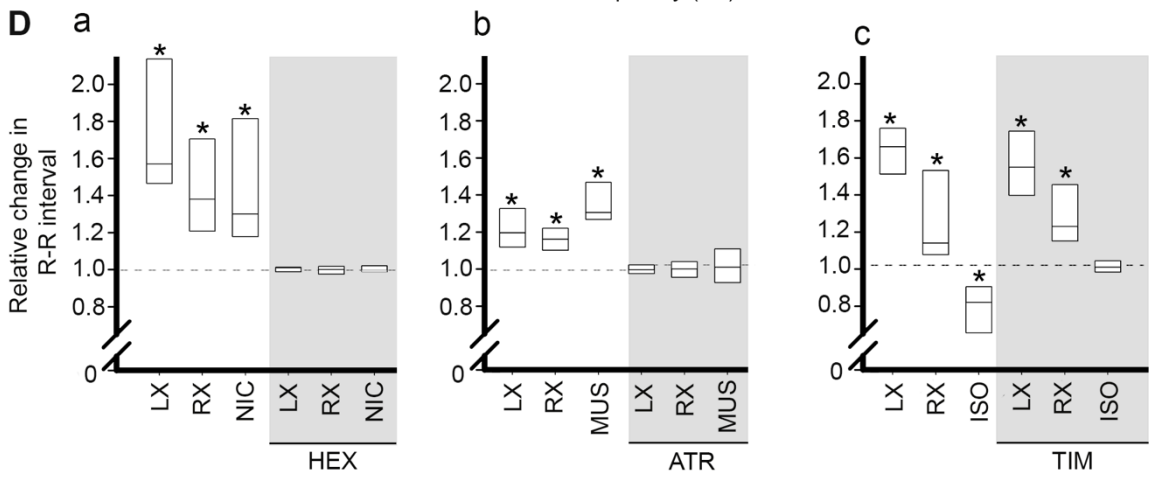
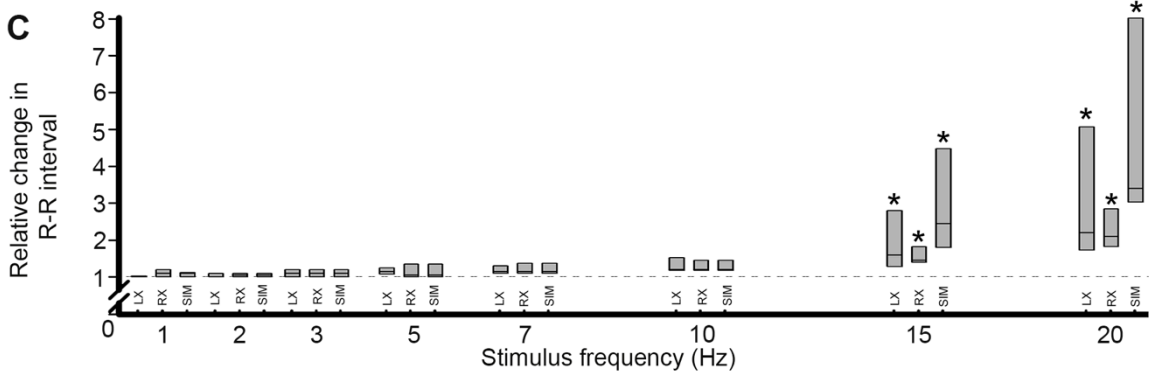
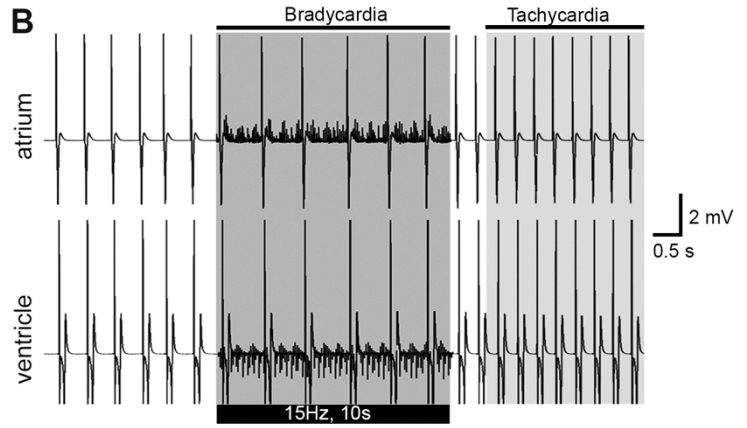
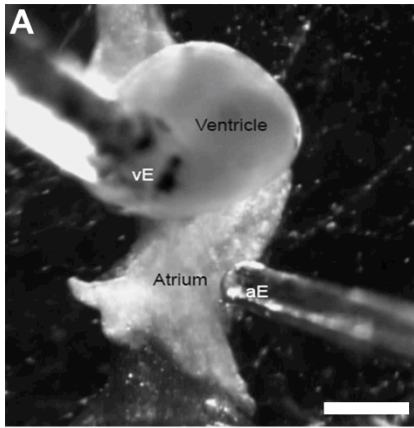


Figure 3.2. Atrioventricular dissociation, modulation of AVR activity, and stimulation of branchiocardiac nerve trunk. **A:** Sample atrial (top trace) and ventricular (bottom trace) ECG traces in intact heart. Inset shows atrioventricular delay in one cardiac cycle at a faster recording speed. **B:** Surgical dissociation of AVR from the SAR caused desynchronization of the chambers and a slowed ventricular rate. **C:** Nicotine (NIC) increased the ventricular R-R interval; this response was blocked by hexamethonium (HEX, grey shading). Isoproterenol (ISO) caused the ventricular R-R interval to decrease; this effect was blocked by timolol (TIM, grey shading). **D:** Electrical stimulation of the branchiocardiac nerve trunk (BCT) in the intact heart reduced R-R interval. This response was eliminated by timolol (TIM, grey shading), but not hexamethonium (HEX, grey shading). *P < 0.05 vs. control by paired Student's *t*-test; *n*=6 for each group.

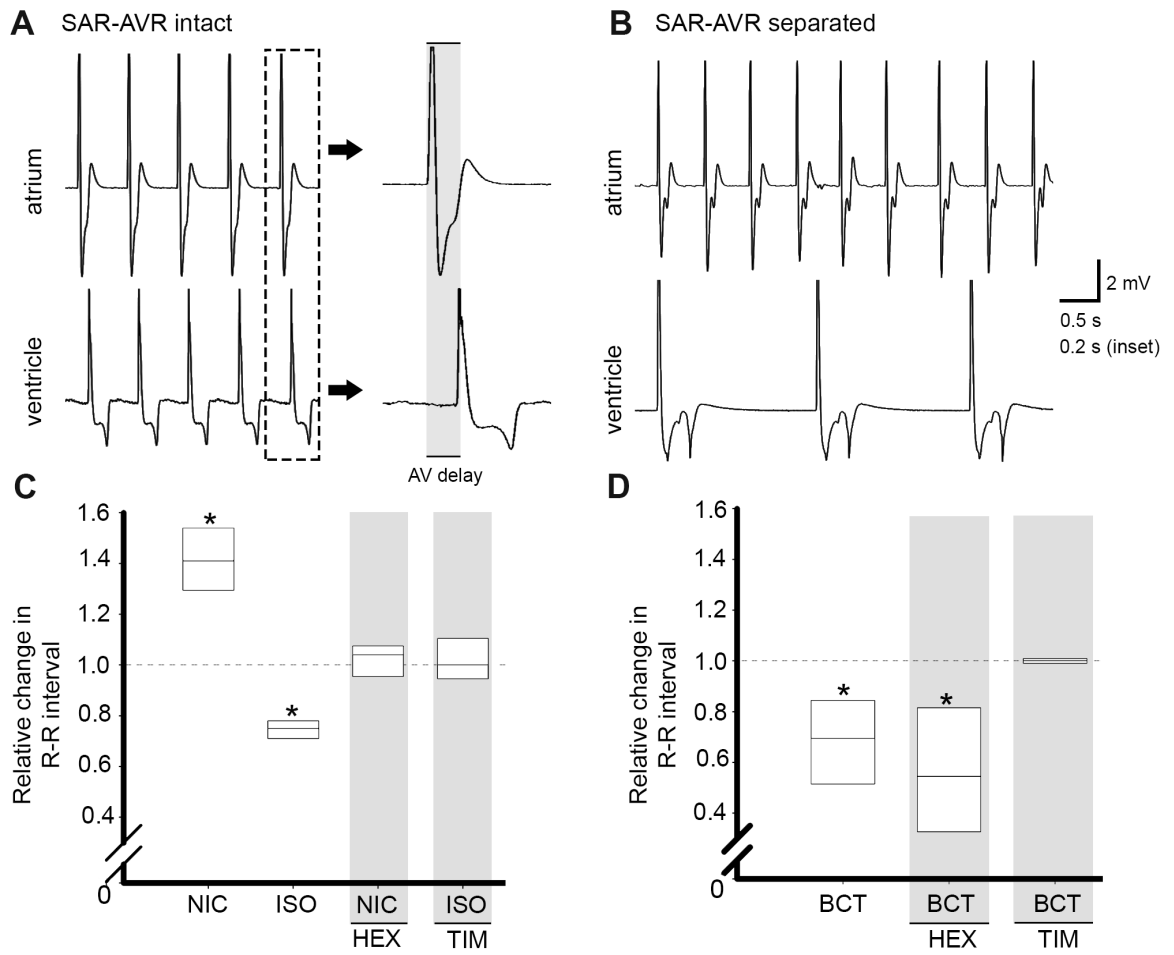


Figure 3.3. Optical mapping of origin and spread of excitation in atrium and ventricle. **A-E:** Sequence of images showing progression of depolarization from the region of origin in the SAR (* in panel A) into the atrial wall (a, panels B and C) across the atrioventricular junction (D) and into the ventricle (v, panel E). Arrows indicate the direction of propagation of the main excitation wavefront. **F:** Isochronal map (isochrones = 8 ms) summarizing the regional spread of electrical activity from the site of origin (*) in the SAR, across the atrium, and into the ventricle. Colour scale represents time to activation from initial excitation. **G-J:** Sequence of images showing progression of depolarization during simultaneous stimulation of both cardiac VSN rami, demonstrating a shift in the site of origin toward the AVR (Arrows indicate direction of propagation). The site of first depolarization occurred at the AVR (* in panel G), followed by multiple foci outside of the SAR (* in panel H) which depolarised the atrium (I). After a delay at the AVR (I) the depolarising activity invades the ventricle (J). **K-M:** Sequence of images showing progression of depolarization from the AVR into the ventricle after surgical isolation from the atrium (K). The main excitation wavefront initiates in the AVR (L) and propagates through the ventricle (M). Scale bars represent 1 mm (A- J), and 50 μ m (K-M).

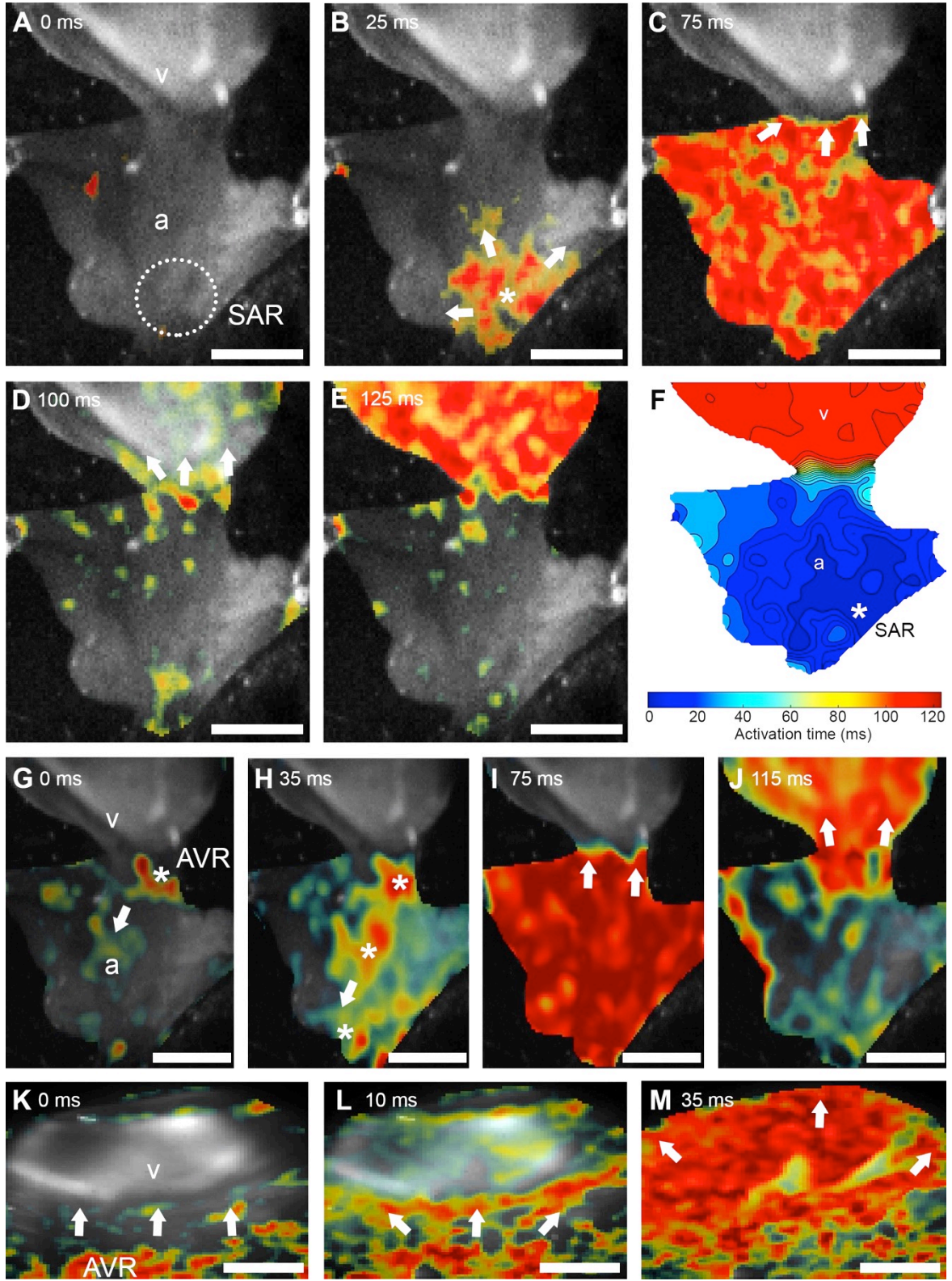


Figure 3.4. Regional distribution of putative pacemaker cells and muscarinic receptors detected by immunohistochemistry. **A:** Schematic showing the cardiac regions: atrium, a; atrioventricular region, AVR; bulbus arteriosus, ba; sinoatrial region, SAR; sinus venosus, sv; ventricle, v. Boxes indicate the locations of images in panels B-H. **B-D:** Organization of putative pacemakers and associated muscarinic receptors in SAR. **B:** Low-magnification overview shows HCN4-immunoreactive (-IR) cells (red) embedded in musculature (Phal, green) surrounding the sinoatrial valves. **C:** Islet-1 (Isl1, blue) co-localized with cells expressing HCN4. **D:** Type 2 muscarinic receptors (M₂R) appeared to be associated with the membrane of Isl1-IR cells. **E:** Putative pacemaker cells expressing HCN4 were present in AVR, embedded in musculature (Phal) of atrioventricular valves. **F:** Type 2 muscarinic receptors (M₂R) associated with the membrane of cells of similar morphology to HCN4-IR cells in the AVR. **G-I:** M₂R were more plentiful in the compact and trabecular myocardium (Phal) of the atrium (G, H; arrows) than in the ventricular trabecular myocardium (I; arrows). Scale bars represent 200 μm (B), 40 μm (C), 20 μm (D), 50 μm (E-I).

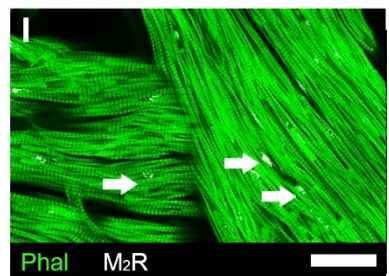
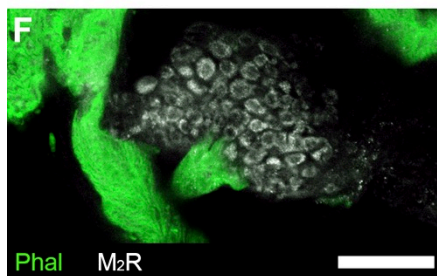
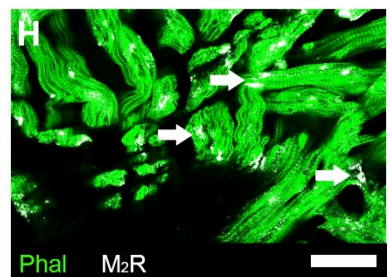
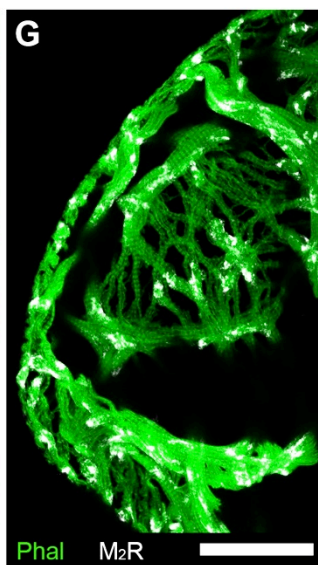
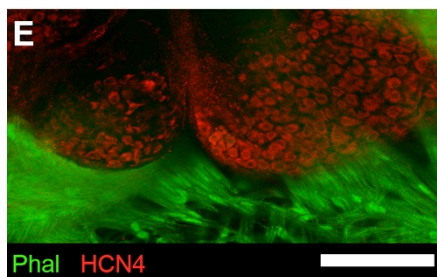
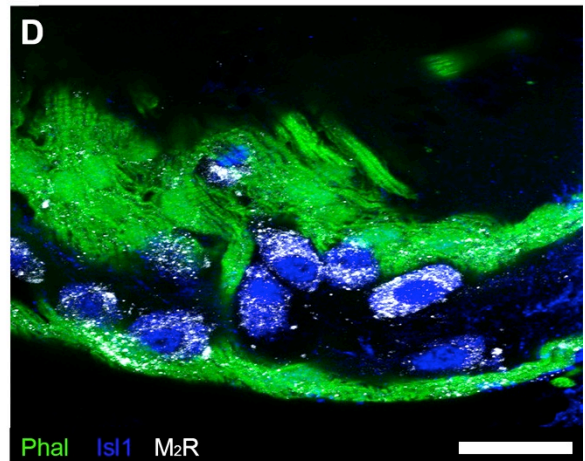
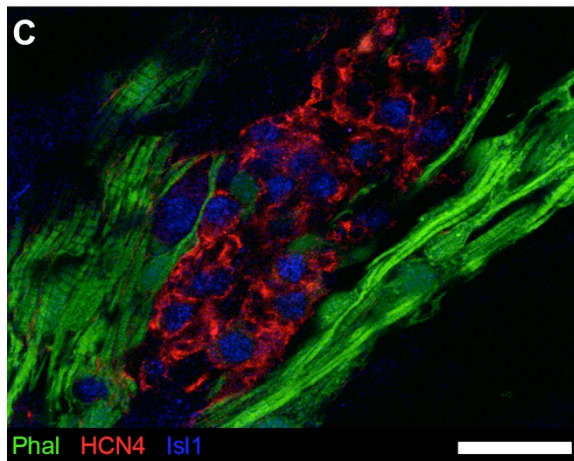
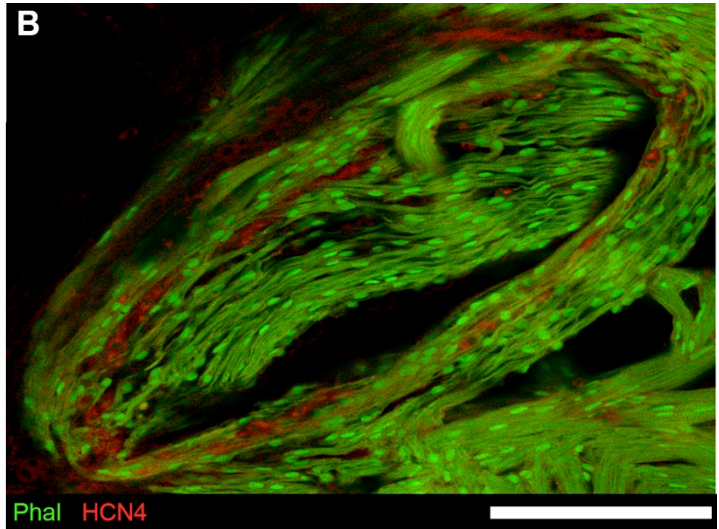
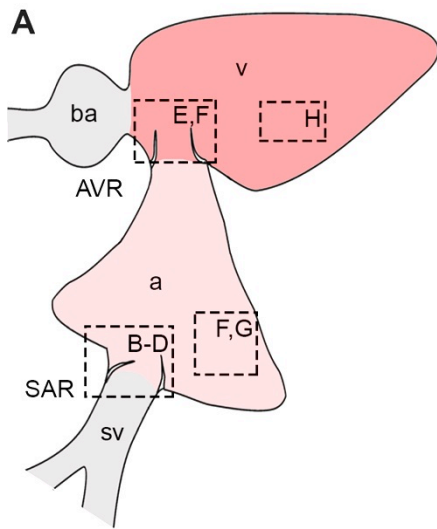
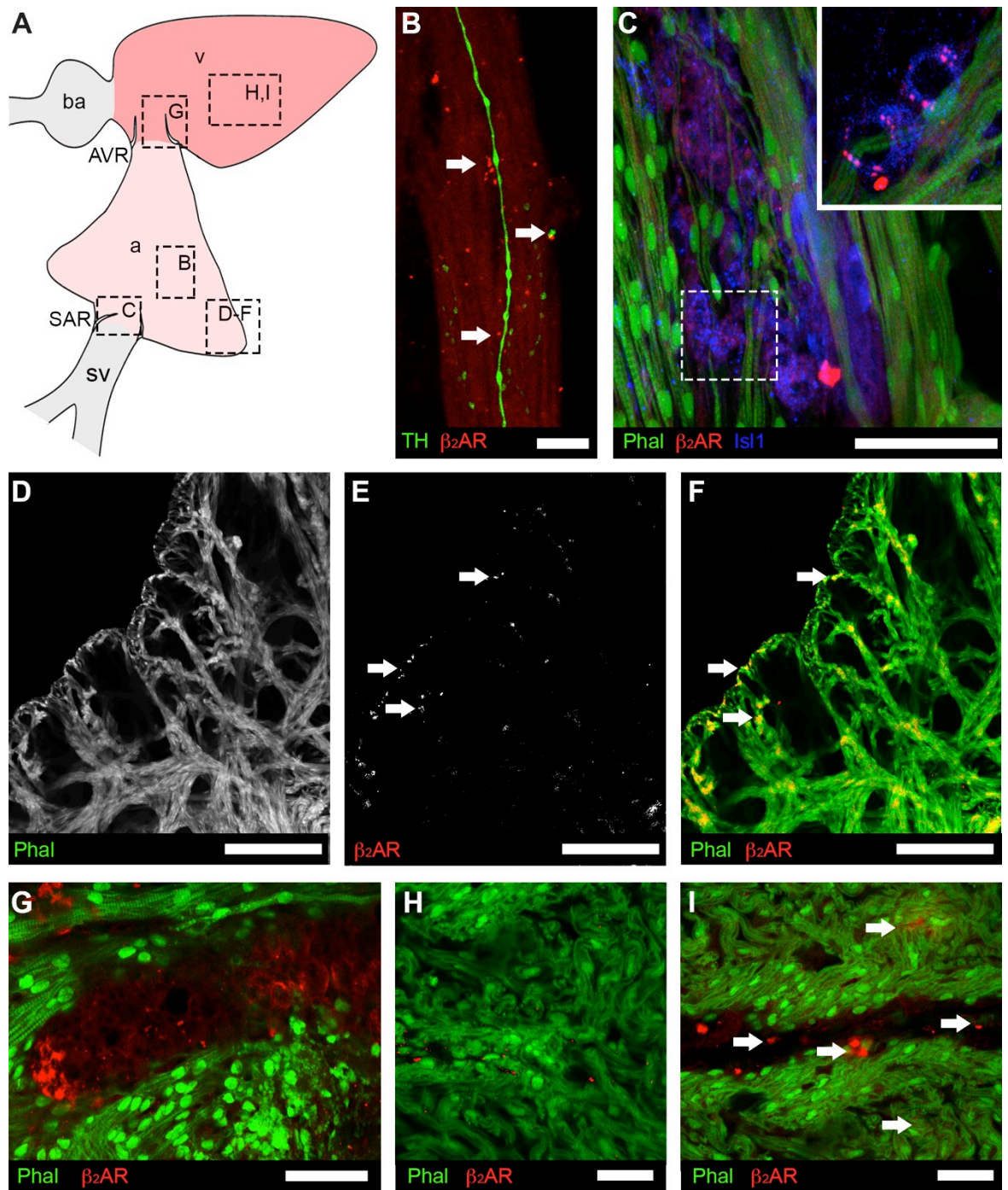


Figure 3.5. Regional distribution of β_2 AR receptors associated with putative pacemaker cells and myocardium. **A:** Schematic showing the cardiac regions; boxes indicate the locations of images in panels B-I. **B:** β_2 AR (red) were detected adjacent to TH-positive innervation (green) in the atrial wall. **C:** In the sinoatrial region Isl1 (blue) was co-localized with cells expressing β_2 AR. Inset shows a single confocal section from boxed region at a higher magnification. **D-F:** β_2 AR-IR was detected in the compact and trabecular myocardium (Phal) of the atrium (E, F; arrows). **G:** β_2 AR -IR associated with the membrane of cells of similar morphology to HCN4-IR cells in the AVR. **H, I:** β_2 AR -IR was more plentiful in the compact myocardium (Phal) of the ventricle than in the atrium, especially proximate to coronary vasculature (I). Scale bars represent 10 μ m (B), 40 μ m (C), 20 μ m (D-F), 20 μ m (G-I).



CHAPTER 4

EFFECTS OF VAGAL NERVE STIMULATION ON PACEMAKER ACTIVITY AND INTRACARDIAC NEURONAL ACTIVATION IN THE ZEBRAFISH

4.1 Introduction

To date the topographical organization axons of within the left and right VSN and their intracardiac targets and functions have not been resolved in any vertebrate species. In the mammalian heart, populations of efferent vagal preganglionic neurons in the dorsal motor nucleus and the nucleus ambiguus project to anatomically separate ganglionic targets in the ICNS (Irisawa, 1978; Chi *et al.*, 2008; Nemtsas *et al.*, 2010; 16). In these studies, axons from cells in each vagal nuclei course in both vagi, but the lateral organization of these projections were not reported. In the cat heart, axons from left and right vagal preganglionic neurons have been shown to target different subpopulations of intracardiac neurons (Akiyama and Yamakazi, 2001).

In the zebrafish, it has been shown that axon terminals from the left and right cardiac vagosympathetic nerves (VSN) are differentially distributed within the sinoatrial region (SAR; Stoyek *et al.*, 2015), suggesting that these inputs may activate different subpopulations of intracardiac neurons (ICN), some of which target nearby pacemaker cells. In a subsequent study, it was shown that activation of individual VSN in zebrafish evoked differing effects on heart rate (HR), with simultaneous activation of both VSN altered HR in a manner suggesting that the effects of activation of both VSN was summative (Stoyek *et al.*, 2016). Taken together, this anatomical and functional evidence suggests that axons in the left and right VSN likely target different subpopulations of cardio-inhibitory ICNs with parallel chronotropic functions.

In order to address this issue, the detection of changes in the expression of the protooncogene cFOS, as well as phosphorylated extracellular signal-regulated kinase (pERK), were used as indicators of subpopulations of vagally activated ICNs in the

present study. The use of cFOS for the immunohistochemical detection of neuronal activation has been established in the brain and central nervous system (CNS) of mammals and teleosts (Grenberg *et al.*, 1986; Herdegen *et al.*, 1993; Bosch *et al.*, 1995; Hua *et al.*, 2004; Lau *et al.*, 2011). The activation of *c-fos* is thought to be stimulated by the binding of a neurotransmitter to excitatory membrane receptors on neurons, and is therefore termed an immediate early gene (Gao and Ji, 2009). While cFOS offers the benefits of low basal levels of expression and dramatic increases in expression following neuronal activation (see review in Gao and Ji, 2009), there exist questions regarding the level of stimulus and time required to induce activity (Bosch *et al.*, 1984; Randlett *et al.*, 2015).

In response to neuronal depolarization, calcium influx activates the Ras (rapidly activated sarcoma protein)-ERK pathway, leading to the phosphorylation of ERK (Randlett *et al.*, 2015). Recent studies have shown rapid, robust neuronal pERK activity in response to stimuli (see review in Gao and Ji, 2009; Randlett *et al.*, 2015). This is the first time these markers have been used in the heart to investigate activation of discrete populations of intracardiac neurons.

In the mammalian heart it has been well established that vagal input not only causes bradycardia, but also influences the locus of the operational pacemaker site (Meek and Eyster, 1913; Boineau *et al.*, 1988; Shibata *et al.*, 2001; Fedorov *et al.* 2006). It has been suggested that such shifts in pacemaker site could result from the differential activation of neurons within the ICNS, some of which target pacemaker cells (Meek and Eyster, 1913; Bouman *et al.*, 1968; Boineau *et al.*, 1988). In the zebrafish heart, simultaneous stimulation of the cardiac VSNs induces bradycardia and a shift in the pattern

of initiation and propagation of electrical activity (Stoyek *et al.*, 2016). Thus, in both zebrafish and mammalian hearts, when vagal tone is elevated and bradycardia occurs, there may be an accompanying shift of the primary pacemaker locus. This represented the first report of a neutrally mediated shift in pacemaker locus in the zebrafish heart (Stoyek *et al.*, 2016), and indicates that this powerful system for cardiac control is conserved from fish to mammals. In the current study it was sought to determine the capability of graded VSN drive on pacemaker locus using a range of stimulus frequencies that fell within the range of tonic vagal nerve discharge in intact fish (Taylor *et al.*, 2009; Sandblom and Axelsson, 2011). Taken together the results of this study will begin to identify the organization of ICNs that receive direct extrinsic input, and describe the of such on the location of the pacemaker itself, more comprehensively than has been previously possible in the mammalian heart.

4.2 Methods

4.2.1 Animals.

A total of 42 adult, AB strain zebrafish (12-18 months post-fertilization; 33 ± 5 mm standard body length) of both sexes were used in this study. Institutional approval for animal use in this study was obtained from the Dalhousie University Committee on Laboratory Animals.

4.2.2 Heart isolation.

Zebrafish were anaesthetised in a buffered solution (pH 7.2) of tricaine (MS-222; 1.5 mM) in tank water (28.5°C) until opercular respiratory movements ceased and the

animals lacked response to a spinal pinch with forceps. A ventral midline incision was made through the body wall to expose the heart, and a block of tissue encompassing the ventral aorta, ventricle, atrium, sinus venosus and ducts of Cuvier (containing the cardiac VSN rami) was then removed for whole-mount immunohistochemistry or *in vitro* recordings.

4.2.3 VSN stimulation for assessment of ICN activation by *cFOS*.

Left or right VSN ($n = 6$ each) were stimulated with bipolar wire electrodes driven by a constant-current stimulator (S88; Grass Instruments, Quincy, MA, USA) that delivered trains of rectangular pulses (pulse duration 500 μ s; train duration 10 s, pulse frequency 20Hz, stimulus current 300 μ A) every 3 minutes for a total of 20 stimulation periods. To eliminate the possibility of pERK-IR in neurons other than those that were activated by VSN stimulations, hearts were immediately (>30 s) transferred to fixative (see below) following each experiment.

4.2.4 VSN stimulation for assessment of ICN activation by *pERK*.

Left or right VSN ($n = 6$ each) were stimulated with bipolar wire electrodes driven by a constant-current stimulator (S88; Grass Instruments, Quincy, MA, USA) that delivered trains of rectangular pulses (pulse duration 500 μ s; train duration 10 s, pulse frequency 15Hz, stimulus current 300 μ A) every 1 minute for a total of 5 stimulation periods. To eliminate the possibility of pERK-IR in neurons other than those that were activated by VSN stimulations, hearts were immediately (less than 30 s) transferred to fixative (see below) following each experiment.

4.2.5 *cFOS* and *pERK* immunohistochemistry.

The general procedures used for immunohistochemistry in this study were similar to those previously described (Stoyek *et al.*, 2015). Whole hearts were labelled with antibodies against *cFOS* (1:100) or *pERK* (1:100). In all experiments antibodies against acetylated tubulin (AcT, axons) and human neuronal protein C/D (Hu, neuronal somata) were used in combination to show the general innervation of the heart (see Appendix B). After exposure to primary antibodies, preparations were incubated with appropriate secondary antibodies conjugated to AlexaFluor 488, 555, or 647 fluorophores washed in PBS and placed in Scale CUBIC-1 clearing solution (Susaki *et al.*, 2014) overnight at room temperature with gentle agitation. Processed specimens were examined as whole-mounts. Counts of ICNs expressing *cFOS*- or *pERK*-like-immunoreactivity (LIR) were performed using Fiji software; data are shown as percent of ICNs that were immunoreactive for *cFOS* or *pERK* compared to the total ICN number as estimated by AcT-Hu immunoreactivity.

4.2.6 *Controls*.

Both *cFOS* and *pERK* antibodies used in this study have previously been used in zebrafish (Randlett *et al.*, 2015; Yabuki *et al.*, 2016). As a control for basal *cFOS* or *pERK* expression, subsets of hearts were fixed immediately after isolation ($n = 6$), or were isolated put in the bath for the same duration as the above experiments without receiving VSN stimulation ($n = 6$), before being fixed and processed for immunohistochemistry. For all antibodies used in this study, tissues for negative controls were processed as outlined

above, except that either the primary or secondary antibody was omitted. In all trials this eliminated detection of histofluorescence.

4.2.7 Voltage optical imaging.

Whole hearts ($n = 6$) were isolated in a 5 mL chamber filled with zebrafish saline and allowed to equilibrate for 30 min (25°C). During this time, the heart was exposed to a voltage-sensitive dye (10 μ M di-4-ANBDQPO) in the perfusate for 10 min, and then washed with fresh saline containing excitation-contraction uncoupler blebbistatin (10 μ M) to eliminate motion artifacts during optical recordings. Blebbistatin was present for the duration of the experiment. For imaging experiments, two controls were run ($n = 3$ each): 1) hearts were isolated and pacemaker initiation site was monitored in the bath every 30 min for 3 h, a period longer than any experiment in this study; 2) hearts were isolated, VSN stimulations were performed every 2 minutes for 40 minutes, and pacemaker site was observed after every stimulation.

As an index of changes in conduction, the time from initial breakthrough to full depolarization of the sinoatrial regions for three successive cycles was averaged from the recordings using custom Matlab routines. To map changes in the site of initial sinoatrial depolarization, binary images were created for three successive cycles and the initiation site averaged. An oval was fit to the image to encompass the sinoatrial valve region and the binary images were normalized (rigid transformation) to a brightfield exemplar image of the sinoatrial region for mapping using Fiji software.

4.2.8 VSN stimulation for assessment of pacemaker shift.

Left and right VSN trunks were stimulated with bipolar wire electrodes delivering trains of rectangular pulses (pulse duration 0.5ms; train duration 10 s, pulse frequency 1-15 Hz, 300 μ A). A minimum of 2 minutes was allowed for recovery of the preparation between VSN stimulations. To control for the possibility that repeated VSN stimulation alone might alter the pacemaker initiation site over time, a subset of hearts ($n = 3$) was sampled for 30 minutes following the last VSN stimulation. .

4.2.9 Pharmacological blockade.

Hexamethonium (10 μ M) was dissolved in saline the day of experiments and put in the bath 15 minutes prior to recordings.

4.2.10 Data presentation.

Numerical values were expressed as mean \pm 1 standard error of the mean (SEM). One-way ANOVA with a Tukey's *post hoc* was used to detect significant differences among means. P values \leq 0.05 were considered significant.

4.3 Results

4.3.1 ICN activation as revealed by cFOS-like immunoreactivity.

cFOS-like-immunoreactivity (LIR) was observed within the somata and processes of ICNs within the sinoatrial plexus (SAP) ipsilateral to each VSN (Figures 4.1-4.2); ICN distribution is summarized in Figure 4.3. In hearts in which the left VSN was stimulated, cFOS-LIR ICNs were located within the ganglia associated with the junction of the left VSN (LXG) and the SAP (Figure 4.2D,E). In hearts in which the right VSN was

stimulated, ICNs within the ganglia associated with the junction of the right VSN (RXG) and the SAP expressed cFOS-LIR (Figure 4.3D,E) cFOS-LIR was not observed outside the vagal ganglia ipsilateral to stimulation, or in the dorsal or ventral sinoatrial plexus ganglia in any of the hearts examined. In control hearts not receiving VSN stimulation, cFOS-LIR was not observed supporting that ICNs expressing cFOS-LIR were the result of activation by VSN stimulation.

4.3.2 ICN activation as revealed by pERK-like immunoreactivity.

pERK-LIR was observed within the somata and processes of ICNs, and was widely distributed within the SAP ipsilateral to VSN (Figures 4.1-4.2); ICN distribution is summarized in Figure 4.3. In hearts in which the left VSN was stimulated, ICNs within the LXG expressed pERK-LIR (Figure 4.2H,I). In hearts in which the right VSN was stimulated, ICNs within the RXG expressed pERK-LIR (Figure 4.3H,I). In contrast with results of the activation experiments investigating cFOS-LIR, pERK-LIR was also observed in ganglia of the SAP contralateral to the stimulated VSN. In hearts in which the left VSN was stimulated ICN within the RXG were found to express pERK-LIR, while in those hearts in which the right VSN was stimulated ICNs within the LXG expressed pERK-LIR. In all of the hearts examined pERK-LIR was not observed in the dorsal or ventral regions of the SAP. In control hearts put in the bath, but not receiving VSN, pERK-LIR was minimal ($3 \pm 1\%$ of total ICN in 4 of 6 hearts) or not detected (2 of 6 hearts), supporting that ICN expressing pERK were the result of activation by VSN stimulation.

4.3.3 Pacemaker activity in vitro.

Basal heart rate (rate at the start of each experiment after isolating the heart) was 104 ± 7 (range 82-144) and the effects of left and right cardiac VSN stimulation were similar to those previously reported in the isolated zebrafish heart (Stoyek *et al*, 2016). In preliminary experiments of hearts observed over 3 h there was $< 10\%$ change in heart rate from the basal rate, and there was no change in the spontaneous pacemaker initiation site. In preliminary experiments in hearts that had VSN stimulations performed periodically, there was no detectable change in either spontaneous pacemaker site or the chronotropic responses to VSN over time (data not shown). Thus, the next experiments in which the cardiac VSN rami were stimulated at varying frequencies, focused on any changes observed within the sinoatrial region, which were assumed to be resultant from ICNS activity on ICNs and effector cells within this region.

4.3.4 Effects of graded VSN stimulation on pacemaker activity within the sinoatrial region.

Shifts in pacemaker initiation site during periods of electrical stimulation of either the left (Figure 4.4) or right (Figure 4.5) cardiac VSN were observed to occur with a stimulation frequency as low as 1 Hz. Overall it was found that increasing the stimulation frequency up to 15 Hz resulted in highly variable shifting of the pacemaker initiation site within the sinoatrial region with no discernable trends in stimulus frequency-related changes in localization. Within the 8 hearts tested a variety of patterns was observed: 1) three hearts in which a single focal origin of activity was found to change to multiple focal origins, 2) two hearts in which multiple focal origins of initiation were observed prior to VSN that changed to a single focal origin of activity during VSN, 3) two hearts in which

there was observed a shift ipsilateral to the stimulated VSN, 4) two hearts in which there was observed a shift contralateral to the stimulated VSN, 5) three hearts in which an observed shift resulted in movement of the initiation site toward the atrial myocardium, 6) two hearts in which an observed shift resulted in movement of the initiation site towards the sinus venosus, and 7) one heart in which the origin of electrical activity was found to show minimal change in response to VSN stimulation. Within these patterns there were no trends observed with with greater VSN stimulation frequency, or specifically with the stimulation of either the right or left cardiac VSN. In fact, the shifts observed at a given frequency could be different from those observed at a high or lower stimulation frequency delivered to the same heart. Overall, shifts observed during either left or right VSN stimulation in the same heart at the same frequency appeared qualitatively similar. In all hearts observed, the variability of pacemaker initiation site was not observed during left or right VSN in the presence of hexamethonium (Figures 4.4 and 4.5).

4.4 Discussion

The first aim of this study was to investigate the organization of ICNs that are activated by VSN input, using detection of changes in the expression of cFOS- and pERK-LIR. Using these markers it was possible to identify and map distinct populations of ICNs activated in response to VSN stimulation. To date, this represents the first time that cFOS and pERK have been used to detect neuronal activation within the heart. The second aim of the present study was to determine the detailed effects of vagally-mediated pacemaker site shift, recently described to occur in zebrafish (Stoyek *et al.*, 2016), and whether these effects may correlate with patterns of activated ICNs. In the present study, graded VSN

stimulation in the isolated zebrafish heart resulted in a variable shifting of the primary site of initiation within the sinoatrial region. The implications of these findings are discussed below.

4.4.1 ICN activation patterns revealed by cFOS- and pERK-LIR.

Though much is known of the regional innervation of mammalian hearts, there exists no comprehensive understanding of the topographical organization of the ICNs within this system. There exist populations of ICNs, distributed throughout the heart, which although located in one region of the heart, may influence cardiac regions at a distance, or to which there has been little to no known function ascribed (Gray *et al.*, 2004). Further complicating this picture are reports that the level of individual ICN activity within these ganglia could be modulated by extrinsic inputs, and that some ICNs simply did not have extrinsic inputs (Smith 2001; Gray *et al.*, 2004; Gibbons *et al.*, 2012; Beaumont *et al.*, 2013; Beaumont *et al.*, 2015). It has been hypothesized that the latter class represents local circuit, or processing, neurons within the ICNS (see Armour, 2008).

In the current study the expression patterns of cFOS- and pERK-LIR that were observed within the ICNS showed subtle differences from each other. Generally, cFOS-LIR was limited to ICNs in the vagal ganglia ipsilateral to the VSN that was stimulated, while pERK-LIR was associated with ICNs in both ipsilateral and contralateral vagal ganglia. A possible explanation for this observation is the differing stimulation paradigms required to induce the expression of cFOS and pERK in the hearts tested. The temporal responses of both cFOS and pERK, have been reported as variable, though the general trend emerging is that given similar stimulus intensities pERK will be expressed more

rapidly than will cFOS (Hua *et al.*, 2004; Randlett *et al.*, 2015). As such, the stimulation paradigm used in cFOS experiments involved more VSN stimulations over a longer time than did that used in experiments aimed at detecting pERK. It is tempting to speculate that differences in expression, specifically the expression of pERK in contralateral ICNs, could be the result of rundown or changes in firing patterns of those ICNs with repeated stimulations as has been seen in decentralized mammalian ICN (Smith *et al.*, 2001).

That the expression of both cFOS- and pERK-LIR was restricted largely to the vagal ganglia ipsilateral to VSN suggests that the current paradigm likely resulted only in activation of ICNs with direct inputs. The detection of cFOS- and pERK-LIR, as performed in this study, does not permit the distinction between neurons being directly activated by VSN stimulation from those ICNs that may have been activated through indirect pathways. While it has not been described with cFOS, intensity dependent reactivity has been described for pERK (Gao and Ji, 2009; Randlett *et al.*, 2015). In preliminary experiments it was found that the current stimulation paradigms were just beyond the threshold of that which would induce cFOS- or pERK-LIR in ICNs. Thus, another explanation could simply be that varying the stimulation or frequency of VSN stimulations could result in more similar patterns of detected activation for cFOS- and pERK-LIR.

In mammals cFOS expression is present transiently in the cytoplasm, before being rapidly taken up to the cell nucleus (Morgan and Curran, 1991). In teleosts the cFOS-like reaction is known to be distinct; the localization of immunoreactivity is entirely outside the nucleus, and was described throughout the cytoplasm of the soma and primary dendrites (Bosch *et al.*, 1995). As the polyclonal cFOS antibody utilized was directed against a

conserved region of a mammalian FOS protein, and the nature of the protein recognized in fish is unknown, immunoreactivity for cFOS is referred to as cFOS-like (Bosch *et al.*, 1995). Thus, the cFOS-LIR throughout ICN soma and processes observed within this study agrees with previous reports. It is currently unknown if this is due to cFOS antibody being unable to access cFOS within the nucleus, or if the antibody is recognizing a protein other than FOS (Bosch *et al.*, 1995). Both cFOS and pERK are constitutively expressed within the neurons of the CNS, which can complicate determination of neurons responding to a given stimulus (see review Gao and Ji, 2009; cFOS, Bosch *et al.*, 1995; pERK, Randlett *et al.*, 2015). This did not seem to be the case in the current study, as no immunoreactivity for cFOS was detectable in control hearts. Expression of pERK, which is known to occur in all cells, was minimal in controls, and constitutive levels are unlikely to have affected the counts of activated ICNs. Thus, reactivity for either marker is taken to indicate activation directly resulting from VSN stimulation. Though the results of this study show that both cFOS and pERK, detected immunohistochemically, can be used to identify activated neurons within the zebrafish heart, given the abundance of transgenic strains, the results of the current study should be used to guide future works using activity dependent reporters (e.g. calcium or voltage sensitive) with targeted expression in ICNs.

4.4.2 Pacemaker site changes in response to VSN stimulation.

Brown and Eccles (1934) first showed in the cat that brief vagal stimulations resulted in complex heart rate changes, potentially explained by pacemaker shift (Shibata *et al.*, 2001). That autonomic activity has the ability to induce shifts in pacemaker site has subsequently been reported in several mammalian models and humans (e.g. Boineau *et al.*,

1968; Opthof, 1988; Shibata *et al.* 2001; Fedorov *et al.*, 2006). Previous anatomic reports of the patterns of extrinsic inputs within the ICNS of zebrafish have showed that extrinsic axons form distinct terminal fields in discrete regions of the sinoatrial region rich with cholinergic ICNs (Stoyek *et al.*, 2015). In teleosts bradycardia has been shown as the dominant effect of activation of the cardiac rami acting through cholinergic pathways (Saito, 1973; Stoyek *et al.*, 2016), and putative pacemaker cells have been shown to express muscarinic receptors, indicating that these effector cells could respond to endogenously released acetylcholine (Steel *et al.*, 2009; Stoyek *et al.*, 2016). From this it could be hypothesized that activation of individual cardiac VSN rami could activate distinct regions of ICNs and effector cells; the most likely result would be activation of inhibitory cholinergic pathways. Given that the comparatively simple sinoatrial pacemaker of the zebrafish displays robust responses to autonomic input, and that the entire ICNS is visible in the whole heart, it was sought to investigate if the identified populations of ICNs, responding to extrinsic inputs, influenced alterations in sinoatrial activity in a predictable manner.

In the zebrafish it was found that the site of initiation of the sinoatrial node became highly variable during increased vagal drive. In preliminary studies in which the same heart was observed over a 3 h period in the absence of VSN stimulation, the pacemaker initiation site remained relatively stable. However during periods of VSN stimulation, pacemaker initiation could 1) move ipsilateral or contralateral to the stimulated VSN, 2) variable changes between single- and multi-focal origin or 3) could show no detectable shift. A limitation in the current study is the qualitative description of the pacemaker shift events: that the points of origin were highly variable; that there were

no distinct spatial trends with stimulus frequency, and that when there were multiple foci of origin the variability of averaged position of origin was high.

As the results of previous work has shown that cholinergic effects dominate the cardiac response to VSN stimulation in the zebrafish (Chapter 2; Stoyek *et al.*, 2016), it was next investigated whether blockade of this pathway would affect the pacemaker initiation site variability. The results of experiments in which hexamethonium was used to block cholinergic neurotransmission within the intracardiac nervous system supported the hypothesis of a neural origin to the altered pacemaker activity during VSN stimulation: the site of origin was stabilized during blockade. Taken together these results suggest that when VSN inputs to the ICNS are activated, these inputs are capable of modulating activity in ICNs which then results in the origin of the pacemaker signal becoming highly variable. One possible explanation for the lack of a consistent pattern in the shifts observed in the pacemaker site in the current study is the potential for a differential responsiveness to ACh between cardiac cell types, and within the same cell over time (Fedorov *et al.*, 2006). In this context, Fedorov *et al.* (2006) hypothesized that the differential excitability existing between primary and subsidiary pacemaker cells, could be the result of differences in vagal innervation patterns, muscarinic receptor density on pacemaker cells, or the influence of pacemaker-myocyte coupling within the sinoatrial region. Further to this, Bouman *et al.* (1968) showed an involvement of cholinergic receptors in the maintenance of the sinoatrial initiation site, as well as in site shifting during pathology. Interestingly, Boineau *et al.* (1988) showed the development of multi-focal origins from single origin sites in human hearts, a finding that was replicated in zebrafish in the present

study. As was mentioned above, it is currently not possible to assess such influences, given that these factors are not well described in the zebrafish sinoatrial region.

In mammalian studies there are numerous reports of predictable pacemaker shifts with changes in extracardiac input drive; furthermore the nature of these shifts was predictable (Lu, 1970; West and Belardinelli, 1985; Shibata *et al.*, 2001; Fedorov *et al.*, 2006). In the zebrafish heart, the current results imply that such predictability was not evident. This could, in part, be due to the structural differences between the sinoatrial regions in mammals and zebrafish. The mature sinoatrial node in mammals is a discrete area in the intercaval region, in which the tissue composition and cell connectivity (e.g. presence of surrounding connective tissue and the expression of gap junction proteins) is well described (see Christoffels *et al.*, 2010). Such factors have, in fact, been proposed to limit the capability for pacemaker shifts in the human sinoatrial node (Fedorov *et al.*, 2010). In the rabbit, Allesie and Bonke (1979) concluded that the site of origin was determined mainly by electrotonic interactions with the depolarization wave at the center of a node. However, the sinoatrial pacemaker of zebrafish is a distributed system (Arrenberg *et al.*, 2009; Tessadori *et al.*, 2012; Stoyek *et al.*, 2016) and not a discrete node as is found in mammals, and at this point, knowledge of the organization, tissue composition and cellular connectivity in this region in the zebrafish heart is scant. Thus, a better understanding of the cellular composition and connectivity of the zebrafish sinoatrial region will aid in putting the results of the current study into a more appropriate context.

4.4.3 Conclusions.

The shift from primary to subsidiary pacemaker sites has been implicated in arrhythmogenesis often leading to atrial fibrillation (Effimov and Fedorov, 2005; Hansen *et al.*, 2015). Further to this, it is now known that these arrhythmias are not strictly myogenic in origin, and numerous studies have shown the ANS has a prominent role in the generation and maintenance of these phenomenon (see Effimov and Fedorov, 2005). Though the overall patterns of pacemaker shift vary in zebrafish from mammals, there is a conservation of the function, innervation, and cellular mechanisms in zebrafish (see reviews in Nemtsas *et al.*, 2010; Verkerk and Remme, 2012; Vornanen and Hassinen, 2016). As such, the current work will act as a foundation, onto which future studies investigate the cellular basis of the effects described in the current study will build, potentially providing valuable insights into cardiac function.

Figure 4.1. Organization of intracardiac neurons demonstrating cFOS and pERK immunoreactivity following left VSN stimulation. **A:** Example of intracardiac projections of the extrinsic right vagosympathetic inputs to sinoatrial plexus (SAP) shown after neurobiotin/FM1-43X application to left (IX) extrinsic nerve. Overall innervation to the region is shown AcT-Hu immunoreactivity (from Stoyek et al., 2015). dG, dorsal ganglia; LXG, left vagal ganglia; RX, right vagosympathetic nerve trunk; RXG, right vagal ganglia; vG, ventral ganglia. Dashed boxes indicate regions shown in B-E. **B-C:** Sample of cFOS and AcT-Hu double labeling, presented as separate panels for clarity. AcT-Hu-IR immunoreactivity at the LX (B) and RX (C) junctions with the SAP. **B¹-C¹:** cFOS immunoreactivity in the same regions as panels B and C. cFOS-IR somata were observed only within the LXG, proximal to the RX junction with the SAP (ipsilateral to VSN stimulation; arrowheads). **D-E:** Sample of pERK and AcT-Hu double labeling (presented as separate panels for clarity). AcT-Hu-IR immunoreactivity at the LX (D) and RX (E) junctions with the SAP. **D¹-E¹:** pERK immunoreactivity in the same regions as panels D and E. pERK-IR somata were observed primarily within the LXG, proximal to the LX junction with the SAP, as well as in the RXG. Scale bars: 100 μ m in A; 50 μ m in B-E.

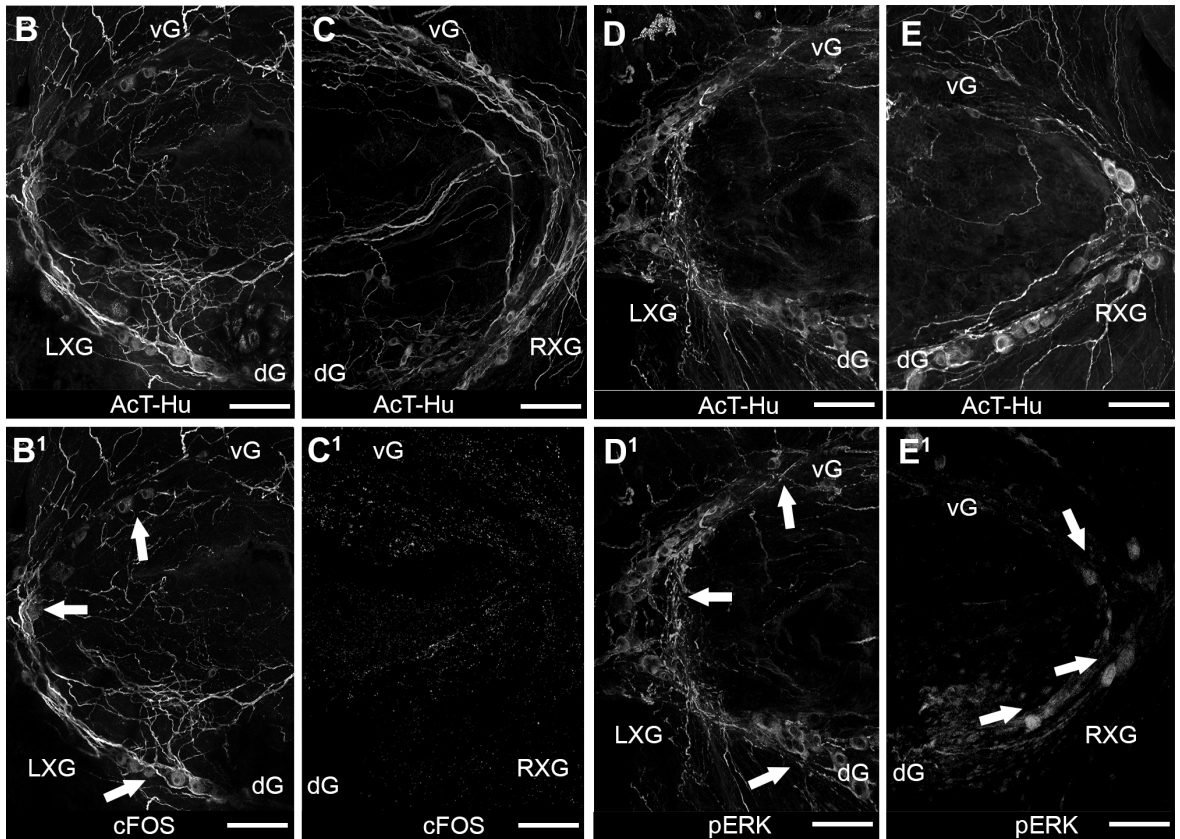
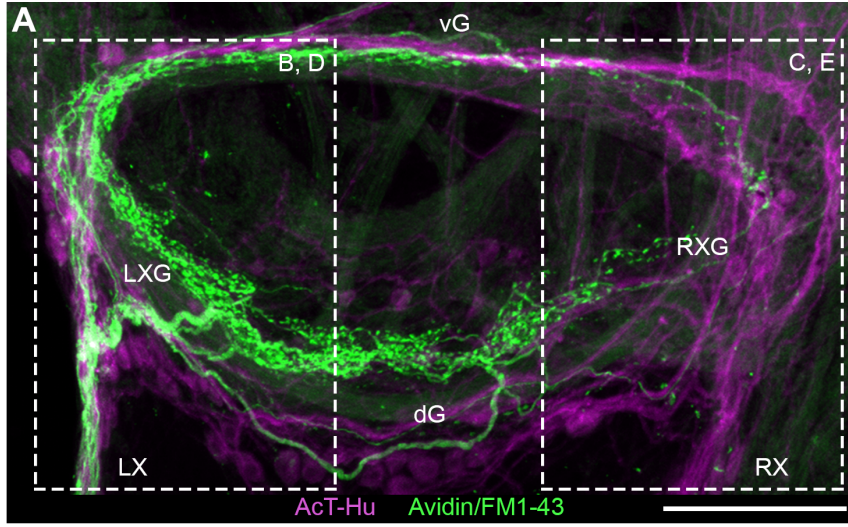


Figure 4.2. Organization of intracardiac neurons demonstrating cFOS and pERK immunoreactivity following right VSN stimulation. **A:** Example of intracardiac projections of the extrinsic right vagosympathetic inputs to sinoatrial plexus (SAP) shown after neurobiotin/FM1-43X application to right (RX) extrinsic nerve. Overall innervation to the region is shown AcT-Hu immunoreactivity (from Stoyek et al., 2015). dG, dorsal ganglia; LXG, left vagal ganglia; RX, right vagosympathetic nerve trunk; RXG, right vagal ganglia; vG, ventral ganglia. Dashed boxes indicate regions shown in B-E. **B-C:** Sample of cFOS and AcT-Hu double labeling (presented as separate panels for clarity). AcT-Hu-IR immunoreactivity at the LX (B) and RX (C) junctions with the SAP. **B¹-C¹:** cFOS immunoreactivity in the same regions as panels B and C. cFOS-IR somata were observed only within the RXG and right dorsal and ventral ganglia proximal to the RX junction with the SAP (ipsilateral to VSN stimulation; arrowheads). **D-E:** Sample of pERK and AcT-Hu double labeling (presented as separate panels for clarity). AcT-Hu-IR immunoreactivity at the LX (D) and RX (E) junctions with the SAP. **D¹-E¹:** pERK immunoreactivity in the same regions as panels F and G. pERK-IR somata were observed primarily within the LXG, proximal to the LX junction with the SAP, as well as in the RXG. Scale bars: 100 μ m in A; 50 μ m in B-E.

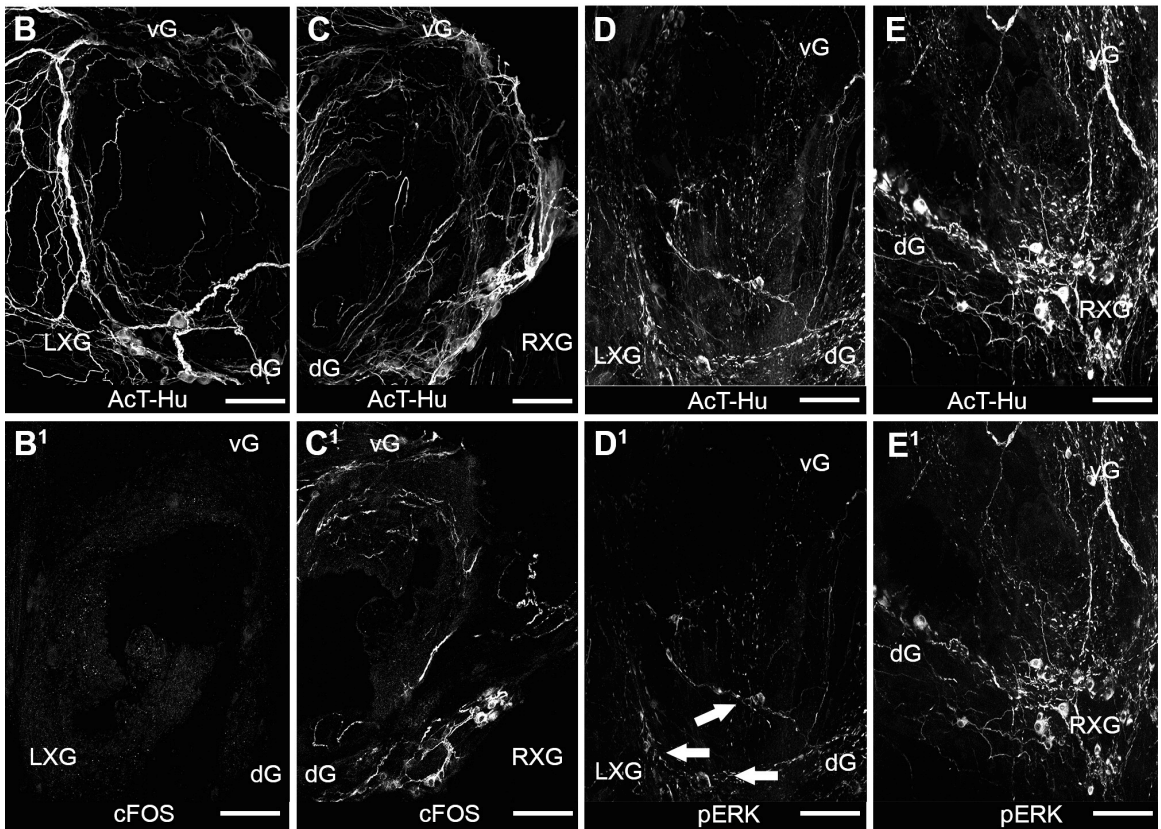
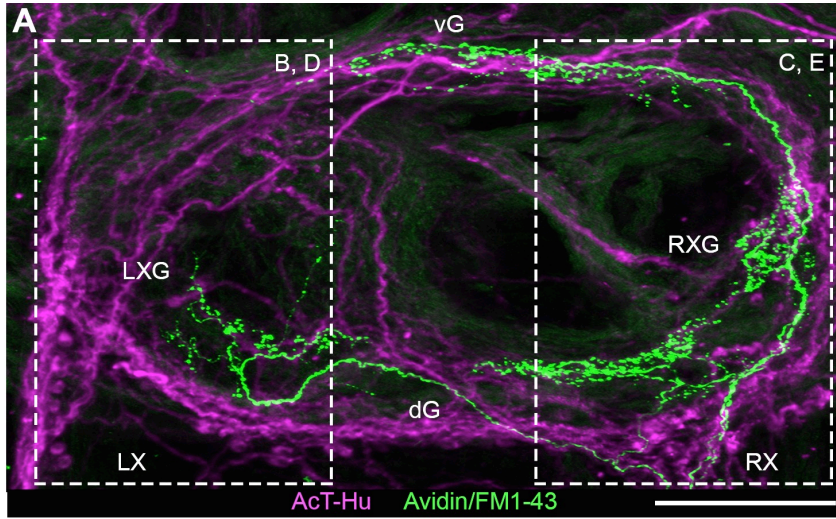


Figure 4.3. Proportion of intracardiac neurons activated by VSN stimulation. The relative proportion of intracardiac neurons expressing cFOS- ($n = 6$; white boxes) or pERK-like immunoreactivity ($n = 6$; grey boxes) within the left (LXG) and right (RXG) as compared to total number ICNs within each region. cFOS-LIR was observed only in the ganglia ipsilateral to vagosympathetic nerve (VSN) stimulation. pERK-LIR was observed in a higher proportion in the ganglia associated with the stimulated VSN, however were also observed at lower proportion in the vagal ganglia contralateral to VSN. * $P \leq 0.05$ by one-way ANOVA.

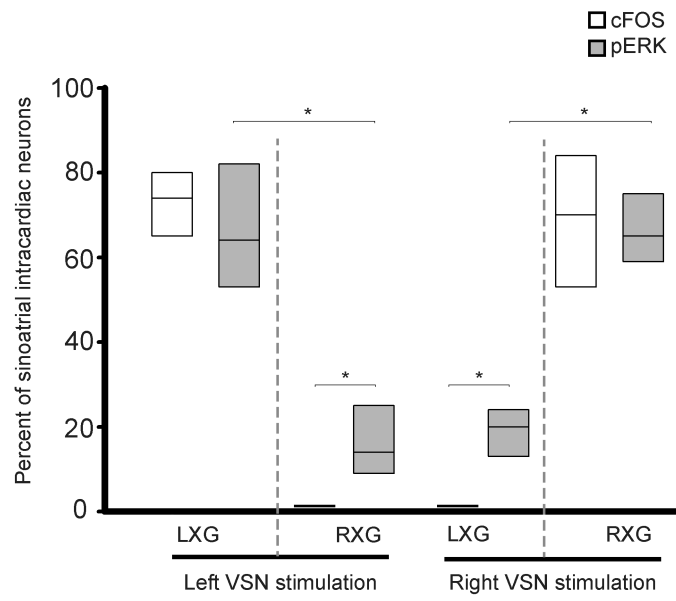


Figure 4.4. Maps of the initial pacemaker site breakthrough in the sinoatrial region with varying levels of electrical stimulation of the left cardiac vagosympathetic nerve (VSN). Each color represents an individual animal, and locations have been normalized over a representative sinoatrial nodal region. Initiation site could reliably be mapped prior to VSN stimulation (A). Increasing levels of left VSN stimulation resulted in variable pacemaker shifts from 1-15 Hz (B-E), displaying as highly variability in initiation site. A, atrium; SAV; sinoatrial valves; SV, sinus venosus.

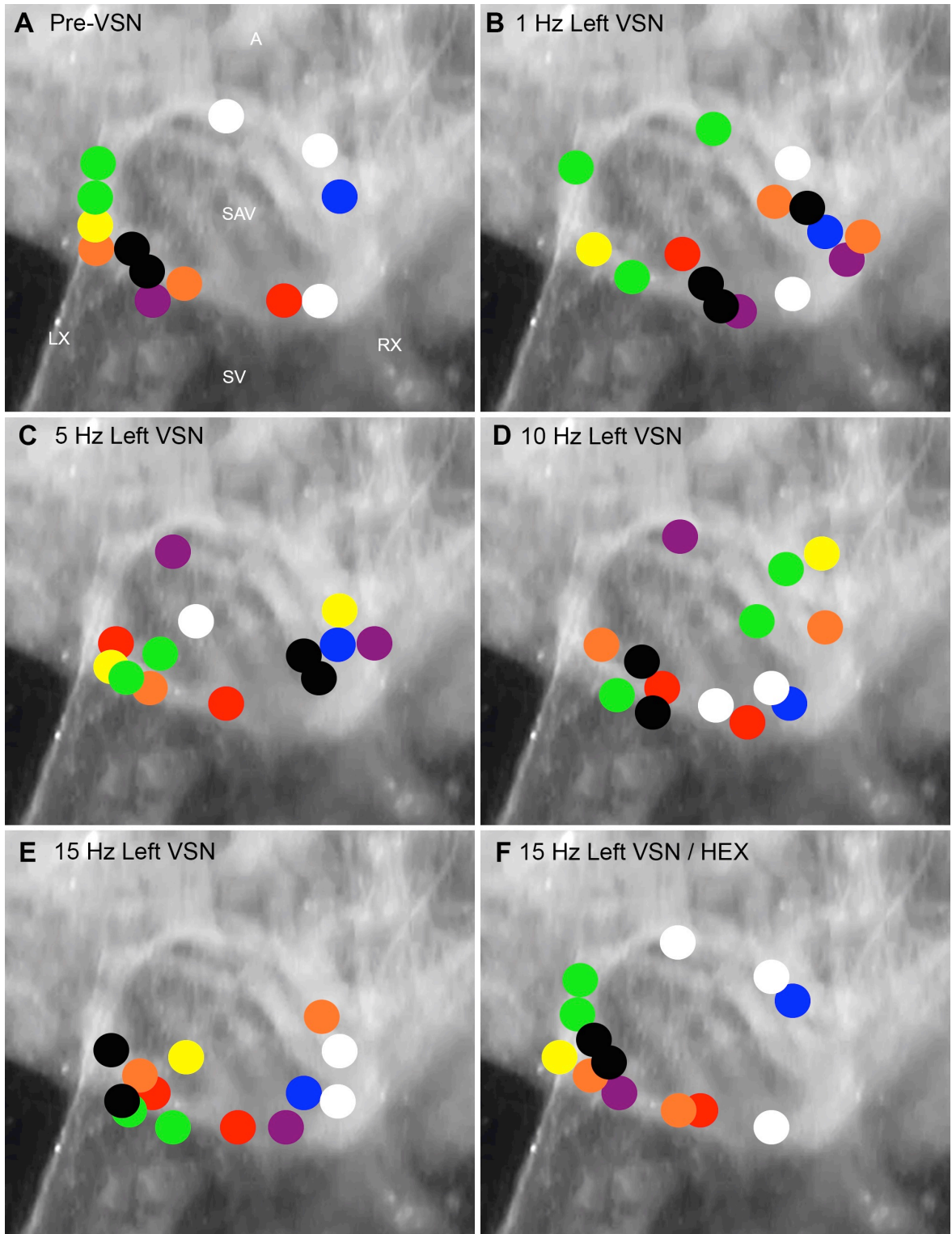
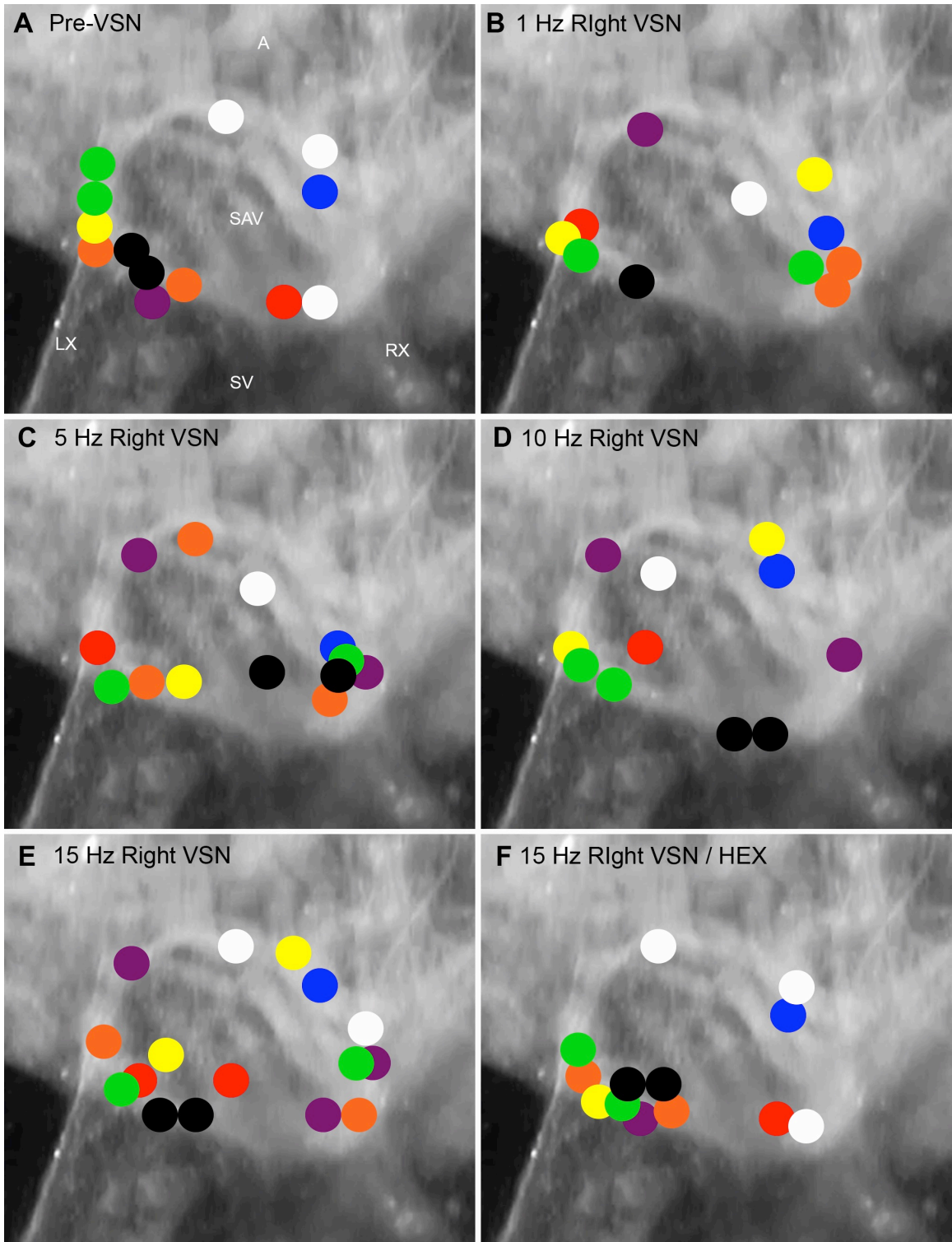


Figure 4.5. Maps of initial pacemaker site breakthrough in the sinoatrial region with varying levels of electrical stimulation of the right cardiac vagosympathetic nerve (VSN). Each color represents an individual animal, and locations have been normalized over a representative sinoatrial nodal region. Initiation site could reliably be mapped prior to VSN stimulation (A). Increasing levels of left VSN stimulation resulted in variable pacemaker shifts from 1-15 Hz (B-E), displaying as highly variability in initiation site. A, atrium; SAV; sinoatrial valves; SV, sinus venosus.



CHAPTER 5

CARDIAC DISTRIBUTION AND CHRONOTROPIC EFFECTS OF SEROTONIN IN THE ZEBRAFISH

5.1 Introduction

Serotonin (5-hydroxytryptamine; 5-HT) was first isolated from blood and described as a vasoconstrictor (Nebigil and Maroteaux, 2001), but has been also shown to have diverse cardio-physiological effects (Frishman and Grewall, 2001). The effects of 5-HT in the cardiovascular system are complex, and previous accounts have shown conflicting biological actions of 5-HT in the cardiovascular system. These effects include bradycardia or tachycardia, hypotension or hypertension, and vasodilation or vasoconstriction (Nebigil and Maroteaux, 2001). 5-HT signaling in the central and peripheral nervous systems takes place through at least 15 receptors, divided into 7 families; all but one of these families belonging to G-protein coupled receptor superfamilies (Levy, 2006).

Recent reports (Briggs, 2002; Chi *et al.*, 2008; Dvornikov *et al.*, 2014; Nemtsas *et al.*, 2010; Rider *et al.*, 2012; Tessadori *et al.*, 2012) have established the zebrafish heart as a powerful tool for studying cardiac electrophysiology, with the potential to provide broad insights into cardiovascular function. The study of serotonergic processes in zebrafish behavior has been well established. Previous reports have described similar responses to those observed in mammalian studies, indicating the potential validity of the zebrafish model in such studies (Airhart *et al.*, 2007; Prieto *et al.*, 2012; Maximino *et al.*, 2013; Stewart *et al.*, 2013). Studies of the physiological effects of 5-HT in zebrafish, however, are more limited and have focused on the role of serotonergic pathways involved with chemosensory neuroepithelial cells in the gills (see review in Jonz and Nurse, 2008). While 5-HT is known to be present in the circulatory system of the zebrafish (Steele *et al.*, 2011), information on the cardiac effects of 5-HT in the zebrafish is lacking, with only a

single report alluding to chronotropic effects of fluoxetine, a commonly used SSRI, at high doses (Airhart *et al.*, 2007).

In a previous study (Stoyek *et al.*, 2015; Chapter 2), the basic structure of the ICNS in zebrafish was described, which is consistent with that of humans and other mammalian models (Irisawa, 1978; Mangoni and Nargeot, 2008; Pauza *et al.*, 2013; Pauza *et al.*, 2014; Li *et al.*, 2015). Further to this, it is known that the zebrafish heart is responsive to agents that affect rate (Arnaout *et al.*, 2007; Stoyek *et al.*, 2016). Therefore, the aim of the present study was to elaborate on these findings and investigate the cardiac distribution and chronotropic responses of 5-HT in the zebrafish heart. A combined anatomical, electrophysiological, and pharmacological approach was used to investigate the involvement of 5-HT pathways, and to compare neural and direct myocardial pathways of biological action. Immunohistochemical methods characterized the relationship of 5-HT and tryptophan hydroxylase (TPH), the rate-limiting enzyme in the production of 5-HT (Levy, 2006), within intracardiac neurons (ICN) and myocardial cells. Electrocardiogram (ECG) recordings combined with pharmacological agents demonstrated that 5-HT acted predominantly through direct myocardial pathways to modulate heart rate. The results of this study establish the isolated zebrafish heart as a tractable preparation to investigate serotonergic function in a whole, functioning heart.

5.2 Methods

5.2.1 Animals.

A total of 32 adult, AB strain zebrafish (12-18 months post-fertilization; 33 ± 5 mm standard body length) of both sexes were used in this study. Institutional approval for

animal use in this study was obtained from the Dalhousie University Committee on Laboratory Animals.

5.2.2 Heart isolation.

Zebrafish were anaesthetised in a buffered solution (pH 7.2) of tricaine in tank water (28.5°C) until opercular respiratory movements ceased and the animals lacked response to a spinal pinch with forceps. A ventral midline incision made through the body wall to expose the heart, and tissues encompassing the ventral aorta, ventricle, atrium, sinus venosus and ducts of Cuvier (containing the cardiac VSN) were removed for *in vitro* recordings or immunohistochemistry.

5.2.3 Immunohistochemical detection of 5-HT and TPH.

The general procedures used for immunohistochemistry in this study were similar to those we have previously described (Stoyek *et al.*, 2015). Tissues were fixed overnight in 4% paraformaldehyde in phosphate-buffered saline (PBS) before processing for immunohistochemistry in whole-mount format. Hearts were labelled with antibodies against 5-HT, tyrosine hydroxylase (rate limiting enzyme in the synthesis of norepinephrine; TH), or tryptophan hydroxylase (rate limiting enzyme in the synthesis of 5-HT; TPH; see Appendix B). Antibodies against acetylated tubulin (AcT; axons) and human neuronal protein C/D (Hu; neuronal somata) were used in combination to show the relationship of 5-HT elements in comparison to the overall innervation of the heart. After exposure to these primary antibodies, preparations were incubated with appropriate secondary antibodies conjugated to AlexaFluor 488, 555, or 647 fluorophores, washed in

PBS and placed in Scale CUBIC-1 clearing solution (Susaki *et al.*, 2014) overnight at room temperature with gentle agitation. Processed specimens were examined as whole-mounts. For all antibodies used in this study, negative control tissues were processed as outlined above, except that either the primary or secondary antibody was omitted. In all trials this eliminated detection of histofluorescence.

5.2.4 Whole-heart ECG recordings.

Isolated hearts were bath perfused with zebrafish saline and allowed to equilibrate for 30 min. ECG signals were recorded from the surface of the atrium with a bipolar suction electrode and cardiac responses were assessed by the time interval between adjacent R-waves of the ECG (R-R interval).

5.2.5 Pharmacological agents.

5-HT was delivered to the tissues in 200 μ l boluses (1 mM). Serotonergic agents ketanserin (10 μ M), fluoxetine (5 μ M), or spiperone (10 μ M) were continuously perfused starting 15 minutes prior to recording. The combination of autonomic antagonists atropine (cholinergic M₂ receptor antagonist; 10 μ M) and timolol (adrenergic β receptor antagonist; 100 μ M) were continuously perfused starting 15 minutes prior to recording. Experiments involving atropine and timolol will henceforth be referred to as “autonomic blockade” (AB).

5.2.6 Imaging, data analysis and presentation.

Tissues were viewed using a Zeiss LSM510 confocal microscope with Zeiss Zen2009 software. Images were processed into plates with Photoshop CS6. During composition of the figure plates the brightness of some images was adjusted so that panel-to-panel contrast in the plate was consistent. Numerical values were expressed as mean \pm 1 SEM. One-way ANOVA with Tukey's *post-hoc* test, was used to detect significant differences among means; to further investigate interactions pairwise t-tests were also performed.

5. 3 Results

5.3.1 Cardiac distribution of 5-HT detected by immunohistochemistry.

Three distinct 5-HT-like-immunoreactive (-LIR) cell types were found within the heart of the zebrafish. For the purposes of this study, these cell types have been classified based upon their morphology, location, and their immunoreactivity with the antibodies tested.

The most numerous of the 5-HT-LIR cells were found within the atrium, associated with the luminal surfaces of the trabeculae. These cells did not co-label with phalloidin-positive myocytes (Figure 5.1B-D). Though it could not be resolved with the markers used in this study it was assumed that these cells were endocardial. These atrial cells, though 5-HT-LIR, did not show TPH (nor TH) immunoreactivity, suggesting that they were sequestering rather than synthesizing 5-HT. In AcT-Hu co-labelled preparations, the myocardial 5-HT-LIR cells were closely associated with axons with varicosities, but did not show direct innervation. To control for the possibility that 5-HT immunoreactivity in the atrial myocardium was due to platelets or erythrocytes that remained within the

trabeculae, and which contained 5-HT, blood smears were made with blood taken from a subset ($n = 3$) of the hearts tested. Blood was collected from the cardiac vessels after fixation and treated with 5-HT and TPH antibodies. In all samples while no 5-HT-immunoreactive erythrocytes were found, 5-HT immunoreactive platelets were found; though the latter constituted less than 1% of the total number of formed elements within a sample.

Within the tissues at the junction of the sinus venosus and atrial myocardium within the sinoatrial valve region (SAR) a 5-HT-LIR ($n = 12$) population of cells was detected in which this marker occurred within the cytoplasm of the cell soma (Figure 5.2C,D). These cells often had numerous small projections from the soma, though the exact targets of these projections could not be determined within the current study. Given this morphology these cells are thus referred to as multipolar cells for the remainder of this study. In preparations co-labelled with either TH ($n = 6$) or AcT-Hu ($n = 6$), no immunoreactivity for either antibody was observed within the multipolar cells. In AcT-Hu/5-HT or TH/5-HT co-labelled preparations, the multipolar 5-HT-LIR cells were closely associated with axons with varicosities, but these cells did not themselves appear to receive direct innervation. As the TPH antibody was raised in the same host as the 5-HT antibody, it was not possible to do co-labelling in the same heart. In hearts labelled with TPH ($n = 6$), no multipolar cells within this region exhibited immunoreactivity, suggesting that, as with the endocardial cells, these cells were sequestering rather than synthesizing the 5-HT they contained.

Within the sinoatrial plexus a small and variable number of ICNs showed 5-HT-LIR (Figure 5.2D); their occurrence was variable among the hearts examined. In 9 of 12

hearts examined 8 5-HT-LIR ICNs were found, in 2 hearts 4 5-HT-LIR ICNs were observed, while no 5-HT-LIR ICNs were observed in one heart. 5-HT-LIR ICNs were restricted to the dorsal sinoatrial plexus (SAP; see Stoyek *et al.*, 2015) region, though the distribution of such ICNs within this region was highly variable. 5-HT-LIR ICNs ranged in size from 40-75 μm . In hearts in which 5-HT-LIR ICNs were observed, all cells of this type showed co-labelling with AcT-Hu ($n = 6$). In hearts in which 5-HT was co-labelled with TH ($n = 6$), there was no co-expression of the two labels in any ICN of any heart. In hearts labelled with TPH ($n = 12$), a population of ICNs with similar spatial distribution to 5-HT-LIR ICNs (Figure 5.2E) was observed. In all hearts labelled with TPH, there was a variable number of TPH-LIR ICNs that were observed in the dorsal SAP. In 7 of 12 hearts 6 TPH-LIR ICNs were observed, in 5 hearts 4 TPH-LIR ICNs were observed, while in 2 hearts no TPH-LIR ICNs were observed. In all preparations TPH-LIR ICNs ranged in size from 42-70 μm . TPH-LIR ICNs showed co-labelling with AcT-Hu ($n = 6$) in all hearts examined; while in preparations co-labelled with TH ($n = 6$) no co-labelling observed was observed. As was previously mentioned, co-labelling of 5-HT and TPH could not be performed, however, based upon similar immunoreactive ICN number, morphology and location within the SAP, it is assumed that 5-HT-LIR ICNs are also TPH-LIR.

5.3.2 Basal heart rate.

In the current study the initial rate of the isolated hearts in the bath was 112 ± 5 beats $\cdot\text{min}^{-1}$ ($n = 40$; range 88 – 144 beats per minute). Chronotropic changes presented below are shown as proportional changes in R-R interval relative to these values obtained prior to the experimental trials (“controls”).

5.3.3 Effects of 5-HT on R-R interval.

The effects of 5-HT and serotonergic agents are summarized in Figure 5.3. 5-HT alone resulted in a significant increase in R-R interval. In hearts exposed to ketanserin (KET; a 5-HT₂ receptor family antagonist) and spiperone (SPIP; a general 5-HT and dopamine 2 receptor antagonist) the elongation of the R-R interval during exposure to 5-HT was blocked and R-R interval was found to not differ significantly from control (1.04 ± 0.04 and 1.11 ± 0.05 times control, respectively). In hearts exposed to fluoxetine (FLX; 5-HT reuptake inhibitor at presynaptic membrane) there was significant increase in 5-HT-induced R-R elongation to 2.63 ± 0.27 times control, which was significantly different from control and those receiving 5-HT alone. In hearts exposed to 5-HT during autonomic input blockade (AB) a significant elongation of the R-R interval was still observed.

5.4 Discussion

Though the reported actions of 5-HT are complex and often contradictory, several lines of evidence now suggest that 5-HT has a regulatory role in cardiovascular function from embryogenesis through adulthood (Nebigil and Maroteaux, 2001). The complex effects of 5-HT in the cardiovascular system, its involvement in the initiation and progression of pathology, and the growing targeting of 5-HT-related mechanisms for developing pharmaceutical therapies, taken together reinforce the need to better understand the distribution and basic actions of 5-HT in the heart.

5.4.1 Distribution of 5-HT within the zebrafish heart.

5-HT has previously been identified in the hearts of rats (Beauvallet *et al.*, 1968; Berkowitz *et al.*, 1974), cats (Votavova *et al.*, 1971), dogs (Madan *et al.*, 1971), and humans (Singh *et al.*, 1998). Although previous studies have described the distribution of 5-HT in the periphery of zebrafish (Jonz and Nurse, 2003; Qin *et al.*, 2010), the current study represents the first description of the distribution of 5-HT within the zebrafish heart.

In the current study cells within the atrial myocardium represented the most plentiful source of 5-HT immunoreactivity. These cells ranged in shape from round to spindle shaped, with the most common morphology being ovoid. Spindle shaped cells associated with atrial trabeculae frequently had long, thin cytoplasmic extensions from the cell somata; however, this was not a feature in all 5-HT-LIR cells. 5-HT-LIR cells were found to be associated with atrial trabeculae, as demonstrated by co-labelling with phalloidin, but these did not extend into the working myocardium. 5-HT has previously been reported in endocardial cells (Yavarone *et al.*, 1993) and it has been proposed that atrial 5-HT-LIR cells currently described likely represent an endocardial cell type; final confirmation of this in zebrafish will require the use of a combination of markers for 5-HT and for endothelial cells. The atrial 5-HT-IR cells in zebrafish did not express TPH, indicating that 5-HT content was most likely the result of uptake and not synthesis. Sari and Zhou (2003) showed in cultured rat myocytes that 5-HT was detected in the absence of TPH, indicating that the 5-HT content of the myocytes was due to uptake and not synthesis, in agreement with our findings and those in other species (Yavarone *et al.*, 1993). Though it was determined that the 5-HT immunoreactivity within the atrial myocardium described above was likely not due to platelets remaining within the trabeculae as platelet size (<3 μm) was found to be inconsistent with 5-HT-IR cells

observed in the atrial wall, it is possible that minimal 5-HT immunoreactivity observed within the atrium was due to this source.

In the tissue at the junction of the sinus venosus and atrium, distributed between the vascular tissue of the sinus venosus and atrial myocytes, there existed a second population of 5-HT-IR cells, which given their morphology, have been termed multipolar cells. These cells were smaller than ICNs, with numerous short projections from the cell somata, imparting a glial- or astrocyte-like appearance. The 5-HT-IR multipolar cells, though, did not show immunoreactivity for the synthesizing enzyme TPH, indicating that 5-HT within these cells is likely the result of uptake and not synthesis. In the CNS it is known that glia and astrocytes actively sequester neurotransmitter substances including NE, dopamine, and 5-HT (Henn and Hamberger, 1971). It is thus tempting to speculate that the 5-HT-IR multipolar cells in the heart of the zebrafish represent a peripheral variant of these cells. Further to this, 5-HT-IR multipolar cells were not observed to express immunoreactivity for general neuronal markers AcT-Hu. Though AcT-Hu has previously been established as a general neuronal marker in the zebrafish (Olsson, 2009; Stoyek *et al.*, 2015), it is not currently known how efficacious these markers are for detecting all neuron types in the zebrafish. That multipolar cells shown in this study were Hu-negative, and display glial- or astrocyte-like morphology, does not necessarily eliminate the possibility that such cells represent a class of neurons that is Hu-negative, and further investigation into their cellular identity must be performed.

Cardiac ganglia have long been thought to contain only cholinergic post-ganglionic neurons, though there is accumulating evidence that cardiac ganglia of zebrafish as well as numerous other vertebrate species contain a heterogenous population of neurons that

synthesize or respond to numerous neuromodulators (Singh *et al.*, 1999, Pauza *et al.*, 2014; Stoyek *et al.*, 2015). Singh *et al.* (1999) previously reported that ICNs in the human heart were the only cells that contained TPH, indicating that they were capable of synthesizing 5-HT. In the zebrafish heart, a population of ICNs with similar morphology and distribution to those expressing 5-HT immunoreactivity expressed TPH. This finding indicates that in zebrafish these ICNs could potentially actively synthesize 5-HT, and that this may be a feature of serotonergic ICNs conserved in mammals.

5-HT can also be taken up by sympathetic neurons for later co-release with NE and other aminergic transmitters and peptides (Nebigil and Maroteaux, 2001; Jaffre *et al.*, 2009). In the current study, however, co-labelling of either 5-HT or TPH with TH in ICNs was not observed, suggesting that such co-release may not occur in the zebrafish heart. It has been suggested that inconsistencies in the literature regarding 5-HT-immunoreactivity could be due to the sensitivity of the technique used to detect 5-HT, the state and source of the tissues examined, or the species examined (Singh *et al.*, 1999). This is supported by reports that pre-treatment with serotonergic agents greatly altered 5-HT detected by immunohistochemical methods (see Yavarone *et al.*, 1993). Therefore it is possible that pretreatment with serotonergic compounds could potentially enhance the content of 5-HT contained within ICNs, which may reveal such colocalization of these markers in the zebrafish heart. Future investigation of the serotonin transporter (5-HTT; Sari and Zhou, 2003) serotonin binding protein (SBP; Tamir and Gershon, 1993), as well as the modulation of 5-HT and its activity by compounds such as angiotensin, could also provide valuable insights to the function of serotonin in control of the heart in zebrafish.

5.4.2 5-HT effects on heart rate.

Given the broad distribution, and potential influence, of 5-HT within the zebrafish heart, the chronotropic response to exogenously applied 5-HT was investigated. In the isolated zebrafish heart 5-HT application, presumably mimicking the endogenous release of 5-HT, resulted in a degree of bradycardia similar to that observed in the hearts of rats (Yamano *et al.*, 1994; Chuang *et al.*, 1993), cats (Schneider and Yonkman, 1953, Jacobs and Comroe, 1971), and dogs (MacCanon and Horvath, 1954). The intent of the current study was to characterize cardiac responses elicited by 5-HT. A potential limitation to this study is that 5-HT was delivered as a focal bolus directly over the heart tissues, therefore neither the absolute concentration in the bath, nor at the receptors within the heart, could be determined.

In the current study serotonergic antagonists ketanserin and spiperone prevented 5-HT-induced bradycardia, supporting that serotonin receptor activation was likely responsible for the negative chronotropic effects. Spiperone is known to act at both 5-HT₁ and 5-HT₂, suggesting that the observed rate effects could be the result of the action of 5-HT at either of these receptors. In the zebrafish it has been shown that ketanserin, a selective antagonist of 5-HT₂ receptors, blocks the physiologic effects of 5-HT on chemosensory afferent fibres of the gills (Shakarchi *et al.*, 2013). That both spiperone and ketanserin blocked 5-HT-induced bradycardia, suggests a role for the 5-HT₂ receptor in the zebrafish heart. In mammals the diversity of 5-HT receptors, and the lack of 5-HT receptor-subtype-specific antagonists have previously complicated the identification of specific receptors involved in controlling cardiac indices (Nebigil and Maroteaux, 2001). Further to this are reports of multiple serotonergic agents interacting with lipid membrane

organization, which may confound the interpretation of receptor-mediated responses through action indirect, non-specific actions (Tessier *et al.*, 2008).

A potential confound to the pharmacological identification of receptor subtypes in zebrafish is that there exist reports of similar results with broadly ranging antagonists that have been suggested to be due to a structural commonality in post-synaptic serotonergic receptors (Maximino *et al.*, 2013). In addition, is the duplication event that occurred in teleosts which produced numerous genes that were later lost. In the zebrafish this duplication includes the 5-HT₁ receptor and 5-HT transporter (5-HTT); though it is assumed that functional proteins are still coded for both the 5-HT₁ receptor and 5-HTT, as the signaling and binding properties of both are retained (Maximino *et al.*, 2013; Stewart *et al.*, 2013). It is currently not known if, or how, other 5-HT receptors may have been affected by this duplication event.

The SSRI fluoxetine has previously been reported as minimally associated with cardiac effects (see review in Gorman and Sloan, 2000). However, the phenotype of transgenic mice overexpressing 5-HT_{1R} autoreceptors, which would recapitulate a reuptake inhibition, included a marked bradycardia, which frequently progressed to death (Audero *et al.*, 2008). The concentration of fluoxetine used in this study was based upon previous publications in zebrafish which described it as lowest dosage capable of blocking CNS effects, but that did not result in reduction of heart rate (Prieto *et al.*, 2012). It is therefore assumed that the enhanced bradycardic effects of 5-HT observed in the current study during exposure to fluoxetine were the result of increased 5-HT exposure, due to the prevention of 5-HT reuptake, and not a cardiac action of fluoxetine itself. The electrophysiologic effects of serotonergic compounds, such as fluoxetine, are known to

include alterations in ion channel function, lengthening of depolarization and repolarization phases of the cardiac action potential, widening of the QRS complex, prolongation of the QT interval, or alterations in L-type calcium and transient outward potassium currents (Park *et al.*, 1999; Sala *et al.*, 2000). It is thus possible, that such changes could represent the underlying cause for the fluoxetine-induced bradycardia observed in this study.

In previous reports an increase in arrhythmogenesis has been described with the use of ketanserin or fluoxetine (Saman *et al.*, 1985; Rajamani *et al.*, 2006). In preliminary experiments for this study exposure to fluoxetine or ketanserin at concentrations between 20-100 μM was found to induce bradycardia and arrhythmias, demonstrating that this phenomenon also occurs in the zebrafish heart. In the presence of ketanserin the initial presentation was brady-arrhythmia, which as concentration was increased, progressively led to cardiac standstill. Injection of 5-HT during the period of ketanserin-induced arrhythmogenic susceptibility would inevitably lead to a rapid increase in R-R interval and deteriorating to cessation of contraction.

In the presence of fluoxetine at concentrations between 20-50 μM , arrhythmias often presented as premature depolarizations on the ECG, which did not initiate an ectopic beat. If fluoxetine concentration was then increased or 5-HT injected, these premature depolarizations increased in frequency, leading in some cases to fibrillation. At the highest concentration of fluoxetine tested (100 μM), there was frequent spontaneous initiation of premature depolarizations, which in all cases led to cardiac fibrillation within 1 minute of exposure. The presence of these arrhythmogenic effects of serotonergic compounds in the

zebrafish heart, similar to those observed in mammalian hearts, thus establishes the potential utility of this model for studying the effects of 5-HT in pathological states.

5.4.3 Conclusions.

5-HT-related mechanisms have been implicated in normal cardiac processes (Xu *et al.*, 2002; Sari and Zhou; 2003; Yavarone *et al.*, 2005; Yabanoglu *et al.*, 2009), as well as in the initiation and progression of pathological states including cardiac hypertrophy (Bianchi *et al.*, 2005; Jaffre *et al.*, 2009), heart failure (Sole *et al.*, 1979), coronary and pulmonary hypertension (Vikenes *et al.*, 1999; Fishman 1999), and cardiac arrhythmias (Saman *et al.*, 1985; Fishman, 1999; (Nebigil and Maroteaux, 2003). As a result the actions of 5-HT, and related pathways, have been widely explored for pharmaceutical development for the treatment of pathologies ranging from antidepressants to appetite suppressants (Levy 2006). Perhaps the best studied of these is the interactions of antidepressants with the cardiovascular system (see Levy, 2006; Gorman and Sloan, 2000; Dawood *et al.*, 2007). The most commonly prescribed medications for depression are selective serotonin reuptake inhibitors (SSRIs; Prieto *et al.*, 2012). While SSRIs have been shown to have minimal effects on cardiac conduction, there exist a growing number of reports implicating SSRIs in fibrillation and arrhythmic events (Pacher *et al.*, 1999). Compounding this are reports implicating that psychosocial factors, such as mood and anxiety disorders, as having a significant role in the prognosis of adverse cardiac events; meaning that a population already potentially susceptible to cardiac dysfunction could be taking drugs which themselves are known to potentially adversely affect cardiac function (Roose and Miyazaki, 2005; Gorman and Sloan, 2000) emphasizing the need to better

understand the cardiac effects of serotonergic agents on cardiac performance. Taken together the results of this study lay the foundation for future studies to investigate in greater depth the pharmacology of 5-HT in the heart.

Figure 5.1. 5-HT-immunoreactivity in the atrial wall. **A:** Schematic showing the cardiac regions: atrium, a; bulbus arteriosus, ba; sinoatrial region, SAR; sinus venosus, sv; ventricle, v. Box indicates the approximate location of images in panels B-D. **B:** Acetylated tubulin and human neuronal protein C/D (AcT-Hu; white) and 5-HT (green) immunoreactivity in the atrial myocardium. Musculature is labelled with phalloidin (Phal; magenta). 5-HT-IR cells were localized to the luminal edges of atrial trabeculae. Dashed box indicates the region of panels C-D. **C-D:** Single confocal images enlarged to show the variety of 5-HT-immuoreactive (-IR) cell morphologies from panel A. 5-HT-IR cells within the atrial wall were restricted to the endocardium. Most 5-HT-IR cells were round to ovoid in shape (C, arrows) with some elongated spindle-shaped cells also observed (D, arrows). In all preparations AcT-Hu-IR somata and axons were observed in close proximity to 5-HT-IR cells; though direct innervation was not observed. Scale bars: 150 μm in B; 75 μm in C-D.

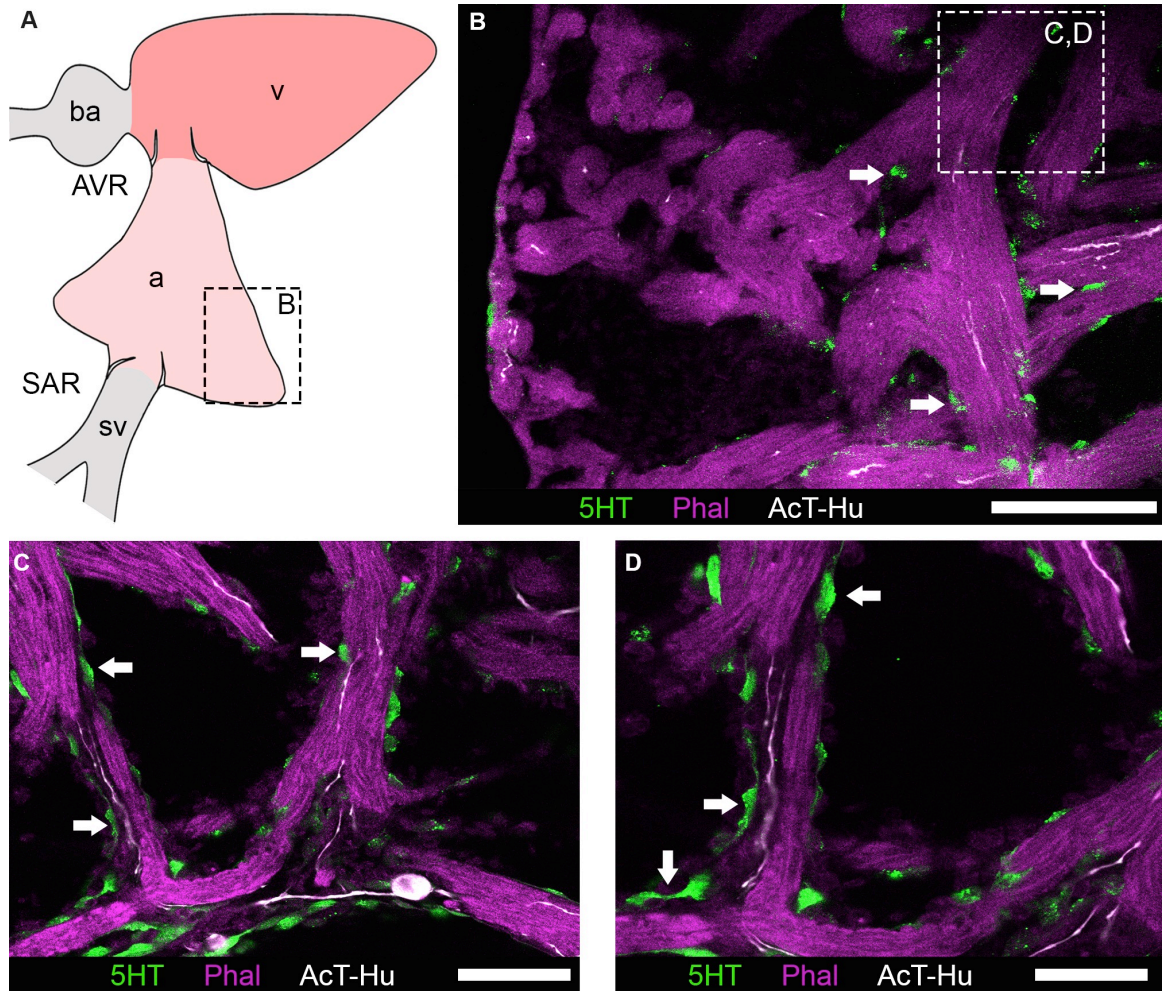


Figure 5.2. Organization of 5-HT-immunoreactivity in the sinoatrial region (SAR). **A:** Schematic showing the cardiac regions: atrium, a; bulbus arteriosus, ba; sinoatrial region, SAR; sinus venosus, sv; ventricle, v. Boxes indicate the locations of images in panels B-E. **B:** Acetylated tubulin and human neuronal protein C/D (AcT-Hu) and 5-HT immunoreactivity at the junctions of the left vagosympathetic trunk with the SAP. Dashed box indicates the region of panel C. **C:** A single confocal image enlarged to show the 5-HT-immuoreactive (-IR) cell morphology from panel A. Cells in this region showed 5-HT-IR most strongly in the cell somata, with small, short projections observed off most somata. These cells did not express immunoreactivity with AcT-Hu. **D:** Within the SAR, some neuronal somata contained 5-HT, and did co-express AcT-Hu (indicated by arrowheads). **E:** In a separate group of hearts neuronal somata of the same morphology as 5-HT-IR somata co-expressed AcT-Hu with tryptophan hydroxylase (TPH; indicated by arrowheads). Scale bars: 75 μm in A; 40 μm in B, 40 μm in D-E.

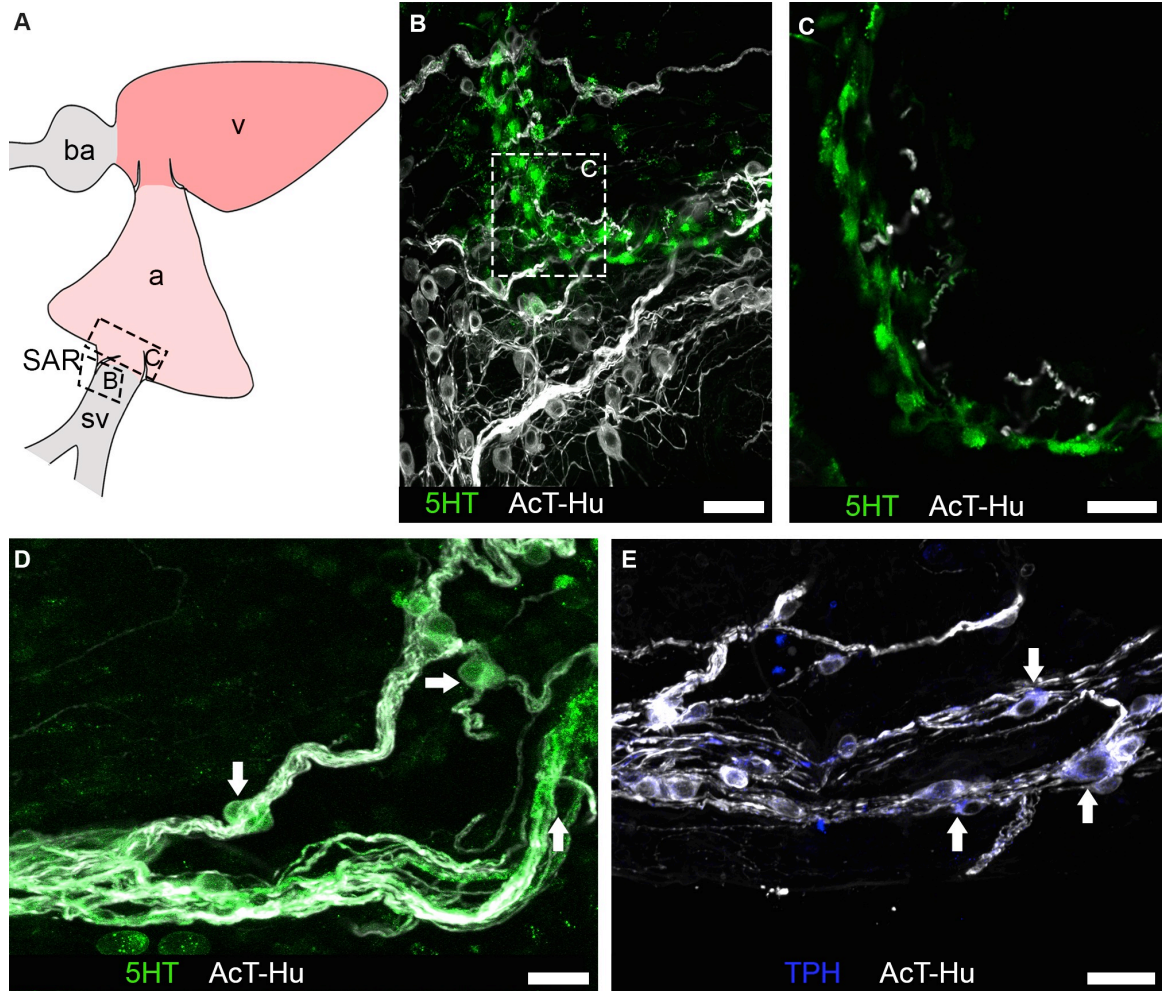
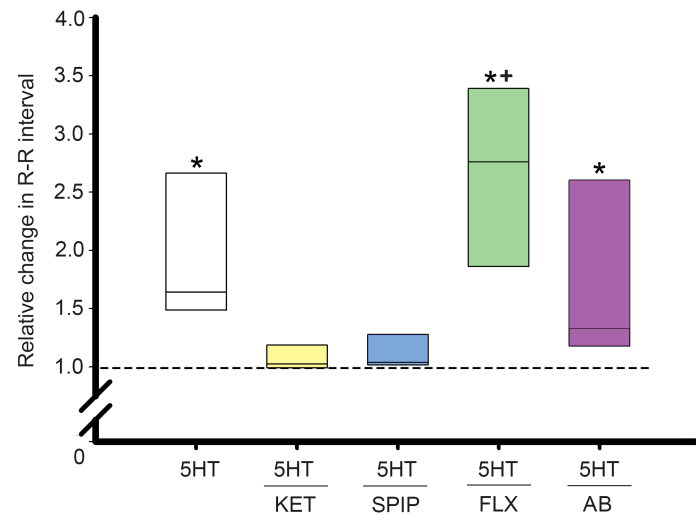


Figure 5.3. Chronotropic responses to 5-HT and serotonergic agents. Exposure to 5-HT increased R-R interval. Effects of 5-HT were eliminated during exposure to ketanserin (KET) and spiperone (SPIP). Fluoxetine (FLX) increased the R-R interval change during exposure to 5-HT. A reduced, but still significant R-R elongation occurred during autonomic input blockade (combined atropine and timolol). *P < 0.05 vs. control by one-way ANOVA with Tukey's *post hoc* test; + P < 0.05 vs. 5-HT by Pair-wise t-test; n=8 for each group.



CHAPTER 6

THE ISOLATED ZEBRAFISH HEART AS A MODEL TO STUDY THE CHRONOTROPIC EFFECTS OF VAPOUR ANAESTHETICS

6.1 Introduction

Anaesthetic agents act at multiple cellular and biochemical target sites to cause widespread depression within the vertebrate central nervous system (CNS). These agents evoke unconsciousness, immobility and inhibition of sensory inputs (Fish *et al.*, 2008; Flecknell, 2009), thereby allowing invasive surgeries and experimental procedures to be performed. Within the CNS the effects of anaesthetics involve several mechanisms, including modulation of ligand-gated ion channels and facilitation or depression of neurotransmission (Hemmings *et al.*, 2005; Mashour and Lydic, 2011).

In addition to their desired effects, all general anaesthetic agents in common use have a broad array of detrimental intra- and post-operative side effects on organs and systems including the nervous system and heart (Ross and Ross, 2008; Fowler and Speiss, 2009). Ligand-gated receptor mechanisms, upon which general anaesthetics act in the CNS, are also present in peripheral components of the autonomic nervous system, including the intracardiac nervous system (ICNS), which forms a common pathway for neural control of the vertebrate heart (Armour, 2008; Stoyek *et al.*, 2015). Furthermore, many of the same ligand-gated receptors, and ion channels, are present on cardiac myocytes and atrial pacemaker cells, so circulating anaesthetics may also directly target these cells. Anaesthetics can suppress or compromise autonomically regulated homeostatic functions (such as breathing, heartbeat and blood pressure) to varying degrees (Mashour and Lydic, 2011). Cardiac side effects of general anaesthetics are documented in species from fishes to mammals and include dose- and exposure-time dependent heart rate changes, arrhythmias and alterations in electrocardiogram (ECG) properties, conduction and myocardial contractility, which together culminate in reduced cardiac output

(Dershwitz and Roscow, 2008; Forman and Mashour, 2008; Sear, 2008; Angelottiv, 2011).

The major cardiac side effect of anesthesia is bradycardia, or reduction in heart rate, which increases the danger that the heart will not be able to supply sufficient blood to the body tissues during surgery. The basic mechanisms underlying the cardiovascular side effects of anaesthetics, however, are not clear in any vertebrate species (see Fish *et al.*, 2008).

Zebrafish are being increasingly used as model organisms for the assessment of drug- and anaesthetic-induced heart rate effects (Moore *et al.*, 1994; Huang *et al.*, 2010; Chen *et al.*, 2015). Recent reports have described significant advantages of the zebrafish model over more traditional mammalian models such as rodents, canine or porcine species for evaluating cardiac function and dysfunction. These advantages include: reduced expense, the requirement for smaller amounts of test compounds, and the possibility for increased sample sizes (Chaudhari *et al.*, 2013). Although the zebrafish heart is two-chambered, and thus simpler than the four-chambered mammalian heart, the operation of the fish heart is fundamentally similar to that of mammals, matching cardiac output to blood perfusion requirements, and employing the same pacemaker system and its neural control (Stoyek *et al.*, 2015; Stoyek *et al.*, 2016). Moreover, the basic electrical properties of the zebrafish heart, including underlying ion channels, better parallel those of the human heart than murine models (see Arnaout *et al.*, 2007). In addition, the small size of the zebrafish heart permits the whole organ to be visualized at once using standard microscopy. These advantages allow precise experimental control of isolated hearts, and the small volume of the *in vitro* bath requires minimal quantities of the test drugs. The basic structure of the ICNS in zebrafish has been described (Stoyek *et al.*, 2015), which is consistent with that of humans and other mammalian models (Irisawa, 1978; Mangoni and

Nargeot, 2008; Pauza *et al.*, 2013; Pauza *et al.*, 2014; Li *et al.*, 2015). Further to this, the physiological aspects of the neural control of chronotropy, and advantages for studies investigating modulation of chronotropy, in the isolated zebrafish heart have been previously described (Stoyek *et al.*, 2016; Chapter 3). The *in vitro* zebrafish heart thus provides an ideal model for allows the investigation of cardiac responses to anaesthetic agents, independent of influences by other systems within the body that may complicate experiments on cardiac function *in vivo*.

In the current study, isolated zebrafish hearts were exposed to vapor anaesthetics over a range of doses to determine their effects on beating rate, measured by quantification of interbeat (R-R) intervals in recorded ECGs. To investigate the contributions of neural and myocardial mechanisms involved in the disruption of heart rate by anaesthetics autonomic antagonists were used to block neural influences. The results of the current study will further our understanding of the cardiotropic roles of modern anaesthetics, their pathways of action and biological activity, which is critical to advance our understanding of the regulation of cardiac output during anesthesia.

6.2 Methods

An expanded Methods section is provided in Appendix A

6.2.1 Animals.

A total of 72 adult, AB strain zebrafish (12-18 months post-fertilization) of both sexes were used in this study. Institutional approval for animal use in this study was obtained from the Dalhousie University Committee on Laboratory Animals.

6.2.2 Heart isolation.

Zebrafish were anaesthetised in a buffered solution (pH 7.2) of tricaine (MS-222; 1.5 mM) and the heart was exposed through a ventral midline incision. A block of tissue encompassing the ventral aorta, ventricle, atrium, sinus venosus and ducts of Cuvier was then removed for *in vitro* recordings.

6.2.3 Measurement of heart rate and vagosympathetic nerve electrical stimulation.

Hearts were bath perfused with zebrafish saline and allowed to equilibrate for 30 minutes to ensure stable heart rate (HR) and to allow for washout of any residual tricaine (see Potential effects of tricaine as overdosing agent). ECG signals were recorded from the atrium and ventricle with bipolar suction electrodes. Cardiac responses were analyzed by measuring the time between R-waves of the ECG (R-R interval; see Figure 6.1). Bipolar wire electrodes were used to deliver trains of rectangular pulses (0.5 ms pulses, 300 μ A, 1-20 Hz) to cardiac VSN. Atrioventricular delay was measured by the latency between atrial and ventricular R-waves within individual cardiac cycles.

6.2.4 Potential effects of tricaine as overdosing agent.

As a tricaine can alter HR in zebrafish (Huang *et al.*, 2010), preliminary experiments were performed to investigate if the use of this anaesthetic compound may have affected the hearts. Residual tricaine from the initial overdose was washed out for 30 minutes, and then the hearts were exposed to a solution of tricaine in the perfusate that was equal in concentration to that used in the overdose procedure for 1 minute before being

switched back to fresh perfusate. Tricaine exposure caused an increase in mean R-R interval to 1.9 ± 0.12 times the mean pre-exposure value, and recovery to pre-tricaine R-R interval occurred by 8.5 ± 1 minutes after the switch to fresh saline. A standardized washout time of 30 minutes for all hearts in the bath was performed before experiments were done in this study.

6.2.5 Anaesthetic agents.

Desflurane (DSF), isoflurane (ISF) or sevoflurane (SVF) were mixed with room air through standard vaporizers that bubbled into a sealed reservoir of zebrafish saline; the tissue was then perfused with this mixture. Concentration of anaesthetics in the perfusate was measured by sampling with a standard patient vapor-phase anaesthetic monitor from the air space in the reservoir. The dose of each anaesthetic was adjusted relative to the minimum alveolar concentration for that agent required to maintain a clinical level of anaesthesia in patients (designated "1.0 MAC" for the purposes of the present study). Desflurane was mixed at 3-12% (6% = 1 MAC), while isoflurane and sevoflurane were mixed at 0.75-3% (1.5% = 1 MAC).

6.2.6 Anaesthetic test procedures.

All anaesthetics used have negligible solubility in water. To test anaesthetic dosage in the perfusate, random samples were drawn into a sealed container from the perfusate reservoir during experiments and allowed to off-gas. Dosages measured from the off-gassing samples were assumed to be in equilibrium with the perfusate, and were statistically similar to those recorded during the initial setup stage for each experiment (t-

test; data not shown). The apparatus for anaesthetic procedures is summarized in Figure 6.1.

For studies on time-dependent cardiac effects, preliminary results showed that changes in R-R period from the pre-anaesthetic value (control) at 15 minutes and 1 h of exposure were statistically similar for all anaesthetics (data not shown). Therefore in all subsequent experiments, hearts were exposed to anaesthetic for a standardized period of 15 minutes.

For concentration-effect studies, the minimum dosage that evoked a detectable change in heart rate over a 30 minute exposure period was 0.5 MAC (data not shown). For the purposes of this study, anaesthetics were applied in dosages increasing from 0.5 MAC to 2.5 MAC (this dosage represented the highest concentration that could be delivered by the vaporizers).

As a control for anaesthetic exposure, in pilot experiments a group of hearts was perfused with saline that had been bubbled through the vaporizer system with no anaesthetic present. Cardiac responses were observed only when the vaporizer was delivering anaesthetic to the perfusate. It was thus assumed that chronotropic effects of anaesthetics were in fact due to these agents reaching the isolated heart.

6.2.7 Pharmacologic agents.

Atropine (10 μ M) and timolol (100 μ M) were delivered in combination starting at 15 minutes prior to and continuing through the period of anaesthetic delivery. Experiments involving atropine and timolol will henceforth be referred to as “autonomic blockade” (AB).

6.2.8 Data Analyses.

All data are presented as means \pm standard error of the mean (SEM). One-way ANOVA with Tukey's *post-hoc*, student's T-test and linear regression were used to analyze the data, using SPSS. P values ≤ 0.05 were considered to indicate significant differences among mean values.

6.3 Results

6.3.1 Heart function in vitro.

Mean initial HR was 103 ± 3 beats \cdot minute⁻¹ (range 77-166 beats \cdot minute⁻¹), and mean initial atrioventricular delay (AVd) was 57 ± 2 ms (range 41-84 ms). For each specimen, HR and AVd varied by <10% between treatments over the 2 hr experimental period. For the purposes of the experiments in this study, control HR and AVd for each treatment were taken as the values measured immediately prior to applying each treatment, and responses are presented as relative changes during anaesthetic exposure relative to pre-exposure values.

6.3.2 Time course of anaesthetic-induced changes in HR and AVd

The HR effects of exposure to 1.0 MAC of a given anaesthetic are summarized in Table 1 and Figure 6.2. All anaesthetics tested showed a tendency to increase R-R intervals starting at 5 minute exposure; these changes reached significance at 15 minutes exposure. Anaesthetic-induced changes in AVd were not significantly time-dependent

with the exception of ISF, which evoked a significant increase in delay at 15 minutes exposure.

6.3.3 Concentration-dependent changes in HR and AVd.

Given that the effects of all anaesthetics on HR reached a plateau level at 15 minutes exposure time, this was used as the standard exposure time for evaluating concentration-dependent effects; these are summarized in Table 1 and Figure 3. Significant bradycardia was observed during exposure to DSF and SVF with at all concentrations tested. Exposure to ISF evoked significant changes in rate at concentrations of 1.0 MAC and above.

AVd was not significantly altered by any anaesthetic at 0.5 MAC, while only ISF caused AVd to change significantly at 1.0 MAC. In contrast, all anaesthetics caused AVd to increase significantly at 2.5 MAC (Table 1; Fig. 6.3).

At the highest dosage used in this study, all anaesthetics caused arrhythmias during prolonged exposure. For instance, in 3 of 6 hearts exposed to ISF arrhythmias resembling fibrillation developed by 25 minutes exposure at 2.5 MAC (data not shown). DSF also caused a fibrillation-like arrhythmia in 2 hearts exposed at 2.5 MAC for 25-30 minutes, while another heart developed a conduction block in which the relationship of atrio-ventricular contraction varied between 2:1 and 3:1.

6.3.4 Effects of autonomic blockade and vagosympathetic nerve stimulation.

To investigate the contributions of neurally-mediated and myocardial mechanisms involved in anaesthetic-mediated disruption of heart rate, isolated hearts were exposed to

anaesthetics under autonomic blockade using a combination of atropine (parasympatholytic) and timolol (sympatholytic). The effects of autonomic blockade during exposure to anaesthetic are summarized in Table 2 and Figure 6.4. In the presence of autonomic blockade, significant bradycardia was still observed after 15 minutes exposure to DSF and DSF, while there was no significant change in HR during exposure to SVF. During autonomic blockade as there were no changes in AVd at 1.0 MAC with anaesthetic alone for DSF and SVF, and there would be no expected changes, HR alone was measured.

Stimulation of the vagosympathetic nerve trunks caused a significant R-R interval elongation in the absence of anaesthetic (Table 2 and Figure 6.5). During exposure to DSF, repeat nerve stimulation resulted in a further elongation of R-R interval that was significantly greater than the change evoked by nerve stimulation alone. This effect was not observed during combined nerve stimulation and exposure to either ISF or SVF (Table 2; Fig. 6.5). As a control for the efficacy of vagosympathetic nerve stimulation in these experiments, cardiac nerve stimulation, anaesthetic and autonomic blockade were combined; no chronotropic changes were observed under these conditions for any anaesthetic agent (Table 2).

6.4 Discussion

General anaesthetics have been a mainstay of surgical practice for more than 150 years, but the mechanisms by which they mediate their clinical actions remain unclear (Chen *et al.*, 2005). These agents often produce undesirable side effects, in particular respiratory and cardiovascular depression, each of which involve unknown targets

(Hemmings *et al.*, 2005). Clinically, a growing number of non-cardiospecific drugs, particularly anaesthetic agents, have been shown to affect cardiac function and thus carry an increased risk of adverse cardiovascular events (Ross and Ross, 2008; Fowler and Speiss, 2009). In research on a wide variety of animal models for cardiovascular diseases, it has been found that the type and dosage of anaesthetic that is used may have a significant impact on cardiovascular measurements. The literature in this field reflects a wide range of anaesthetic and dosing regimes that have been utilized depending on the type of experimental intervention, study design, species and strain differences, and institutional regulations (Janssen *et al.*, 2004).

In this study the viability of the isolated zebrafish as a novel model for the study of the cardiac effects of vapor anaesthetics has been established. The adoption of zebrafish into anaesthetic research programs has been hampered by specific limitations, including difficulties in determining the exact dose of anaesthetic compound administered, uniformity in interpretation of results and correlation of dosages that may cause adverse effects in the zebrafish heart to dosages effective in other species (Chaudhari *et al.*, 2013). One issue addressed in the current study was that of the potential lack of anaesthetic solubility in aqueous solutions. The vapor-phase anaesthetics used in the current study are considered to be insoluble in water, but preliminary experiments anaesthetic concentrations reported by the patient monitor correlated with anaesthetic concentration in the perfusate as shown by off-gassing controls. In addition only R-R period changes were observed only when the anaesthetic was being actively vaporized, indicating that the observed changes were in fact a result of exposure of the isolated heart to anaesthetic agent. While the exact form that the anaesthetic agents took in the perfusate was unknown,

it is possible that these agents entered the aqueous phase as a result of ‘microbubbles’ formed during passage of the gas through the aerator, eventually reaching the heart.

That the intracardiac elements of neural control and basic operation of the sinoatrial pacemaker, are highly conserved from zebrafish to humans (Stoyek *et al.*, 2015; Stoyek *et al.*, 2016) were key factors in the choice of model. This, together with reports demonstrating conservation of gene and protein and function for many established sedative hypnotic pathways throughout the vertebrates, further supports the applicability of using the zebrafish heart in such studies (Renier *et al.*, 2007). While the use of the isolated zebrafish heart may be oversimplified in terms of addressing the broadly integrated mechanisms underlying anaesthetic side effects during surgery, it could be argued that eliminating all non-cardiac factors to focus on effects of intracardiac origin is a strength of the model. Thus, it is felt that such research in the zebrafish ultimately has the potential to provide useful insights into the cardiac effects of anesthesia and their underlying intracardiac mechanisms in the clinical setting.

6.4.1 Effects of anaesthetics on HR and AVd.

In previous studies in mammals a variety of responses, including tachycardia (Ebert and Muzi, 1993; Yli-Hankala *et al.*, 1993; Ebert and Muzi, 1994; Weiskopf *et al.*, 1994; Ebert *et al.*, 1995a; Ebert *et al.*, 1995b; Marano *et al.*, 1996) and bradycardia (Poterack *et al.*, 1991; Park *et al.*, 1999; Preckel *et al.*, 1998; Janssen *et al.*, 2004; Constantinides *et al.*, 2011) as well as stabilized HR (Holaday and Smith, 1981; Manohar and Parks, 1984; Bernard *et al.*, 1990; Harkin *et al.*, 1994; Ebert *et al.*, 1995a) have been described in response to exposure to inhalational anaesthetics. However, the prevailing

cardiac response is a depression of cardiac output, most likely mediated by slowing of HR (Hanley *et al.*, 2002; Janssen *et al.*, 2004). Such a variety of responses reinforce the need for a model to better understand the underlying mechanisms of such effects.

In the isolated zebrafish heart there was a general reduction in HR with all anaesthetics, occurring in a time- and dose-dependent manner similar to effects described in the mammalian heart. At 1.0 MAC, DSF, ISF, and SVF all evoked elongation of the R-R interval within 5 minutes of exposure to the anaesthetic in perfusate, with significant changes in interval occurring at 15 minutes exposure.

AVd tended to be highly variable during exposure to the anaesthetics used in this study, but only ISF evoked a significant increase in this factor. The current findings accord with those of previous studies in the isolated zebrafish heart (Lin *et al.*, 2014; Stoyek *et al.*, 2016). Furthermore, AVd seems to be unaffected by autonomic agents (Stoyek *et al.*, 2016). The relative lack of apparent effect of inhalational anaesthetics on AVd could have resulted because subtle changes in delay time were masked by the inherently high beat-to-beat variability observed in the zebrafish heart. As alterations in AVd are known to be involved in arrhythmogenesis and re-entry, especially when there exist co-morbidities (Goldreyer and Damato, 1971; El-Sharif *et al.*, 1977; Aurricchio *et al.*, 1999), this result warrants further investigation to be properly understood.

In a previous study it was found that ISF co-delivered with tricaine resulted in a more stable and maintainable HR during recoverable anesthesia in intact adult zebrafish (Huang *et al.*, 2010). While Huang *et al.* (2010) described the HR effects of tricaine alone, and co-administration of ISF with tricaine in the *in vivo* and *in vitro* zebrafish heart; the effects of ISF alone were not investigated. These authors concluded that the more stable

HR observed with ISF and tricaine together was due to a positive synergistic interaction between these agents on the heart, the mechanisms of which were not described (Huang *et al.*, 2010). In the present study a significant bradycardia was observed with ISF alone in isolated hearts, and previous studies have shown that tricaine anaesthetic can have variable cardiovascular effects in zebrafish (Huang *et al.*, 2010; Chen *et al.*, 2015). For instance, Chen *et al.* (2015) showed that HR decreased to different degrees after anesthesia of 4 day post fertilization zebrafish with 1 mM tricaine. In this study, after the tricaine had been replaced with embryo medium without anaesthetic, the zebrafish began to recover from anaesthetic effects. Although no timeline for recovery was reported for these experiments, in the current study exposing the isolated adult heart to tricaine resulted in a decrease in HR similar to that shown in intact larval fish. Also, in the current experiments, as in the larval experiments reported by Chen *et al.* (2015), recovery from tricaine effects began rapidly after switching the perfusate to fresh saline without tricaine. As in all experiments there was an acclimation period of 30 minutes post-isolation, in which the heart was being perfused with fresh saline, it is assumed that any tricaine that may have reached the heart, would have been washed out. Thus, the effects that were observed during exposure to DSF, ISF, and SVF were assumed to be due to those anaesthetics alone.

6.4.2 Concentration-dependent effects.

The clinical potencies of inhaled anaesthetics were established in studies by Eger *et al.* (1965), who defined the ‘minimum alveolar concentration’ (MAC) as that concentration necessary to inhibit response to a noxious stimulus in 50% of subjects (Hemmings *et al.*, 2005). While 1.0 MAC, as used in these experiments, represents a

“clinically-relevant” dosage, effective concentrations of inhalational anaesthetics may vary between individuals, or between induction of anesthesia and maintenance in the same individual. Thus, to investigate potential concentration effects, the concentration in the perfusate was varied from 0.5 – 2.5 MAC. R-R interval was significantly elongated following a 15 minute exposure to both DSF and SVF at a concentration of 0.5 MAC. Exposure to 2.5 MAC of all anaesthetics resulted in a stable, but significant R-R period elongation. Previous mammalian studies in which concentration of ISF was increased above 1.0 MAC have more consistently reported decreases in HR (see Poterack *et al.*, 1991)

At 2.5 MAC concentrations AVd was significantly increased revealing, contrary to previous reports showing no alterations (Lin *et al.*, 2014; Stoyek *et al.*, 2016), that anaesthetics could alter AVd. That AVd was elongated at these relatively high concentrations suggests that the lack of alteration in AV delay at 1.0 MAC was, in fact, likely masked by the high interbeat AV delay variability.

It has been proposed that an anaesthetic’s cardiac effects cannot be adequately addressed by noting only that the heart shows no arrhythmias (Meek *et al.*, 1937). In preliminary experiments prolonged exposure (≥ 25 minutes) or rapid increases ($>1\%$) to high concentration of DSF and ISF anaesthetic resulted in increased probability of arrhythmogenesis, in accord with reports that these anaesthetics may be proarrhythmogenic. The mechanism of this effect has been proposed to be through modification of cardiac ion channel activity (Moore *et al.*, 1994; Hünenke *et al.*, 2004; Zhou *et al.*, 2012). DSF has also been associated with periods of substantial sympatho-excitation and tachycardia when it is first introduced into the inspired gas after intravenous

induction of anesthesia (Ebert and Muzi, 1993; Yli-Hankala *et al.*, 1993; Ebert and Muzi, 1994) and during periods of steady state anesthesia when the inspired concentration is abruptly increased (Ebert and Muzi, 1993; Moore *et al.*, 1994; Weiskopf *et al.*, 1994). ISF has been shown to provoke a response that is qualitatively similar to that of DSF when abruptly increased, but the magnitude of the response is far less (Ebert and Muzi, 1994; Weiskopf *et al.*, 1994). The administration of SVF in rapidly increasing inspired concentrations has not been associated with such effects (Ebert *et al.*, 1995a).

6.4.3 Effects of autonomic blockade and vagosympathetic nerve stimulation.

Enhancement of inhibitory postsynaptic responses and inhibition of excitatory synaptic transmission are generally thought to be the predominant mode of general anaesthetic action in the central nervous system (Yamashita *et al.*, 2005). Such disruption of central neural control elements, some of which modulate tonic sympathetic and parasympathetic outflow to the periphery, may also contribute to changes in cardiovascular regulation (Price *et al.*, 1963; Poterack *et al.*, 1991). As many the receptors involved in anaesthetic effects in the CNS are also present in the heart, it is not surprising that disruption of the regulation of the circulation via direct actions of anaesthetics on the heart, independent of autonomic activity, has been demonstrated (Wig *et al.*, 1979; Saarnivaara and Lindgren, 1983; Seagard *et al.*, 1985; Aypar *et al.*, 2007; Pauza *et al.*, 2014). In previous studies all hallmarks of autonomic innervation, and the physiology of neural control, in the zebrafish heart have been shown analogous to those in humans (Stoyek *et al.*, 2015; Stoyek *et al.*, 2016). Therefore, in this study, isolated hearts were exposed to a combination of ATR (post-junctional muscarinic receptor blocker) and TIM

(post-junctional beta-adrenergic receptor blocker), which blocked all effects of adrenergic and cholinergic drive to the myocardium. This allowed differentiation of direct cardiac actions of anaesthetics from those effects mediated via the ICNS.

It was found that of the agents tested, only the SVF-evoked bradycardia was prevented by autonomic blockade, suggesting that the HR effect of this anaesthetic was mainly of neural origin in the isolated zebrafish heart. Many volatile anaesthetics inhibit neuronal nicotinic and muscle-type muscarinic acetylcholine receptors, even at sub-anaesthetic concentrations (Flood *et al.*, 1997; Violet *et al.*, 1997; Yamashita *et al.*, 2005). The activation of muscarinic receptors in the CNS during anaesthetic has been shown in the rat (Hudetz *et al.*, 2003). Thus, it is may be that the results for SVF during autonomic blockade represent, at least in part, a disruption in cholinergic receptor-mediated actions of SVF in the CNS.

In contrast to SVF, even in the presence of autonomic blockade, a reduced, but still significant bradycardia was observed with both DSF and ISF, suggesting that the cardiac effects of these anaesthetics were mainly the result of actions directly on cardiac pacemaker cells. This finding agrees with previous reports describing bradycardia due to direct negative chronotropic effects of DSF when ANS activity was depressed or abolished (Skovsted and Saphavihaikul, 1977). Given the likelihood of direct myocardial effects of DSF and ISF, the most likely mechanism would be inhibition of cardiac pacemaker cells. In zebrafish and mammalian species hyperpolarization-activated, cyclic-nucleotide gated channels (HCN), are known to contribute a major portion of the diastolic depolarizing current in cardiac pacemaker cells (Irisawa, 1978; Mangoni and Nargeot, 2008). The inhibition of HCN channels by inhaled anaesthetics occurs through a hyperpolarizing shift

in the voltage dependence of activation of these cells and thus a decrease in maximal available current, effectively blocking conductance over the typical subthreshold voltage range (Chen *et al.*, 2005).

In humans, reflex heart rate and changes in sympathetic nerve activity in response to arterial pressure perturbations are diminished with increasing MAC of SVF; these responses are generally similar to those produced by ISF and DSF (Ebert *et al.*, 1995b). Previous reports have described alterations in cardiac sympathetic and parasympathetic vagal nerve traffic during periods of anesthesia, which were proposed to play a role in the observed chronotropic effects (Kurosawa *et al.*, 1989). In order to test the responsiveness of the zebrafish heart to extrinsic cardiac nerve input, these nerves were stimulated during exposure to anaesthetic, thus simulating CNS input to the intracardiac nervous system. During exposure to DSF and ISF, VSN stimulation resulted in a significant bradycardia, which was summative with anaesthetic effects. Though these results support the hypothesis that DSF and ISF are acting on myocardial targets, they stand in contrast with a previous description of ISF dose-dependently attenuating chronotropic responses during CNS stimulation (Poterack *et al.*, 1991). VSN stimulation during exposure to SVF had no chronotropic effect, which could be the result of depression of the intracardiac nervous system by this agent, providing further support to the results of the autonomic blockade experiments and suggesting that the chronotropic effects of SVF were of neural origin.

6.4.4 Conclusions.

Of the most important effects to understand about any anaesthetic agent is its action on the heart and how such an agent may influence indices such as contractility,

conductivity, or automaticity (Meek *et al.*, 1937). There is now ample evidence that clinical concentrations of most general anaesthetics, particularly volatile anaesthetics, have interactions with multiple targets (Hemmings *et al.*, 2005), and that interactions with these targets can drastically alter normal function of the heart (Hünenke *et al.*, 2004). There exist many studies that have analyzed isolated cardiomyocytes in the presence of commonly used anaesthetic vapours which have produced valuable insights into the side-effects of anaesthetics at the molecular and cellular level (see Hünenke *et al.*, 2004); however interactions and effects at the level of the organ may differ. Though the small size of the zebrafish heart presents its own technical challenges, its size also permits a level of visualization, accessibility, and experimental manipulability of the whole organ, than has previously been possible with other models.

On the basis of the current study, it appears most likely that no single target is responsible for the chronotropic changes observed during anaesthesia, and that in all probability the observed effects are the result of multiple interacting factors of neural and myocardial origin. While the current study was designed to directly assess effects of intracardiac origin, at the same time it excluded several mechanisms that may also be important in the *in vivo* situation, such as modulation by autonomic centres within the CNS. Consequently, the effect of inhalation anaesthetics in the *in vivo* zebrafish heart may differ from what was observed in this study. Techniques developed in this study can now be applied to “open-chest” preparations, akin to those used in canine studies, of the *in vivo* zebrafish heart to investigate how the cardiac effects described here differ with direct CNS input. Determining how and why commonly used anaesthetics cause a drop in HR, and subsequently cardiac output, will provide insights into the improvement of such

anaesthetics or the development of new ones which reduce or eliminate these effects. The basic knowledge arising from the experiments described here will allow for the investigation and identification of cardiac specific mechanisms and pathways to pursue in reducing the cardiotropic consequences of anesthesia.

Table 1: Summary of effects of desflurane (DSF), isoflurane (ISF), or sevoflurane (SVF) on heart rate (HR) or atrioventricular delay (AVd) represented relative change in as compared to pre-treatment values. Values are group ($n = 6$) means \pm SEM. AB, autonomic blockade. * $P < 0.05$ by one-way ANOVA.

			DSF	ISF	SVF
Time (min at 1.0 MAC)	RR	5	1.25 \pm 0.09	1.38 \pm 0.14	1.28 \pm 0.09
		10	1.34 \pm 0.08	1.44 \pm 0.16	1.33 \pm 0.11
		15	1.61 \pm 0.09*	2.05 \pm 0.23*	1.45 \pm 0.05*
	AVd	5	1.03 \pm 0.10	1.17 \pm 0.06	1.13 \pm 0.05
		10	1.25 \pm 0.27	1.24 \pm 0.11	1.23 \pm 0.05
		15	1.33 \pm 0.14	1.54 \pm 0.11*	1.28 \pm 0.09
Concentration (15min at MAC)	RR	0.5	1.30 \pm 0.06*	1.59 \pm 0.15	1.30 \pm 0.04*
		1.0	1.59 \pm 0.10*	2.05 \pm 0.21*	1.45 \pm 0.07*
		2.5	1.84 \pm 0.08*	2.59 \pm 0.11*	1.57 \pm 0.05*
	AVd	0.5	1.16 \pm 0.08	0.96 \pm 0.03	1.21 \pm 0.05
		1.0	1.30 \pm 0.07	1.48 \pm 0.07*	1.28 \pm 0.09
		2.5	1.47 \pm 0.06*	1.53 \pm 0.11*	1.88 \pm 0.12*
AB (15 min at 1.0 MAC)	RR	1.41 \pm 0.13*	1.29 \pm 0.09*	1.01 \pm 0.02	

Table 2: Summary of effects of vagosympathetic nerve stimulation on heart rate (HR) during exposure to desflurane (DSF), isoflurane (ISF), or sevoflurane (SVF). * P < 0.05 compared to pre-treatment (VSN or AB) control values. † P < 0.05 compared to pre-anesthetic VSN by one-way ANOVA. Values are group (n = 6 each) means ± SEM.

		DSF	ISF	SVF
PRE	VSN	1.36 ± 0.10*	1.42 ± 0.06*	1.33 ± 0.11*
	VSN	2.48 ± 0.11†	1.76 ± 0.08†	1.40 ± 0.13*
ANESTH	VSN / AB	1.26 ± 0.06	1.49 ± 0.05	1.01 ± 0.01

Figure 6.1. Schematic of the perfusion and electrocardiogram (ECG) recording system for the zebrafish heart. **A:** Standard zebrafish saline or zebrafish saline treated with desflurane, isoflurane, and sevoflurane were delivered to the heart from gravity fed reservoirs, with saline type controlled by a three-way valve. Cardiac electrical activity was monitored by via surface ECG, from atrial and ventricular leads, differentially amplified and recorded to a PC. Anaesthetic concentration was monitored via a gas-chromatograph patient monitor. **B:** Sample ECG recording from atrial and ventricular leads, showing P-, R-, and T-waves. Chronotropic responses were quantified by changes in the interbeat (R-R; grey bar) interval calculated from the atrial lead. Atrioventricular delay was quantified by changes in P-R interval (grey bar; inset) calculated from atrial and ventricular leads.

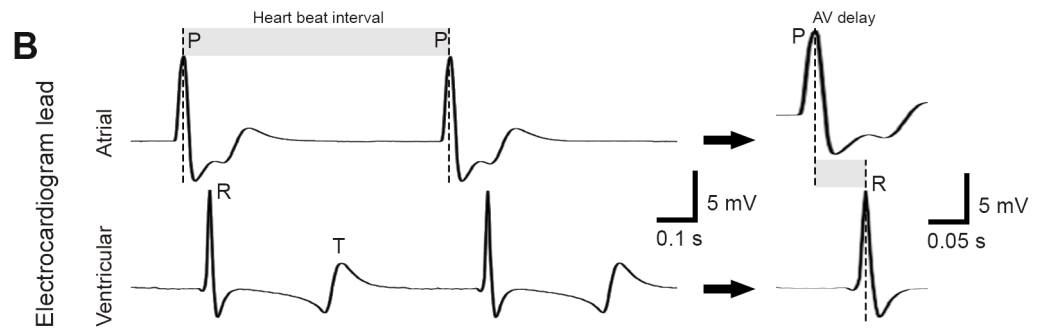
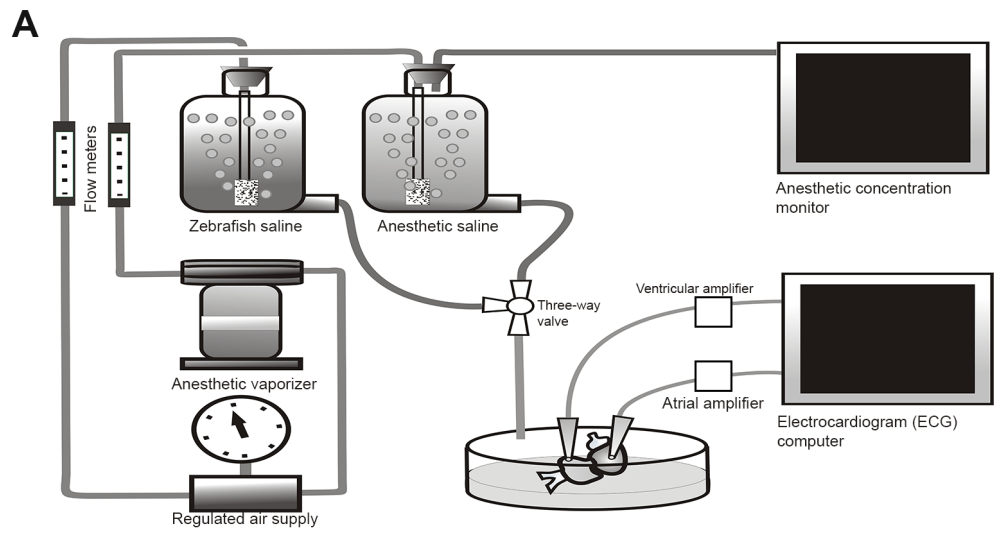


Figure 6.2. Time-dependent chronotropic responses of the isolated zebrafish heart to anaesthetics. **A:** Interbeat (R-R) interval began to elongate within 1 minute of anaesthetic exposure to desflurane (DSF), isoflurane (ISF), and sevoflurane (SVF), and showed a maximal response at 15 minutes post-exposure. **B:** Atrioventricular delay (AVd) began to elongate within 1 minute of anaesthetic exposure to desflurane (DSF), isoflurane (ISF), and sevoflurane (SVF), and showed a maximal response at 15 minutes post-exposure. Dashed line indicates the pre-treatment heart rate. *P < 0.05 vs. pre-exposure values by paired One-way ANOVA; *n*=6 for each group.

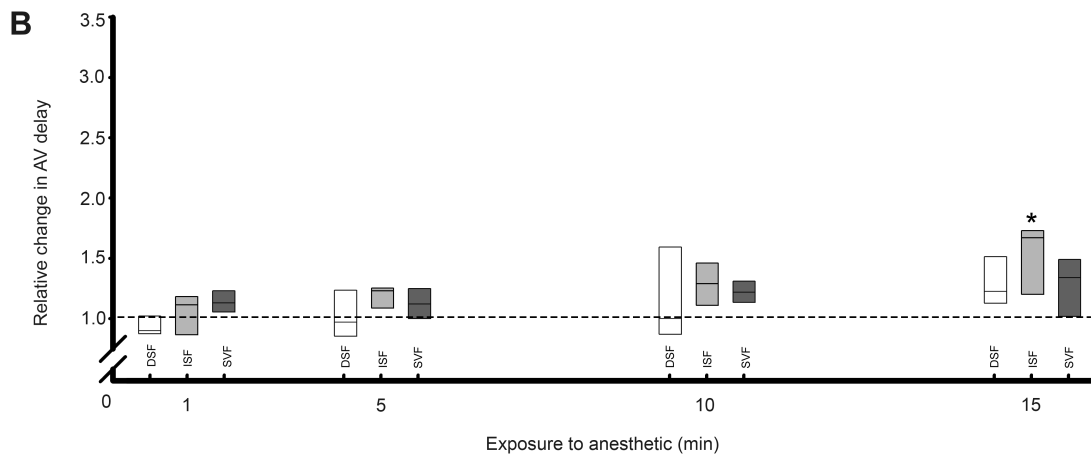
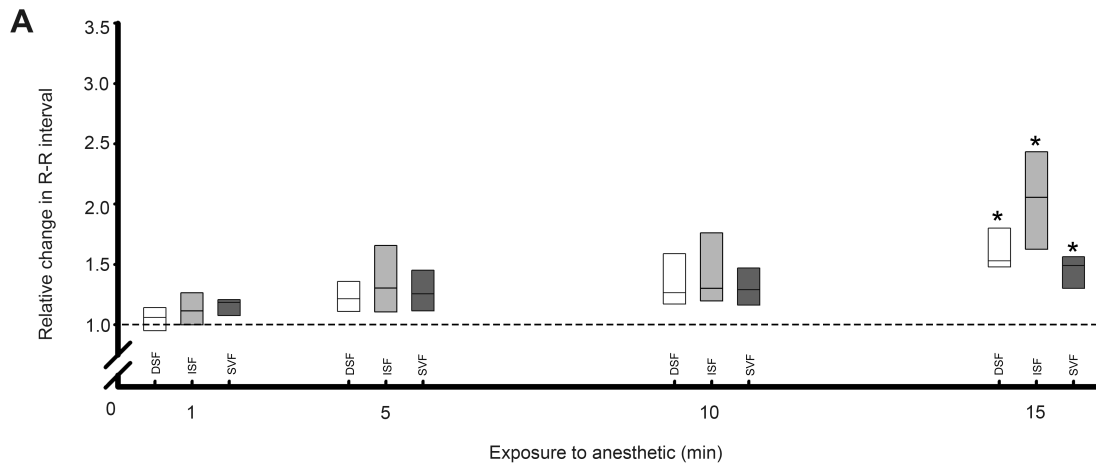


Figure 6.3. Concentration-dependent chronotropic responses of the isolated zebrafish heart to anaesthetics relative to a 1.0 human minimum alveolar concentration (MAC) as calculated by patient monitor. **A:** Effective concentrations inducing bradycardia in the zebrafish heart were similar to clinical concentrations. Chronotropic responses were observed beginning at 0.5 MAC and increasing at higher concentrations. **B:** Effects of altering anaesthetic concentrations on atrioventricular delay in the zebrafish heart were similar to clinical concentrations. Dashed line indicates the pre-treatment heart rate. *P < 0.05 vs. pre-exposure values by paired One-way ANOVA; *n*=6 for each group.

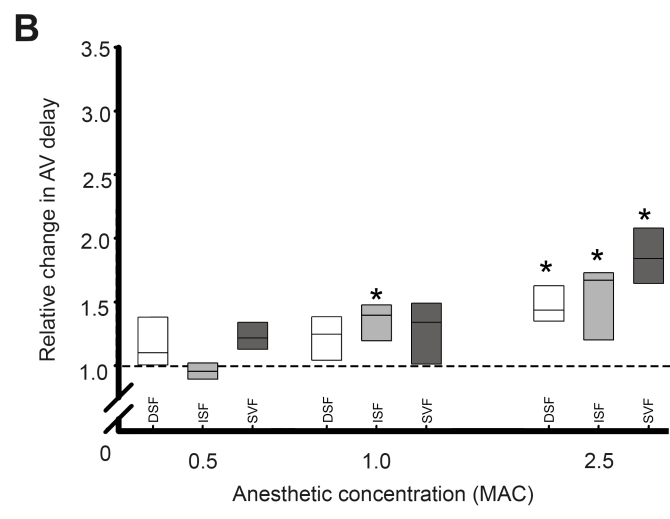
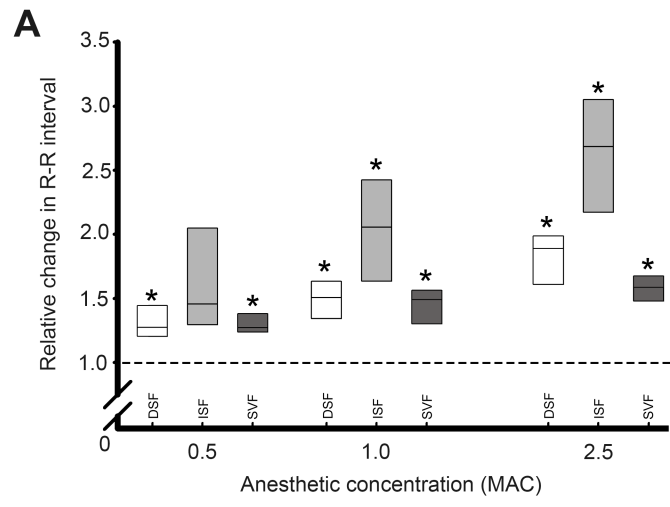


Figure 6.4. Effects of anesthetic exposure during autonomic blockade on heart rate.

Isolated hearts were exposed to a combination of atropine (200 μ M; parasympatholytic) and timolol (100 μ M; sympatholytic) to investigate the involvement of the intracardiac autonomic nervous system. In the presence of autonomic blockade the significant elongation of the R-R interval were still observed during exposure to desflurane (DSF) and isoflurane (ISF) were maintained. Autonomic blockade prevented the elongation of the R-R interval during exposure to sevoflurane (SVF). Dashed line indicates the pre-treatment heart rate. * $P < 0.05$ vs. pre-exposure values by paired Student's *t*-test; $n=6$ for each group.

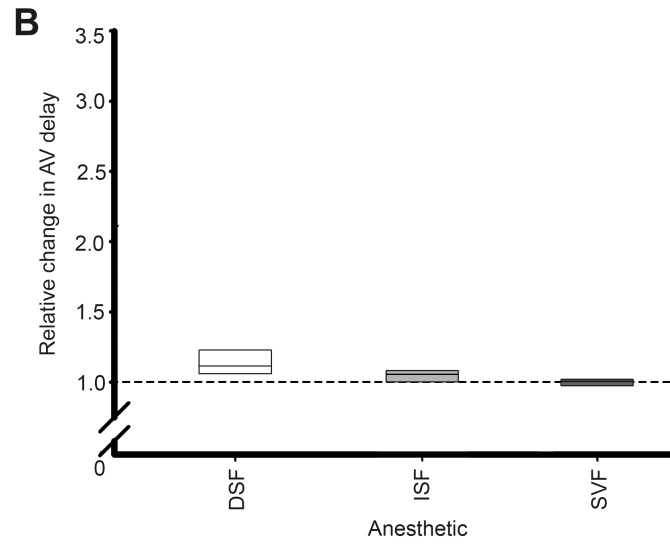
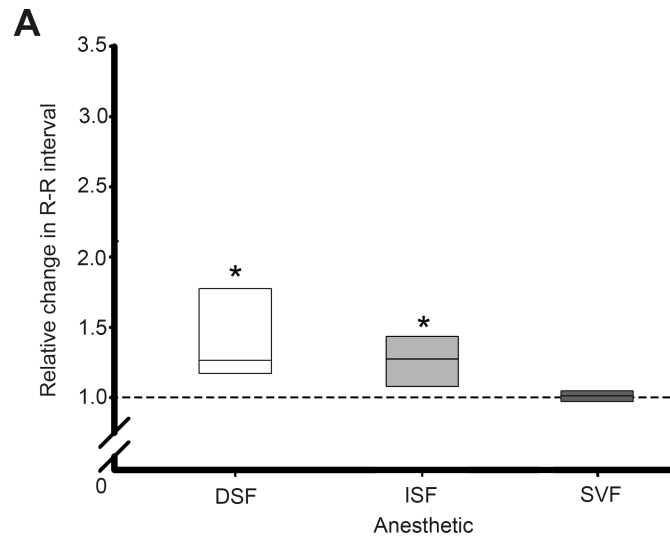
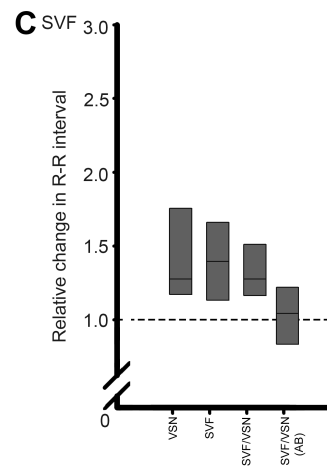
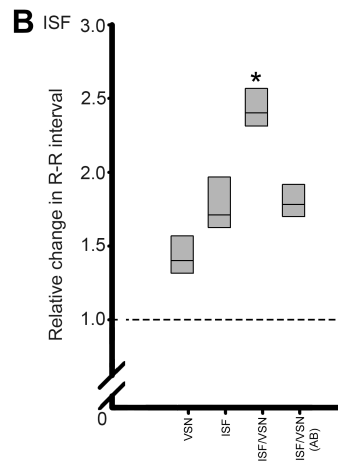
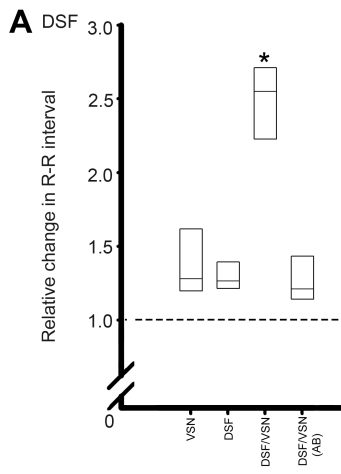


Figure 6.5. Effects of vagosympathetic nerve stimulation on HR during anesthetic exposure. Isolated hearts were exposed to anaesthetic or a combination of anaesthetic and autonomic blockade to investigate the involvement of the intracardiac autonomic nervous system. In all cases pre-anaesthetic VSN resulted in a significant elongation of the R-R interval. In the presence of desflurane (A; DSF) and isoflurane (B; ISF) the effects of VSN- and anaesthetic-induced R-R elongation were summative. Sevoflurane (C; SVF) prevented the VSN-induced R-R elongation. Dashed line indicates the pre-treatment heart rate. *P < 0.05 vs. pre-exposure values, ⁺P < 0.05 vs. pre-exposure VSN by paired Student's *t*-test; *n*=6 for each group.



CHAPTER 7

CONCLUSIONS

In the vertebrate heart the intracardiac nervous system is a common pathway for autonomic control of cardiac output. Neural elements modulate the activity of effectors within the heart to adjust cardiac output, maintaining optimal perfusion of the body tissues under a wide range of metabolic activities. In this thesis I investigated the organization and function of the intracardiac nervous system of the zebrafish heart. The focus of this work is on the role of this part of the autonomic nervous system in controlling pacemaker cells that determine heart rate, a key component in setting cardiac output. My work has revealed within the zebrafish intracardiac nervous system a complex neuroanatomy in addition to the classic cholinergic and adrenergic vertebrate hallmarks of cardiac control. Overall, the results of my studies contribute significant advances in the establishment of the zebrafish as a new model for studies of integrative autonomic cardiac control.

In Chapter 2 I have described the neuroanatomy of the zebrafish intracardiac nervous system, distribution of intracardiac neurons, and their neurotransmitter phenotypes. Most ICNs were located at the venous pole in a plexus around the sinoatrial valve; the plexus contained cholinergic, adrenergic, and nitrergic ICNs and vasoactive intestinal polypeptide-positive terminals. For these studies, I applied preliminary immunohistochemical screening in the zebrafish heart using antibodies for the major autonomic neurotransmitters known to be involved in the mammalian intracardiac nervous system. Putative pacemaker cells near the plexus were identified with hyperpolarization-activated, cyclic nucleotide-gated channel 4 (HCN4), a known marker for mammalian pacemaker cells, and establishing one of the first putative pacemaker markers in zebrafish.

Extrinsic axons from the left and right vagosympathetic trunks innervated both the sinoatrial plexus and atrial and ventricular walls. Results of this study have shown that the

intracardiac nervous system in the adult zebrafish is anatomically and neurochemically complex, providing a substrate for autonomic control of cardiac effectors in all chambers. To further compare similarities, as well as potential differences, of the zebrafish intracardiac nervous system with common mammalian models, future studies should focus on other transmitters, peptides and modulators (e.g. angiotensins, kinins, and natriuretic factors) known to be present in the heart of other species.

Given the rich cardiac innervation I described in Chapter 2, I next sought to investigate the mechanisms through which the ICNS coordinates function. In Chapter 3 I presented the isolated, innervated zebrafish heart as a novel alternative model for functional studies of autonomic control of heart rate. Stimulation of individual cardiac vagosympathetic nerve trunks evoked biphasic rate changes; these effects were mimicked by direct application of cholinergic and adrenergic agents and blocked by autonomic antagonists. Optical mapping of electrical activity confirmed the sinoatrial region as the site of origin of normal pacemaker activity, and identified a secondary pacemaker in the atrioventricular region. In addition putative pacemaker cells in the sinoatrial and atrioventricular regions expressed adrenergic and cholinergic receptors. As with Chapter 2, this study focused on the investigation of classical neurotransmitter modulators of heart rate. In preliminary experiments it was observed that drastic, and dose dependent changes could be induced by nitric oxide donors, as has been reported in mammals, and suggesting that the zebrafish heart is responsive to other modulators. Future studies should therefore focus on other known modulators of heart rate and their effects in the zebrafish heart. Collectively, it was demonstrated that the zebrafish heart contains all the hallmarks of cardiac control, establishing this preparation as a viable model for studies of integrative

physiological control of cardiac function by intracardiac neurons.

In Chapter 4 I investigated the bilateral extrinsic vagosympathetic inputs to the zebrafish heart, and through immunohistochemical detection of cFOS and pERK upregulation, identified distinct populations of intracardiac neurons that were activated during VSN stimulation. This represents the first study in which these markers have been used to show the patterns of neuronal activation in the heart as a result of changes in extrinsic drive, establishing a new method to investigate cardiac function. It is known that activation of the intracardiac nervous system shifts the locus of the sinoatrial pacemaker and the pattern of electrical activity to the myocardium in mammals. Given the distinct patterns of vagosympathetic terminal fields (Chapter 2) and ICNs activated during stimulation (Chapter 3), I sought to resolve if such spatial organization existed within the effector cells. My studies reveal that the site of sinoatrial initiation can become progressively more variable during graded vagal activation. That this disruption could be blocked by autonomic antagonists supports the hypothesis that these effects have a neural origin. This is the first detailed report of neurally mediated shifts in pacemaker locus in the teleost heart. This powerful system is common to all mammalian models that have been studied, and my results show that it is present also in the zebrafish heart. Therefore the mechanisms, not only for autonomic control of pacemaker rate, but for the location of the pacemaker itself, is conserved from fish to mammals.

In the preceding chapters I have established the basic neuroanatomy and function of the ICNS in controlling heart rate in the zebrafish. In Chapters 5 and 6, I performed studies to investigate the applicability of the isolated zebrafish heart for studies oriented to more clinical issues. In Chapter 5, I demonstrated the intracardiac distribution of serotonin

and its chronotropic effects, as well as dissected the proportion of these effects resulting from direct serotonergic actions on the pacemaker cells versus those acting indirectly through the ICNS for the first time. Serotonin distribution, as well as the chronotropic effects of serotonin applied to the heart, mimicked those observed in mammalian species and humans. That these effects could also be blocked or enhanced by the same pharmacological agents that act in mammals supports the hypothesis that serotonergic pathways and their actions are conserved from zebrafish to mammals. In my study, only the cellular localization of serotonin was investigated, and while the staining patterns I showed permit some inferences about the mechanisms of reuptake and synthesis, future studies must confirm the roles of these processes within the cells I have identified. A potential way to investigate this would be to perform immunohistochemical detection of 5-HT, as well as precursors or enzymes, in hearts that have been treated with serotonergic compounds which will alter endogenous 5-HT levels such as reserpine (to deplete sequestered serotonin), permitting greater insights into these mechanisms.

In Chapter 6 I determined the chronotropic responses to vapour anesthetics and the proportion of these responses resulting from direct effects on pacemaker cells versus those acting indirectly through the ANS to alter rate were determined. Anesthetics that are commonly used clinically had profound inhibitory effects on heart rate in the isolated zebrafish heart. For two of three anaesthetics tested such inhibitions resulted from direct effects on the myocardium, presumably acting on pacemaker cells. For the third anesthetic used, I presented evidence that its action on heart rate occurred at least in part via the intracardiac nervous system. Overall, the results of the studies in Chapters 5 and 6 offer a new model for studies to further our understanding the direct and neurally mediated

pathways involved in heart rate regulation that may potentially be responsible for heart dysfunction known to occur in patients using serotonergic anti-depressants as well as those observed in patients undergoing clinical anesthesia. Given that the studies in Chapters 2 and 3 implicate HCN4, a channel crucial to the characteristic diastolic depolarization of pacemaker cells, and that there exist pharmacologic blockers for this channel (e.g. ivabradine and zatebradine), experiments combining exposure to these compounds with anesthetics will need to be performed to determine this.

In conclusion the major goal of this thesis was to undertake studies into the integrative control of cardiac function in the zebrafish. My work has provided information about the anatomy and function of the elements involved in chronotropic control in a whole heart in a way previously not possible. Zebrafish offer an interesting model to provide further answers to these questions given the high degree of conservation of their heart in terms of function, molecular pathways and genetics. Despite its apparent simplicity, the zebrafish heart appears to be capable of the same finely coordinated regulation of cardiac output as are the hearts of vertebrates with more complex hearts and circulatory systems. Findings from these studies provide the basis for normal physiology of autonomic control in the zebrafish heart, and given the rapid, recent advances in genetic modification of zebrafish, there exists the potential to more fully understand the mechanisms governing autonomic control of the heart in pathologic conditions. The zebrafish heart thus represents a unique opportunity for investigating key roles of the ICNS, identifying the organization and roles of intracardiac neurons in specific effector-control pathways within this system. Overall, the results of these studies contribute significant advances in the establishment of the zebrafish as a new model for studies of integrative autonomic cardiac control.

CITATIONS

- Ackermann, G. E., and B. H. Paw.** "Zebrafish: a genetic model for vertebrate organogenesis and human disorders." *Frontiers in Bioscience* 8 (2003): d1227-53.
- Airrt, M. J., et al.** "Movement disorders and neurochemical changes in zebrafish larvae after bath exposure to fluoxetine (PROZAC)." *Neurotoxicology and teratology* 29.6 (2007): 652-664.
- Akiyama, T., and T. Yamazaki.** "Effects of right and left vagal stimulation on left ventricular acetylcholine levels in the cat." *Acta Physiologica Scandinavica* 172.1 (2001): 11-16.
- Allessie, M.A., and F. I. Bonke.** "Direct demonstration of sinus node reentry in the rabbit heart." *Circulation Research* 44.4 (1979): 557-568.
- Ampatzis, K., and C. R. Dermon.** "Regional distribution and cellular localization of β 2-adrenoceptors in the adult zebrafish brain (*Danio rerio*)." *Journal of Comparative Neurology* 518.9 (2010): 1418-1441.
- Ardell, J. L., et al.** "Activity of in vivo atrial and ventricular neurons in chronically decentralized canine hearts." *American Journal of Physiology-Heart and Circulatory Physiology* 260.3 (1991): H713-H721.
- Ardell, J. L., and W. C. Randall.** "Selective vagal innervation of sinoatrial and atrioventricular nodes in canine heart." *American Journal of Physiology-Heart and Circulatory Physiology* 251.4 (1986): H764-H773.
- Ardell, J. L., et al.** "Chronic spinal cord stimulation modifies intrinsic cardiac synaptic efficacy in the suppression of atrial fibrillation." *Autonomic Neuroscience* 186 (2014): 38-44.
- Armour, J. A.** "Potential clinical relevance of the 'little brain' on the mammalian heart." *Experimental Physiology* 93.2 (2008): 165-176.
- Arnaut, R., et al.** "Zebrafish model for human long QT syndrome." *Proceedings of the National Academy of Sciences* 104.27 (2007): 11316-11321.
- Arrenberg, A. B., et al.** "Optogenetic control of cardiac function." *Science* 330.6006 (2010): 971-974.
- Audero, E., et al.** "Sporadic autonomic dysregulation and death associated with excessive serotonin autoinhibition." *Science* 321.5885 (2008): 130-133.
- Auricchio, A., et al.** "Effect of pacing chamber and atrioventricular delay on acute systolic function of paced patients with congestive heart failure." *Circulation* 99.23 (1999): 2993-3001.

- Ausoni, S., and S. Sartore.** "From fish to amphibians to mammals: in search of novel strategies to optimize cardiac regeneration." *Journal of Cell Biology* 184.3 (2009): 357-364.
- Aypar, E., et al.** "The effects of sevoflurane and desflurane anesthesia on QTc interval and cardiac rhythm in children." *Pediatric Anesthesia* 17.6 (2007): 563-567.
- Bakkers, J.** "Zebrafish as a model to study cardiac development and human cardiac disease." *Cardiovascular Research* 91.2 (2011): 279-288.
- Barrionuevo, W. R., and W. W. Burggren.** "O₂ consumption and heart rate in developing zebrafish (*Danio rerio*): influence of temperature and ambient O₂." *American Journal of Physiology-Regulatory, Integrative and Comparative Physiology* 276.2 (1999): R505-R513.
- Baruscotti, M., and R. B. Robinson.** "Electrophysiology and pacemaker function of the developing sinoatrial node." *American Journal of Physiology-Heart and Circulatory Physiology* 293.5 (2007): H2613-H2623.
- Beaumont, Eric, et al.** "Network interactions within the canine intrinsic cardiac nervous system: implications for reflex control of regional cardiac function." *Journal of Physiology* 591.18 (2013): 4515-4533.
- Beaumont, E., et al.** "Vagus nerve stimulation mitigates intrinsic cardiac neuronal and adverse myocyte remodeling postmyocardial infarction." *American Journal of Physiology-Heart and Circulatory Physiology* 309.7 (2015): H1198-H1206.
- Beauvallet, M., F. Godefroy, and J. Weil-Fugazza.** "Modification of the heart 5-hydroxytryptamine level during a diet high in sodium chloride." *Comptes rendus des seances de la Societe de biologie et de ses filiales* 162.12 (1967): 2085-2088.
- Berdougo, E., et al.** "Mutation of weak atrium/atrial myosin heavy chain disrupts atrial function and influences ventricular morphogenesis in zebrafish." *Development* 130.24 (2003): 6121-6129.
- Berkowitz, B. A., C-H. Lee, and S. Spector.** "Disposition of serotonin in the rat blood vessels and heart." *Clinical and Experimental Pharmacology and Physiology* 1.5 (1974): 397-400.
- Bernard, J-M, et al.** "Effects of sevoflurane and isoflurane on cardiac and coronary dynamics in chronically instrumented dogs." *Anesthesiology* 72.4 (1990): 659-662.
- Betz, W. J., F. Mao, and G. S. Bewick.** "Activity-dependent fluorescent staining and destaining of living vertebrate motor nerve terminals." *Journal of Neuroscience* 12.2 (1992): 363-375.

- Bianchi, P., et al.** "A new hypertrophic mechanism of serotonin in cardiac myocytes: receptor-independent ROS generation." *The FASEB Journal* 19.6 (2005): 641-643.
- Bisgrove, B. W., et al.** "Expression of c-ret in the zebrafish embryo: Potential roles in motoneuronal development." *Journal of Neurobiology* 33.6 (1997): 749-768.
- Blinder, K. J., et al.** "Central control of atrio-ventricular conduction and left ventricular contractility in the cat heart: synaptic interactions of vagal preganglionic neurons in the nucleus ambiguus with neuropeptide Y-immunoreactive nerve terminals." *Autonomic Neuroscience* 131.1 (2007): 57-64.
- Blinder, K. J., T. A. Johnson, and V. John Massari.** "Negative inotropic vagal preganglionic neurons in the nucleus ambiguus of the cat: neuroanatomical comparison with negative chronotropic neurons utilizing dual retrograde tracers." *Brain Research* 804.2 (1998): 325-330.
- Boineau, J. P., et al.** "Demonstration of a widely distributed atrial pacemaker complex in the human heart." *Circulation* 77.6 (1988): 1221-1237.
- Bosch, T. J., S. Maslam, and B. L. Roberts.** "A polyclonal antibody against mammalian FOS can be used as a cytoplasmic neuronal activity marker in a teleost fish." *Journal of Neuroscience Methods* 58.1 (1995): 173-179.
- Bouman, L. N., et al.** "Pacemaker shift in the sino-atrial node during vagal stimulation." *Pflügers Archiv* 302.3 (1968): 255-267.
- Briggs, J. P.** "The zebrafish: a new model organism for integrative physiology." *American Journal of Physiology-Regulatory, Integrative and Comparative Physiology* 282.1 (2002): R3-R9.
- Brodde O-E.** β -adrenoceptors, in *Receptor Pharmacology and Function* (Williams M, Glennon RA, & Timmermans PBMWM eds). Pp 207-255. Marcel Dekker Inc., New York, 1989.
- Brodde, O-E, and M. C. Michel.** "Adrenergic and muscarinic receptors in the human heart." *Pharmacological Reviews* 51.4 (1999): 651-690.
- Brown, G. L., and J. C. Eccles.** "The action of a single vagal volley on the rhythm of the heart beat." *Journal of Physiology* 82.2 (1934): 211.
- Brüning, G., K. Hattwig, and B. Mayer.** "Nitric oxide synthase in the peripheral nervous system of the goldfish, *Carassius auratus*." *Cell and Tissue Research* 284.1 (1996): 87-98.
- Brunton, L. L., B. Chabner, and B. C. Knollmann,** eds. *Goodman & Gilman's the pharmacological basis of therapeutics*. Vol. 12. New York: McGraw-Hill Medical, 2011.

- Burnstock, G.** "Evolution of the autonomic innervation of visceral and cardiovascular systems in vertebrates." *Pharmacological Reviews* 21.4 (1969): 247-324.
- Caulfield, M. P.** "Muscarinic receptors—characterization, coupling and function." *Pharmacology & Therapeutics* 58.3 (1993): 319-379.
- Chaudhari, G. H., et al.** "Optimization of the adult zebrafish ECG method for assessment of drug-induced QTc prolongation." *Journal of Pharmacological and Toxicological Methods* 67.2 (2013): 115-120.
- Chen, H., et al.** "In vivo reversal of general anesthesia by cucurbit [7] uril with zebrafish models." *RSC Advances* 5.78 (2015): 63745-63752.
- Chen, J-N, et al.** "Mutations affecting the cardiovascular system and other internal organs in zebrafish." *Development* 123.1 (1996): 293-302.
- Chen, X., et al.** "HCN subunit-specific and cAMP-modulated effects of anesthetics on neuronal pacemaker currents." *Journal of Neuroscience* 25.24 (2005): 5803-5814.
- Cheng, Z. J., et al.** "Differential control over postganglionic neurons in rat cardiac ganglia by NA and DmnX neurons: anatomical evidence." *American Journal of Physiology-Regulatory, Integrative and Comparative Physiology* 286.4 (2004): R625-R633.
- Chi, N. C., et al.** "Genetic and physiologic dissection of the vertebrate cardiac conduction system." *PLoS Biology* 6.5 (2008): e109.
- Christoffels, V. M., et al.** "Development of the pacemaker tissues of the heart." *Circulation Research* 106.2 (2010): 240-254.
- Chuang, J. I., S. S. Chen, and M. T. Lin.** "Melatonin decreases brain serotonin release, arterial pressure and heart rate in rats." *Pharmacology* 47.2 (1993): 91-97.
- Constantinides, C., R. Mean, and B. J. Janssen.** "Effects of isoflurane anesthesia on the cardiovascular function of the C57BL/6 mouse." *ILAR Journal/National Research Council, Institute of Laboratory Animal Resources* 52 (2011): e21.
- Coppola, E., et al.** "Phox2b expression in the taste centers of fish." *Journal of Comparative Neurology* 520.16 (2012): 3633-3649.
- Dahme, T., H. A. Katus, and W. Rottbauer.** "Fishing for the genetic basis of cardiovascular disease." *Disease Models and Mechanisms* 2.1-2 (2009): 18-22.
- Davies, P. J., J. A. Donald, and G. Campbell.** "The distribution and colocalization of neuropeptides in fish cardiac neurons." *Journal of the Autonomic Nervous System* 46.3 (1994): 261-272.

- Dawood, T., et al.** "Specific serotonin reuptake inhibition in major depressive disorder adversely affects novel markers of cardiac risk." *Hypertension Research* 30.4 (2007): 285.
- Dershwitz M., and Rosow C.** "Pharmacology of intravenous anaesthetics." *Anesthesiology*. New York: McGraw-Hill, pp. 849-868, 2008.
- Dhein, S., C. J. Van Koppen, and O-E Brodde.** "Muscarinic receptors in the mammalian heart." *Pharmacological Research* 44.3 (2001): 161-182.
- Dodd, A., et al.** "Modeling human disease by gene targeting." *Methods in Cell Biology* 76 (2004): 593-612.
- Donald J.** Autonomic nervous system. In: Evans DH, editor. *The Physiology of Fishes*. Second ed. Boca Raton, FL, USA: CRC Press. (1998): 407-439.
- Dumbarton, T. C., et al.** "Adrenergic control of swimbladder deflation in the zebrafish (*Danio rerio*)." *Journal of Experimental Biology* 213.14 (2010): 2536-2546.
- Dvornikov, A. V., et al.** "Novel approaches to determine contractile function of the isolated adult zebrafish ventricular cardiac myocyte." *Journal of Physiology* 592.9 (2014): 1949-1956.
- Ebert T. J., and M. Muzi.** Sympathetic activation with desflurane in humans. In: Bosnjak Z, Kampine JP, eds. *Advances in pharmacology*, vol 31: anesthesia and cardiovascular disease. Academic Press, San Diego, pp. 369-78, 1994.
- Ebert, T. J., and M. Muzi.** "Sympathetic hyperactivity during desflurane anesthesia in healthy volunteers. A comparison with isoflurane." *Anesthesiology* 79.3 (1993): 444-453.
- Ebert, T. J., C. P. Harkin, and M. Muzi.** "Cardiovascular responses to sevoflurane: a review." *Anesthesia & Analgesia* 81.6S (1995a): 11S-22S.
- Ebert, T. J., M. Muzi, and C. W. Lopatka.** "Neurocirculatory Responses to Sevoflurane in Humans: A Comparison to Desflurane." *Journal of the American Society of Anesthesiologists* 83.1 (1995b): 88-95.
- Efimov, I. R., and V. V. Fedorov.** "Chessboard of atrial fibrillation: reentry or focus? Single or multiple source (s)? Neurogenic or myogenic?." *American Journal of Physiology-Heart and Circulatory Physiology* 289.3 (2005): H977-H979.
- Eger, E. I., L. J. Saidman, and B. Brandstater.** "Minimum Alveolar Anesthetic Concentration A Standard of Anesthetic Potency." *Journal of the American Society of Anesthesiologists* 26.6 (1965): 756-763.

- El-Sherif, N. A. B. I. L., et al.** "Re-entrant ventricular arrhythmias in the late myocardial infarction period. 2. Patterns of initiation and termination of re-entry." *Circulation* 55.5 (1977): 702-719.
- Eyster, J. A. E., and W. J. Meek.** "Experiments on the origin and propagation of the impulse in the heart: point of primary negativity in the mammalian heart and the spread of negativity to other regions." *Heart* 5.119 (1913): 1913-1914.
- Farrell A. P., and D. G. Jones.** The heart. In: Hoar WS, Randall DJ, Farrell AP, editors. *Fish Physiology*. Toronto: Academic Press. (1992): 1-88.
- Fedorov, V. V., et al.** "Optical mapping of the isolated coronary-perfused human sinus node." *Journal of the American College of Cardiology* 56.17 (2010): 1386-1394.
- Fedorov, V. V., et al.** "Postganglionic nerve stimulation induces temporal inhibition of excitability in rabbit sinoatrial node." *American Journal of Physiology-Heart and Circulatory Physiology* 291.2 (2006): H612-H623.
- Finney, J. L., et al.** "Structure and autonomic innervation of the swim bladder in the zebrafish (*Danio rerio*)." *Journal of Comparative Neurology* 495.5 (2006): 587-606.
- Fish R. E., M. E. Brown, P.J. Danneman, and A. Z. Karas,** ed. (2008). *Anesthesia and Analgesia in Laboratory Animals*. Elsevier, Amsterdam.
- Fishman, A. P.** "Aminorex to fen/phen an epidemic foretold." *Circulation* 99.1 (1999): 156-161.
- Flood, P., J. Ramirez-Latorre, and L. Role.** "Alpha4beta2 neuronal nicotinic acetylcholine receptors in the central nervous system are inhibited by isoflurane and propofol, but alpha7-type nicotinic acetylcholine receptors are unaffected." *Journal of the American Society of Anesthesiologists* 86.4 (1997): 859-865.
- Forman S. A., and G. A. Mashour.** "Pharmacology of inhalational anaesthetics." *Anesthesiology*. New York, McGraw-Hill Companies, pp.739-766, 2008.
- Fowler M. A., and B. D. Spiess.** (2009). In *Clinical Anesthesia*, ed. Barash PG, Cullen BF, Stoelting RK, Cahalan MK & Stock MC, pp. 1421-1443. Lippincott Williams and Wilkins, Philadelphia.
- Frishman, W. H., and P. Grewall.** "Serotonin and the heart." *Annals of Medicine* 32.3 (2000): 195-209.
- Funakoshi, K., and M. Nakano.** "The sympathetic nervous system of anamniotes." *Brain, Behavior and Evolution* 69.2 (2007): 105-113.
- Furness, J. B., et al.** "Intrinsic primary afferent neurons and nerve circuits within the intestine." *Progress in Neurobiology* 72.2 (2004): 143-164.

- Gannon, B. J., and G. Burnstock.** "Excitatory adrenergic innervation of the fish heart." *Comparative Biochemistry and Physiology* 29.2 (1969): 765-773.
- Gao, Y-J, and R-R Ji.** "c-Fos and pERK, which is a better marker for neuronal activation and central sensitization after noxious stimulation and tissue injury?." *The Open Pain Journal* 2 (2009): 11.
- Gibbins I.** Comparative anatomy and evolution of the autonomic nervous system. In: Nilsson S, Holmgren S, editors. *Comparative Physiology and Evolution of the Autonomic Nervous System*. Switzerland: Harwood Academic Publishers. (1994): 1-67.
- Gibbons, D. D., et al.** "Neuromodulation targets intrinsic cardiac neurons to attenuate neuronally mediated atrial arrhythmias." *American Journal of Physiology-Regulatory, Integrative and Comparative Physiology* 302.3 (2012): R357-R364.
- Glassman, A. H., S. P. Roose, and J. T. Bigger.** "The safety of tricyclic antidepressants in cardiac patients: risk-benefit reconsidered." *Journal of the American Medical Association* 269.20 (1993): 2673-2675.
- Goldberg, J. M., et al.** "Sympathetically induced pacemaker shifts following sinus node excision." *American Journal of Physiology--Legacy Content* 224.6 (1973): 1468-1474.
- Goldreyer, B. N., and A. N. Damato.** "The essential role of atrioventricular conduction delay in the initiation of paroxysmal supraventricular tachycardia." *Circulation* 43.5 (1971): 679-687.
- Goldstein, A. M., B. S. Ticho, and M. C. Fishman.** "Patterning the heart's left-right axis: From zebrafish to man." *Developmental Genetics* 22.3 (1998): 278-287.
- Gorman, J. M., and R. P. Sloan.** "Heart rate variability in depressive and anxiety disorders." *American Heart Journal* 140.4 (2000): S77-S83.
- Gould, R. A., et al.** "Hierarchical approaches for systems modeling in cardiac development." *Wiley Interdisciplinary Reviews: Systems Biology and Medicine* 5.3 (2013): 289-305.
- Gray, A. L., et al.** "Parasympathetic control of the heart. II. A novel interganglionic intrinsic cardiac circuit mediates neural control of heart rate." *Journal of Applied Physiology* 96.6 (2004): 2273-2278.
- Greenberg, M. E., E. B. Ziff, and L. A. Greene.** "Stimulation of neuronal acetylcholine receptors induces rapid gene transcription." *Science* 234.4772 (1986): 80-83.

- Hancock, J. C., and D. B. Hoover.** "Capsaicin-evoked bradycardia in anesthetized guinea pigs is mediated by endogenous tachykinins." *Regulatory Peptides* 147.1 (2008): 19-24.
- Hanley, P. J., et al.** "Halothane, isoflurane and sevoflurane inhibit NADH: ubiquinone oxidoreductase (complex I) of cardiac mitochondria." *Journal of Physiology* 544.3 (2002): 687-693.
- Hansen, B. J., et al.** "Atrial fibrillation driven by micro-anatomic intramural re-entry revealed by simultaneous sub-epicardial and sub-endocardial optical mapping in explanted human hearts." *European Heart Journal* (2015): ehv233.
- Harkin, C. P., et al.** "Direct negative inotropic and lusitropic effects of sevoflurane." *Anesthesiology* 81.1 (1994): 156-167.
- Haverinen, J., and M. Vornanen.** "Temperature acclimation modifies sinoatrial pacemaker mechanism of the rainbow trout heart." *American Journal of Physiology-Regulatory, Integrative and Comparative Physiology* 292.2 (2007): R1023-R1032.
- Heath, B. M., et al.** "Translation of flecainide-and mexiletine-induced cardiac sodium channel inhibition and ventricular conduction slowing from nonclinical models to clinical." *Journal of Pharmacological and Toxicological Methods* 63.3 (2011): 258-268.
- Hecker, L., et al.** "Functional evaluation of isolated zebrafish hearts." *Zebrafish* 5.4 (2008): 319-322.
- Hedberg, A., K. P. Minneman, and P. B. Molinoff.** "Differential distribution of beta-1 and beta-2 adrenergic receptors in cat and guinea-pig heart." *Journal of Pharmacology and Experimental Therapeutics* 212.3 (1980): 503-508.
- Hemmings, H. C., et al.** "Emerging molecular mechanisms of general anesthetic action." *Trends in Pharmacological Sciences* 26.10 (2005): 503-510.
- Henn, F. A., and A. Hamberger.** "Glial cell function: uptake of transmitter substances." *Proceedings of the National Academy of Sciences* 68.11 (1971): 2686-2690.
- Herdegen, T., et al.** "Expression of JUN, KROX, and CREB transcription factors in goldfish and rat retinal ganglion cells following optic nerve lesion is related to axonal sprouting." *Journal of Neurobiology* 24.4 (1993): 528-543.
- Hoage, T., Y. Ding, and X. Xu.** "Quantifying cardiac functions in embryonic and adult zebrafish." *Cardiovascular Development: Methods and Protocols* (2012): 11-20.
- Holaday, D. A., and F. R. Smith.** "Clinical characteristics and biotransformation of sevoflurane in healthy human volunteers." *Anesthesiology* 54.2 (1981): 100-106.

- Holmgren, S.** "Regulation of the heart of a teleost, *Gadus morhua*, by autonomic nerves and circulating catecholamines." *Acta Physiologica Scandinavica* 99.1 (1977): 62-74.
- Howe, K., et al.** "The zebrafish reference genome sequence and its relationship to the human genome." *Nature* 496.7446 (2013): 498-503.
- Hua, F., et al.** "c-Fos expression in rat brain stem and spinal cord in response to activation of cardiac ischemia-sensitive afferent neurons and electrostimulatory modulation." *American Journal of Physiology-Heart and Circulatory Physiology* 287.6 (2004): H2728-H2738.
- Huang, W-C, et al.** "Combined use of MS-222 (tricaine) and isoflurane extends anesthesia time and minimizes cardiac rhythm side effects in adult zebrafish." *Zebrafish* 7.3 (2010): 297-304.
- Hucker, W. J., V. P. Nikolski, and I. R. Efimov.** "Autonomic control and innervation of the atrioventricular junctional pacemaker." *Heart Rhythm* 4.10 (2007): 1326-1335.
- Hudetz, A. G., J. D. Wood, and J. P. Kampine.** "Cholinergic reversal of isoflurane anesthesia in rats as measured by cross-approximate entropy of the electroencephalogram." *Journal of the American Society of Anesthesiologists* 99.5 (2003): 1125-1131.
- Hulme, E. C., N. J. M. Birdsall, and N. J. Buckley.** "Muscarinic receptor subtypes." *Annual Review of Pharmacology and Toxicology* 30.1 (1990): 633-673.
- Hüneke, R., et al.** "Effects of volatile anesthetics on cardiac ion channels." *Acta Anaesthesiologica Scandinavica* 48.5 (2004): 547-561.
- Irisawa, H.** "Comparative physiology of the cardiac pacemaker mechanism." *Physiological Reviews* 58.2 (1978): 461-498.
- Jacob, E., et al.** "Influence of hypoxia and of hypoxemia on the development of cardiac activity in zebrafish larvae." *American Journal of Physiology-Regulatory, Integrative and Comparative Physiology* 283.4 (2002): R911-R917.
- Jacobs, L., and J. H. Comroe.** "Reflex Apnea, Bradycardia, and Hypotension Produced by Serotonin and Phenylidguanidecting on the Nodose Ganglia of the Cat." *Circulation Research* 29.2 (1971): 145-155.
- Jaffré, F., et al.** "Serotonin and angiotensin receptors in cardiac fibroblasts coregulate adrenergic-dependent cardiac hypertrophy." *Circulation Research* 104.1 (2009): 113-123.
- Jänig W.** *The Integrative Action of the Autonomic Nervous System: Neurobiology of Homeostasis.* Cambridge, UK: Cambridge University Press. 610 p. (2006).

- Janssen, B. J. A., et al.** "Effects of anesthetics on systemic hemodynamics in mice." *American Journal of Physiology-Heart and Circulatory Physiology* 287.4 (2004): H1618-H1624.
- Jonz, M. G., et al.** "Peripheral chemoreceptors in fish: a brief history and a look ahead." *Comparative Biochemistry and Physiology Part A: Molecular & Integrative Physiology* 186 (2015): 27-38.
- Jonz, M. G., I. M. Fearon, and C. A. Nurse.** "Neuroepithelial oxygen chemoreceptors of the zebrafish gill." *Journal of Physiology* 560.3 (2004): 737-752.
- Kimmel, C. B., et al.** "Stages of embryonic development of the zebrafish." *Developmental Dynamics* 203.3 (1995): 253-310.
- Kloos, W., H. A. Katus, and B. Meder.** "Genetic cardiomyopathies." *Herz* 37.6 (2012): 612-618.
- Kurosawa, M., et al.** "Effects of sevoflurane on autonomic nerve activities controlling cardiovascular functions in rats." *Journal of Anesthesia* 3.2 (1989): 109-117.
- Kuscha, V., et al.** "Lesion-induced generation of interneuron cell types in specific dorsoventral domains in the spinal cord of adult zebrafish." *Journal of Comparative Neurology* 520.16 (2012): 3604-3616.
- Kuwajima, T., et al.** "ClearT: a detergent-and solvent-free clearing method for neuronal and non-neuronal tissue." *Development* 140.6 (2013): 1364-1368.
- Lakatta, E. G., and D. DiFrancesco.** "JMCC Point-Counterpoint: What keeps us ticking, a funny current, a Calcium clock, or both?." *Journal of Molecular and Cellular Cardiology* 47.2 (2009): 157.
- Lakatta, E. G., V. A. Maltsev, and T. M. Vinogradova.** "A coupled SYSTEM of intracellular Ca²⁺ clocks and surface membrane voltage clocks controls the timekeeping mechanism of the heart's pacemaker." *Circulation Research* 106.4 (2010): 659-673.
- Lang, S. A., H. Zieske, and M. N. Levy.** "Insignificant bilateral convergence of preganglionic vagal fibers on postganglionic neurons to the canine heart." *Circulation Research* 67.3 (1990): 556-563.
- Langley J. N.** *The Autonomic Nervous System Part I.* Cambridge, UK: W Heffer and Sons Ltd. (1921): 80 p.
- Lau, B. Y. B., et al.** "Identification of a brain center whose activity discriminates a choice behavior in zebrafish." *Proceedings of the National Academy of Sciences* 108.6 (2011): 2581-2586.

- Laurent, P., S. Holmgren, and S. Nilsson.** "Nervous and humoral control of the fish heart: structure and function." *Comparative Biochemistry and Physiology Part A: Physiology* 76.3 (1983): 525-542.
- Leger, J., R. P. Croll, and F. M. Smith.** "Regional distribution and extrinsic innervation of intrinsic cardiac neurons in the guinea pig." *Journal of Comparative Neurology* 407.3 (1999): 303-317.
- Levy, R. J.** "Serotonin transporter mechanisms and cardiac disease." *Circulation* 113.1 (2006): 2-4.
- Li, N., et al.** "Molecular mapping of sinoatrial node HCN channel expression in the human heart." *Circulation: Arrhythmia and Electrophysiology* 8.5 (2015): 1219-1227.
- Lin, E., et al.** "Construction and use of a zebrafish heart voltage and calcium optical mapping system, with integrated electrocardiogram and programmable electrical stimulation." *American Journal of Physiology-Regulatory, Integrative and Comparative Physiology* 308.9 (2015): R755-R768.
- Lin, E., et al.** "Optical mapping of the electrical activity of isolated adult zebrafish hearts: acute effects of temperature." *American Journal of Physiology-Regulatory, Integrative and Comparative Physiology* 306.11 (2014): R823-R836.
- Liu, J., and D. Y. R. Stainier.** "Zebrafish in the study of early cardiac development." *Circulation Research* 110.6 (2012): 870-874.
- Llach, A., et al.** "Detection, properties, and frequency of local calcium release from the sarcoplasmic reticulum in teleost cardiomyocytes." *PLOS One* 6.8 (2011): e23708.
- Lu, H. H.** "Shifts in pacemaker dominance within the sinoatrial region of cat and rabbit hearts resulting from increase of extracellular potassium." *Circulation Research* 26.3 (1970): 339-346.
- MacCanon, D. M., and S. M. Horvath.** "Some effects of serotonin in pentobarbital anesthetized dogs." *American Journal of Physiology--Legacy Content* 179.1 (1954): 131-134.
- Madan, B. R., et al.** "Changes in the 5-hydroxytryptamine (5-HT) content of the heart during ectopic ventricular arrhythmia and consequent to its reversion by quinidine." *The Indian Journal of Medical Research* 58.1 (1970): 130.
- Mangoni, M. E., and J. Nargeot.** "Genesis and regulation of the heart automaticity." *Physiological Reviews* 88.3 (2008): 919-982.
- Manohar, M. U. R. L. I., and C. M. Parks.** "Porcine systemic and regional organ blood flow during 1.0 and 1.5 minimum alveolar concentrations of sevoflurane anesthesia

- without and with 50% nitrous oxide." *Journal of Pharmacology and Experimental Therapeutics* 231.3 (1984): 640-648.
- Marano, G., et al.** "Effects of isoflurane on cardiovascular system and sympathovagal balance in New Zealand white rabbits." *Journal of Cardiovascular Pharmacology* 28.4 (1996): 513-518.
- Mashour G. A., and R. Lydic.** *Neuroscientific Foundations of Anesthesiology*. Oxford University Press, 2011.
- Matiukas, A., et al.** "Near-infrared voltage-sensitive fluorescent dyes optimized for optical mapping in blood-perfused myocardium." *Heart Rhythm* 4.11 (2007): 1441-1451.
- Maximino, C., et al.** "Role of serotonin in zebrafish (*Danio rerio*) anxiety: relationship with serotonin levels and effect of buspirone, WAY 100635, SB 224289, fluoxetine and para-chlorophenylalanine (pCPA) in two behavioral models." *Neuropharmacology* 71 (2013): 83-97.
- McDevitt, D. G.** "In vivo studies on the function of cardiac b-adrenoceptors in man." *European Heart Journal* 10.suppl B (1989): 22-28.
- McLean, I. W., and P. K. Nakane.** "Periodate-lysine-paraformaldehyde fixative a new fixative for immunoelectron microscopy." *Journal of Histochemistry & Cytochemistry* 22.12 (1974): 1077-1083.
- Meek, W. J., H. R. Hathaway, and O. S. Orth.** "The effects of ether, chloroform and cyclopropane on cardiac automaticity." *Journal of Pharmacology and Experimental Therapeutics* 61.3 (1937): 240-252.
- Milan, D. J., et al.** "In vivo recording of adult zebrafish electrocardiogram and assessment of drug-induced QT prolongation." *American Journal of Physiology-Heart and Circulatory Physiology* 291.1 (2006): H269-H273.
- Moore, M. A., et al.** "Rapid 1% increases of end-tidal desflurane concentration to greater than 5% transiently increase heart rate and blood pressure in humans." *Anesthesiology* 81.1 (1994): 94-98.
- Moreno, N., et al.** "Islet1 as a marker of subdivisions and cell types in the developing forebrain of *Xenopus*." *Neuroscience* 154.4 (2008): 1423-1439.
- Moreno, N., et al.** "Characterization of the bed nucleus of the stria terminalis in the forebrain of anuran amphibians." *Journal of Comparative Neurology* 520.2 (2012): 330-363.

- Morgan, J. I., and T. Curran.** "Stimulus-transcription coupling in the nervous system: involvement of the inducible proto-oncogenes fos and jun." *Annual Review of Neuroscience* 14.1 (1991): 421-451.
- Nebigil, C. G., and L. Maroteaux.** "A novel role for serotonin in heart." *Trends in Cardiovascular Medicine* 11.8 (2001): 329-335.
- Nebigil, C. G., and L. Maroteaux.** "Functional consequence of serotonin/5-HT_{2B} receptor signaling in heart role of mitochondria in transition between hypertrophy and heart failure?." *Circulation* 108.7 (2003): 902-908.
- Nemtsas, P., et al.** "Adult zebrafish heart as a model for human heart? An electrophysiological study." *Journal of Molecular and Cellular Cardiology* 48.1 (2010): 161-171.
- Newton, C. M., et al.** "Regional innervation of the heart in the goldfish, *Carassius auratus*: a confocal microscopy study." *Journal of Comparative Neurology* 522.2 (2014): 456-478.
- Nilsson S., and S. Holmgren,** editors. 1994. *Comparative Physiology and Evolution of the Autonomic Nervous System*. Chur, Switzerland: Harwood Academic Publishers.
- Nilsson S.** *Autonomic Nerve Function in the Vertebrates*. Berlin: Springer-Verlag. (1983): 253 p
- Nilsson, S.** "Comparative anatomy of the autonomic nervous system." *Autonomic Neuroscience* 165.1 (2011): 3-9.
- Olsson, C.** "Autonomic innervation of the fish gut." *Acta Histochemica* 111.3 (2009): 185-195.
- Opthof, T.** "The mammalian sinoatrial node." *Cardiovascular drugs and therapy* 1.6 (1988): 573-597.
- Pacher, P., et al.** "Speculations on difference between tricyclic and selective serotonin reuptake inhibitor antidepressants on their cardiac effects. Is there any?." *Current Medicinal Chemistry* 6.6 (1999): 469-480.
- Park, K. S., et al.** "Fluoxetine inhibits L-type Ca²⁺ and transient outward K⁺ currents in rat ventricular myocytes." *Yonsei Medical Journal* 40.2 (1999): 144-51.
- Pauza, D. H., et al.** "Innervation of sinoatrial nodal cardiomyocytes in mouse. A combined approach using immunofluorescent and electron microscopy." *Journal of Molecular and Cellular Cardiology* 75 (2014): 188-197.

- Pauza, D. H., et al.** "Morphology, distribution, and variability of the epicardiac neural ganglionated subplexuses in the human heart." *The Anatomical Record* 259.4 (2000): 353-382.
- Pauza, D. H., et al.** "Neuroanatomy of the murine cardiac conduction system: a combined stereomicroscopic and fluorescence immunohistochemical study." *Autonomic Neuroscience* 176.1 (2013): 32-47.
- Peralta, E. G., et al.** "Distinct primary structures, ligand-binding properties and tissue-specific expression of four human muscarinic acetylcholine receptors." *The EMBO Journal* 6.13 (1987): 3923.
- Pieperhoff, S., et al.** "Heart on a plate: histological and functional assessment of isolated adult zebrafish hearts maintained in culture." *PloS One* 9.5 (2014): e96771.
- Poterack, K. A., J. P. Kampine, and W. T. Schmeling.** "Effects of isoflurane, midazolam, and etomidate on cardiovascular responses to stimulation of central nervous system pressor sites in chronically instrumented cats." *Anesthesia & Analgesia* 73.1 (1991): 64-75.
- Preckel, B., et al.** "Effects of enflurane, isoflurane, sevoflurane and desflurane on reperfusion injury after regional myocardial ischaemia in the rabbit heart in vivo." *British Journal of Anaesthesia* 81.6 (1998): 905-912.
- Price, H. L., H. W. Linde, and H. T. Morse.** "Central nervous actions of halothane affecting the systemic circulation." *Journal of the American Society of Anesthesiologists* 24.6 (1963): 770-778.
- Prieto, M. J., et al.** "Effect of risperidone and fluoxetine on the movement and neurochemical changes of zebrafish." (2012).
- Qin, Z., J. E. Lewis, and S. F. Perry.** "Zebrafish (*Danio rerio*) gill neuroepithelial cells are sensitive chemoreceptors for environmental CO₂." *Journal of Physiology* 588.5 (2010): 861-872.
- Rajamani, S., et al.** "Drug-induced long QT syndrome: hERG K⁺ channel block and disruption of protein trafficking by fluoxetine and norfluoxetine." *British Journal of Pharmacology* 149.5 (2006): 481-489.
- Rajendran, P. S., et al.** "Myocardial infarction induces structural and functional remodelling of the intrinsic cardiac nervous system." *Journal of Physiology* 594.2 (2016): 321-341.
- Randlett, O., et al.** "Whole-brain activity mapping onto a zebrafish brain atlas." *Nature Methods* 12.11 (2015): 1039-1046.

- Renier, C., et al.** "Genomic and functional conservation of sedative-hypnotic targets in the zebrafish." *Pharmacogenetics and Genomics* 17.4 (2007): 237-253.
- Rider, S. A., et al.** "Techniques for the in vivo assessment of cardio-renal function in zebrafish (*Danio rerio*) larvae." *Journal of Physiology* 590.8 (2012): 1803-1809.
- Robertson, G. N., et al.** "The contribution of the swimbladder to buoyancy in the adult zebrafish (*Danio rerio*): a morphometric analysis." *Journal of Morphology* 269.6 (2008): 666-673.
- Roose, S. P., and M. Miyazaki.** "Pharmacologic treatment of depression in patients with heart disease." *Psychosomatic Medicine* 67 (2005): S54-S57.
- Ross L. G., and B. Ross.** Anesthetic and Sedative Techniques for Aquatic Flecknell PA. Anaesthesia of common laboratory species: special considerations. In *Laboratory Animal Anaesthesia*, 3rd ed.(Flecknell, P. ed.), Academic Press, London (2009):181, 2009. Animals. Blackwell Publishing, Oxford, UK.
- Saarnivaara, L., and L. Lindgren.** "Prolongation of QT interval during induction of anaesthesia." *Acta Anaesthesiologica Scandinavica* 27.2 (1983): 126-130.
- Sabeh, M. K., H. Kekhia, and C. A. MacRae.** "Optical mapping in the developing zebrafish heart." *Pediatric Cardiology* 33.6 (2012): 916-922.
- Saito, T., and K. Tenma.** "Effects of left and right vagal stimulation on excitation and conduction of the carp heart (*Cyprinus carpio*)." *Journal of Comparative Physiology* 111.1 (1976): 39-53.
- Saito, T.** "Effects of vagal stimulation on the pacemaker action potentials of carp heart." *Comparative Biochemistry and Physiology Part A: Physiology* 44.1 (1973): 191-199.
- Sala, M., et al.** "Antidepressants: their effects on cardiac channels, QT prolongation and Torsade de Pointes." *Current Opinion in Investigational Drugs* 7.3 (2006): 256-263.
- Saman, S., F. Thandroyen, and L. H. Opie.** "Serotonin and the heart: effects of ketanserin on myocardial function, heart rate, and arrhythmias." *Journal of Cardiovascular Pharmacology* 7 (1985): 70-75.
- Sandblom, E., and M. Axelsson.** "Autonomic control of circulation in fish: a comparative view." *Autonomic Neuroscience* 165.1 (2011): 127-139.
- Sari, Y., and F. C. Zhou.** "Serotonin and its transporter on proliferation of fetal heart cells." *International Journal of Developmental Neuroscience* 21.8 (2003): 417-424.
- Schneider, C. A., Wayne S. Rasband, and Kevin W. Eliceiri.** "NIH Image to ImageJ: 25 years of image analysis." *Nature Methods* 9.7 (2012): 671-675.

- Schneider, J. A., and F. F. Yonkman.** "Action of serotonin (5-hydroxytryptamine) on vagal afferent impulses in the cat." *American Journal of Physiology--Legacy Content* 174.1 (1953): 127-134.
- Schwerte, T., et al.** "Development of the sympatho-vagal balance in the cardiovascular system in zebrafish (*Danio rerio*) characterized by power spectrum and classical signal analysis." *Journal of Experimental Biology* 209.6 (2006): 1093-1100.
- Seagard J. L., et al.** Cardiovascular effects of general anesthesia. In: Covino BG, Fozzard HA, Rehder K, Strichartz G, eds. Effects of anesthesia. Bethesda, American Physiological Society, pp. 149-77, 1985.
- Sear, J. W.** "Perioperative control of hypertension: when will it adversely affect perioperative outcome?." *Current Hypertension Reports* 10.6 (2008): 480-487.
- Sedmera, D., et al.** "Functional and morphological evidence for a ventricular conduction system in zebrafish and *Xenopus* hearts." *American Journal of Physiology-Heart and Circulatory Physiology* 284.4 (2003): H1152-H1160.
- Sehnert, A. J., and D. Y. R. Stainier.** "A window to the heart: can zebrafish mutants help us understand heart disease in humans?." *Trends in Genetics* 18.10 (2002): 491-494.
- Shakarchi, K., P. C. Zachar, and M. G. Jonz.** "Serotonergic and cholinergic elements of the hypoxic ventilatory response in developing zebrafish." *Journal of Experimental Biology* 216.5 (2013): 869-880.
- Shibata, N., et al.** "Pacemaker shift in the rabbit sinoatrial node in response to vagal nerve stimulation." *Experimental Physiology* 86.02 (2001): 177-184.
- Shvilkin, A., et al.** "Vagal release of vasoactive intestinal peptide can promote vagotonic tachycardia in the isolated innervated rat heart." *Cardiovascular Research* 28.12 (1994): 1769-1773.
- Singh, S., et al.** "Monoamine- and histamine-synthesizing enzymes and neurotransmitters within neurons of adult human cardiac ganglia." *Circulation* 99.3 (1999): 411-419.
- Singleman, C., and N. G. Holtzman.** "Analysis of postembryonic heart development and maturation in the zebrafish, *Danio rerio*." *Developmental Dynamics* 241.12 (2012): 1993-2004.
- Skovsted, P., and S. Saphavichaiikul.** "The effects of isoflurane on arterial pressure, pulse rate, autonomic nervous activity, and barostatic reflexes." *Canadian Anaesthetists' Society Journal* 24.3 (1977): 304-314.
- Small, J-V, et al.** "Visualising the actin cytoskeleton." *Microscopy Research and Technique* 47.1 (1999): 3-17.

- Smith, D. G., et al.** "Nervous control of the blood pressure in the Atlantic cod, *Gadus morhua*." *Journal of Experimental Biology* 117.1 (1985): 335-347.
- Smith, F. M.** "Extrinsic inputs to intrinsic neurons in the porcine heart in vitro." *American Journal of Physiology-Regulatory, Integrative and Comparative Physiology* 276.2 (1999): R455-R467.
- Smith, F. M., et al.** "Effects of chronic cardiac decentralization on functional properties of canine intracardiac neurons in vitro." *American Journal of Physiology-Regulatory, Integrative and Comparative Physiology* 281.5 (2001): R1474-R1482.
- Smith, F. M., and D. R. Jones.** "Localization of receptors causing hypoxic bradycardia in trout (*Salmo gairdneri*)." *Canadian Journal of Zoology* 56.6 (1978): 1260-1265.
- Sole, M. J., A. Shum, and G. R. Van Loon.** "Serotonin metabolism in the normal and failing hamster heart." *Circulation Research* 45.5 (1979): 629-34.
- Stainier, D. Y. R., et al.** "Mutations affecting the formation and function of the cardiovascular system in the zebrafish embryo." *Development* 123.1 (1996): 285-292.
- Stainier, D. Y. R.** "Zebrafish genetics and vertebrate heart formation." *Nature Reviews Genetics* 2.1 (2001): 39-48.
- Steele, S. L., et al.** "In vivo and in vitro assessment of cardiac β -adrenergic receptors in larval zebrafish (*Danio rerio*)." *Journal of Experimental Biology* 214.9 (2011): 1445-1457.
- Steele, S. L., et al.** "Loss of M2 muscarinic receptor function inhibits development of hypoxic bradycardia and alters cardiac β -adrenergic sensitivity in larval zebrafish (*Danio rerio*)." *American Journal of Physiology-Regulatory, Integrative and Comparative Physiology* 297.2 (2009): R412-R420.
- Steele, Shelby L., Marc Ekker, and Steve F. Perry. "Interactive effects of development and hypoxia on catecholamine synthesis and cardiac function in zebrafish (*Danio rerio*)." *Journal of Comparative Physiology B* 181.4 (2011): 527-538.
- Stewart, A. M., et al.** "Perspectives on experimental models of serotonin syndrome in zebrafish." *Neurochemistry International* 62.6 (2013): 893-902.
- Stoyek, M. R., R. P. Croll, and F. M. Smith.** "Intrinsic and extrinsic innervation of the heart in zebrafish (*Danio rerio*)." *Journal of Comparative Neurology* 523.11 (2015): 1683-1700.
- Stoyek, M. R., R. P. Croll, and F. M. Smith.** "Zebrafish heart as a model to study the integrative autonomic control of pacemaker function. *American Journal of Physiology – Heart and Circulatory Physiology* (2016), doi: 10.1152/ajpheart.00330.2016.

- Susaki, E. A., et al.** "Whole-brain imaging with single-cell resolution using chemical cocktails and computational analysis." *Cell* 157.3 (2014): 726-739.
- Tamir, H., and M. D. Gershon.** "Serotonin-Storing Secretory Vesicles." *Annals of the New York Academy of Sciences* 600.1 (1990): 53-67.
- Taylor E.W., et al.** "The role of the vagus nerve in the generation of cardiorespiratory interactions in a neotropical fish, the pacu, *Piaractus mesopotamicus*." *Journal of Comparative Physiology A* 195.8 (2009): 721-731.
- Taylor, E. W., D. Jordan, and J. H. Coote.** "Central control of the cardiovascular and respiratory systems and their interactions in vertebrates." *Physiological Reviews* 79.3 (1999): 855-916.
- Tessadori, F., et al.** "Identification and functional characterization of cardiac pacemaker cells in zebrafish." *PloS One* 7.10 (2012): e47644.
- Tessier, C., et al.** "Modification of membrane heterogeneity by antipsychotic drugs: an X-ray diffraction comparative study." *Journal of Colloid and Interface Science* 320.2 (2008): 469-475.
- Tota, B., et al.** "NO modulation of myocardial performance in fish hearts." *Comparative Biochemistry and Physiology Part A: Molecular & Integrative Physiology* 142.2 (2005): 164-177.
- Tsutsui, H., et al.** "Visualizing voltage dynamics in zebrafish heart." *Journal of Physiology* 588.12 (2010): 2017-2021.
- Uyttebroek, Leen, et al.** "Neurochemical coding of enteric neurons in adult and embryonic zebrafish (*Danio rerio*)." *Journal of Comparative Neurology* 518.21 (2010): 4419-4438.
- Verkerk, A. O., and C. A. Remme.** "Zebrafish: a novel research tool for cardiac (patho) electrophysiology and ion channel disorders." *Frontiers in Physiology* 3 (2012): 255.
- Vikenes, K., M. Farstad, and J. E. Nordrehaug.** "Serotonin is associated with coronary artery disease and cardiac events." *Circulation* 100.5 (1999): 483-489.
- Violet, J. M., et al.** "Differential sensitivities of mammalian neuronal and muscle nicotinic acetylcholine receptors to general anesthetics." *Journal of the American Society of Anesthesiologists* 86.4 (1997): 866-874.
- Vornanen, M., and M. Hassinen.** "Zebrafish heart as a model for human cardiac electrophysiology." *Channels* 10.2 (2016): 101-110.

- Vornanen, M., M. Hälinen, and J. Haverinen.** "Sinoatrial tissue of crucian carp heart has only negative contractile responses to autonomic agonists." *BMC Physiology* 10.1 (2010): 1.
- Votavova, M., D. J. Boullin, and E. Costa.** "Specificity of action of 6-hydroxydopamine in peripheral cat tissues:: Epletion of noradrenaline without depletion of 5-hydroxytryptamine." *Life Sciences* 10.2 (1971): 87-91.
- Warren, K. S., and M. C. Fishman.** "'Physiological genomics': mutant screens in zebrafish." *American Journal of Physiology-Heart and Circulatory Physiology* 275.1 (1998): H1-H7.
- Warren, K. S., K. Baker, and M. C. Fishman.** "The slow mo mutation reduces pacemaker current and heart rate in adult zebrafish." *American Journal of Physiology-Heart and Circulatory Physiology* 281.4 (2001): H1711-H1719.
- Weinberger, F., et al.** "Localization of islet-1-positive cells in the healthy and infarcted adult murine heart." *Circulation Research* 110.10 (2012): 1303-1310.
- Weiskopf, R. B., et al.** "Rapid increase in desflurane concentration is associated with greater transient cardiovascular stimulation than with rapid increase in isoflurane concentration in humans." *Anesthesiology* 80.5 (1994): 1035-1045.
- West, G. A., and L. Belardinelli.** "Sinus slowing and pacemaker shift caused by adenosine in rabbit SA node." *Pflügers Archiv* 403.1 (1985): 66-74.
- Wig J., et al.** Prolonged QT interval syndrome. Sudden cardiac arrest during anaesthesia. *Anaesthesia* 34: 37-40, 1979.
- Wilson, C. M., et al.** "Phylogeny and effects of anoxia on hyperpolarization-activated cyclic nucleotide-gated channel gene expression in the heart of a primitive chordate, the Pacific hagfish (*Eptatretus stoutii*)." *Journal of Experimental Biology* 216.23 (2013): 4462-4472.
- Woo, K., J. Shih, and S. E. Fraser.** "Fate maps of the zebrafish embryo." *Current Opinion in Genetics & Development* 5.4 (1995): 439-443.
- Wyeth, R. C., and R. P. Croll.** "Peripheral sensory cells in the cephalic sensory organs of *Lymnaea stagnalis*." *Journal of Comparative Neurology* 519.10 (2011): 1894-1913.
- Xu, J., et al.** "Serotonin mechanisms in heart valve disease II: the 5-HT₂ receptor and its signaling pathway in aortic valve interstitial cells." *American Journal of Pathology* 161.6 (2002): 2209-2218.
- Yabanoglu, S., et al.** "Platelet derived serotonin drives the activation of rat cardiac fibroblasts by 5-HT_{2A} receptors." *Journal of Molecular and Cellular Cardiology* 46.4 (2009): 518-525.

- Yabuki, Yoichi, et al.** "Olfactory receptor for prostaglandin F2 [alpha] mediates male fish courtship behavior." *Nature Neuroscience* (2016).
- Yamano, M., et al.** "Serotonin (5-HT) 3-receptor antagonism of 4, 5, 6, 7-tetrahydrobenzimidazole derivatives against 5-HT-induced bradycardia in anesthetized rats." *Japanese Journal of Pharmacology* 65.3 (1994): 241-248.
- Yamashita, M., et al.** "Isoflurane modulation of neuronal nicotinic acetylcholine receptors expressed in human embryonic kidney cells." *Journal of the American Society of Anesthesiologists* 102.1 (2005): 76-84.
- Yavarone, M. S., et al.** "Serotonin and cardiac morphogenesis in the mouse embryo." *Teratology* 47.6 (1993): 573-584.
- Yelon, D.** "Developmental biology: Heart under construction." *Nature* 484.7395 (2012): 459-460.
- Yli-Hankala, A., et al.** "Increases in hemodynamic variables and catecholamine levels after rapid increase in isoflurane concentration." *Anesthesiology* 78.2 (1993): 266-271.
- Yuan, B-X, et al.** "Gross and microscopic anatomy of the canine intrinsic cardiac nervous system." *The Anatomical Record* 239.1 (1994): 75-87.
- Zaccone, D., et al.** "Morphology and innervation of the teleost physostome swim bladders and their functional evolution in non-teleostean lineages." *Acta Histochemica* 114.8 (2012): 763-772.
- Zaccone, G., F. Marino, and D. Zaccone.** "Intracardiac neurons and neurotransmitters in fish." *Encyclopedia of fish physiology: from genome to environment* 2 (2010): 1067-72.
- Zaccone, G., et al.** "Postganglionic nerve cell bodies and neurotransmitter localization in the teleost heart." *Acta Histochemica* 112.4 (2010): 328-336.
- Zaccone, G., et al.** "Postganglionic nerve cell bodies and neurotransmitter localization in the teleost heart." *Acta Histochemica* 112.4 (2010): 328-336.
- Zhou, C., J. Liu, and X-D Chen.** "General anesthesia mediated by effects on ion channels." *World Journal of Critical Care Medicine* 1.3 (2012): 80.

Appendix A

Expanded Materials and Methods

GENERAL – ALL CHAPTERS

Ethics approval.

Procedures for animal care and use followed the "Guidelines on the Care and Use of Fish in Research, Teaching and Testing" document issued by the Canadian Council of Animal Care (2005 ed.). Institutional approval for animal use in this study was obtained from the Dalhousie University Committee on Laboratory Animals.

Animal husbandry.

Animals were acquired from breeding stocks in the Faculty of Medicine Zebrafish Facility at Dalhousie University. Fish were maintained in standard 3-10 l tanks (Aquatic Habitats, nif-0000-31933, Apopka, FL, USA) at 28.5°C, supplied continuously with conditioned water from a recirculating water system, and subjected to a 14hour light: 10hour dark illumination cycle. Fish were fed commercial dry fish food (Golden Pearl pellets, Brine Shrimp Direct, Ogden, UT, USA) and live artemia (raised in-house) twice a day.

Heart isolation.

Zebrafish were anaesthetised in a buffered solution (pH 7.2) of tricaine (MS-222; 1.5 mM; Sigma–Aldrich, Oakville, ON, Canada) in tank water (28.5°C) until opercular respiratory movements ceased and the animals lacked response to a fin pinch with forceps. A ventral midline incision was made through the body wall to expose the heart, and a block of tissue encompassing the ventral aorta (containing the branchiocardiac nerve trunk, BCT), ventricle, atrium, sinus venosus and ducts of Cuvier (containing the cardiac

vagosympathetic rami) was then removed for whole-mount immunohistochemistry or *in vitro* recordings.

Imaging and data presentation.

Tissues were viewed using a Zeiss LSM510 or Zeiss LSM710 confocal microscope using Zeiss Zen2009 software (Zeiss Canada, Mississauga, ON). Preparations were epilluminated with a mercury lamp (X-Cite 120Q; Lumen Dynamics) reflected by a 488/543/633 nm dichroic mirror (HFT 488/543/633; Carl Zeiss AG) on to the preparation. Emitted fluorescence was collected with a 10 \times , 0.45 NA objective (Plan-Apochromat SF25; Carl Zeiss AG), a 25 \times , 0.80 NA objective (LCI Plan-Neofluar; Carl Zeiss AG), a 40 \times , 0.95 NA objective (Plan-Apochromat M27; Carl Zeiss AG), or a 63 \times , 1.30 NA objective (LCI Plan-Neofluar M27; Carl Zeiss AG). For fluorescence collected from the specimens, 480-520 nm and 500-615 nm band-pass filters (BP565-615; Carl Zeiss AG) and a 565-615 nm long pass filter (LP565-615; Carl Zeiss AG) were used. Z-stacks were taken from regions of interest surrounding immunoreactive tissues, and ranged from 20-100 μ m in depth. Z-stack scans also encompassed a region, of 5-25 μ m above and below the regions of interest to ensure that all structures were captured, while limiting issues of light scattering associated with deeper scans. Confocal image stacks were processed with Zeiss Zen2009 software. These images were processed into plates with Photoshop CS6 (Adobe Systems Inc, San Jose, CA, USA). During composition of the figure plates some images originally in color were converted to greyscale values; the brightness of these images was adjusted slightly so that panel-to-panel contrast in the plate was consistent. Numerical values were expressed as mean \pm 1 standard error (SE). Statistical analyses

(one-way ANOVA, student's T-test and regression) to detect significant differences among means were performed using SPSS (IBM Canada, Markham, ON).

CHAPTER 2 – ANATOMY OF THE ZEBRAFISH INTRACARDIAC NERVOUS SYSTEM

Animals.

A total of 60 adult AB wild type zebrafish (12-18 months post fertilization; mixed sex; mean standard body length 44 ± 7 mm (\pm SE) were used in this study.

Tissue fixation.

Tissue was fixed overnight in 4% paraformaldehyde (PFA; RT-15710, Electron Microscopy Sciences, Hatfield, PA, USA) in phosphate-buffered saline (PBS, composition in mM: 50 Na₂HPO₄, 140 NaCl, pH 7.2) before processing for immunohistochemistry in whole-mount format. Tissues processed for tryosine hydroxylase immunohistochemistry were fixed in a 9:1 (v/v) solution of methanol and formalin (HT501128, Sigma Aldrich) for 6-8 hours at room temperature.

General and neurotransmitter-specific labelling.

The general procedures used for immunohistochemistry in this study were similar to those described in previous publications on cyprinid neuroanatomy (Finney *et al.*, 2006; Robertson *et al.*, 2008; Dumbarton *et al.*, 2010; Newton *et al.*, 2014). Briefly, fixed tissues were rinsed in PBS, transferred to a PBS solution containing 2% Triton X-100 (X100, Sigma Aldrich), 1 % bovine serum albumin (BSA; A9576, Sigma Aldrich) and 1% normal goat serum (NGS; G9023, Sigma Aldrich) for 48 hours at 4°C with agitation, and then

incubated with primary antibodies (see below for descriptions). Primary antibodies were diluted in a solution containing 0.25% Triton X-100, 1 % BSA and 1 % NGS in PBS (designated PBS-T). Tissues were incubated 3-5 d with agitation at 4°C, rinsed in PBS-T, then transferred to a solution of PBS-T containing the appropriate secondary antibody conjugated to AlexaFluor 488 or 555 fluorophores (Life Technologies, Burlington, ON, Canada). Incubation time with secondary antibodies was 3-5 d with agitation at 4°C. Final rinsing of tissues was done in PBS before clearing and mounting in ClearT2 (Kuwajima *et al.*, 2013) containing 2% propyl gallate (P3130, Sigma Aldrich) to reduce fluorophore photobleaching.

Antibody specificity.

The primary antibodies used in this study have been used previously in zebrafish and in the goldfish heart, a cyprinid species closely related to the zebrafish (see Appendix B). In the present study, to determine the general innervation of the heart antibodies against acetylated tubulin (AcT, axons; T6793, Sigma Aldrich) were combined with human neuronal protein C/D (Hu, neuronal somata; A21271, Life Technologies). An antibody against synaptic vesicle protein 2 (SV-2; SV2, Developmental Studies Hybridoma Bank, Iowa City, IA, USA) was used to detect axon terminals. Cholinergic axons and somata were detected by immunoreactivity for choline acetyltransferase (ChAT; AB144P, Millipore, Etobicoke, ON, Canada), an enzyme involved in acetylcholine (ACh) synthesis. In a subset of specimens an antibody against vesicular acetylcholine transporter (VAcHT; AB1588, Millipore) was used together with ChAT to double-label putative cholinergic elements. The VAcHT antibody used was the same as used by Uyttebroek *et*

al. (2010), who reported that pre-adsorption with a synthetic peptide that corresponded to the C-terminus sequence eliminated immunoreactivity in the zebrafish gill. The expression of tyrosine hydroxylase (TH; 22941, Immunostar, Hudson, WI, USA), the rate-limiting enzyme in the synthesis of noradrenaline (NE), indicated adrenergic elements. Neurons capable of generating nitric oxide were detected by the presence of neuronal nitric oxide synthase (nNOS; ab5586, Abcam, Toronto, ON, Canada). Antibodies directed against vasoactive intestinal polypeptide (VIP; 20077, Immunostar) demonstrated the distribution of this peptide in neural elements in the heart.

To label putative pacemaker cells, an antibody against hyperpolarization-activated, cyclic-nucleotide-gated ion channels was used (HCN4; APC-052, Alomone Laboratories, Jerusalem, Israel). Expression of the transcription factor Islet-1 (Isl1) has been shown to partly overlap that of HCN4 in the zebrafish heart (Tessadori *et al.*, 2012), so an analysis of the distribution of immunoreactivity for this factor has been included in this study. The anti-Isl1 antibody used here (Developmental Studies Hybridoma Bank) was the same as that used by Tessadori *et al.* (2012) and others in zebrafish (e.g., Kuscha *et al.*, 2012; Ericson *et al.*, 1992) and its pattern of expression matches the labelling of motor neurons in *in situ* hybridization experiments in the hindbrain of developing zebrafish (Coppola *et al.*, 2012). These authors also showed that anti-Isl1 antibody detection was eliminated after injection of morpholinos directed against Isl1 and by preabsorption with Isl1 peptide (Moreno *et al.*, 2008; 2012).

Controls.

For all antibodies used in this study, negative control tissues were processed as outlined above, except that either the primary or secondary antibody was omitted. In all trials this eliminated detection of histofluorescence. As a control for the anti-HCN4 antibody, the HCN4 antibody was pre-treated with fusion protein (1 µg primary antibody: 3 µg fusion protein; Alomone Labs, Israel) in PBS-T. Tissue was then incubated in the presence of the pre-adsorbed antibody following the procedures outlined above. In 6 trials no immunoreactivity was observed.

Myocardial labelling.

In order to determine how immunohistochemically labelled neuronal elements were related to the regional structure of the myocardium, some specimens were double-labelled with the F-actin marker phalloidin (77418, Sigma Aldrich; Small *et al.*, 1999; Newton *et al.*, 2014), conjugated with tetramethyl rhodamine isothiocyanate to show cardiac myocytes.

Tracing extrinsic vagosympathetic inputs.

To visualize the intracardiac projections and termination patterns of axons in the cardiac rami of the vagosympathetic trunks a combination of the actively transported neurotracer neurobiotin (SP1120, Vector Laboratories, Burlingame, CA, USA; Wyeth and Croll, 2011) and a fluorescent styryl dye, FM1-43X (F35355, Life Technologies) was used. This dye, which appears to label the membranes of recycled synaptic vesicles, becomes concentrated in active synaptic terminals over time (Betz *et al.*, 1992) so will

accumulate in the intracardiac terminals of extracardiac axons when those axons are stimulated. In this procedure hearts were isolated as described above and pinned to the rubber bottom of a chamber (3 mL volume) that was perfused with zebrafish saline (in mM: 124.1 NaCl, 5.1 KCl, 2.9 Na₂HPO₄, 1.9 MgSO₄·7H₂O, 1.4 CaCl₂·2H₂O, 11.9 NaHCO₃; pH 7.2; gassed with room air). A length of approximately 1 mm of the left or right vagosympathetic trunk was freed from the wall of the duct of Cuvier and the cut end of the nerve was drawn by suction into a tip of a closely fitting glass pipette filled with saline. This was then replaced with a solution containing neurobiotin and FM1-43X (1 mM each) in distilled water. This preparation was maintained at room temperature for 6-8 hours and maintained spontaneous cardiac contractions throughout this period. The nerve was then removed from the pipette and hearts were perfused for a further 2-3 hours. During the last hour of this period the dye-loaded nerve was stimulated with a bipolar wire electrode driven by a constant-current stimulator (S88; Grass Instruments, Quincy, MA, USA) to load axonal terminals with FM1-43X. Trains of rectangular pulses (pulse duration 500µs; train duration 30 s, pulse frequency 15Hz, stimulus current 300 µA) were delivered every 5 minutes for a total of 12 stimulation periods. Following this procedure hearts were fixed as described above for immunohistochemistry. The presence of neurobiotin in neural elements was detected with avidin conjugated to AlexaFluor 488 (A212370, Life Technologies). Two controls were used for this procedure: nerves were loaded with neurobiotin and FM1-43X but not stimulated, or neurobiotin without FM1-43X was applied and nerves were stimulated. In both cases no terminals were observed.

CHAPTER 3 - AUTONOMIC CONTROL OF CHRONOTROPY IN THE ZEBRAFISH

Animals.

A total of 96 adult, AB strain zebrafish (12-18 months post-fertilization; 35 ± 8 mm standard body length, 693 ± 154 mg wet weight) of both sexes were used in this study.

Heart viability.

In preliminary experiments, to control for possible deterioration of function in the isolated hearts over the duration of the experiments, heart rate and responses to VSN stimulation were monitored in sample hearts for up to 6 h, a period longer than any experiments in this study.

Whole-heart ECG recordings and VSN stimulation.

Isolated hearts ($n=24$) were pinned through the ventral aorta and walls of the ducts of Cuvier to the Sylgard rubber (Dow Corning, Midland, MI, USA) bottom of a 5 mL chamber and perfused with zebrafish saline (composition in mM: 124.1 NaCl, 5.1 KCl, 2.9 Na₂HPO₄, 1.9 MgSO₄-7H₂O, 1.4 CaCl₂-2H₂O, 11.9 NaHCO₃; pH 7.2; aerated with room air; 25°C) at a rate of 10 mL min⁻¹ and allowed to acclimate for 30 min prior to experiments. Approximately 1 mm of the left and right cardiac rami of the vagosympathetic trunks were exposed in the walls of the ducts of Cuvier. Vagosympathetic trunks were stimulated individually or simultaneously with bipolar wire electrodes attached to constant-current isolation units (PSIU6; Grass Instruments, Quincy, MA, USA) driven by a stimulator (S88; Grass Instruments) delivering trains of rectangular pulses (pulse duration 0.5ms; train duration 10 s, pulse frequency 1-20 Hz). In all

experiments, a standard stimulus current of 300 μA was used. This current was chosen as optimal for this preparation as it was double the intensity (140 μA) that reliably activated all axons in the vagi in preliminary experiments measuring compound action potentials. ECG signals were recorded from the surface of the atrium and ventricle *via* bipolar suction electrodes, differentially amplified (total gain 1000-10000) and stored on a personal computer after analog-digital conversion (Digidata 1322A, Axon Instruments, Foster City, CA, USA). To quantify cardiac responses, time between adjacent R-waves of the ECG (R-R interval) and latency between atrial and ventricular R-waves within individual cardiac cycles (atrioventricular delay) were processed using Axoscope software (Axon Instruments). To control for the possibility of electrotonic spread of current from the site of the stimulating electrodes to active cardiac tissue, in some preparations the electrodes were placed on the duct wall away from the nerve ($n=6$) or moved off the nerve into the bath ($n=6$); repeated stimulation with the same parameters had no effect on heart rate.

Isolated ventricular pacemaker recordings.

To investigate the function of putative pacemaker cells at the atrioventricular region, ECG signals were recorded first from intact hearts ($n=6$), followed by isolation of the ventricle along with a small margin of atrial tissue proximal to the atrioventricular valve (<500 μm from atrioventricular valves). Subsequent ECG recordings were made from the dissociated ventricular and atrial tissues (as per *Whole-heart ECG recordings and VSN stimulation*). As it was not possible to directly access the intracardiac nerves in the walls of the isolated ventricle to study the direct effects of nerve stimulation on ventricular rate, cholinergic and adrenergic agents were used to evaluate the potential for neural

control in this tissue (see *Pharmacological agents*).

BCT stimulation.

To evaluate the effects of stimulating the BCT, an electrode was placed over the nerve as it coursed along the ventral aorta between the origins of the afferent arteries supplying the fourth gill arches and the bulbus arteriosus. Perfusion and stimulation parameters were similar to those for vagosympathetic trunk stimulation. To control for electrotonic current spread, the stimulating electrode was moved away from the nerve, and placed on the ventral aorta between the afferent vessels supplying the third and fourth gill arches; repeated stimulation in this region had no effect on heart rate ($n=3$).

Pharmacological agents.

Nicotine (agonist at excitatory nicotinic channels on the membrane of cholinergic intracardiac neurons), muscarine (agonist at post-junctional muscarinic receptors on cardiac effector cells) and isoproterenol (agonist at post-junctional beta-adrenergic receptors on cardiac effector cells) were dissolved in saline (all 1 mM; Sigma Aldrich) on the day of the experiment. Agonists were delivered to the bath directly above the tissue in 200 μ L boluses through a micropipette *via* a calibrated syringe attached to a screw-drive microinjector (IM-4B; Narishige, East Meadow, NY, USA). As a control 200 μ L boluses of saline were delivered in the same manner and did not elicit chronotropic responses. Hexamethonium (a non-depolarising nicotinic receptor blocker at nicotinic acetylcholine receptors on parasympathetic and sympathetic pre-ganglionic neurons) and atropine (post-junctional muscarinic receptor blocker) (10 μ M each; Sigma Aldrich) and timolol (post-

junctional beta-adrenergic receptor blocker) (100 μ M; Sigma Aldrich) were dissolved in saline and perfused continuously starting 15 min prior to recording.

Voltage optical mapping.

Voltage changes in isolated hearts ($n=6$) or AVR-ventricular tissue ($n=5$) were optically mapped to determine the normal time course and spread of cardiac excitation from the pacemaker initiation site, to assess whether shifts in the point of initiation occurred with vagal nerve stimulation, and to establish the characteristics of AVR-initiated ventricular activity. Whole hearts or isolated tissues were isolated and pinned to the Sylgard rubber bottom of a 3 mL chamber filled with perfusate and allowed to equilibrate for 30 min (aerated with room air; 25°C; as per *Whole-heart ECG recordings and VSN stimulation*). During this time, the heart was exposed to a voltage-sensitive dye (10 μ M di-4-ANBDQPQ [Matiukas *et al.*, 2007]; University of Connecticut Health Center, Farmington, CT, USA) in the perfusate for 10 min, and then washed with fresh saline containing excitation-contraction uncoupler blebbistatin (10 μ M (\pm)-blebbistatin; Cayman Chemical Company, Ann Arbor, MI, USA) to eliminate motion artifacts during optical recordings. Blebbistatin was present for the duration of the experiment. In a subset of hearts ($n=3$), simultaneous stimulation of both cardiac vagal nerve rami (20 Hz; described above) was performed to test for changes in the pacemaker initiation site.

Preparations were epi-illuminated through a compound microscope with a red light-emitting diode (CBT-90-R; Luminus Devices Incorporated, Billerica, MA, USA) directed through a 640 ± 10 nm band-pass filter (D640/20X, Chroma Technology Corporation, Bellows Falls, VT, USA) and reflected by a 660 nm dichroic mirror (FF660;

Semrock, Rochester, NY, USA) on to the preparation. Emitted fluorescence was collected with a 5 \times , 0.15 NA objective (Plan; Zeiss Canada, Mississauga, ON, Canada) or a 10 \times , 0.25 NA objective (EA10; Olympus Canada Incorporated, Richmond Hill, ON, Canada) through a 700 nm long-pass filter (HQ700LP, Chroma) and captured by a 128 \times 128 pixel, 16-bit electron-multiplying charge-coupled device camera (Cascade 128+; Photometrics, Tucson, AZ, USA) at 511 frames \cdot s⁻¹. Previous investigations of the penetrance of 640 \pm 20 nm light into myocardium has shown 50% intensity at a depth of 1 mm (TA Quinn, unpublished). At a depth of 200-400 μ m, which is the maximum thickness of the zebrafish tissue preparations used in this study, light intensity is \sim 70-80%, resulting in excitation and collection of voltage signals from the entire transmural thickness of the heart.

The camera was controlled and signals were acquired using MultiRecorder software (S. Luther and J. Schröder-Schetelig, Max Planck Institute for Dynamics and Self-Organization, Göttingen, Germany; <http://www.bmp.ds.mpg.de/multirecorder.html>). As all recordings contained some degree of readout noise, pre-treatment activation patterns were mapped from signal-averaged values taken from ten consecutive beats immediately prior to introduction of the stimuli. Isochronal activation maps were generated using an activation threshold of 60% of action potential amplitude. Atrioventricular delay was estimated as the time from arrival of the excitation wavefront at the atrioventricular junction to the first occurrence of depolarization in ventricular tissue. All optical data were analysed with custom routines written in Matlab (The MathWorks, Natick, MA, USA).

Pacemaker cell immunohistochemistry.

Hearts ($n=16$) were fixed in a modified periodate-lysine-paraformaldehyde fixative (1.3 mM paraformaldehyde, 250 μ M L-lysine, 10 mM sodium metaperiodate; [McLean and Nakane, 1974]) in phosphate buffered saline (PBS). Whole hearts were labelled with antibodies against HCN4 (1:50; APC-052, Alomone Laboratories, Jerusalem, Israel) and the transcription factor, Islet-1 (Isl1; 1:100; Developmental Studies Hybridoma Bank, Iowa City, IA, USA; [Tessadori *et al.*, 2012]) to detect putative pacemaker cells as previously described (see Appendix B). To reveal the presence of autonomic receptors associated with these cells, antibodies against muscarinic receptor subtype 2 (M_2R ; 1:100; M9558; Sigma-Aldrich) and adrenergic receptor subtype beta-2 (β_2AR ; 1:50; sc569 clone H20; Santa Cruz Biotechnology, Dallas, TX, USA; [Ampatzis and Dermon, 2010]) and tyrosine hydroxylase (TH; 1:100; 22941; Immunostar, Hudson, WI, USA) were used. To image β_2AR immunoreactivity a biotin-avidin fluorophore amplification process modified from Ampatzis and Dermon (2010) was used. Whole-mount tissue samples were first processed with the β_2AR primary antibody as previously described (Stoyek *et al.*, 2015), then incubated in a biotinylated anti-rabbit IgG antibody (1:100; Vector Laboratories, Burlington, ON, Canada) for two days at 4°C. Tissues were then rinsed in PBS, incubated with fluorophore-conjugated streptavidin (Rhodamine B; S871; Life Technologies) and processed for either anti-TH or anti- β_2AR antibodies raised in mouse. After exposure to these primary antibodies, preparations were incubated with appropriate secondary antibodies conjugated to AlexaFluor 488, 555, or 647 fluorophores (Life Technologies, Burlington, ON, Canada), washed in PBS and placed in Scale CUBIC-1 clearing solution (Susaki *et al.*, 2014) overnight at room temperature with gentle agitation. Processed

specimens were examined as whole-mounts. Omission controls for the antibody against M₂R were run as previously described for the HCN4 and Isl11 antibodies (Tessadori *et al.*, 2012; Stoyek *et al.*, 2015). Omission of either primary or secondary antibodies from the incubation protocol resulted in absence of immunoreactivity. Omission controls for the antibody against adrenergic receptor subtype beta-2 were performed by omitting 1) the β_2 AR primary antibody, 2) the biotinylated secondary, 3) the rhodamine-conjugated streptavidin, or both 2 and 3. In all cases omission of antibody or fluorophore-conjugated streptavidin resulted in an absence of immunoreactivity.

The relative distribution of β_2 ARs and M₂Rs were estimated from digital images of the atrium and ventricle of 6 specimens. In images from each specimen, five regions were selected at random from both the atrium and ventricle; these regions measured 10 × 10 μ m (100 μ m² each, 500 μ m² total area per chamber). To estimate relative receptor density, the number of immunoreactive punctata, which represent clusters of post-synaptic receptors, were counted using ImageJ software (50).

CHAPTER 4 – EFFECTS OF VAGAL NERVE STIMULATION ON PACEMAKER SITE AND NEURONAL ACTIVATION IN ZEBRAFISH

Animals.

A total of 42 adult, AB strain zebrafish (12-18 months post-fertilization; 33 ± 5 mm standard body length) of both sexes were used in this study.

VSN stimulation for assessment of ICN activation by cFOS.

Left or right VSN ($n = 6$ each) were stimulated with bipolar wire electrode driven by a constant-current stimulator (S88; Grass Instruments, Quincy, MA, USA) that

delivered trains of rectangular pulses (pulse duration 500 μ s; train duration 10 s, pulse frequency 20Hz, stimulus current 300 μ A) every 3 minutes for a total of 20 stimulation periods. To eliminate the possibility of pERK-IR in neurons other than those that were activated by VSN stimulations, hearts were immediately (>30 s) transferred to fixative (see below) following each experiment.

VSN stimulation for assessment of ICN activation by pERK.

Left or right VSN ($n = 6$ each) were stimulated with bipolar wire electrode driven by a constant-current stimulator (S88; Grass Instruments, Quincy, MA, USA) that delivered trains of rectangular pulses (pulse duration 500 μ s; train duration 10 s, pulse frequency 15Hz, stimulus current 300 μ A) every 1 minute for a total of 5 stimulation periods. To eliminate the possibility of pERK-IR in neurons other than those that were activated by VSN stimulations, hearts were immediately (less than 30 s) transferred to fixative (see below) following each experiment.

cFOS and pERK immunohistochemistry.

The general procedures used for immunohistochemistry in this study were similar to those we have previously described (Stoyek *et al.*, 2015). Tissues were fixed overnight in 4% paraformaldehyde (PFA; RT-15710, Electron Microscopy Sciences, Hatfield, PA, USA) in phosphate-buffered saline (PBS, composition in mM: 50 Na₂HPO₄, 140 NaCl, pH 7.2) before processing for immunohistochemistry in whole-mount format. Whole hearts were labelled with antibodies against cFOS (1:100; sc-253; Sanata Cruz Biotechnologies) or pERK (1:100; 4370S; Cell Signalling Technologies). In all experiments antibodies

against acetylated tubulin (AcT, axons; T6793, Sigma Aldrich) and human neuronal protein C/D (Hu, neuronal somata; A21271, Life Technologies) were used in combination to show the general innervation of the heart. After exposure to primary antibodies, preparations were incubated with appropriate secondary antibodies conjugated to AlexaFluor 488, 555, or 647 fluorophores (Life Technologies, Burlington, ON, Canada), washed in PBS and placed in Scale CUBIC-1 clearing solution (Susaki *et al.*, 2014) overnight at room temperature with gentle agitation. Processed specimens were examined as whole-mounts. Counts of ICNs expressing cFOS- or pERK-like-immunoreactivity (LIR) were performed using Fiji software; data is shown as percent of ICNs that were immunoreactive for cFOS or pERK compared to the total ICN number as estimated by AcT-Hu immunoreactivity.

Controls.

Both cFOS and pERK antibodies used in this study have previously been used in zebrafish (Randlett *et al.*, 2015; Yabuki *et al.*, 2016; see Appendix B). As a control for basal cFOS or pERK expression, subsets of hearts were fixed immediately after isolation ($n = 6$), or were isolated put in the bath for the same duration as the above experiments without receiving VSN stimulation ($n = 6$), before being fixed and processed for immunohistochemistry. For all antibodies used in this study, tissues for negative controls were processed as outlined above, except that either the primary or secondary antibody was omitted. In all trials this eliminated detection of histofluorescence.

Volatage optical imaging.

Whole hearts ($n = 6$) were isolated and pinned to the Sylgard rubber bottom of a 5 mL chamber filled with zebrafish saline and allowed to equilibrate for 30 min (composition in mM: 124.1 NaCl, 5.1 KCl, 2.9 Na₂HPO₄, 1.9 MgSO₄-7H₂O, 1.4 CaCl₂-2H₂O, 11.9 NaHCO₃; pH 7.2; 25°C). During this time, the heart was exposed to a voltage-sensitive dye (10 μM di-4-ANBDQPQ [Matiukas *et al.*, 2007]; University of Connecticut Health Center, Farmington, CT, USA) in the perfusate for 10 min, and then washed with fresh saline containing excitation-contraction uncoupler blebbistatin (10 μM (±)-blebbistatin; Cayman Chemical Company, Ann Arbor, MI, USA) to eliminate motion artifacts during optical recordings. Blebbistatin was present for the duration of the experiment. For imaging experiments, two controls were run ($n = 3$ each), 1) hearts were isolated and pacemaker initiation site was monitored in the bath every 30 min for 3 h, a period longer than any experiment in this study, 2) hearts were isolated, VSN stimulations were performed every 2 minutes for 40 minutes, and pacemaker site was observed after every stimulation.

Preparations were epi-illuminated through a macro zoom microscope (Olympus MVX10; Olympus Corporation) with a mercury lamp (Olympus U-HGLGPS) directed through a 640 ± 10 nm band-pass filter (D640/20X, Chroma Technology Corporation, Bellows Falls, VT, USA) and reflected by a 685 nm dichroic mirror (FF85-Di02; Semrock, Rochester, NY, USA) on to the preparation. Emitted fluorescence was collected with a 2×, 0.50 NA objective (Olympus MV PLAPO 2XC) at 4-6.3× magnification through a 700 nm long-pass filter (ET700LP, Chroma). Recordings were captured by a 128 × 128 pixel, 16-bit electron-multiplying charge-coupled device camera (Cascade 128+; Photometrics, Tucson, AZ, USA) at 511 frames·s⁻¹. Previous investigations of the

penetrance of this range of light wavelengths into myocardium was at 50% intensity at a depth of 1 mm (TA Quinn, unpublished). At a depth of 200-400 μm , which is the range of thickness of the zebrafish tissue preparations used in this study, light intensity is \sim 70-80%, resulting in excitation and collection of voltage signals from the entire transmural thickness of the heart. The camera was controlled and signals were acquired using MultiRecorder software (S. Luther and J. Schröder-Schetelig, Max Planck Institute for Dynamics and Self-Organization, Göttingen, Germany; <http://www.bmp.ds.mpg.de/multirecorder.html>).

As an index of changes in conduction, the time from initial breakthrough to full depolarization of the sinoatrial regions for three successive cycles was averaged from the recordings using custom Matlab routines. To map changes in the site of initial sinoatrial depolarization, binary images were created for three successive cycles and the initiation site averaged. An oval was fit to the image to encompass the sinoatrial valve region and the binary images were normalized (rigid transformation) to a brightfield exemplar image of the sinoatrial region for mapping using Fiji software.

VSN stimulation for assessment of pacemaker shift.

Left and right VSN trunks were stimulated with bipolar wire electrodes attached to constant-current isolation units (PSIU6; Grass Instruments, Quincy, MA, USA) driven by a stimulator (S88; Grass Instruments) delivering trains of rectangular pulses (pulse duration 0.5ms; train duration 10 s, pulse frequency 1-15 Hz). In all experiments, a standard stimulus current of 300 μA was used (Stoyek *et al.*, 2016). Between stimulation trains, a minimum of 2 min was allowed for recovery of the preparation between VSN

stimulations. To control for the potential that repeated VSN stimulation alone may alter the pacemaker initiation site, a subset of hearts ($n = 3$) was sampled for 30 minutes following the last VSN stimulation. .

Pharmacological blockade.

Hexamethonium (a non-depolarising nicotinic receptor antagonist that blocks cholinergic neurotransmission; 10 μ M; Sigma Aldrich) was dissolved in saline the day of experiments. Saline in the bath was replaced with saline containing hexamethonium 15 minutes prior to recordings.

Data presentation.

Numerical values were expressed as mean \pm 1 standard error of the mean (SEM). One-way ANOVA with a Tukey's *post hoc* (SPSS, IBM Canada, Markham, ON) was used to detect significant differences among means. P values ≤ 0.05 were considered significant.

CHAPTER 5 CARDIAC DISTRIBUTION AND CHRONOTROPIC EFFECTS OF SEROTONIN IN THE ZEBRAFISH

Animals.

A total of 72 adult, AB strain zebrafish (12-18 months post-fertilization) of both sexes were used in this study.

Tissue preparation.

Tissue was fixed overnight in 4% paraformaldehyde (PFA; RT-15710, Electron Microscopy Sciences, Hatfield, PA, USA) in phosphate-buffered saline (PBS, composition in mM: 50 Na₂HPO₄, 140 NaCl, pH 7.2) before processing for immunohistochemistry in whole-mount format. The general procedures used for immunohistochemistry in this study were similar to those described in previous publications on cyprinid neuroanatomy (Finney *et al.*, 2006; Robertson *et al.*, 2008; Dumbarton *et al.*, 2010; Newton *et al.*, 2014; Stoyek *et al.*, 2015; Stoyek *et al.*, 2016). Briefly, fixed tissues were rinsed in PBS, transferred to a PBS solution containing 2% Triton X-100 (X100, Sigma Aldrich), 1 % bovine serum albumin (BSA; A9576, Sigma Aldrich) and 1% normal goat serum (NGS; G9023, Sigma Aldrich) for 48 hours at 4°C with agitation, and then incubated with primary antibodies (see Appendix B). Primary antibodies were diluted in a solution containing 0.25% Triton X-100, 1 % BSA and 1 % NGS in PBS (designated PBS-T). Tissues were incubated 3-5 d with agitation at 4°C, rinsed in PBS-T, then transferred to a solution of PBS-T containing the appropriate secondary antibody conjugated to AlexaFluor 488 or 555 fluorophores (Life Technologies, Burlington, ON, Canada). Incubation time with secondary antibodies was 3-5 d with agitation at 4°C. Final rinsing was done in PBS and before specimens were placed in Scale CUBIC-1 clearing solution (Susaki *et al.*, 2014) overnight at room temperature with gentle agitation.

Serotonin and tryptophan hydroxylase antibodies.

Serotonergic elements were detected by immunoreactivity with an anti-serotonin (5-hydroxytryptamine; 5-HT) antibody (dilution 1:100; 20080, Immunostar; see Appendix

B). The 5-HT antibody used was the same as used by Uyttebroek *et al.* (2010) in zebrafish. The expression of tryptophan hydroxylase (TPH; dilution 1:100; P21961, Life Technologies), the rate-limiting enzyme in the synthesis of 5-HT, indicated was used as an indicator of elements capable of synthesizing 5-HT. To determine the general innervation of the heart antibodies against acetylated tubulin (AcT, axons; T6793, Sigma Aldrich) were combined with human neuronal protein C/D (Hu, neuronal somata; A21271, Life Technologies) as previously described (Stoyek *et al.*, 2015).

Controls.

For all antibodies used in this study, negative control tissues were processed as outlined above, except that either the primary or secondary antibody was omitted. In all trials this eliminated detection of histofluorescence.

Myocardial labelling.

In order to determine how immunohistochemically labelled neuronal elements were related to the regional structure of the myocardium, some specimens were double-labelled with the F-actin marker phalloidin (77418, Sigma Aldrich; Small *et al.*, 1999; Newton *et al.*, 2014), conjugated with tetramethyl rhodamine isothiocyanate to show cardiac myocytes.

Measurement of heart rate.

Isolated hearts were pinned through the ventral aorta and walls of the ducts of Cuvier to the Sylgard rubber (Dow Corning, Midland, MI, USA) bottom of a 5 mL

chamber which was perfused with zebrafish saline (composition in mM: 124.1 NaCl, 5.1 KCl, 2.9 Na₂HPO₄, 1.9 MgSO₄-7H₂O, 1.4 CaCl₂-2H₂O, 11.9 NaHCO₃; aerated with room air; pH 7.2; 25°C) at a rate of 10 mL min⁻¹. Hearts were allowed to equilibrate in the bath for 30 min prior to testing. Electrocardiogram (ECG) signals were recorded from the surface of the atrium and ventricle *via* bipolar suction electrodes, differentially amplified (total gain ×1000-10000), and stored on a personal computer after analogue-digital conversion (Digidata 1322A, Axon Instruments, Foster City, CA, USA). To quantify cardiac responses, time between adjacent P-waves of the atrial ECG (R-R interval) for HR effects was processed using Axoscope software (Axon Instruments) (Stoyek *et al.*, 2016).

Pharmacological agents.

5-HT was dissolved in saline (1 mM; H7752, Sigma Aldrich) on the day of the experiment and delivered to the bath directly above the tissue in 200 µL boluses through a micropipette *via* a calibrated syringe attached to a screw-drive microinjector (IM-4B; Narishige, East Meadow, NY, USA). As a control 200 µL boluses of saline were delivered in the same manner and did not elicit chronotropic responses. Serotonergic agents ketanserin (5-HT₂-receptor blocker; 10 µM; S006, Sigma Aldrich), spiperone (5-HT₁-receptor blocker; 10 µM; S7395, Sigma Aldrich), and fluoxetine (selective 5-HT reuptake inhibitor at presynaptic receptors; 5 µM; F132, Sigma Aldrich) were dissolved in saline and perfused continuously starting 15 minutes prior to recording. Autonomic antagonists atropine (post-junctional muscarinic receptor blocker; 10 µM; A0132, Sigma Aldrich) and timolol (post-junctional beta-adrenergic receptor blocker; 100 µM; T6394, Sigma Aldrich) were dissolved in saline and perfused continuously starting 15 minutes prior to recording.

CHAPTER 6 - THE ISOLATED ZEBRAFISH HEART AS A MODEL TO STUDY THE CHRONOTROPIC EFFECTS OF VAPOUR ANAESTHETICS

Animals.

A total of 72 adult, AB strain zebrafish (12-18 months post-fertilization) of both sexes were used in this study.

Measurement of heart rate and vagosympathetic nerve electrical stimulation.

Isolated hearts were pinned through the ventral aorta and walls of the ducts of Cuvier to the Sylgard rubber (Dow Corning, Midland, MI, USA) bottom of a 5 mL chamber which was perfused with zebrafish saline (composition in mM: 124.1 NaCl, 5.1 KCl, 2.9 Na₂HPO₄, 1.9 MgSO₄-7H₂O, 1.4 CaCl₂-2H₂O, 11.9 NaHCO₃; aerated with room air; pH 7.2; 25°C) at a rate of 10 mL min⁻¹. Hearts were allowed to equilibrate in the bath for 30 minutes prior to testing, to ensure stable HR and to allow for washout of any residual tricaine (see *Potential effects of triacaine as an overdosing agent*).

Electrocardiogram (ECG) signals were recorded from the surface of the atrium and ventricle *via* bipolar suction electrodes, differentially amplified (total gain ×1000-10000), and stored on a personal computer after analogue-digital conversion (Digidata 1322A, Axon Instruments, Foster City, CA, USA). To quantify cardiac responses, time between adjacent R-waves of the atrial ECG (R-R interval) for HR effects, and delay between the atrial R-wave and ventricular R-wave for atrioventricular delay (Fig. 1), were processed using Axoscope software (Axon Instruments) (Stoyek *et al.*, 2016).

Stimulation of vagosympathetic trunks was performed with bipolar wire electrodes attached to constant-current isolation units (PSIU6; Grass Instruments, Quincy, MA, USA)

driven by a stimulator (S88; Grass Instruments) delivering trains of rectangular pulses (pulse duration 0.5ms; train duration 10 s, pulse frequency 15 Hz, stimulus current 300 μ A [Stoyek *et al.*,2016]). In previous work the effects of left and right vagosympathetic nerve stimulation on HR were statistically similar, thus in this study only the right vagosympathetic nerve was stimulated to test the effects of activation. To control for the possibility of electrotonic spread of current into the myocardium from the site of nerve stimulation, in some preparations the stimulating electrodes were placed on the duct wall away from the nerve ($n=6$) or moved off the nerve into the bath ($n=6$); repeated stimulation with the same parameters then had no effect on heart rate.

Potential effects of tricaine as overdosing agent.

As a tricaine overdose was used on the animals in this study and a previous report showed that tricaine can alter HR in zebrafish (Huang *et al.*,2010), preliminary experiments were performed to investigate if the use of this compound may have affected the hearts. Residual tricaine from the initial overdose was washed out for 30 minutes, then the hearts were exposed to a solution of tricaine in the perfusate that was equal in concentration to that used in the overdose procedure. Hearts were perfused with this solution for 1 minute before being switched back to fresh perfusate and rate was monitored throughout this period and during washout. Tricaine exposure caused an increase in mean R-R interval to 1.9 ± 0.12 times the mean pre-exposure value, and recovery to pre-tricaine R-R interval occurred by 8.5 ± 1 minutes after the switch to fresh saline. Therefore to ensure that tricaine exposure did not affect the experimental outcomes, a standardized

washout time of 30 minutes for all hearts in the bath was performed before experiments were done in this study.

Anaesthetic agents.

Desflurane (DSF; Baxter Corporation, Mississauga, ON, Canada), isoflurane (ISF; Baxter Corporation) or sevoflurane (SVF; Abbott Canada, Saint-Laurent, PQ, Canada) were mixed with room air through standard vaporizers (Draegerwerk AG, Lübeck, Germany) that bubbled into a sealed reservoir of zebrafish saline; the tissue was then perfused with this mixture. Concentration of anaesthetics in the perfusate was measured by sampling with a standard patient vapor-phase anaesthetic monitor (Datex-Ohmeda, Madison, WI, USA) from the air space in the reservoir; the partial pressure of anaesthetic in the gas phase and in the perfusate were assumed to be in equilibrium. The dose of each anaesthetic was adjusted to match the minimum alveolar concentration for that agent to maintain a clinical level of anaesthesia in patients (this dose was designated "1.0 MAC" for the purposes of the present study). Desflurane was mixed at 3-12% (6% = 1 MAC), while isoflurane and sevoflurane were mixed at 0.75-3% (1.5% = 1 MAC) with air through the vaporizers.

Anaesthetic test procedures.

Their manufacturers have described all anaesthetics tested as having negligible solubility in water, so determining the exact dose of anaesthetic compound administered in the present study could have posed potential limitations in determining comparative cardiac responses. Thus, to test anaesthetic dosage in the perfusate, random samples were

drawn into a sealed container from the perfusate reservoir during experiments. The perfusate was allowed to off-gas and the dose of anaesthetic present was sensed with the patient monitor. Dosages measured from the off-gassing samples were assumed to be in equilibrium with the perfusate, as indicated previously. Values for anaesthetic dosages were statistically similar to those recorded during the initial setup stage for each experiment (t-test; data not shown).

For studies on time-dependent cardiac effects, a series of preliminary experiments was done in which anaesthetic agents were introduced following a period of acclimation in the bath. HR was monitored for up to 1 h in the presence of the agent under test. Analysis of changes in R-R period from the pre-anaesthetic value (control) at 15 minutes and 1 h of exposure were statistically similar for all anaesthetics (data not shown). Therefore in all subsequent experiments, hearts were exposed to anaesthetic for a standardized period of 15 minutes.

For concentration-effect studies, preliminary experiments were done to determine the lowest dose of each anaesthetic that had an effect. After an acclimation period, the minimum dosage that evoked a detectable change in heart rate over a 30 minute exposure period was 0.5 MAC (data not shown). For the purposes of this study, anaesthetics were applied in dosages increasing from 0.5 MAC to 2.5 MAC (this dosage represented the highest concentration that could be delivered by the vaporizers).

As a control for anaesthetic exposure, in trial experiments a group of hearts was perfused with saline that had been bubbled through the vaporizer system with no anaesthetic present; the results of these trials were compared with the effects of anaesthetic in the vaporizer. Cardiac responses occurred only when the vaporizer was delivering

anaesthetic to the perfusate. It was thus assumed that chronotropic effects of anaesthetics were in fact due to these agents reaching the isolated heart.

Pharmacologic agents.

Atropine (post-junctional muscarinic receptor blocker; 10 μ M; Sigma Aldrich) and timolol (post-junctional beta-adrenergic receptor blocker; 100 μ M; Sigma Aldrich) were dissolved in zebrafish saline on the day of experiments (Stoyek *et al.*, 2016). For experiments investigating autonomic blockade, these drugs were delivered in combination starting at 15 minutes prior to and continuing through the period of anaesthetic delivery. The order of exposure to autonomic antagonists was tested in two paradigms: 1) exposure to autonomic antagonists and then anaesthetics in the continued presence of antagonists; or 2) exposure to anaesthetics and then to autonomic antagonists in the continued presence of anaesthetics. In these preliminary experiments the responses to these paradigms were statistically similar, so in all subsequent experiments responses were first measured during antagonist exposure alone, then in the presence of antagonists with anaesthetics.

Appendix B

Table of immunohistochemical agents

Primary Antibody	Immunogen / Host	Source	Dilution	Reference / Species
Anti-acetylated tubulin, clone 6-11B-1 (AcT)	Epitope of <i>Chlamydomonas</i> axonemal α -tubulin α 3 isoform / mouse, monoclonal	Sigma (T6793)	1:200	Olsson <i>et al.</i> (2008) / zebrafish
Anti-beta 2 adrenergic receptor, clone H-20 (β_2 AR)	C-terminus peptide of human beta-2 receptor (mapping to 5q32) / rabbit, polyclonal	Santa Cruz Biotechnologies (sc-569)	1:50	Ampatzis and Dermon (2010) / zebrafish
Anti-choline acetyltransferase (ChAT)	Human ChAT (NM_020549.3) / goat, polyclonal	Chemicon (AB144P)	1:100	Clemente <i>et al.</i> (2004) / zebrafish
Anti-cFOS, clone K-25 (cFOS)	Peptide mapping within internal region of human c-Fos, mapping to 14q24.3 / rabbit, polyclonal	Santa Cruz Biotechnologies (sc-253)	1:100	See text
Anti-human neuronal protein C/D (Hu)	Human neuronal proteins C/D, product of ELAVL3 gene / mouse monoclonal	Life Technologies (A21271)	1:200	Olsson <i>et al.</i> (2008) / zebrafish
Anti-hyperpolarization-activated, cyclic-nucleotide gated channel 4 (HCN4)	GST protein to AA119-155 (Q9Y3Q4) of human HCN4 (N-terminus) / rabbit, polyclonal	Alomone Laboratories (APC-052)	1:50	See text
Anti-Islet 1 & 2 homeobox 4D5 (Isl1)	Amino acids 214-379, C-terminal / mouse, monoclonal	Developmental Studies Hybridoma Bank	1:100	Kuscha <i>et al.</i> , 2012; Coppola <i>et al.</i> , 2012 / zebrafish
Anti-muscarinic acetylcholine receptor, subtype 2 (M_2 R)	GST protein to AA 227-356 of the i3 intracellular loop, of human M2 muscarinic acetylcholine receptor / rabbit, polyclonal	Sigma Aldrich (M9558)	1:100	See text
Anti-neuropeptide Y (NPY)	Porcine NPY conjugated to bovine thyroglobuline with gluteraldehyde / rabbit, polyclonal	Immunostar (22940)	1:400	Matsuda <i>et al.</i> (2009) / goldfish
Anti-nitric oxide synthetase, neuronal (nNOS)	Synthetic peptide to AA1411-25 of human nNOS / rabbit, polyclonal	AbCam (ab5586)	1:300	Newton <i>et al.</i> (2014) / goldfish

Primary Antibody	Immunogen / Host	Source	Dilution	Reference / Species
Anti-phosphorylated ERK (pERK)	Synthetic phosphopeptide corresponding to residues surrounding Thr202/Tyr204 of human p44 MAP kinase	Cell Signalling Technologies (4370S)	1:100	Randlett <i>et al.</i> (2015) / zebrafish
Anti-serotonin (5-HT)	Serotonin / rabbit, polyclonal	Immunostar (20080)	1:100	Uyttbroek <i>et al.</i> (2010) / zebrafish
Anti-synaptic vesicle marker 2 (SV2)	<i>Diplobatis ommata</i> synaptic vesicles / mouse	Developmental Studies Hybridoma Bank	1:100	Braubach <i>et al.</i> (2012) / zebrafish
Anti-vesicular acetylcholine transporter (VAChT)	Synthetic peptide corresponding to the C-terminus of the predicted rat VAChT protein	Millipore (AB1588)	1:100	Shakarchi <i>et al.</i> (2013) / zebrafish
Anti-tryptophan hydroxylase (TPH)	Phosphopeptide corresponding to AA residues surrounding phosphor-Ser19 of rat tryptophan hydroxylase / rabbit, polyclonal	Life Technologies (P21961)	1:100	See text
Anti-tyrosine hydroxylase (TH)	TH purified from rat PC12 cells / mouse, monoclonal	Immunostar (22941)	1:100	Olsson <i>et al.</i> (2008) / zebrafish
Anti-vasoactive intestinal polypeptide (VIP)	Porcine VIP conjugated to bovine thyroglobulin with carbodiimide / rabbit, polyclonal	Immunostar (20077)	1:400	Finney <i>et al.</i> (2006); Olsson <i>et al.</i> (2008); Uyttbroek <i>et al.</i> (2010) / zebrafish
Label / Tracer	Immunogen / Host	Source	Dilution	Reference / Species
Phalloidin	<i>Amanita phalloides</i> toxin	Sigma Aldrich (77418)	1:500	Small <i>et al.</i> , 1999
Neurobiotin	N-(2-aminoethyl) biotinamide hydrochloride	Vector Laboratories (SP-1120)	1:50	Wyeth and Croll, 2011
FM1-43X		Life Technologies (F35355)	1:100	Betz <i>et al.</i> , 1992
Secondary Antibody	Host	Source	Dilution	
AlexaFluor488 anti-goat	donkey	Life Technologies (A11055)	1:100	

Secondary Antibody	Host	Source	Dilution
AlexaFluor488 anti-mouse	donkey	Life Technologioges (A21202)	1:100
AlexaFluor488 anti-rabbit	goat	Life Technologies (A11008)	1:100
AlexaFluor555 anti-goat	donkey	Life Technologies (A21432)	1:100
AlexaFluor555 anti-guinea pig	goat	Life Technologies (A21435)	1:100
AlexaFluor555 anti-mouse	goat	Life Technologies (A21422)	1:100
AlexaFluor555 anti-rabbit	donkey	Life Technologies (A21206)	
AlexaFluor647 anti-mouse	donkey	Life Technologies (A31571)	1:100
AlexaFluor488 Avidin		Life Technologies (A21370)	1:100
Biotinylated anti-rabbit IgG	goat	Vector Laboratories (BA-1000)	1:50

Appendix C

Results from studies of intracardiac innervation in goldfish, *Carassius auratus*

In teleost fishes, details of the organization of the intracardiac nervous system (ICNS) is not well understood. Prior to the studies of zebrafish a number of techniques were developed in investigations of the ICNS in the goldfish (Newton *et al.*, 2014) a species representative of a large group of cyprinids. Antibodies against the neuronal markers acetylated tubulin (AcT), and human neuronal protein C/D (Hu), as well as choline acetyltransferase (ChAT), tyrosine hydroxylase (TH) were used to detect neural elements and their transmitter contents in wholemounts of cardiac tissue. All chambers of the heart were innervated by AcT-positive axons, implying cholinergic regulation; and by TH containing axons, implying adrenergic regulation. The mean total number of intracardiac neurons was 713 ± 78 . Neuronal somata were mainly located in a ganglionated plexus around the sinoatrial valves. Putative pacemaker cells, identified by immunoreactivity for hyperpolarization activated, cyclic nucleotide-gated channel 4 (HCN4), were located in the base of the sinoatrial valves, and this region was densely innervated by cholinergic and adrenergic terminals. These results show that the goldfish heart possesses the necessary neuroanatomical substrate for fine, region-by-region autonomic control of the myocardial effectors that are involved in determining cardiac output.

Methods

Immunohistochemistry.

The general immunohistochemical procedures used in this study were similar to those used previously in zebrafish (Finney *et al.*, 2006; Robertson *et al.*, 2007). After rinsing in phosphate buffered saline (PBS), fixed tissues were transferred to a solution of 0.25% Triton X-100 (Sigma-Aldrich) and 1% bovine albumen serum in PBS for 4 hours at

4°C with agitation before exposure to primary antibodies, to permeabilize tissue and reduce nonspecific binding of antibodies. Tissues were then placed in a solution of the appropriate primary antibody (Table 1) diluted in 0.25% Triton X-100, 2% dimethylsulfoxide (Sigma-Aldrich) 1% normal goat serum (Sigma Aldrich) and 1% bovine serum albumen (Sigma Aldrich) in PBS (designated “PBS-T”), and incubated at 4°C for 5–7 days with agitation. Following incubation with primary antibody, tissues were rinsed in PBS-T and incubated with the appropriate secondary antibody conjugated to AlexaFluor 488 or 555 fluorophores (Molecular Probes, Eugene, OR or Invitrogen, Burlington, ON, Canada) diluted in PBS-T at 4°C for 5–7 days with agitation. This was followed by a final rinsing in PBS. For combined AcT and Hu labeling, tissues were incubated in a solution of PBS-T containing AcT and Hu primary antibodies together for 5–7 days at 4°C with agitation. A single anti-mouse antibody conjugated to either AlexaFluor 488 or 555 was used to visualize both primary antibodies in the same tissue specimens. Tissues were exposed to the secondary antibody in PBS-T for 5-7 days at 4°C. In order to determine the relationship of the innervation with cardiac and smooth muscle, some specimens were incubated with phalloidin (Small *et al.*, 1999), conjugated with tetramethyl rhodamine isothiocyanate (TRITC) (Sigma #77418, dilution 1:500 in PBS) at 4°C overnight. Tissues were mounted in a glycerol solution (3:1 glycerol to Tris buffer, pH 8.0) with 1–2% n-propyl gallate added to prevent fluorophore bleaching.

Results

Neuronal somata in the sinoatrial plexus.

Neuronal somata were detected by a combination of AcT and Hu to label neuronal

processes and somata, respectively, in the same tissue samples. The appearance and relative density of AcT-positive axons in the SAP (Figure B1) Labeling with AcT-Hu antibodies revealed that ICN somata were organized into ganglia at the junctions of the left and right vagosympathetic trunks with the plexus (Figure B1F,H, respectively) as well as in the intervagal regions of the plexus. Individual somata or ganglia containing 2–5 somata were also observed along both vagosympathetic trunks for a distance of up to 200 μm from the vagoplexus junctions (e.g., ganglion associated with left vagosympathetic trunk, Figure B1G). Most neuronal somata visualized with AcT-Hu in the SAP (and elsewhere in the heart) were oval or spherical and there was typically only one visible process, with an apparent axon hillock emerging from one end of the soma (i.e., Figure B1G).

Somata were present in all parts of the SAP, displaying a wide range of soma size. Long-axis somatic dimension ranged from 10 to 80 μm (mean 35 μm), while short-axis dimension ranged from 5 to 60 μm (mean 25 μm). Frequency distributions of these dimensions, when plotted as histograms (not shown), were continuous across their ranges, peaking at the mean values ($n = 5$; 4,368 neurons). In these plots there was no evidence of bi- or multimodal frequency distribution that might have indicated discrete classes of soma size. In the SAP of seven hearts there was a mean total number of 713 ± 78 (SEM) ICNs. The SAP was divided this into four regions each representing one-quarter of the total SAP area in wholemout specimens in order to determine if there was differential regional distribution of neurons within this plexus. The dorsal intervagal region contained 38% of SAP ICNs (mean number 267 ± 30). Neurons proximal to the left vagal junction constituted 25% of ICNs (mean 179 ± 23); this value was not significantly different from that in the dorsal region. The ventral intervagal region contained 20% of ICNs (mean 143

± 25) while the region associated with the right vagal junction encompassed 17% (mean 122 ± 17). The values for these regions were significantly less than the value for the dorsal intervagal region but not significantly different from that for the left vagal region, or from each other.

Putative pacemaker tissue in SAV region.

In wholemount preparations of the sinoatrial region, cells labeled with antibodies against HCN4 were generally oval-shaped and less than 10 μm in longest dimension (Figure B1). The majority of these cells were located within the valve leaflets, mainly in the basal regions. Along the length of each leaflet the greatest density of labeled cells was near the valve commissures, close to the entry of the vagosympathetic trunks into the SAP. In the example shown in Figure 1, the left vagosympathetic trunk is at the lower left of the image. Double labeling with AcT-Hu and HCN4 showed that axon bundles and single axons coursed through and terminated within the region containing HCN4-positive cells (Figure B1).

Atrial wall innervation.

Multiple axon bundles and nerves arose from the SAP and entered the atrial wall. Of these, the largest continued toward the ventricle, but some nerve bundles and single axons diverged to innervate myocytes in atrial trabeculae (AcT-Hu, Figure B2A). The relative densities of axons within trabeculae in different regions of the atrial wall were similar (data not shown). In all specimens examined there were also 5–10 ICN somata located in the atrial wall near the apex (Figure B2B,C). Atrial wall trabeculae were

innervated by both ChAT- and TH-positive axons (Figure B2D,E, respectively). While the relative densities of these axonal types was not quantitatively analyzed, there appeared to be more cholinergic than adrenergic axons in this part of the heart.

Atrioventricular funnel, ventricular wall, and ventriculobulbar junction.

There were several axonal bundles coursing directly from the SAP via the wall of the atrioventricular funnel into the ventricle (Figure B3, schematic). These bundles converged to form a plexus at the atrioventricular junction, circumscribing the atrioventricular valves (Figure B3A, dashed line, lower right). A fine network of axons extended into the atrioventricular valve leaflets from the plexus. There was also a small population of neurons associated with this plexus, located mainly on the atrial side, in the area indicated by the asterisk (*) in the lower right of Figure B3A. A portion of the atrioventricular plexus is seen in detail in Figure 3B, showing an axonal bundle with a ganglion of four somata (arrowhead) beside the nerve, along with several isolated somata and individual axons. In four specimens examined, there were 12–15 neuronal somata located here; these appeared to be unipolar (Figure B3B). Figure 3C shows details of the atrioventricular plexus ganglion of another specimen, illustrating a complex arrangement of axons surrounding the somata. The soma indicated by the arrowhead in Figure 3C is shown at higher magnification in panel D. There appeared to be multiple terminals or varicosities associated with this soma (indicated by *), clustered around the putative axon hillock. An extension of the atrioventricular trunk (AVtr, Figure B3) continued within a thickening of the compact ventricular myocardium from the atrioventricular plexus to the ventriculobulbar junction (Figure B3, left side, junction indicated by *). The basal regions

of the atrioventricular valves were attached to the heart wall in the region shown between the two dashed lines on the left side of this image. In the ventricular wall, axons branching from the atrioventricular trunk innervated the subepicardial zone of the compact ventricular myocardium as well as coronary blood vessels. At the ventriculobulbar junction the nerve trunk divided to form a small plexus (AcT-Hu, Figure B3). Some of the axons innervating the ventricular wall were ChAT-positive (Figure B3), targeting both myocytes and coronary vessels. TH-positive axons were also detected in the ventricular wall, particularly adjacent to the ventriculobulbar junction; these axons appeared to target primarily coronary blood vessels.

Innervation of the bulbus arteriosus and ventral aorta.

The general innervation of the bulbus and aorta (Figure B4) appeared to have two origins. Axons from the ventriculobulbar plexus extended caudocranially within the tunica adventitia of the bulbus, contributing to a small plexus at the bulbo-aortic junction. Some of these axons continued a short distance into the wall of the ventral aorta. Figure 4 also shows nerve trunks that coursed craniocaudally within the walls of the ventral aorta, becoming reduced in size as they extended toward the bulbus arteriosus. In the wall of the bulbus close to the bulbo-aortic junction, there was fine innervation of both the tunica adventitia and outer tunica media, visible in wholemount. ChAT-positive axons in this region appeared to be evenly distributed throughout the tunica adventitia while axons expressing TH-immunoreactivity appeared to target mainly adventitial blood vessels. Figure 4A shows the fine innervation of the midregion of the ventral aorta, with axons in the tunica adventitia overlying smooth muscle in the tunica media.

Figure C1. Overview of cardiac innervation and putative pacemaker cells in sinoatrial plexus (SAP) region. Neural elements and putative pacemaker cells in SAP region were labeled with antibodies against acetylated tubulin (AcT, axons), human neuronal protein C/D (Hu, intracardiac neuron [ICN] somata) and the ion channel HCN4. AcT and Hu were detected using the same fluorescent secondary antibody. **A:** Ganglia at the junction of left vagosympathetic trunk with the SAP. **B:** ICN somata (arrowheads) associated with left vagosympathetic trunk in the wall of the duct of Cuvier approximately 200 μm distal to the SAP. Note typical “unipolar” appearance of somata. **C:** Ganglia at the junction of the right vagosympathetic trunk with the SAP. **D-E:** Overview (D) and enlarged detail (E) of SAV leaflet showing small cells immunoreactive for HCN4 (green, arrowheads) in the leaflet base. This area was well-innervated and close to SAP ganglia (note AcT-Hu double-labeled axons and somata, red). Scale bars 50 μm in A-C; 40 μm in I; 20 μm in J.

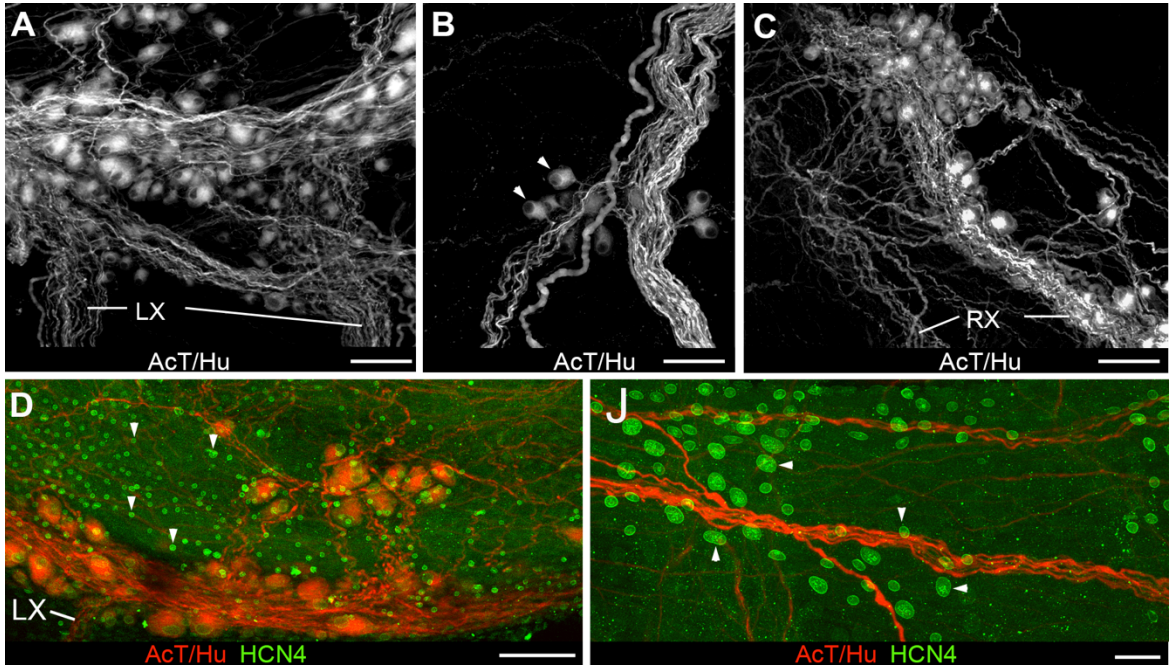


Figure C2. Innervation of atrial wall. **A:** Combined AcT-Hu (green) and phalloidin (Phal; red) labeling showed dense innervation of cardiac myocytes in atrial trabeculae. **B,C:** Detailed views of AcT-Hu labeled ICNs and axons in the atrial wall near the apex. Note axonal varicosities, and double nucleoli in soma, panel C. **D:** Example of ChAT-positive axons innervating atrial trabeculae near sinoatrial junction. **E:** Example of TH-positive axons innervating atrial trabeculae near the atrioventricular junction. Scale bars 100 μm in A,E; 200 μm in D; 25 μm in C (applies to B).

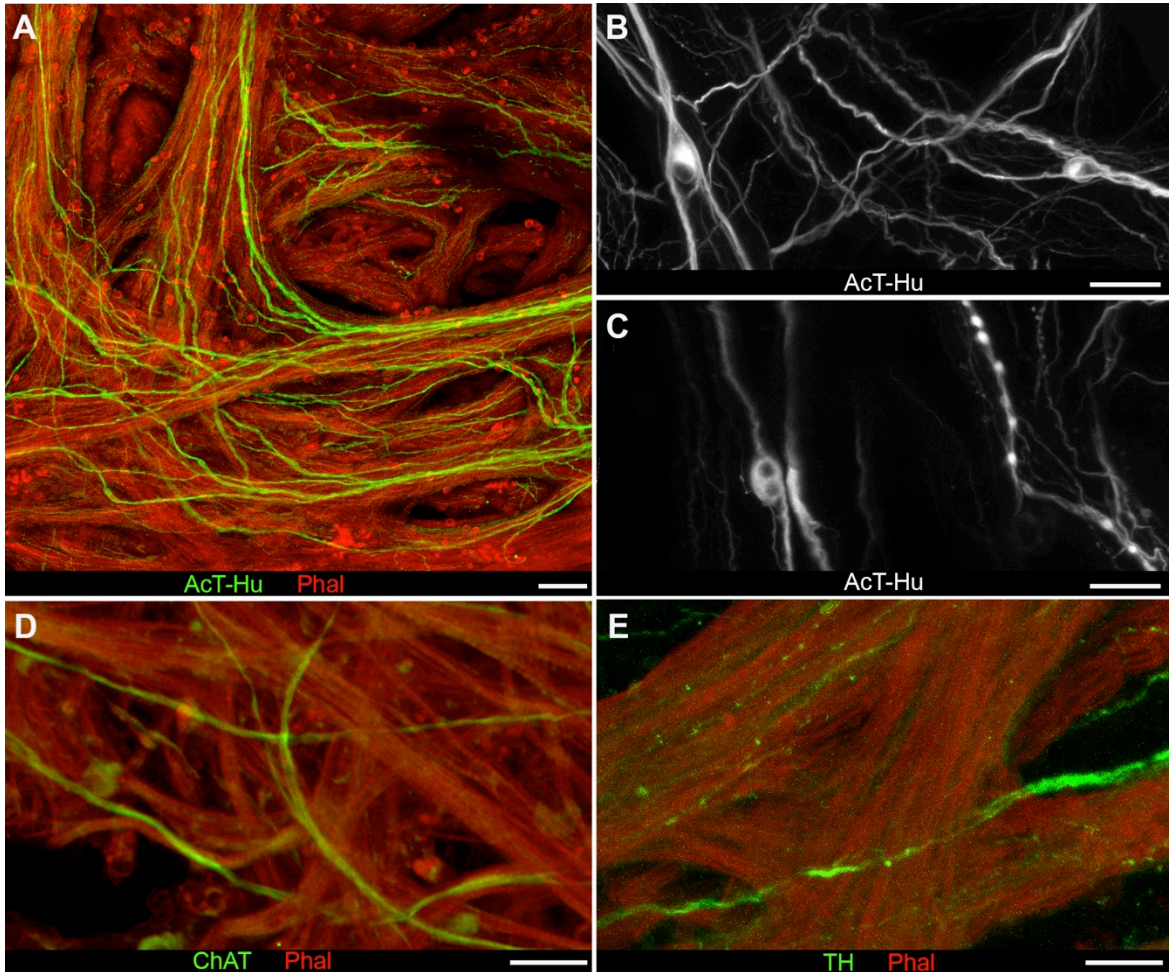


Figure C3. Innervation of atrial funnel, ventricle, and ventriculobulbar junction.

Schematic view of this region is shown in panel at lower left; AVtr, atrioventricular nerve trunk; other labels as for Figure 1A. **A:** Low-magnification overview of region in box in schematic, including a portion of the atrium (A, *, lower right) proximal to the atrioventricular junction region (single dashed line) and ventricular wall (V) between the atrioventricular junction and ventriculobulbar junction (* between two dashed lines on left). The bases of the AV valves were anchored to the cardiac wall in this region. Cranial is toward top of panel. The AVtr coursed from the AV valve plexus via the ventricular subepicardium to join a plexus at the ventriculobulbar junction. Part of this nerve trunk was obscured by the thickness of the wholemount tissue. **B–D:** Details of ICNs in the atrioventricular plexus. **B:** Ganglionic somata and complex neuropil from another specimen; arrowhead indicates a soma illustrated in detail in panel D. **C:** Multiple varicosities (putative axonal terminals, arrowheads) were associated with this soma (*). **D:** Four somata constituted a small ganglion (arrowhead) associated with a nerve trunk. Scale bars 100 μm in A; 20 μm in B; 10 μm in C; 50 μm in D.

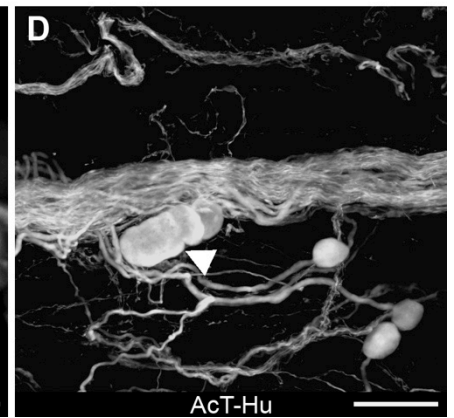
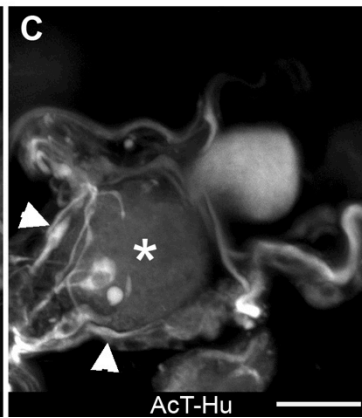
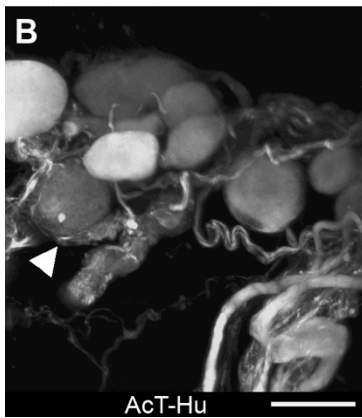
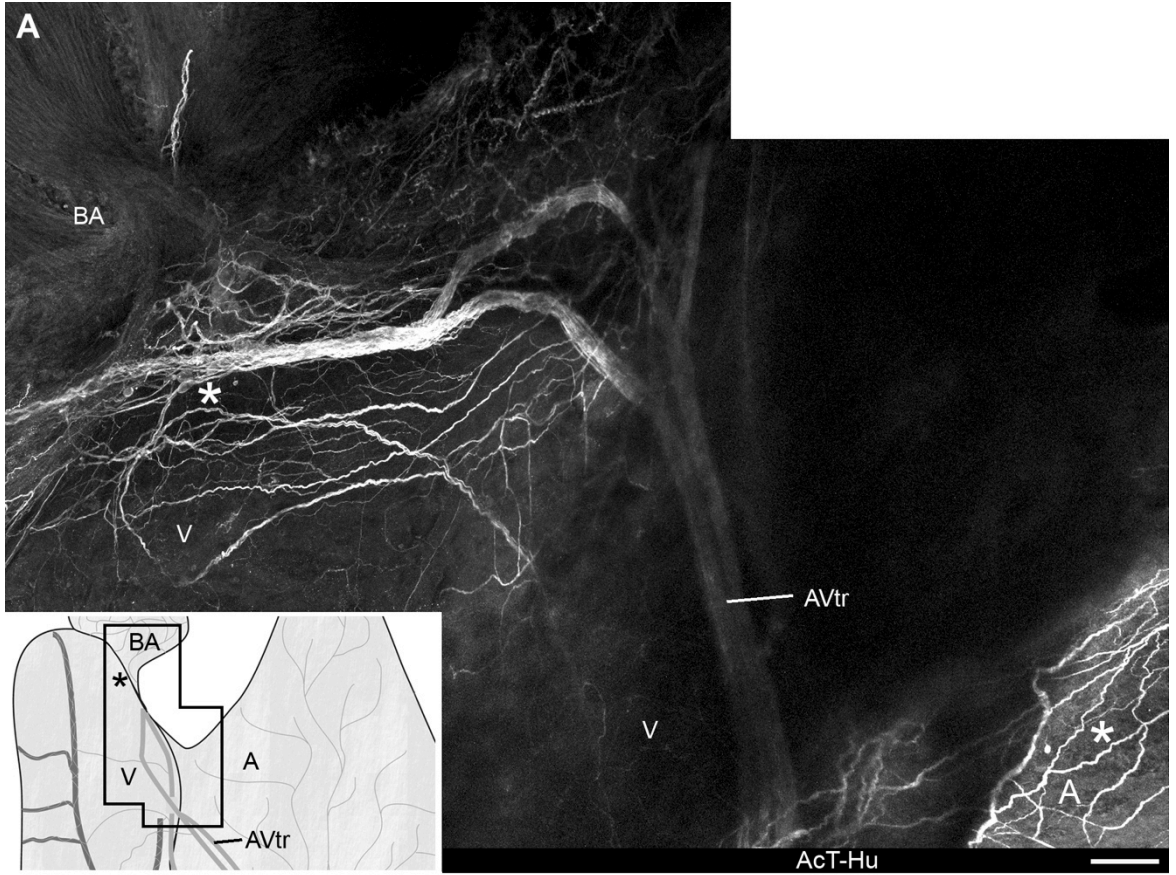
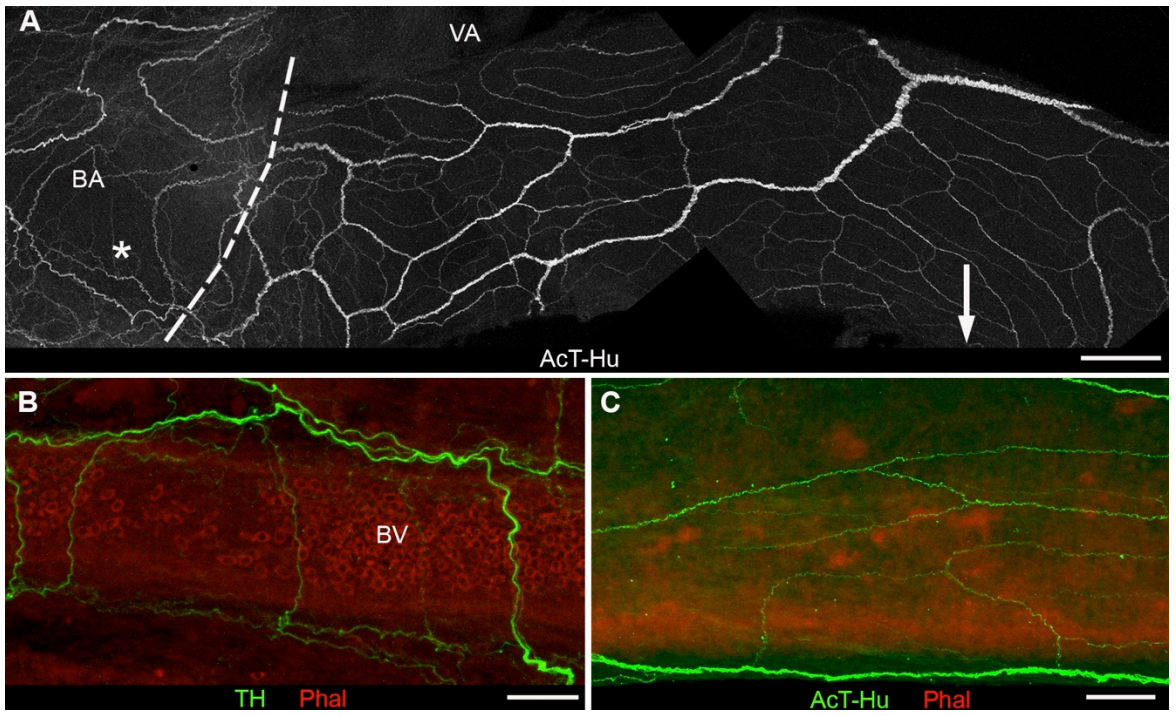


Figure C4. Innervation of the ventricular wall, ventriculobulbar junction, and outflow tract. **A:** Composite micrograph showing general innervation (AcT-Hu) of bulbus arteriosus (BA, left side of panel; dashed line marks approximate location of bulbus ventral aorta junction) and ventral aorta (VA) to origin of first afferent branchial artery (arrow). Caudal is to left, cranial is to right of this panel. **B:** Blood vessel in bulbus wall innervated by TH-positive axons (green; phalloidin, red). **C:** Axons (AcT-Hu, green) in mid-ventral aorta innervated mainly adventitia that overlay phalloidin-labeled smooth muscle (red) in media. Scale bars 200 μm in A; 50 μm in B,C.



Appendix D

Copyright permissions

Chapter 2: *Regional intrinsic and extrinsic innervation of the heart in zebrafish*

This chapter was previously published in the Journal of Comparative Neurology (Volume 523, Issue 11, pp. 1683-1700) and is reproduced here with permission from John Wiley and Sons (Wiley Periodicals), as per the license agreement following.

Citation:

Stoyek, M. R., R. P. Croll, and F. M. Smith. "Intrinsic and extrinsic innervation of the heart in zebrafish (*Danio rerio*)." Journal of Comparative Neurology 523.11 (2015): 1683-1700.

Chapter 3: *Integrative autonomic control of heart rate in zebrafish*

This work is accepted and awaiting publication with the American Journal of Physiology: Heart and Circulatory Physiology.

Citation:

Stoyek, M. R., R. P. Croll, and F. M. Smith. Zebrafish heart as a model to study the integrative autonomic control of pacemaker function. American Journal of Physiology – Heart and Circulatory Physiology, (2016), doi: 10.1152/ajpheart.00330.2016.

Appendix 2: *Results from studies in goldfish*

This work represents part of a study previously published in the Journal of Comparative Neurology (Volume 522, Issue 2, pp. 456-478) and is reproduced here with permission from John Wiley and Sons (Wiley Periodicals), as per the license agreement following.

Citation:

Newton, C. M., et al. "Regional innervation of the heart in the goldfish, *Carassius auratus*: a confocal microscopy study." Journal of Comparative Neurology 522.2 (2014): 456-478.

Copyright permission for Chapter 3: *Regional intrinsic and extrinsic innervation of the heart in zebrafish*


**JOHN WILEY AND SONS LICENSE
TERMS AND CONDITIONS**

May 14, 2016

This Agreement between Matthew R Stoyek ("You") and John Wiley and Sons ("John Wiley and Sons") consists of your license details and the terms and conditions provided by John Wiley and Sons and Copyright Clearance Center.

License Number	3867810628468
License date	May 14, 2016
Licensed Content Publisher	John Wiley and Sons
Licensed Content Publication	Journal of Comparative Neurology
Licensed Content Title	Intrinsic and extrinsic innervation of the heart in zebrafish (<i>Danio rerio</i>)
Licensed Content Author	Matthew R. Stoyek, Roger P. Croll, Frank M. Smith
Licensed Content Date	Apr 9, 2015
Pages	18
Type of use	Dissertation/Thesis
Requestor type	Author of this Wiley article
Format	Print and electronic
Portion	Full article
Will you be translating?	No
Title of your thesis / dissertation	Autonomic innervation and control the heart in the zebrafish
Expected completion date	Aug 2016
Expected size (number of pages)	350
Requestor Location	Matthew R Stoyek 5850 College Street PO Box 15000 Halifax, NS B3H 4R2 Canada Attn: Matthew R Stoyek
Billing Type	Invoice
Billing Address	Matthew R Stoyek 5850 College Street PO Box 15000 Halifax, NS B3H 4R2 Canada Attn: Matthew R Stoyek

Copyright permission for Chapter 3: *Integrative autonomic control of heart rate in zebrafish*



About | Testimonial | Jobs | Store | FASEB Directory

Search

Support APS

Awards | Careers | Education | Meetings | Membership | Publications | Science Policy

» Copyright

home / publications / information for authors / copyright

Twitter | Facebook | LinkedIn | YouTube | Email | RSS

Login

In this section

- [Cost of Publication](#)
- [Authorship Changes](#)
- [Manuscript Formatting Requirements](#)
- [Manuscript Composition](#)
- [Preparing Figures](#)
- [Data Repository Standards](#)
- [Data Supplements](#)
- [Special Instructions for Physiological Reviews](#)
- [Special Instructions for Physiology in Medicine](#)
- [Peer Review Policy](#)
- [Open Access](#)
- [Policy on Depositing Articles in PMC](#)
- [Copyright](#)
- [Permissions](#)
- [Policy on Use of Previously Published Data in Illustrations](#)
- [APS Ethics Policy](#)
- [Human Fetuses, Fetal Tissue, Embryos, and Embryonic Cells](#)
- [Guiding Principles for Research Involving Animals and Human Beings](#)
- [Ethics Posters](#)

Information For...

- [Advertising / Marketing](#)
- [Advocacy and Outreach](#)
- [Authors](#)
- [Chapters](#)
- [Committees](#)
- [Early Career Professionals](#)
- [Graduate/Professional Students](#)
- [Groups](#)
- [K-12 Education](#)
- [Minority Scientists](#)
- [Postdoctoral Fellows](#)
- [Public / Press](#)
- [Sections](#)
- [Subscription/Help Information](#)
- [Undergraduate Students](#)

"Science has just the privilege of

Copyright

The APS Journals are copyrighted for the protection of authors and the Society. The Mandatory Submission Form serves as the Society's official copyright transfer form.

Rights of Authors of APS Articles

- For educational purposes only:
 - Authors may republish parts of their final-published version articles (e.g., figures, tables), without charge and without requesting permission, provided that full acknowledgement of the source is given in the new work.
 - Authors may use their articles (in whole or in part) for presentations (e.g., at meetings and conferences). These presentations may be reproduced on any type of media in materials arising from the meeting or conference such as the proceedings of a meeting or conference. A copyright fee will apply if there is a charge to the user or if the materials arising are directly or indirectly commercially supported.
- Posting of the accepted or final version of articles or parts of articles is restricted and subject to the conditions below:
 - Theses and dissertations.** APS permits whole published articles to be reproduced without charge in dissertations and posted to thesis repositories. Full citation is required.
 - Open courseware.** Articles, or parts of articles, may be posted to a public access courseware website. Permission must be requested from the APS. A copyright fee will apply during the first 12 months of the article's publication by the APS. Full citation is required.
 - Websites.** Authors may not post a PDF of the accepted or final version of their published article on any website including social and research networking platforms; instead, links may be posted to the article on the APS journal website (see exception to authors' own institution's repository, as note below).
 - Institutional repositories (non-theses).** Authors may deposit their accepted, peer-reviewed manuscripts into an institutional repository providing:
 - the APS retains copyright to the article¹
 - a 12 month embargo period from the date of final publication of the article is observed by the institutional repository and the author
 - a link to the published article on the APS website is prominently displayed with the article in the institutional repository
 - the article is not used for commercial purposes
 - Self-archived articles posted to repositories are without warranty of any kind

¹Unless it is published under the APS *AuthorChoice* open access option, which allows for immediate public access under a Creative Commons license (CC BY)

(See also the APS [Policy on Depositing Articles in PMC.](#))

Discover the APS

- [Pay Your Membership Dues](#)
- [Apply for Membership](#)
- [APS Council/Leadership](#)
- [Visit the Journals of the APS](#)
- [Support the Society](#)
- [Explore the Living History of Physiology](#)
- [Visit PhysiologyInfo.org](#)
- [Join a Committee](#)
- [Read Our New I Spy Physiology Blog](#)
- [Network on the APS Connect Community](#)
- [Find Us on Social Media](#)

Copyright permission for Appendix 2: *Results from studies in goldfish*

JOHN WILEY AND SONS LICENSE TERMS AND CONDITIONS

May 14, 2016

This Agreement between Matthew R Stoyek ("You") and John Wiley and Sons ("John Wiley and Sons") consists of your license details and the terms and conditions provided by John Wiley and Sons and Copyright Clearance Center.

License Number	3867810781283
License date	May 14, 2016
Licensed Content Publisher	John Wiley and Sons
Licensed Content Publication	Journal of Comparative Neurology
Licensed Content Title	Regional innervation of the heart in the goldfish, <i>Carassius auratus</i> : A confocal microscopy study
Licensed Content Author	Cecilia M. Newton, Matthew R. Stoyek, Roger P. Croll, Frank M. Smith
Licensed Content Date	Dec 6, 2013
Pages	23
Type of use	Dissertation/Thesis
Requestor type	Author of this Wiley article
Format	Print and electronic
Portion	Full article
Will you be translating?	No
Title of your thesis / dissertation	Autonomic innervation and control the heart in the zebrafish
Expected completion date	Aug 2016
Expected size (number of pages)	350
Requestor Location	Matthew R Stoyek 5850 College Street PO Box 15000 Halifax, NS B3H 4R2 Canada Attn: Matthew R Stoyek
Billing Type	Invoice
Billing Address	Matthew R Stoyek 5850 College Street PO Box 15000 Halifax, NS B3H 4R2 Canada Attn: Matthew R Stoyek